MECHANICAL AND STRUCTURAL PROPERTIES OF MICROWAVE SINTERED TIN-COPPER-ANTIMONY ALLOYS

THE UNIVERSITY OF
WAIKATO
Te Whare Wānanga o Waikato

A thesis
submitted in fulfilment
of the requirements for the degree
of

Doctor of Philosophy in Engineering

at

The University of Waikato

by

TASNIM FIRDAUS BINTI MOHAMED ARIFF

The University of Waikato
2009

ABSTRACT

Tin-copper-antimony (pewter) alloys have been traditionally produced by a casting process which consumes large amounts of energy, time and as a result is expensive. This research aims to investigate the possibilities of implementing powder metallurgy for pewter production through a sintering process using microwave energy. The optimum sintering conditions using microwave sintering are also of interest. Pewter alloys were examined to determine the effect of green density, sintering time, and sintering temperature on the mechanical and structural properties of the sintered compacts. Samples were prepared by hydraulic pressing of a well mixed and blended tin alloy powder with three different compositions; 97wt%Sn 2wt%Cu 1wt%Sb, 94wt%Sn 4wt%Cu 2wt%Sb and 91wt%Sn 6wt%Cu 3wt%Sb. Two compaction loads were used to produce the samples with different green densities. Pellets pressed at 96 MPa had an average relative density of 80.7%, while those pressed at 129 MPa had an average green density of 84.6%.

Sixteen different time-temperature combinations were used for the heat treatments at 160 and 220°C for both conventional and microwave sintering. However, the sintering times had to be restricted to 15 and 30 minutes for microwave heating. Meanwhile, 60 and 120 minutes were used for conventional heating. It was found that for all three compositions, samples with a higher green density had a higher sintered density, compared to samples with lower green density, for the same sintering time and temperature. The relative density of sintered pewter alloys increased on average by 13% after conventional sintering and by about 14% after microwave sintering, when the sintering was carried out for the longer of the two sintering times and at the higher of the sintering temperatures selected, for all three compositions.

Moreover, the hardness increased by 25.6%, 23.5% and 7.0% when microwave sintered relative to the conventional sintering for 97Sn2Cu1Sb, 94Sn4Cu2Sb and 91Sn6Cu3Sb alloys respectively. Nevertheless, the grain size remained similar for all three compositions under the same sintering conditions. The degree of grain growth in microwave sintered samples was marginally

smaller (up to 23-24 μm) than in conventionally sintered samples which reached a grain size of 26-27 μm.

In terms of strength, microwave sintering produced samples with similar properties to those conventionally sintered under the same sintering conditions for all three compositions. The tensile strengths obtained compared well with the strengths obtained from the casting process. Nonetheless, tensile strengths for both conventionally and microwave sintered material was higher in the transverse direction than in the longitudinal direction. In conventionally sintered material, there was an increase in transverse strength of about 6.9%, 5% and 4%, while for the microwave sintered material, the strength increase was 9.1%, 5.6% and 4.5% for 97Sn2Cu1Sb, 94Sn4Cu2Sb and 91Sn6Cu3Sb alloys respectively when compared to the longitudinal direction.

The microwave sintered samples in general have improved hardness, better densification and a finer microstructure compared with the conventionally sintered samples and traditionally cast pewter. Increasing the Cu and Sb content increases the hardness and strength but in return, decreases its ductility. Hence, a pewter alloy with a moderate amount of Cu and Sb, i.e. 97Sn2Cu1Sb, microwave sintered at 220°C for 30 minutes would be the best choice for optimum mechanical properties.

Acknowledgements

All praises to Allah, the Almighty for I have successfully completed my PhD research. I would like to thank my chief supervisor, Dr. Brian Gabbitas for his advice, guidance and encouragement throughout this research. He helped me overcome hurdles that came along the way. I would also like to thank my second supervisor, Professor Dr. Deliang Zhang for sharing his views and opinions with me.

I sincerely appreciate all the help my colleagues at the Large Scale Lab have given me throughout my research by indulging in many serious discussions. They are Asma Salman, Aamir Mokhtar, Vijay Nadakuru, Masleeyati Yusop and Bhupinder Singh. Not to forget, appreciation also goes to the technical staff; Yuanji Zhang and Paul Ewart for helping me out with the instruments at the laboratory, Indar Singh for training me with the XRD equipment and Helen Turner for the SEM work. In addition, I would also like to thank Mr. Loh Keng Fong from Royal Selangor Malaysia who has provided me relevant information regarding cast pewter in Malaysia.

My deepest gratitude goes to my family. My parents and parents-in-law have shown their endless love, encouragement and support throughout my studies. They have supported and accepted well the fact of being far away from them during this mission of seeking further knowledge. My husband, Jehabar Sadiq, had sacrificed his career and so many other things for the sake of being together as a family in New Zealand. He had continuously motivated and encouraged me during my studies by giving me academic and emotional support. Last but not least, my children, Afdzaal and Azeemah who have shown their fullest support and love by sacrificing the most by being away from their grandparents, uncles, aunties and cousins back in Malaysia. Their physical presence with me in New Zealand meant a lot to me. This PhD mission has taught me that they are more important to me in life than anything else in the world.

To my parents

Professor Emeritus Datuk Dr. Mohamed Ariff Abdul Kareem

Datin Junaitha Begum Mohamed Abdullah

&

To my husband and children

Jehabar Sadiq Mohamed Nizamuddin

Afdzaal Sadiq

Azeemah Sadiq

TABLE OF CONTENTS

LIST OF FIGURES

LIST OF TABLES

NOMENCLATURE

MW	Microwave sintering
CS	Conventional sintering
Sn	Tin
Sb	Antimony
Cu	Copper
ppm	Particles per minute
m_b	Bouyant mass
w_{sat}	Saturated weight
w_{dry}	Dry weight
ρ	Density
V_b	Bulk volume
V_o	Volume of open pores
V_{cp}	Volume of closed pores
V_t	True volume
l	Mean lineal intercept
L	Length of the line
M	Magnification
N_l	Number of grain boundary intercept
Sv	grain-boundary area per unit volume
D	Grain size
D	Diffusivity
A	Frequency factor of diffusivity
Q	Activation energy
R	Gas constant (8.314472 J/Kmol)
T	Temperature (Kelvin)
r_0	Jump distance in diffusion
N	Number of jumps during diffusion
v	Fixed jump rate
k_t	Dielectric constant
k_p	Piezoelectric constant
δ	Skin depth (μm)
f	Frequency of microwaves (2.45GHz)

μ	Magnetic permeability (Henries/m)
σ_e	Electrical conductivity (Ω/m)
ρ	Electrical resistivity (nΩm)
ε	Absolute permittivity, (C^2/Nm^2)
λ_0	Incident wavelength (12.24cm for 2.45GHz waves)
D_p	Power penetration depth (nm)
E	Electric field (V/m)
E_o	Electric field amplitude at the surface (V/m)
P	Power absorbed per unit area (W/m^2)
J	Surface current
R_s	Surface resistivity (Ω-1)
η_0	Impedance of free space (377Ω)
H	Magnetic field
P_{em}	Electromagnetic power density
P_{conv}	Power loss per unit volume due to convection
P_{rad}	Power loss per unit volume due to radiation
H	*C*onvective heat-transfer coefficient of incoming gas
A/V	Surface area to volume ratio for compact
σ	Stefan-Boltzman constant
T_a	Surrounding temperature
Pr	Prandtl Number
Cp	Specific heat
μ	Viscosity
k	Thermal conductivity
Δt	Temperature as a function of incremental time domain
T_n	Temperature at nth interval
$T_{(n+1)}$	Temperature at the (n+1)th interval

CHAPTER 1

INTRODUCTION

1.1 General Background

Powder metallurgy is a cost effective method for producing simple or complex parts at, or close to, final dimensions at a variety of production rates ranging from a few hundred to several thousand parts per hour. In comparison with material production processes in general, powder metallurgy is a small but important process. It has an advantage of minimizing machining and hence scrap losses, because it is a near net-shape process. It gives good surface finishes and facilitates the manufacture of complex or unique shapes which would be difficult or impossible to make using other metal-working processes. Examples include semi-porous self-lubricating bearings, brake pads with embedded ceramic fibers, or brushes for electric motors combining copper with graphite [1]. Powder Metallurgy is capable of producing near net shape or net shape parts; hence its principal application is in the manufacture of small-to-medium size parts of complex shape such as gears, cams and levers.

Microwave heating is a sensitive function of the material being processed, where heating of the material is very much dependent on the capability of the material to couple in the microwave field. Microwave technology is successfully being used to sinter various powder metal components including small cylinders, rods, gears and automotive components in just 30 to 90 minutes [2]. Additionally, microwave technology is also used for melting metals and casting the melt into various shapes. Microwave sintering of powder metals (already in final net shape) has been demonstrated with a variety of metals and alloys; copper, iron, steel, aluminium, nickel, silver, gold, molybdenum, cobalt, tungsten, tin, titanium, etc. [2].

Microwave sintering is a method of heating that involves energy conversion which is different from the conventional sintering that concerns energy

transfer. In microwave sintering, the heat is generated internally within the material instead of originating from external sources. In the process of microwave heating, the materials absorb microwave energy themselves and then transform it into heat within the sample volume [3]. The energy is directly transferred to the material through the interaction of electromagnetic waves with atoms and molecules leading to heating [4]. Microwave sintering has the potential for rapid processing with refinements in microstructure and enhanced properties. Microwave sintering is much more uniform and effective compared to conventional sintering. This results in a reduction of processing time and energy consumption.

1.2 The importance of this study

Microwave heating is a function of the material being processed, and there is almost 100% conversion of electromagnetic energy into heat, largely within the sample itself, unlike conventional heating, where there are significant thermal energy losses. Bulk metals are excellent reflectors of microwaves and in general are not heated significantly. But in a powdered or unsintered form, all metals, alloys or intermetallics will couple in a microwave field efficiently and effectively to produce highly sintered bodies with improved mechanical properties [5,6].

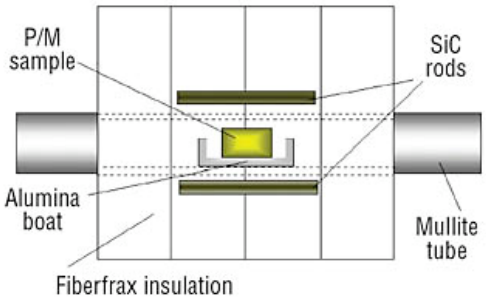

Figure 1.1: Schematic of tube microwave processing setup [2]

The microwave process has many advantages over conventional heating methods [6]:

i) Time and energy saving which leads to lower cost

ii) High heating rates which minimizes grain growth

iii) Uniform and volumetric internal heating which leads to uniform microstructures

iv) Lower sintering time and temperature which leads to energy savings

v) Finer microstructures with improved mechanical properties

vi) Synthesis of new and special materials which leads to new market potential

vii) Improvement in the product performance

viii) Controlled inert atmosphere which is an environmentally friendly process

Since 1984, the Materials Research Institute at The Pennsylvania State University has been a pioneer institution in the microwave processing of a whole range of ceramics, composites, and metallic materials. The 1980s saw successes in sintering and synthesizing of many traditional ceramics such as alumina, zirconia, ZnO, [NZP], hydroxyapatite, zeolites, mullite, silica, etc. The focus in the 1990s was aimed at new materials and in new directions [2].

Many electroceramics such as PZT, $BaTiO_3$, $Ba(Mg_{1/3}Ta_{2/3})O_3$ and transparent ceramics were successfully synthesized, fabricated and sintered in microwave fields. Following this, programs were launched to sinter non-oxides, especially WC/Co based products. The success made in this area led to the innovative approach of continuous microwave sintering, which made it possible to successfully commercialize the developed technology for WC/Co based products applied in the cutting and drilling industry. Another advancement in 1996 was the successful sintering of powder metal parts (steel) with improved performance and better mechanical properties, which opened up completely new avenues of research and commercial exploitation of microwave technology in new applications. Some of these achievements are discussed in the literature review.

A review of the research undertaken in the field of microwave sintering reveals a significant amount of work on oxide ceramics and semi-metals like carbides and nitrides. The applicability of microwave sintering to metals has been overlooked because most metals are known to reflect microwaves [6]. Roy *et al*. [7] discussed the use of microwave sintering and noted that few experiments have

been done with metal powders. Green laboratory and commercial compacts were microwave sintered, typically, at 1100°C to 1300°C for 5 to 30 minutes. The sintered compacts were reported to have uniformly distributed porosity with improved properties in comparison with conventionally processed materials.

1.3 Problem Statement

Tin was one of the first metals known to man. Throughout ancient history, various cultures recognized the virtues of tin in coatings, alloys and compounds, and use of the metal increased with advancing technology. Mostly, tin is used as a protective coating or as an alloy with other metals such as lead or zinc. Tin is used in coatings for steel containers, in solders for joining pipes or electrical/electronic circuits, in bearing alloys, in glass-making, and in a wide range of tin chemical applications. Secondary, or scrap, tin is an important source of tin supply. The bulk of the world's tin is produced by Malaysia, Indonesia, Thailand and Bolivia. The largest producer was once Malaysia. Now it is the third largest producer after Bolivia and Indonesia. The most important uses of tin are in cans and in solder, but substitutes, such as plastics and aluminium, have become more and more important for containers, while the resmelting of tin scrap has increased [8].

At present, the tin-based manufacturing industry in Malaysia consists of three main product sectors namely solder, tinplate and pewter. Domestic consumption of primary tin metal for the first four months of 2007 was 8% lower than that in the comparable period of 2006. During this period, solder remained the leading consumption category, followed by chemicals, tinplate, brass and bronze [9]. Despite progress in the local downstream tin-based manufacturing industry, as reflected by the modest growth in the domestic tin metal consumption, the industry is at present still relatively small in terms of its contribution to the nation's manufacturing value-added activities. However, the potential for the advancement of the industry is considerable, especially in the field of tin chemicals [8].

In an era of globalization, the production and consumption of materials symbolises or encapsulates aspects of national identity. For example, when Sydney staged the 2000 Olympic Games, certain businesses had the "rights" to produce particular icons that were promoted as depicting "Australia". Similarly, in 1998 when the Commonwealth Games were staged in Kuala Lumpur, Malaysia was promoted to the outside world with a wide range of artefacts that represented the modern aspects of Malaysian identity. Royal Selangor produced trophies and gifts to international dignitaries. Sociological dynamics is broadened by national material cultural identities [10].

Malaysia is home to the world's finest pewter and Royal Selangor is its most well known name. Royal Selangor, an Icon of Malaysia, is a Malaysian pewter manufacturer and retailer, the largest of its type in the world. Royal Selangor is the most well-known brand in pewter. Royal Selangor offers over thousands of different varieties of tableware and gift items, ranging from traditional tankards, elegant tea sets, photo frames and handsome desk accessories. Malaysian pewter is composed of tin, with a small fraction of copper and antimony added to strengthen it. Unlike pewter in the olden days, modern pewter produced in Malaysia, for health reasons does not contain lead, and adheres to international standards [11].

As pewter has a low melting point and is relatively soft, it is an ideal material for craftsmen and designers to work with. Designers at Royal Selangor are able to express the individuality, beauty and character of the material in a variety of finishes and forms. The material also lends itself to different manufacturing techniques, some of which have been handed down through many generations. Today, tin is an important metal in industries even though the annual tonnage used is much smaller than that of many other metals. One reason for the small tonnage is that, in most applications, only very small amounts of tin are used at a time. Tin has a low melting point (232°C) and is therefore sintered at a low temperature.

The pewter produced in Malaysia is produced by the casting process where tin, copper and antimony are melted and mixed in the liquid phase to form the pewter alloy. This consumes large amounts of energy, as a result of furnace

time and high production costs. This research investigates alternatives for modern pewter production through a powder metallurgy process and also takes a step further by exploring the possibilities of implementing microwave sintering into processing as a substitute for the conventional sintering method, as a means of further reducing processing costs.

Manufacturing industry in the 21st century will have to reduce its consumption of energy in order to protect the environment. Since the pewter industry uses traditional casting processes to make its products, the use of high temperatures requires large quantities of energy. However, a significant proportion of the energy is consumed in maintaining the temperature of the surrounding furnace material or container rather than being used in product manufacturing. If energy can be efficiently used in the manufacturing of products by improving the sintering process, less energy will be consumed, which will in turn save energy.

Microwave processing has been applied to a wide variety of materials. Microwave heating is fundamentally different from conventional furnace heating. The latter involves radiant/resistance heating followed by transfer of thermal energy via conduction to the inside of the body being processed. Microwave heating, on the other hand, is a volumetric process involving instantaneous, rapid and highly efficient conversion of electromagnetic energy into thermal energy. Thus, the use of microwave energy for materials processing has major potential and advantages over conventional heating. For example, microwaves allow enhanced densification at lower processing temperature and with shorter processing time.

From the literature survey, it has been observed that no microwave sintering work has been done on pewter alloys. There exists a great need for investigating the effect of microwave sintering of pewter alloy on density, porosity, dimensional changes, tensile strength, grain size, microstructure, and degree of densification.

1.4 Hypothesis, Aims and Objectives of the study

The aim of this study is to analyze the mechanical and structural properties of microwave sintered tin-copper-antimony alloys. Therefore the hypothetical questions for this research are:

i) Will the mechanical properties of microwave sintered tin-copper-antimony (pewter) alloys be as good as or better than those produced by casting?
ii) Will the microstructure of the microwave sintered tin-copper-antimony (pewter) alloys be improved through enhanced homogeneity and a more uniform microstructure?
iii) Will the microwave sintered pewter alloys have a significant impact on the Malaysian pewter production when compared to the current pewter industry which uses a casting process?

The main aim of this research is to find optimum conditions that best suits sintering behaviour of tin-copper-antimony alloys.

The objectives of this study are:

i) To study the influence of microwave sintering on the pewter's hardness, tensile strength, density, porosity, dimensional changes, densification parameter, grain size and shape.
ii) To compare microwave sintering of pewter alloys with conventional sintering of pewter alloys.
iii) To analyze the difference between modern pewter, produced through microwave sintering, with the pewter produced through traditional casting processes.
iv) To investigate the influence of three different compositions of tin, copper and antimony in the pewter composition, on the structure and properties relationship.

1.5 The Scope of this Study

In a limited time period, it was not possible to cover the implementation of a wider range of parameters. Of course, the main aim and goal would be to improve the overall mechanical and structural properties of tin-copper-antimony (pewter) alloys. Therefore, only the most relevant and appropriate parameters were chosen for the purpose of experimentation. However, there were only three different compositions of tin alloys that were investigated for a specified range of parameters. The three sets of alloys used in experimental work based on percentage of weight composition, were as follows:

1. 97wt%Sn 2wt%Cu 1wt%Sb
2. 94wt%Sn 4wt%Cu 2wt%Sb
3. 91wt%Sn 6wt%Cu 3wt%Sb

Table 1.1: Control Factor Allocation

Type of Heating	Compaction Load	Sintering Temperature	Sintering Time
Hybrid Microwave Heating	96 MPa, 129 MPa	160°C, 220°C	15 min, 30 min
Conventional Vacuum Heating	96 MPa, 129 MPa	160°C, 220°C	60 min, 120 min

This research however, does have some limitations and constraints. The size of the microwave oven and the thermal pod itself is designed for small or medium sample sizes. Thus, very large samples could not be used. Graphite pellets were used as susceptors in the crucible to allow a controlled two-directional sintering process for low sintering temperature instead of SiC since this caused thermal runaways due to excessive energy being stored during heating. SiC is meant for high temperature application and is unsuitable for low temperatures. Only a type K thermocouple could be used because it is designed for low temperature applications. Moreover, oxidation could not be totally prevented by purging the microwave oven with argon gas. Microwave sintering the sample in a vacuumed capsule was not possible due to the inability of monitoring temperature inside the capsule itself.

1.6 Report Structure

This thesis is divided into five chapters. The literature review presented in Chapter 2 covers various aspects of microwave sintering on materials such as metals, ceramics, and composites. Some of the related research work in previous years are quoted in this chapter to further support and reinforce the author's ideas in terms of the application of microwave energy as an alternative method of sintering compared with conventional sintering in powder metallurgy.

Chapter 2 also discusses the importance of microwave sintering in various research areas and its benefits in terms of mechanical, structural, and economic aspects, particularly in the manufacturing sector where energy consumption and processing time play an important role in cost effectiveness. This chapter also discloses the positive and negative characteristics of materials, sintered by microwave energy.

Chapter 3 describes the research methodology for the preparation of the samples, the sintering process, the measurement of density, porosity, hardness and tensile properties, X-Ray Diffraction (XRD), Scanning Electron Microscope (SEM), and Electron Dispersive X-Ray Spectrometer (EDS) analysis.

Chapter 4 compiles all the experimental results and discusses them in terms of mechanical properties and structural characteristics. The effect of green density, compaction load, sintering time and temperature on the mechanical and structural properties of the conventional and microwave sintered samples are discussed. This chapter also includes a study on diffusion, based on a separate experiment which involved couples of Sn-Cu and Sn-Sb with the aim of verifying the diffusion behaviour using microwave energy. Furthermore, an application of mathematical modelling during microwave sintering is included in this chapter to quantify the effects of microwave energy for sintering purposes.

The research is concluded in Chapter 5 which outlines the most appropriate conditions for the application of microwave sintering for the manufacturing of pewter artefacts. Moreover, this chapter also mentions how the findings of this research might have an impact on the Malaysian pewter industry, by considering powder metallurgy as an alternative method of production instead of the traditional casting process. Additionally, this chapter includes ideas for possible future work and recommendations in this area of research.

CHAPTER 2

LITERATURE REVIEW

2.1 Introduction

Recent developments in the field of microwave sintering have been driven by its potential use for a wide range of materials ranging from wood, bacon and potato chips to rubber, ceramics and semiconductors [12 - 15]. Microwave technology has had a positive impact on many industrial processes through lower energy costs and faster processing times. It is used for synthesis, drying, calcination, debinding and sintering of materials. The Microwave Research Group at the Materials Research Institute of the Pennsylvania State University was the first to demonstrate very rapid sintering in time intervals varying from 3-20 min on many traditional and advanced ceramic materials such as alumina, mullite and hydroxyapatite [7, 16].

"New developments (and innovative ideas) in materials processing have the most profound and wide-ranging impact on the emergence of new materials and technologies. Microwave processing is one such emerging technology of the future." [2]

Due to specific new developments, especially at Pennsylvania State University and in Japan, microwave processing has become an innovative technology for a wide variety of real materials and is attracting worldwide attention. Initially, successes in microwave heating and sintering were confined to mainly oxide and some non-oxide ceramics. Today, this has been extended to cemented carbides for cutting and drilling applications with improved performance, and has been successfully commercialized. Additionally, microwave processing has been effectively and efficiently applied to the sintering of powder metals [2].

The efficacy of microwave heating is a sensitive function of the material being processed; only those materials that couple in microwave fields will get heated. Microwave heating is different from conventional heating because the heat is generated internally during microwave heating, so the thermal gradients are the opposite of those observed in conventional heating. The electrical and magnetic properties of a material determine whether microwave radiation is reflected, absorbed or transmitted. Most materials transmit and/or absorb microwaves to varying degrees. Many ceramics are transparent or poor absorbers of microwave energy but when heated to a critical temperature, they become good microwave absorbers [17]. While it is well recognized that bulk metals are opaque to microwaves and good reflectors, metallic materials in powder or porous form are very good absorbers of microwaves and can be heated very rapidly [2].

The main aim of this research was to determine the feasibility of using microwave heating to sinter pewter alloy effectively and efficiently. Artefacts made from pewter alloy are traditionally made by melting and casting. Furthermore, the effect of green density, sintering time, sintering temperature and percentage content of alloying elements; copper and antimony into the tin alloy on the mechanical and structural properties were studied. The following sections give an overview of microwave sintering on various materials but they mainly focus on the effects on density, hardness, tensile strength, microstructural evolution and grain growth.

2.2 The Microwave Sintering of Metallic Materials

Current work on the microwave sintering of metallic materials is largely based on a laboratory scale. However, the Fraunhofer IFAM Institute in Dresden, Germany, in partnership with the University of Bayreuth are studying microwave sintering of PM ferrous and aluminium alloys and special materials to evaluate the potential for industrial scale production [18]. Their results indicate that lower sintering temperatures, shorter process time and improved material properties may result from effects created by the electro-magnetic field of microwaves.

Microwave sintering has been widely recognized as one such technique and has been extensively used for the consolidation of ceramics and hard metals [14 - 19]. Roy *et al*. [7, 20] were the first to prove that metallic materials can be coupled with microwaves as long as they are in powder form. Rodiger *et al*. [19] reported that sintering of hardmetal with microwaves leads to a finer microstructure because of lower sintering temperatures and shorter processing times compared to conventional sintering. A more recent sintering of premixed and pre-alloyed Cu-12Sn bronze for temperatures corresponding to transient, solid-state, and supersolidus sintering were done by Sethi, Upadhyaya and Agrawal [21]. The study has shown that the hardness of the premixed microwave samples is higher than for the corresponding conventional premixed samples. In addition, the microstructure in the case of microwave sintered samples is more uniform than the conventionally sintered ones.

Subsequently, microwave heating and sintering of several other metal powder compacts has been demonstrated [22 -30]. Recently, Gupta and Wong [31, 32] have revealed the possibilities of consolidating a range of particulate metallic materials (Al-, Mg- and Pb-free solders) and the synthesis of Mg-Al_2O_3 and Mg-Cu composites using two-directional microwave-assisted rapid sintering. These studies have shown that there is an enhancement of the overall mechanical performance of metallic materials. Tensile testing of microwave synthesized materials revealed superior mechanical properties compared with conventionally sintered materials.

There has been some uncertainty among researchers about the benefits of using susceptors in microwave heating. Gupta and Wong [31] implemented the two-directional microwave sintering methodology which uses silicon carbide (SiC) as a susceptor material in an experimental arrangement shown in Figure 2.1. This can be considered as hybrid sintering with direct heating/sintering of the compacts from microwaves forming one component and the radiative heating/sintering from the SiC susceptor forming the second component of the total heat imparted into the compacts. In an earlier study by Roy *et al*. [20], there were indications that susceptors such as SiC may not be useful in sintering and the use of susceptors, separated from the microwave source by only a ceramic wall, was not attempted. In another study, Roy, Agrawal and Cheng [23], used microwaves, without susceptors to sinter their materials but claimed and proved that it was 100% microwave sintering. Gupta and Wong [31] however realized that microwaves assisted the sintering from the inside to the outside of a compact while a SiC-susceptor assisted the sintering from the outside to the inside. This concept of two-directional sintering is shown in Figure 2.2.

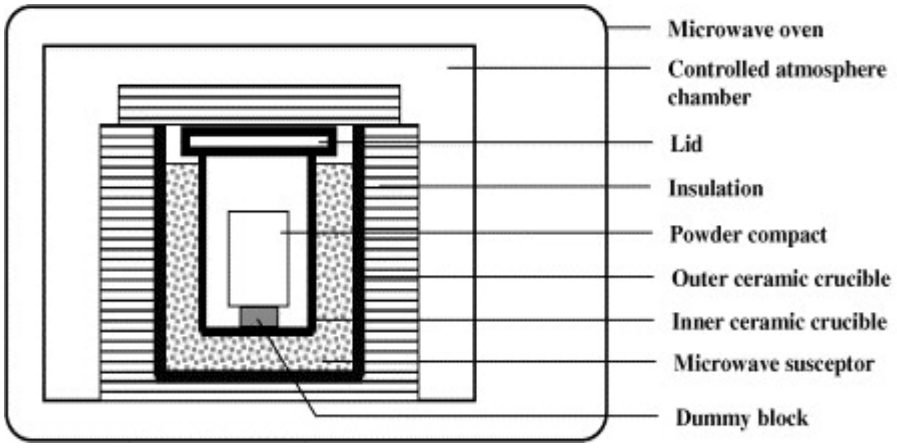

Figure 2.1: Schematic diagram of the experimental set-up used in microwave sintering using SiC (susceptor) heating [31]

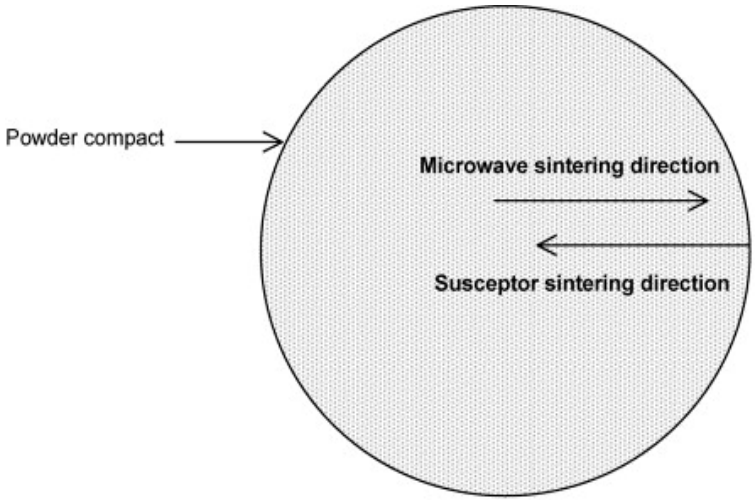

Figure 2.2: Schematic diagram showing the concept of two-directional sintering [31]

Although there is evidence of enhanced mechanical properties after microwave sintering, the influence of heating rate should not be overlooked. In order to avoid thermal shock in conventional heating, the heating rate seldom exceeds 10°C/min. In contrast, in microwave heating, the compact itself acts as a heat source and is subjected to a more rapid and uniform heating which minimizes microstructural coarsening. One of the concerns in microwave heating is the influence of high heating rates on the microstructural homogeneity during sintering. Studies have shown that when compared with conventional sintering, the microwave sintered compacts were denser and exhibited less grain coarsening [28, 29]. These studies have also shown that bronze alloys and W-Ni-Fe alloys can be consolidated through microwave sintering with a significant (~75%) reduction in processing time.

Sorescu *et al*. [3] have found evidence for microwave-induced recrystallization in NiZn ferrites. In another study, comparing the effect of heating mode on the densification, microstructure, strength and hardness of austenitic and ferritic stainless steel, Panda *et al*. [26] reported that while the microwave sintered compacts exhibit a finer microstructure, there was no corresponding improvement found in densification and mechanical properties. This has been correlated with an elongated and irregular pore structure.

In addition to research findings relevant to mechanical and structural properties, several studies [33 - 39] have investigated the synthesis of ferrite materials using the microwave technique. Characterizations of the structural and magnetic properties were carried out successfully. Most significantly, ferrite samples sintered in a microwave field, generally, showed lower dielectric constant values compared with conventionally sintered samples, making microwave sintering particularly suitable for high frequency applications. These results demonstrate the beneficial effect of microwave sintering processes on enhancing the densification of ferrites, as compared with the conventional processes. The authors have reported that the degradation of the magnetic properties was attributed to the strain induced in the ferrites. Figure 2.3 shows the uniform grain size distribution for both conventional and microwave sintered MnZn-ferrites where the former showed larger grains (~10 μm) and the latter smaller grains (~6.5 μm).

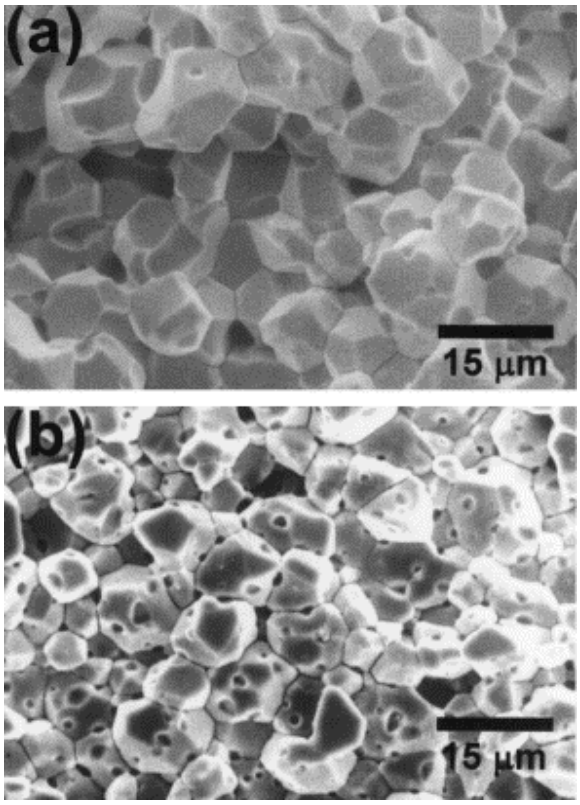

Figure 2.3: Typical SEM microstructure of MnZn-ferrites densified by (a) conventional furnace sintering, cs (b) microwave sintering, ms [34]

2.3 The Microwave Sintering of Ceramic Materials

It is well known that microwaves are widely used in many industrial applications including meat tempering, processing of potato chips, drying of pharmaceutical products and vulcanization of rubber. However, in the case of ceramic processing, microwave energy has been used since the late 1940's with a big push later in the 1980's. The application of microwaves has been limited, but not restricted to process control, drying of ceramic sanitary wares, calcination, decomposition of gaseous species and the sintering of oxide ceramics by microwave plasma [5].

Microwave processing of ceramics is fast emerging as a new field of ceramic processing and material synthesis. In recent years there has been significant progress in the aspect of commercialization and application of the technology to new areas. The most significant developments have been the use of microwaves in the sintering of non-oxides, such as tungsten carbide-based components and powdered metals, the fabrication of transparent ceramics and the design of continuous microwave systems [5].

The use of microwave energy for processing ceramics and ceramic matrix composites has been extensively investigated. The range of materials and processes that have been investigated is shown in Table 2.1 [40]. The potential advantages of microwave processing over conventional methods for ceramics include:

- Reduced processing time
- Improved product uniformity
- Improved microstructure

Table 2.1: Examples of ceramics microwave processing research and development [40]

Materials	Processes											
	Annealing	Binder Burnout	Calcining	Drying	Fiber Drawing	Joining	Melting	Sintering	Combustion Synthesis	Powder Synthesis	Slip Casting	Clinker
Advanced Ceramics		X		X		X		X	X	X		
Cements												X
Composites						X		X				
Ferroelectrics	X	X	X					X				
Ferrites								X				
Glasses					X		X			X		
Minerals			X	X				X				
Refractories			X	X			X	X				
Superconductors	X			X				X		X		
Whitewares				X				X			X	

The microwave processing of ceramics can be used as an alternative method to conventional sintering of ceramics because of the potential advantages that exist, such as rapid heating, more uniform microstructures, penetrating radiation, and higher densities [41-45]. Several studies have been directed towards a comparison of the dielectric behaviour of microwave and conventionally sintered ceramics [46- 53]. All of these studies showed that the microstructure and superconducting properties of microwave sintered material is close to those observed for conventionally sintered ceramic material. Xie *et al*. [52] have reported that green compacts of ferroelectric ceramics achieved more than 98% theoretical density at 960°C. The authors discovered that smaller grain sizes and a more uniform microstructure were developed due to volumetric heating and rapid

sintering during microwave processing. Figure 2.4 shows that the dielectric properties obtained after microwave sintering are comparable to those obtained after conventional sintering at two different temperatures.

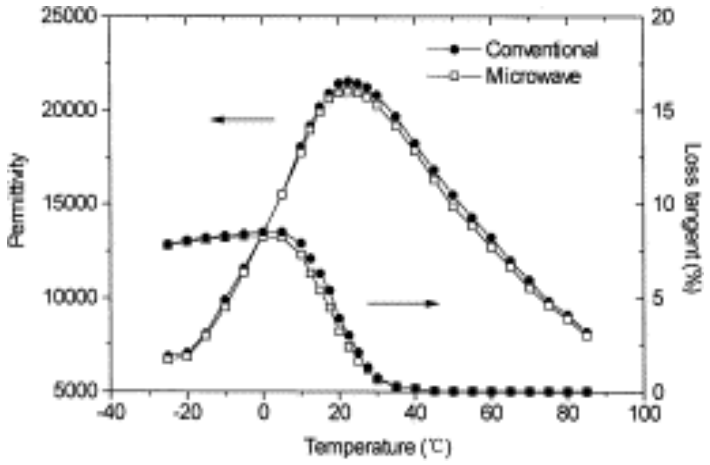

Figure 2.4: Dielectric properties of the samples sintered by microwave and conventional method [52]

Nevertheless, there is evidence of microwave sintered ceramic samples with improved dielectric properties [54-56]. Thakur, Prakash and Agrawal [54,55] carried out a detailed dielectric study on a Barium strontium titanate (BST) (95:5) composition. The material was synthesized conventionally and by microwave processing. The latter technique resulted in material with high density, improved microstructure and dielectric properties. The dielectric properties were studied as a function of frequency and temperature and well-defined ferroelectric behaviour of the first order transition was observed. It followed the Curie–Weiss law above the transition temperature (paraelectric region) where the Curie temperature was found to be slightly higher for microwave sintered material.

In addition to the previous studies mentioned above, Singh *et al*. [57] carried out a research to compare the influence of conventional and microwave sintering techniques on the structural, electrical and piezoelectric properties of PCT ceramics. It was observed that the microwave sintered PCT ceramics showed better densification, a fine and uniform grain size, low dielectric loss and improved dielectric – piezoelectric constant (kt/kp) ratio. The microwave sintering resulted in energy-saving, rapid processing and a uniform temperature distribution throughout the sample. The value of coercive field, E_c was slightly higher for a microwave sintered sample.

Microwave sintering was performed in a modified microwave kitchen oven (2.45 GHz, 1.2 kW) as shown in Figure 2.5. Sintering was done at 1100 °C for 30 min and the total cycle time was 135 min. The temperature–time profile for conventionally sintered and microwave sintered material is shown in Figure 2.6. A specially designed thermocouple (Pt–PT–Rh 13%) was kept close to the sample for measurement of temperature in the microwave oven. To avoid interaction with the high electric field, a platinum tube was used to shield the sheathed thermocouple.

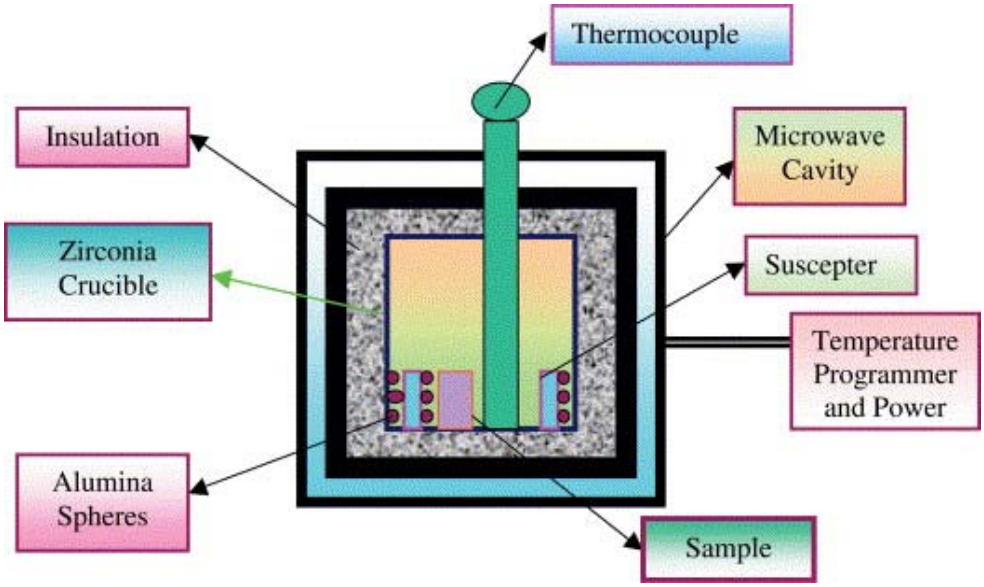

Figure 2.5: Schematic of the microwave sintering system [57]

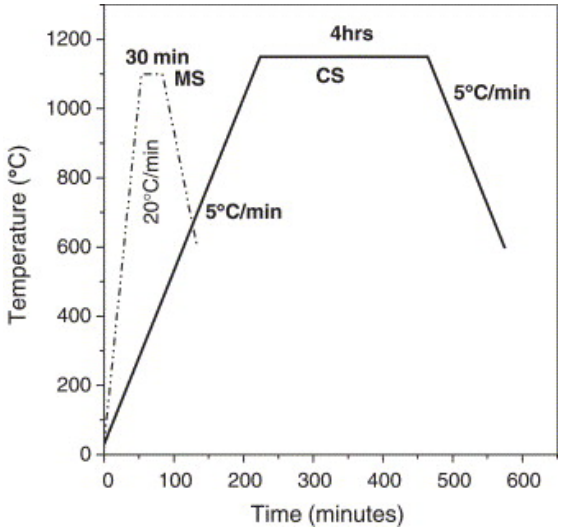

Figure 2.6: Comparison of the time–temperature profiles for modified PT synthesis in microwave and conventional process [57]

Figure 2.7 shows the microstructures of conventionally and microwave sintered PCT ceramics. The grain size distribution for microwave sintered samples is more uniform than that for a conventionally sintered sample. This suggests that the rate of grain growth during microwave sintering is markedly enhanced without inducing abnormal grain growth, which is desired to get the better electrical and electromechanical properties. In addition, the authors also reported that the average grain size is smaller after microwave sintering.

Experiments to examine the feasibility of densifying α-silicon carbide powder compacts based by the use of microwave powered furnaces were attempted [58,59]. The authors discovered that while microwave sintering of silicon carbide (SiC) is feasible, it does not seem to generate practical advantages over conventional heating. The authors have observed that the particle size of SiC did not change with the increase in reaction temperatures.

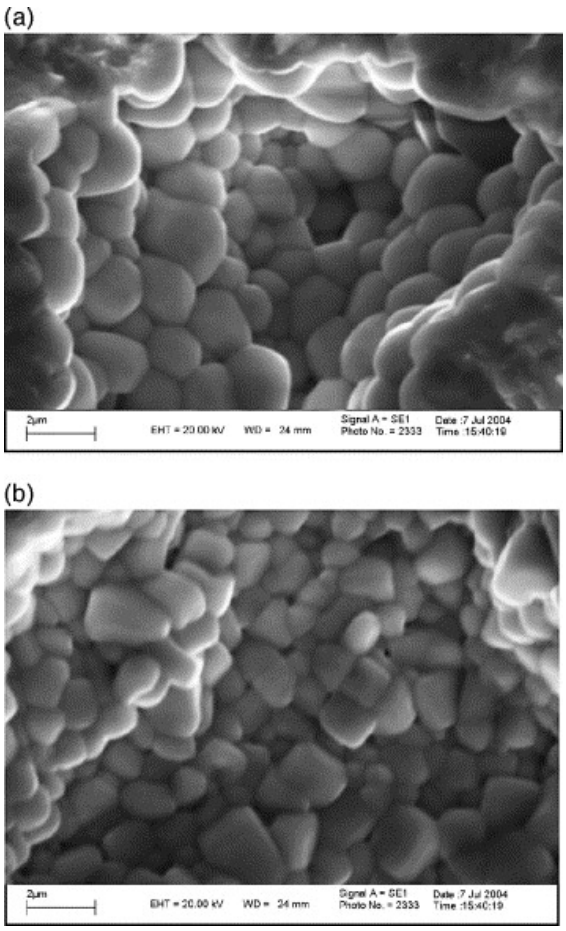

Figure 2.7: Scanning electron micrographs for (a) Conventional Sintered and (b) Microwave Sintered samples of PCT ceramics [57]

Despite various implementations of microwave sintering on ceramic materials, a great deal of work has been done on the research and development of hydroxyapaptite (HAp) ceramics as biomaterials. Hydroxyapatite has a great potential for biomedical applications since it is the main component of bones and teeth. Several studies have been conducted on the fabrication of transparent ceramics using hydroxyapatite. These studies led to the first fabrication of hydroxyapatite by Fang *et al*. [16] using microwave processing. It was shown that useful bodies could be sintered in less than 15 minutes and that the densification was dependent on the starting materials. More recent studies have revealed that microwave processing has been successfully used to fabricate transparent ceramics due to its ability to minimise grain growth and produce a fully dense ceramic in a very short period of time [60-65].

There have been extensive investigations on titanium based ceramics over the last decade. Studies have included observations on the effects of microwave sintering on resistivity, phase transformations, mullitizations, dielectric properties, microcrystal structure, densification and hardness [66-77]. Hart *et al*. [78] faced challenges in producing TiO_2 films by microwave heating. Microwave processing is an attractive alternative to conventional furnace treatment for sintering of TiO_2 nanostructured thin films, but problems arose when they were heated with 2.45-GHz microwaves. It was found that the conducting glass cracked (Figure 2.8) at temperatures above 200°C. By coating a 20-μm-thick film of nanostructured TiO_2 on the transparent conducting oxide (TCO) glass (using a commercially available powder), the temperature at which cracking occurred was raised to about 400°C. When a sol–gel method was used to produce TiO_2, difficulties were encountered in the production of ~10-μm-thick films, including cracking of films during drying.

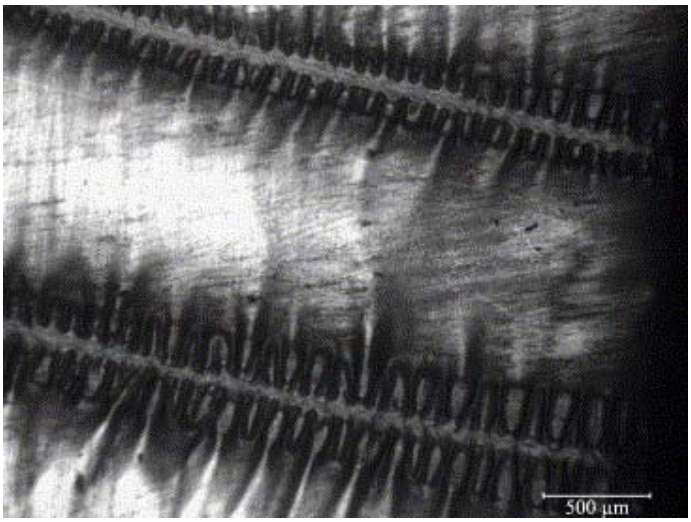

Figure 2.8: Optical micrograph of cracked TCO glass after a microwave heat treatment to ~220 °C [78]

A more recent study performed by Mahboob *et al*. [79], on the dielectric behaviour of microwave sintered rare-earth doped $BaTiO_3$ ceramics, revealed that high values of dielectric constant had been obtained in most of the samples. This was attributed to the effect of microwave sintering. Impedance measurements were also carried out between room temperature and 600 °C over a wide

frequency range. Some interesting features of the samples were reported, such as the separation of grain, grain boundary and electrode effects. Figure 2.9 shows the variation of dielectric constant with temperature for microwave sintered $BaTiO_3$ samples comparing the different doped elements. Results clearly indicate that a Pr doped sample has the largest dielectric constant followed by Ce and Nd.

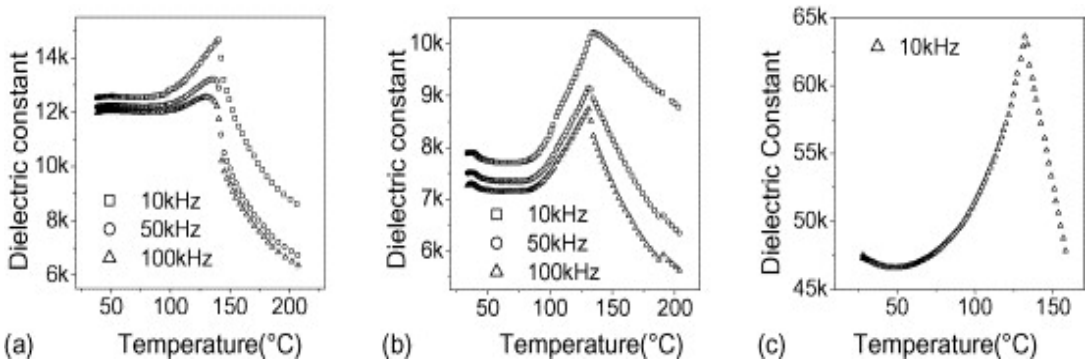

Figure 2.9: (a–c) Variation of dielectric constant with temperature for microwave sintered Ce, Nd and Pr doped $BaTiO_3$ samples respectively [79]

Zirconia based ceramics possess properties which are of interest to engineers. They include high strength, high fracture toughness, wear resistance and good frictional behaviour. The implementation of microwave processing to zirconia based ceramics has not been overlooked. Many experiments have been conducted and these have successfully produced high quality samples with high densification, smaller grain size, more uniform grain structure and higher hardness [80-83].

Huang *et al*. [84] carried out a comparative study on microwave and conventional sintering of CeO_2 and Y_2O_3 co-stabilised ZrO_2 from stabiliser-coated nanopowders. The influence of the composition and the sintering methods on the final phase composition and microstructure were also investigated. Fully dense material grades were obtained by both sintering methods. They observed finer and more uniform microstructures in the microwave sintered ceramics compared with conventionally sintered samples. As expected, average grain size increases with increasing sintering temperatures as shown in Table 2.2. However, the authors

concluded that the fracture toughness increases with decreasing stabiliser content, whereas a reverse relation was found for the Vickers hardness. Comparable toughness and hardness values were obtained for the microwave and conventionally sintered samples.

Table 2.2: Average grain size of $0.7MgTiO_3$–$0.3MgTa_2O_6$ ceramics with different sintering temperature [84]

Temperature (°C)	Average grain size (μm)
1370	4.8
1400	6.6
1430	11.6
1460	13.3
1490	16.1

Despite numerous advantages of microwave sintering on physical and mechanical properties, microwave sintering has also proven to have some negative effects. Goldstein and Kravchik [85] conducted a study on the feasibility of sintering PZT powder compacts by direct microwave heating using multimode applicators at 2.45 GHz. PbO loss and an electromagnetic field intensity with a non-uniform spatial distribution were the main factors with a negative influence on sintering. Cracking-warpage propensity was shown to be a strong function of specimen shape, size and the heating chamber set up. However, dielectric and piezoelectric properties of MW and conventionally sintered specimens appeared to be similar.

To overcome the problem of cracking, Goldstein *et al*. [86] used yttria-stabilized zirconia instead and managed to obtain uncracked fully dense zirconia ceramics. It was found that such a sintering approach can be used in the case of $ZrO_2(Y_2O_3)$ powder compacts. Sintered bulk densities close to the theoretical were obtained after firing cycles of about 2 hours. Sintering rate enhancement in the microwave furnace resulted in a reduction of about 100°C in the minimal temperature required for full densification. However, they reported that the mechanical properties of microwave and conventionally sintered specimens were not significantly different.

Aluminium Oxide (Al_2O_3) is an important engineering material. It offers a combination of good mechanical properties and electrical properties leading to a wide range of applications which include seal rings, medical prostheses, laser tubes, thermocouple tubes and electrical insulators. Alumina can be produced in a range of purities with additives designed to enhance properties. Producing alumina based ceramics using microwave technology has helped to enhance densification and the initiation of nucleation and growth driven phase transformations at lower sintering temperatures [87-92].

Another comparative study of microwave and conventional processing of ceramic materials based on $MgAl_2O_4$ was performed by Gomez *et al*. [93]. According to semi-quantitative X-ray diffraction analysis, approximately 90% of $MgAl_2O_4$ was produced with both processing methods. Scanning electron microscope (SEM) images of the microstructure shown in Figure 2.10 reveal a similar grain morphology for the two methods, but the grain size is much smaller after microwave sintering. A more heterogeneous microstructure was observed in the specimen processed by microwaves.

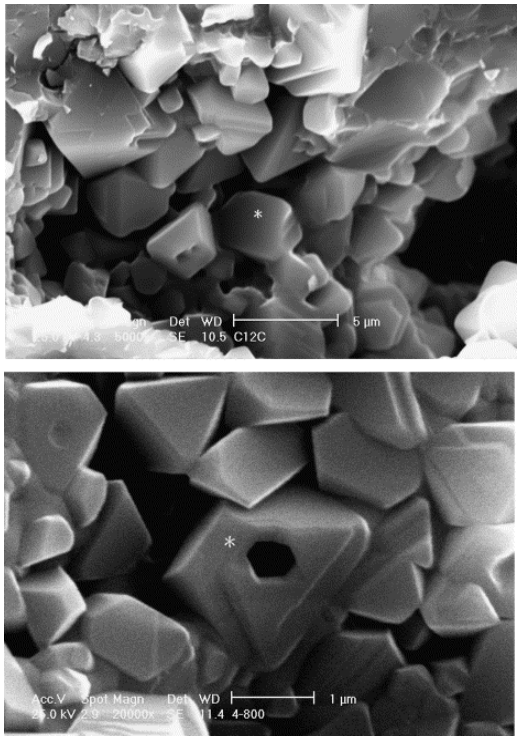

Figure 2.10: SEM images of $MgAl_2O_4$ obtained by conventional (above) and microwave (below) heating [93]

Studies mentioned earlier have indicated smaller grain growth for microwave sintering due to shorter sintering times relative to conventional sintering. However, although improved densification (>95% theoretical density) and grain growth have been observed when sintering UO_2 using microwave energy over short sintering times [94-96], in experimental work carried out by Jae *et al*. [96] on a comparison between microwave and conventional sintering of uranium oxide (UO_2) pellets, the variation of grain size and holding time with temperature shown in Figures 2.11 and 2.12, was obtained. The grain size of microwave-sintered pellets is found to be larger than that for the conventionally sintered pellets for the same sintering temperature and after the same holding time.

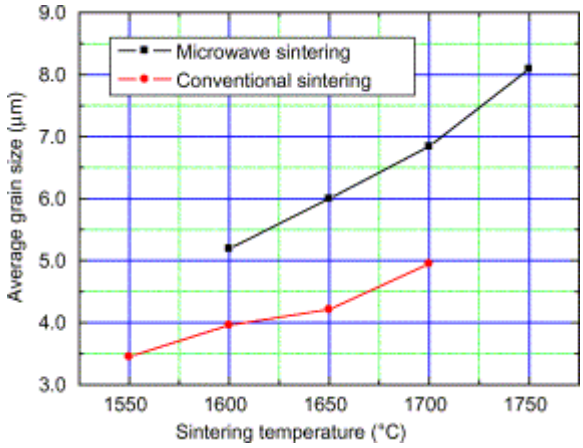

Figure 2.11: Grain size of sintered UO_2 pellets as a function of sintering temperature. Sintering time: 1 h [96]

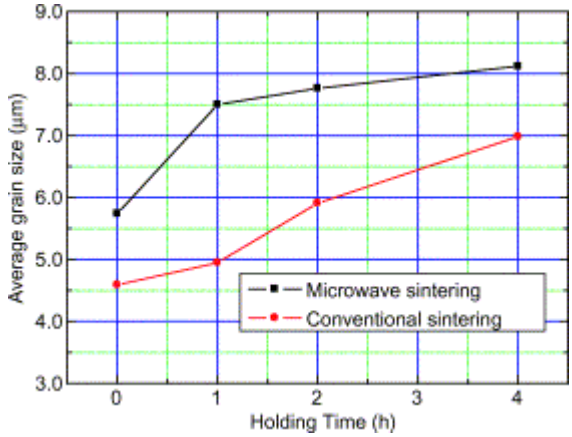

Figure 2.12: Grain size of sintered UO_2 pellets as a function of sintering time. Sintering temperature: 1700°C [96]

2.4 The Microwave Sintering of Composite Materials

Microwave processing has received some attention by workers in the field of composite materials. Studies of the effects of microwave sintering on densification, grain size and the morphological changes have been analysed [98-108]. Results from these studies show that improvements in densification, grain growth, strength and toughness can be achieved. Figure 2.13 shows the influence of sintering temperature on the bulk density of microwave and conventionally sintered Y-TZP/20wt.%Al_2O_3 composites, as reported by Travitzky *et al*. [99]. The microwave sintered composites attain a higher bulk density of about 97% theoretical density (T.D.) at 1200°C, while the conventionally fired materials attained only 95% T.D. at 1500°C. The average bulk density of the specimens, made by microwave sintering at 1500°C, was about 99% T.D. The authors have reported that at a given sintering temperature, microwave fabricated composites exhibited superior bending strength, fracture toughness and hardness (Vickers) when compared with conventionally sintered materials due to the better densification of the MW-sintered specimens.

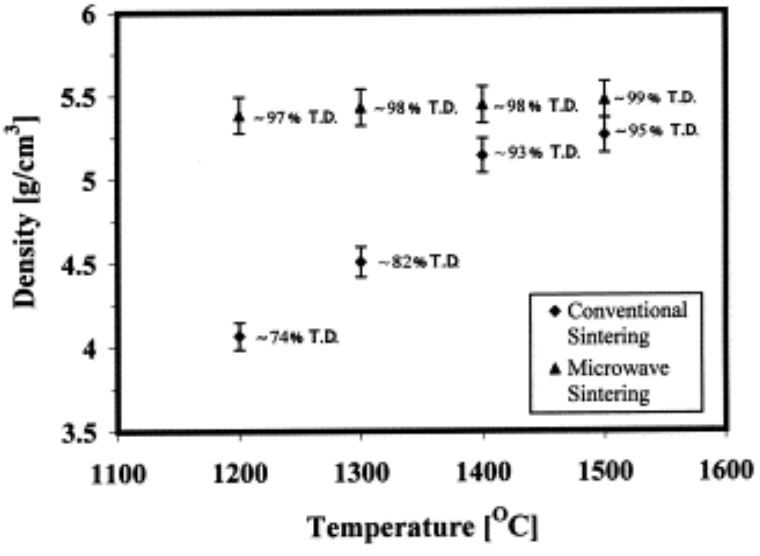

Figure 2.13: Influence of sintering temperature on the bulk density of microwave and conventionally fabricated Y-TZP/20 wt.% Al_2O_3 composites [99]

More recent findings from Tun and Gupta [108] on the fabrication of magnesium nanocomposites using magnesium as the matrix and nano-yttria as a reinforcement revealed a uniform distribution of Y_2O_3 particulates in the matrix and the presence of nanopores. Meanwhile, hardness, 0.2% yield strength, ultimate tensile strength, work of fracture and ductility increased with increasing amount of reinforcement from 0.5 to 2.0 wt%. Further studies by the authors on the effect of heating rate during hybrid microwave sintering on the tensile properties of Mg and Mg/Y_2O_3 revealed that average hardness and strengths of both samples were higher when they were sintered at higher heating rate. The ductility of pure Mg was reduced at a higher heating rate while it remained similar for Mg/Y_2O_3 [109].

Despite positive densification results obtained from researchers mentioned above, there is also some contrary evidence reported [110-111]. Li *et al*. [110] produced porous C_3S samples after microwave sintering at 1500°C, but the formation of C_3S was achieved at temperatures as low as 1350°C when using Al_2O_3 additions. The use of Fe_2O_3 as an additive was not as effective in promoting C_3S formation as expected. Its morphological observation by scanning electron microscopy is shown in Figure 2.14.

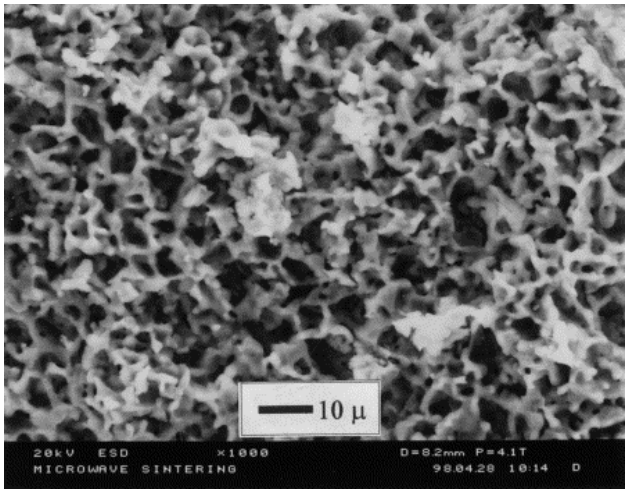

Figure 2.14: Microwave sintered sample at 1400°C. Al_2O_3 = 2.0% [110]

Meanwhile, Oh *et al*. [111] produced porous composites of Al_2O_3/ZrO_2 with improved mechanical properties by microwave sintering. The composite exhibited higher elastic modulus, fracture strength and improved mechanical properties than those prepared by conventional sintering. It is reasonable to suggest that a small particle size in the starting powders and low sintered densities, as shown in Table 2.3, contributed to the distribution of fine pores in the sintered specimens.

Table 2.3: Relative density of the conventional and microwave sintered composites [111]

Sintering temperature (°C)	Relative density (%)	
	Conventional sintering	Microwave sintering
1000	54.9	55.3
1100	55.3	57.0
1200	56.0	62.2
1300	58.6	not measured

Because of their unique combination of hardness, toughness and strength, hard metal composites, especially tungsten (WC) based composites are widely used for cutting tools and drilling operations worldwide. Conventional methods for sintering WC with cobalt (Co) as a binder phase, involves high temperatures and long sintering times. In a conventional sintering method, the carbide is subjected to high temperatures (up to 1500°C) for long periods in order to achieve a high degree of sintering. Such conditions, however, lead to undesirable WC grain growth in the presence of Co liquids [4]. Consequently, the hardness and other mechanical properties of the tool will be lower.

WC/Co samples sintered in a microwave field differ radically in terms of phases, chemistry, and microstructure when compared with conventionally sintered samples. Breval *et al*. [112] did a comparison study between microwave and conventionally sintered WC/Co composites. Microstructural investigations by TEM showed that in microwave sintered material the cobalt phase dissolved a little tungsten, whereas in conventionally sintered samples up to 20 wt% tungsten was dissolved.

It was also observed that smaller WC grains and a finer and more uniform distribution of cobalt binder were formed in microwave sintered samples as shown in Figure 2.15. This resulted in a harder material, which also exhibited better resistance towards both corrosion and erosion. The authors have reported that microwave sintered samples also have a three-dimensional uniform shrinkage, whereas conventionally sintered samples showed a greater vertical shrinkage. It is possible to microwave sinter WC/Co at a lower surface temperature and in much shorter times than is normally needed in a conventional furnace to obtain the same degree of densification.

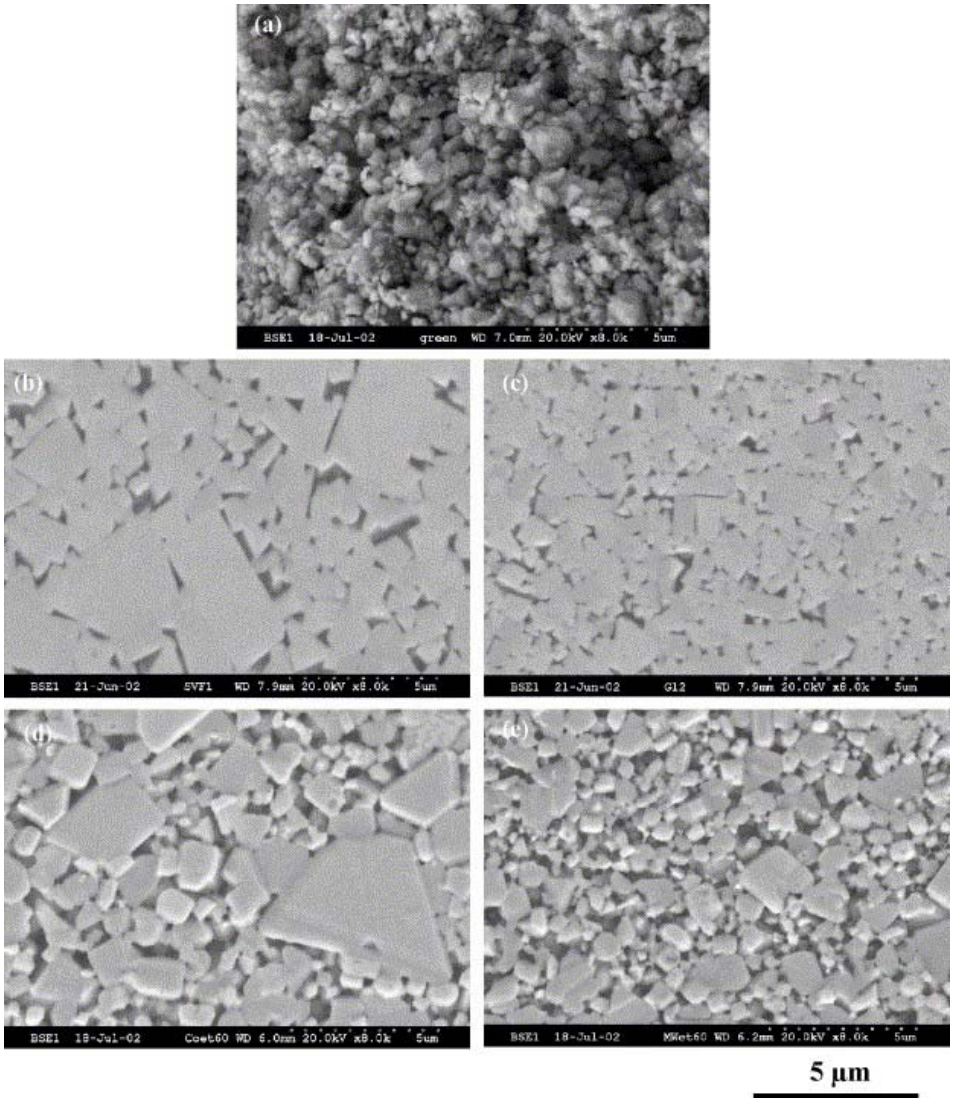

Figure 2.15: SEM images of WC/Co (Specimen E). (a) Fractured green sample, (b) the same material, conventionally sintered and polished, (c) the same material, microwave sintered and polished, (d) the same material, conventionally sintered, polished and etched H_2O_2/HNO_3, 12 min/60 °C, and (e) the same material, microwave sintered, polished and etched H_2O_2/HNO_3, 12 min/60 °C [112]

VaradaRajan *et al*. [113] have attempted to improve the performance of cemented tungsten carbide tools with a post treatment by subjecting them to microwave radiations. Results from this study showed that an irradiated tool performs better during machining of MMC's, suggesting that microwave radiation is a potential post sintering technique for cemented carbide tools to improve machining ability. Typically observed parametric influences on cutting force components are illustrated in Figure 2.16 (a) and (b).

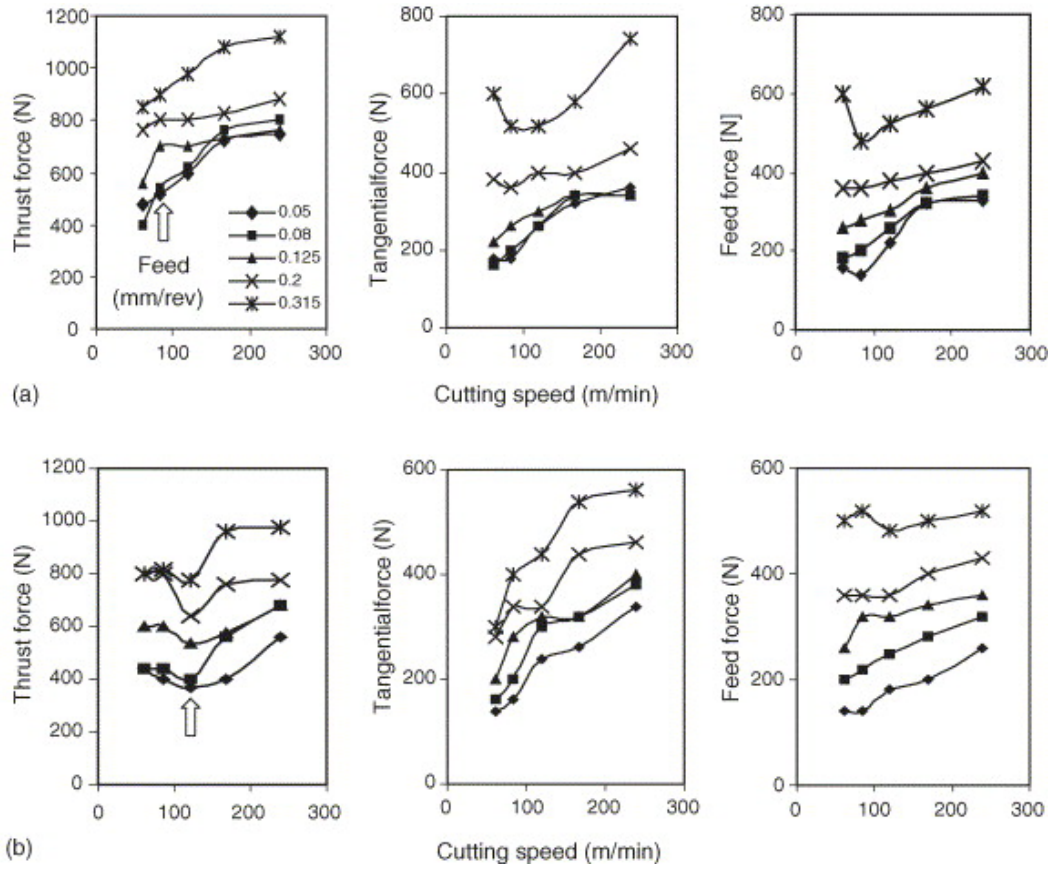

Figure 2.16: Typical variation of machining force components with cutting velocity: (a) untreated tool; (b) microwave irradiated tool (DOC = 0.5 mm) [113]

2.5 Microwave Sintering on Dental Applications

Microwave sintering has also penetrated into dental applications. Any successful implant should be biocompatible, strong and contain surface pores to promote osseointegration. A one-step microwave sintering procedure of titanium powders was attempted by Kutty, Bhaduri S., and Bhaduri S.B [114] in this work. The idea was to take advantage of the peculiar way microwaves couple with metallic powders, i.e. generating heat in the interior of the sample and dissipating it away through the surface. This non-conventional heating of titanium powder produced a dense core with surface porosity.

The authors have revealed that the dense core provides the strength while the surface pores promote bone growth. Microstructural characterization which was carried out by a Scanning Electron Microscope showed that the sintered titanium had gradient porosity on the surface with a thickness of about 100-200 μm depending on the microwave power. The pores were interconnected with size ranging from 30 to 100 μm. This kind of microstructure is favorable for cell growth. Tensile strength values as high as 400 MPa were obtained for these samples.

Other investigations by Pan and Ravaev [115], who were looking for better performance and improvements in dental materials, were concerned with increasing the adherence of ceramics and alloys in metal-ceramic structures. It has been found that microwave sintering of porcelain ceramics on Ni-Cr substrates leads to a two or threefold increase in adherence, compared with conventional sintering. A schematic diagram showing the experimental equipment used by the authors is shown in Figure 2.17.

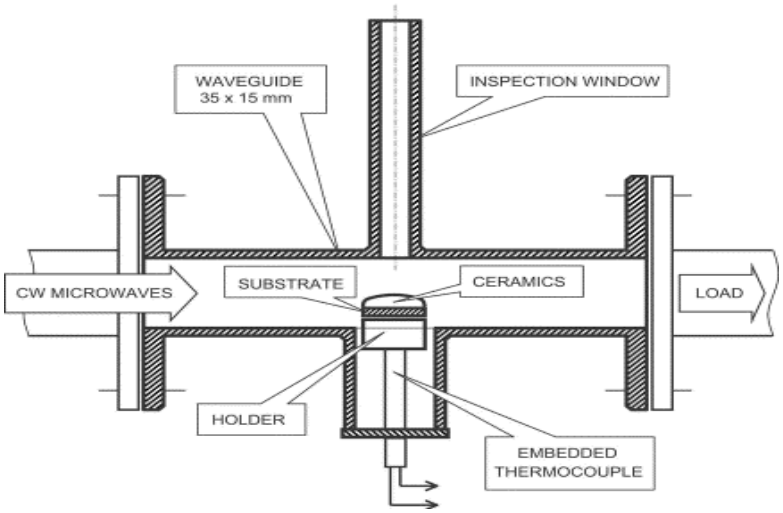

Figure 2.17: Simplified scheme of the experiment: waveguide microwave chamber and its components [115]

2.6 Economics of Microwave Processing

The economic benefits of microwave processing are difficult to define in a general way. The decision or need for microwave processing over other traditional methods for a particular application has to be based on an analysis of a specific process. There are several factors that can influence the usage of microwave processing over other traditional methods of production. They include the location of the processing facility, the product requirements, possible property improvements, alternative sources of energy, availability of capital, the balance between energy costs, labour costs, capital costs and the value added to the product [116]. Other factors besides energy savings account for selecting microwave processing over other conventional methods, like shorter processing times, smaller equipment and space, improvement in productivity and material properties. Moreover, hybrid microwave systems have resulted in providing more savings compared with either direct microwave or conventional systems on their own [116].

2.7 Summary

Powder metallurgy competes with other, more conventional metalworking methods in the fabrication of parts, such as casting, machining, and stamping. Characteristic advantages of powder metallurgy are close tolerances, low cost, net shaping, high production rates, and controlled properties. Other attractive features include compositional flexibility, low tooling costs, available shape complexity, and a relatively small number of steps in most powder metallurgy production operations. New developments in the area of material processing have led to the discovery of new useful materials with interesting properties. Furthermore, they have also advanced into the development of new improved technologies which are much faster, cheaper, better and greener.

Significant developments and advances have taken place in the field of microwave processing of ceramics over the last decade. In the case of composites, particularly tungsten/cobalt composites, the cycle time using microwave processing can be reduced to about one tenth of that needed for conventional processing. The microwave coupling causes extremely rapid reaction kinetics and new reaction paths leading to materials processing at much lower temperatures than normally obtained by conventional heating. The most significant development in microwave processing is in the sintering of powdered metals and transparent ceramics in a single step process. Microwave processing has succeeded in producing materials with rapid densification, enhanced mechanical properties and improved microstructures. There exists a great future for microwave technology for the commercialization of metallic materials.

From literature review, it is quite clear that beneficial results in terms of improved density, hardness, strengths, finer grain size and uniform microstructures have been obtained from microwave sintering. However, the authors have not mentioned whether or not there exists any microwave or ‘athermal’ effect. All the authors on the other hand did clearly state or indicate that the results obtained from microwave sintering are due to the rapid heating effect or simply thermal in nature. There still exists a debate as to whether there are any athermal effects during microwave sintering.

CHAPTER 3

EXPERIMENTAL PROCEDURE

3.1 Preparation of sample

3.1.1 Mixing

1. There were three sets of experiments prepared for the following compositions:

- 97wt% Sn, 2wt% Cu and 1wt% Sb,
- 94wt% Sn, 4wt% Cu and 2wt% Sb,
- 91wt% Sn, 6wt% Cu and 3wt% Sb.

2. Tin powder with 99.5% purity (-100 mesh), copper powder with 99% purity (<75 μm) and antimony powder with 99.5% purity (-100 mesh) were used (supplied from Sigma Aldrich).

3. These powders were first weighed accordingly and placed into their respective containers which were then evacuated in a glove box to remove oxygen to less than 100 ppm and then mixed using a roller mixer (ABB ABS 100) shown in Figure 3.1; for about 12 hours at a frequency of 40 Hz.

Figure 3.1: Roller mixer (ABB ABS 100) used for mixing the tin alloy powder

4. Each set of experiments had sixteen different conditions (see Table 3.1).

5. Sixteen samples from 80 g of powder were prepared from the same die to produce samples with a cross section of 10.1 mm in width and 30.8 mm in length with the height of 42 mm on average. This was the largest obtainable size from the selected die from which tensile specimens from both the transverse and longitudinal directions were obtained.

3.1.2 Compaction

1. Using the percentage of powder and its respective weights, a total of 48 samples for the 3 sets of experiments were prepared from the die shown in Figure 3.2.

Figure 3.2: Die used to prepare the tin alloy compacts

2. Two different pressing pressures were applied to prepare samples for this study. Samples were compacted at 96 MPa and at 129 MPa using the 10 ton Hydraulic Floor Press Machine (D2003K) with a holding time of 5 minutes (see Figure 3.3).

3. Between these limits, samples were defect-free and had sufficient green strength for handling.

Figure 3.3: The 10 ton Hydraulic Floor Press Machine (D2003K) used for compacting the tin alloy powder

4. Below 96 MPa, it was difficult to reproduce the load on the press, resulting in variations in green density. Furthermore, the samples broke and cracked upon removal due to insufficient green strength. On the other hand, it was difficult and almost impossible to produce samples above 129 MPa, either as the pressure applied was almost at a maximum for the equipment, making samples hard to press.

3.2 Sintering

1. Out of the 16 samples prepared from the die, 8 samples were sintered using the vacuum furnace and the other 8 sintered using the microwave furnace for each set of experiment.

2. Following the experimental conditions as stated in Table 3.1, the samples were sintered at two different temperatures (160°C and 220°C) for different durations.

Table 3.1: The experimental conditions for each experiment

Sample No:	Sample Name	Sintering	Compaction Pressure	Sintering Temperature	Sintering Time
1	CS1	conventional	96 MPa	160°C	60 min
2	CS2	conventional	96 MPa	160°C	120 min
3	CS3	conventional	96 MPa	220°C	60 min
4	CS4	conventional	96 MPa	220°C	120 min
5	CS5	conventional	129 MPa	160°C	60 min
6	CS6	conventional	129 MPa	160°C	120 min
7	CS7	conventional	129 MPa	220°C	60 min
8	CS8	conventional	129 MPa	220°C	120 min
9	MW1	microwave	96 MPa	160°C	15 min
10	MW2	microwave	96 MPa	160°C	30 min
11	MW3	microwave	96 MPa	220°C	15 min
12	MW4	microwave	96 MPa	220°C	30min
13	MW5	microwave	129 MPa	160°C	15 min
14	MW6	microwave	129 MPa	160°C	30 min
15	MW7	microwave	129 MPa	220°C	15 min
16	MW8	microwave	129 MPa	220°C	30min

3.2.1 Conventional Sintering

1. A conventional furnace with a cavity size of 5cm x 110cm under vacuum conditions was used as shown in Figure 3.4 below.

2. Temperatures of 160ºC and 220ºC as listed in Table 3.1 were used for sintering the tin-copper-antimony samples.

3. The heating rate for the conventional sintering was maintained at 6ºC/min in order to avoid thermal shock to the equipment.

4. It was ensured that the vacuum pressure reached 10^{-6} MPa before sintering.

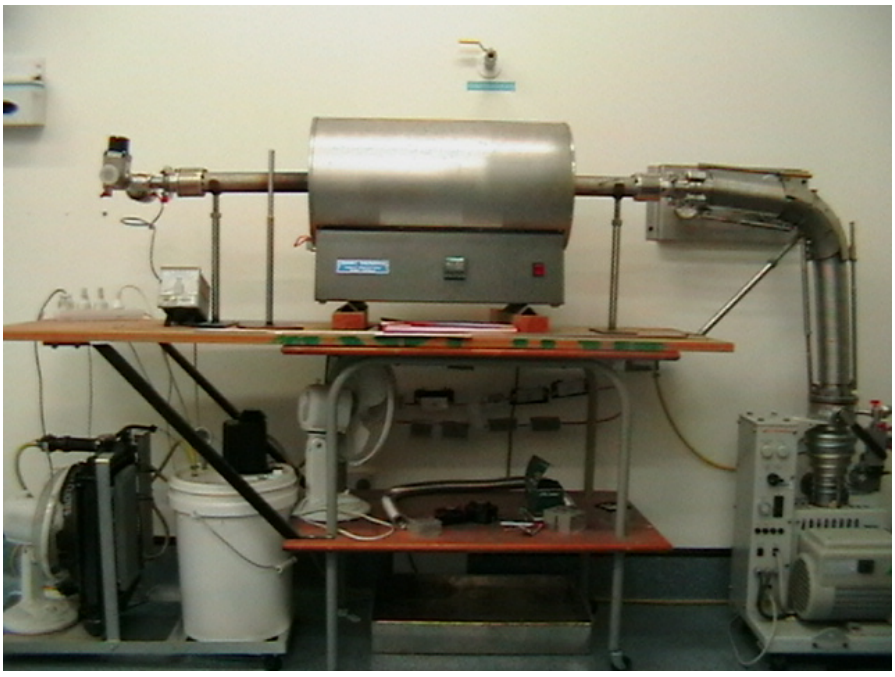

Figure 3.4: The conventional vacuum furnace used for conventional sintering

3.2.2 Microwave Sintering

1. A Panasonic Thermwave Mod.111 multimode microwave system (1.3kW, 2.45GHz, 47cm x 61cm x 64 cm) with a water cooling system, designed for the high temperature processing of materials in a laboratory or small-scale industrial manufacturing, was used for this study (see Figure 3.5).

Figure 3.5: Panasonic Thermwave Mod.111 multimode microwave system used for hybrid microwave sintering

2. The green compacts were placed in a cylindrical thermal box / thermal pod made from ceramic fibre (see Figure 3.6).

3. The sample was sintered with a few (14 pieces) graphite pellets (in the range of 1 to 1.5 cm in length) placed around the sample at the base of the thermal pod which were used as susceptors to ensure a controlled two-directional sintering process took place and that excessive heat and energy did not build up in the system. This helped to give a better control of temperature since low sintering temperatures were used (see Figure 3.7). The number of graphite pellets used was always kept consistent for each experimental run.

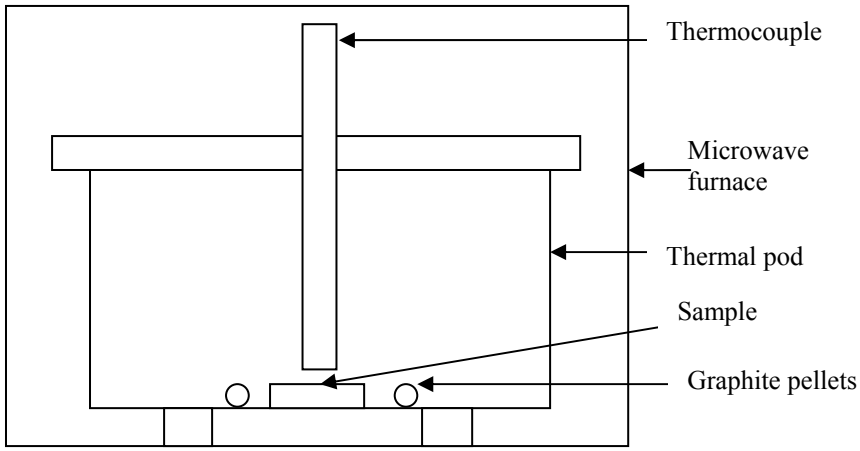

Figure 3.6: Schematic diagram of sample in the multimode microwave system used for hybrid microwave sintering

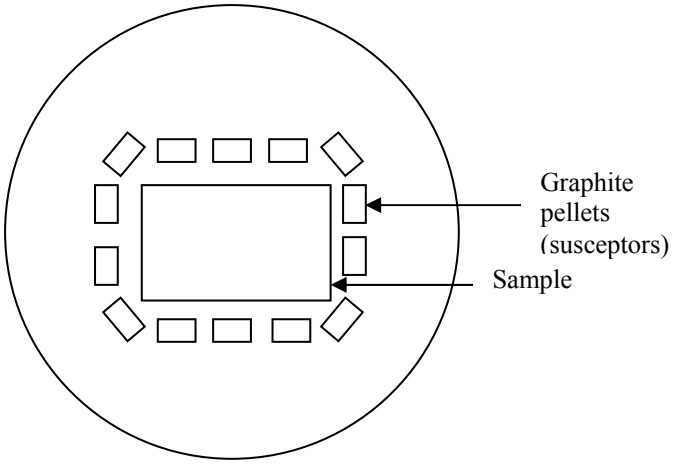

Figure 3.7: Schematic diagram of the susceptors used around the sample in the multimode microwave system (top view)

Susceptors have the capability of absorbing microwave energy, since they comprise a particulate substrate which is substantially non-reflective of microwave energy. Susceptors are typically particles having a thin-film coating. The matrix typically comprises of ceramic materials that are stable at high temperatures. The composition allows reuse of the susceptors, eliminates a decline in heating rate, eliminates arcing, allows the heating rate to be controlled, and also allows overheating to be controlled when operating at high temperatures. Figure 3.8 shows the effects on the heating rate in the microwave furnace with and without susceptors.

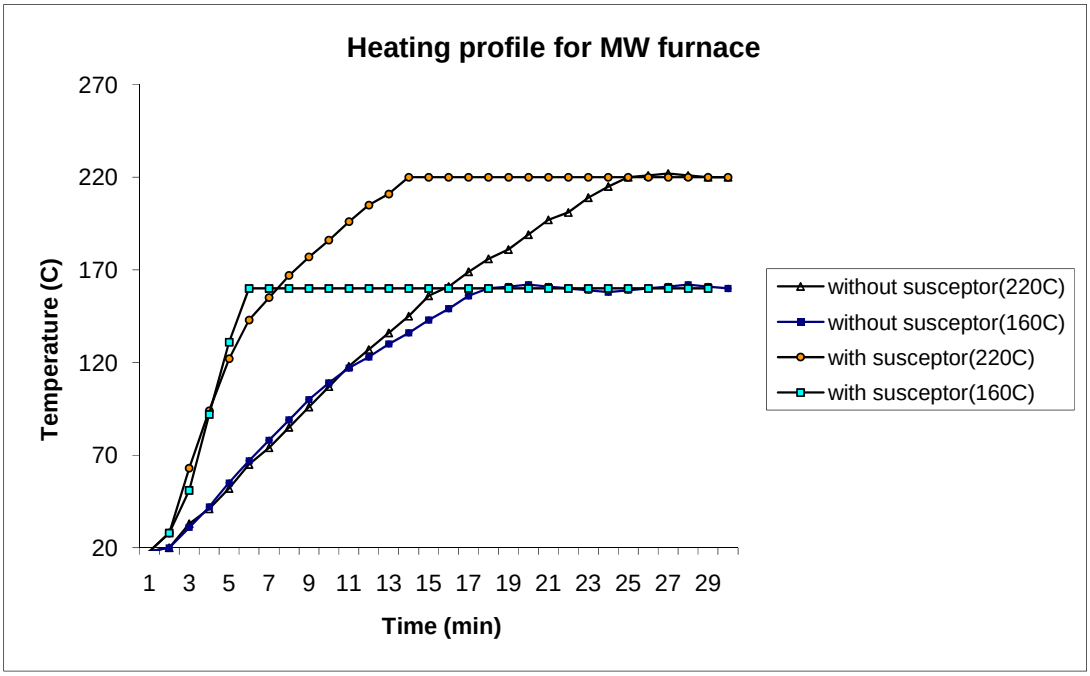

Figure 3.8: The effect of susceptors in the heating behaviour in microwaves

4. The crucible was filled with argon gas (due to the fact that the microwave system could not be operated under vacuum conditions) before the sintering process with a flow rate of 50mL /min and was maintained at this flow rate throughout the sintering process. This hybrid microwave sintering had an average heating rate of 15°C/min.

5. The power dial at the controller was adjusted manually from an output energy level of 50% and the microwave unit was set to 70% input power level to allow high and uniform heating rates since a low temperature application was used.

6. The temperature of the sample in the crucible was measured using a Type K thermocouple shown in Figure 3.9. Once the targeted temperature was achieved, the output power level on the microwave unit was reduced to 30% in order to maintain the sintering temperature and the sintering time was set.

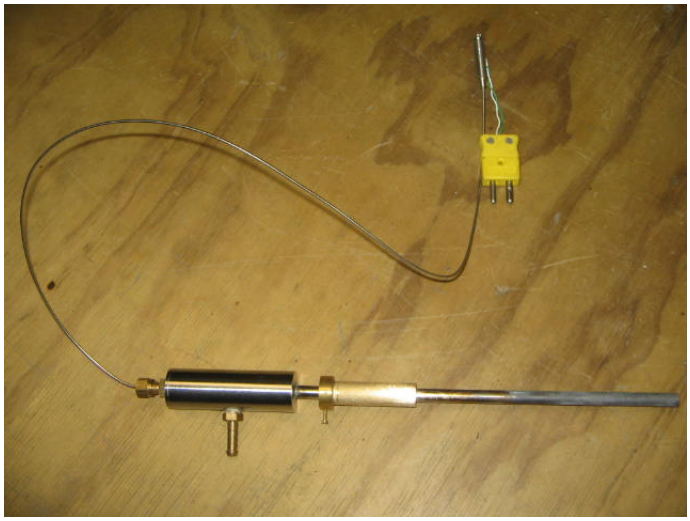

Figure 3.9: Type K thermocouple used for measuring temperature of the sample during microwave sintering

This is a crucial step in the microwave sintering process as failing to do so would result in instability of the desired temperature leading to a temperature overshoot. The following diagram in Figure 3.10 shows the heating profiles for both microwave and conventional furnace.

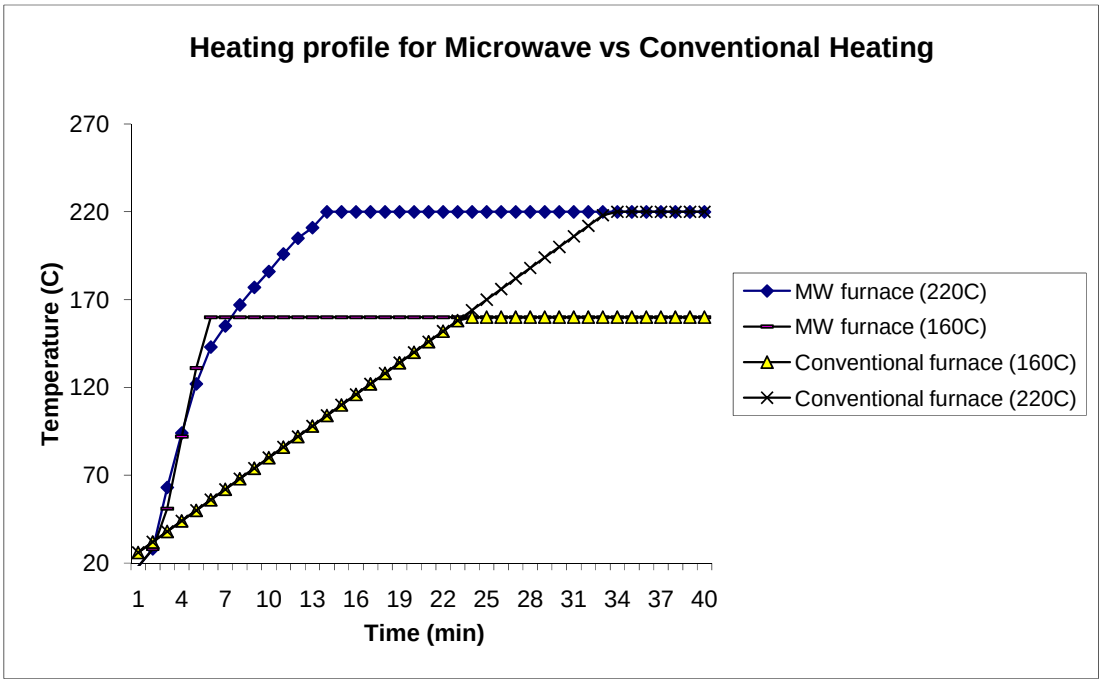

Figure 3.10: The heating profiles obtained from the microwave furnace and conventional vacuum furnace

3.3 Grinding and Polishing of Samples

1. During grinding, new sheets of abrasive papers and excessive pressure was avoided, to prevent pick-up of loose silicon carbide particles which can be easily embedded in relatively soft tin alloys.

2. Grinding with worn abrasive papers with grits of 2000 and 4000 was carried out using the rotary polishing and grinding machine (Struers RotoPol – 21). Coarser papers of 500 and 1000 grit were avoided since they caused too many deep scratches and enabled penetration of SiC particles into the tin alloy.

3. Scratches from the final abrasive papers were removed by polishing for several minutes on a wheel covered with nap cloth impregnated with 0.3 μm agglomerated alpha alumina suspension.

4. Care was taken to make sure that the polishing wheels were free from dust and grit from the previous polishing step.

5. A 2% nital solution, consisting of 2% by volume nitric acid in ethanol, was used for etching. A good etch was achieved after 1 to 2 minutes immersion.

3.4 Measurement of density

3.4.1 Green Compact

1. Accurate density measurements are an important part of characterizing the physical properties of samples. In this experiment, the density of as-pressed pellets was calculated from the sample mass and volume.

2. Mass was measured using a digital balance and sample volume was calculated from the external dimensions of the samples, which were rectangular in shape.

3.4.2 Sintered Samples

1. A liquid displacement method, based on Archimedes' principle, was used to determine the density of the sintered samples. Experiments were carried out at room temperature using distilled water.

   Archimedes' principle states that an object immersed in a liquid will be supported by a pressure equal to the weight of the liquid displaced by the object. Buoyancy acts against the force of gravity and so makes objects seem lighter with respect to gravity. To represent this effect, which is important for sedimentation, it is common to define a buoyant mass, m_b that represents the effective mass of the object with respect to gravity

$$m_b = m_{\text{object}} \cdot \left(1 - \frac{\rho_{\text{fluid}}}{\rho_{\text{object}}}\right) \tag{3.1}$$

   where m_{object} is the true (vacuum) mass of the object, whereas ρ_{object} and ρ_{fluid} are the average densities of the object and the surrounding fluid, respectively. The weight of the displaced fluid is directly proportional to the volume of the displaced fluid (specifically if the surrounding fluid is of uniform density).

2. The sintered sample was weighed in air first and then in water. The density of the immersed object relative to the density of the fluid is easily calculated without measuring any volumes:

$$Relative\ density = \frac{Weight}{Weight - Apparent\ immersed\ weight} \tag{3.2}$$

3. To take into account the influence of the variation in the initial as-pressed density, the compact sinterability was also determined through a densification parameter, which is expressed as:

$$Densification \quad parameter = \frac{sintered\ density - green\ density}{theoretical\ density - green\ density} \tag{3.3}$$

where a negative densification parameter implies compact swelling.

3.5 Measurement of Porosity

1. The volume of open and closed pores can also be calculated using Archimedes' measurements [117]. The volume of open pores, V_o, is given by:

$$V_o = \frac{w_{sat} - w_{dry}}{density_{liq}} \tag{3.4}$$

Where w_{sat} = saturated weight

w_{dry} = weight of dry sample

2. The volume of closed pores can be calculated only if the theoretical density, TD, of the material is known.

3. The dry weight divided by the theoretical density gives the true volume, V_t. True volume is the volume of solid in the pellet. The volume of closed pores, V_{cp}, is then:

$$V_{cp} = V_b - V_o - V_t \tag{3.5}$$

Where: Bulk volume (V_b) = (w_{sat} - w_{susp})/$\rho_{liq.}$

w_{susp} = weight of suspended sample

$\rho_{liq.}$ = density of liquid used

3.6 Microhardness Testing

1. In this work, a LECO Microhardness Tester (LM 700) was used where the diamond indenter is forced into the surface of the material using a calibrated machine with a test load of 25–100 gf to give a micro-indentation.

2. When micro-hardness testing was performed, care was taken to avoid porosity, as the micro-indenter will make a larger impression and record a lower hardness in porous material, compared with fully dense material of the same composition. This is because the pores offer no resistance to deformation.

3. A highly polished, pointed, square-based pyramidal diamond indenter with face angles of 136º between opposite faces was forced into the material under a load F.

4. The micro-indentation left in the surface of the material after removal of the load was measured using the diagonals d_1 and d_2 by means of microscope. Their arithmetic mean d automatically calculated and the micro Vickers hardness value computed.

5. A 25 gf load with a dwell time of 15 seconds was used each time.

6. Five different microhardness readings were taken from five different locations on the sample and the average result was taken for each sample.

3.7 Tensile Testing

1. Tensile testing was used to determine the yield and tensile strength of samples. A tensile testing machine (INSTRON 4204) with a 5 kN load cell and crosshead speed of 1 mm/min was used for testing.

2. The test pieces were cut directly from the sintered material using a metal cutter and then filed manually to its tensile profile. The typical tensile specimen prepared is shown in Figure 3.11. It has enlarged ends or shoulders of 5 mm for gripping.

3. An important part of the specimen is the gauge section. The cross-sectional area of the gauge section (2 mm x 4 mm) is reduced relative to that of the remainder of the specimen so that deformation and failure will be localized in this region.

4. The gauge length (15 mm) is the region over which measurements are made and is centred within the reduced section. The gauge lengths are marked and measured before and after the tensile test in order to obtain percentage of strain to fracture.

5. The distances between the ends of the gauge section and the shoulders should be great enough so that the larger ends do not constrain deformation within the gauge section, and the gauge length should be great relative to its diameter. Otherwise, the stress state will be more complex than simple tension.

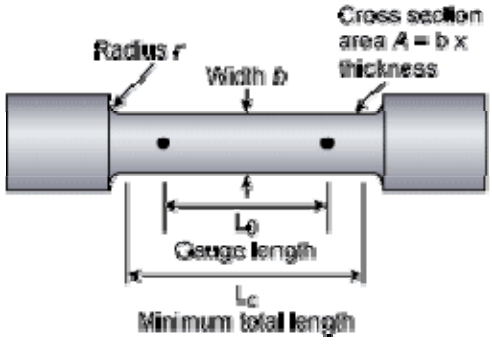

Figure 3.11: Standard shape for the tensile test specimens used [118]

3.8 Characterization of Sample

3.8.1 Scanning Electron Microscopy (SEM)

1. A scanning electron microscope creates high resolution, two dimensional images of a sample's surface. The cross-sections of the polished and etched solid samples which are already conductive were bombarded with a focused beam of electrons which liberates secondary electrons from the sample's surface.

2. A detector in the microscope systematically "counts" these electrons, recording data on their origin and emission intensity which can then be assembled into a high contrast, high resolution image. An SEM S-4700 Hitachi Scanning Electron Microscope, with SIS Ultrascan 2 image acquisition software, was used to generate high quality digital images.

3.8.2 Optical Microscope

1. Grain size was measured using the Lineal Intercept Technique, where lines are drawn in the photomicrograph obtained from an optical microscope (Olympus BX 60), and the number of grain-boundary intercepts, N_l, along a line is counted.

2. The mean lineal intercept is then given as:

$$\bar{l} = \frac{L}{N_l M} \tag{3.6}$$

where L is the length of the line and M is the magnification in the photomicrograph of the material.

3. The most correct way to express the grain size (D) from lineal intercept measurements is:

$$D = \frac{3}{2}\bar{l} \tag{3.7}$$

3.9 Electron Dispersive X-Ray Spectrometer (EDS)

1. The SEM used in this work also features a Kevex electron dispersive x-ray spectrometer (EDS) which can be used to ascertain the elemental composition of the portion of a sample being visualized.

2. When a sample is struck by the SEM's electron beam it emits x-rays which are picked up by the EDS.

3. Because each element emits x-rays of characteristic energies and wavelengths, the EDS unit is able to determine which element is responsible for the emission.

4. These data can be overlaid onto an SEM image to produce a virtual elemental map of a sample's surface.

3.10 X-Ray Diffraction (XRD)

1. X-ray diffraction (XRD) was used to characterize the composition of sintered samples and also to determine the phase constitution of samples after sintering (using CuK_{α} radiation).

2. The peaks also were used to verify the diffusion process occurring during sintering.

3. Gonio scan axis with a step scan of 0.02° and 1.5 second time per step for the scan range from 20°-100° was employed using a Philips X'PERT System.

CHAPTER 4
RESULTS AND DISCUSSION

4.1 Introduction

This chapter aims to identify the optimum processing parameters for sintering tin alloys with varying compositions (97Sn2Cu1Sb, 94Sn4Cu2Sb and 91Sn6Cu3Sb). The variables investigated were sintering temperatures (160°C and 220°C), sintering time (15, 30, 60 and 120 minutes), compaction pressures (96 MPa and 129 MPa) and sintering methods (microwave and conventional sintering). The effect of each variable was assessed by mechanical and structural analysis. Mechanical analysis comprised density measurements, microhardness testing and tensile testing.

Structural analysis was carried out using Scanning Electron Microscopy (SEM) and optical microscopy for structural characterisation and grain size measurement, Electron Dispersive X-Ray Spectroscopy (EDS), X-Ray mapping and X-Ray Diffraction (XRD) were used for elemental dispersion after sintering and phase identification. Such results are used to justify the possibility of using a powder metallurgy method, such as microwave sintering instead of conventional sintering, as an alternative to a casting process.

4.2 Results

4.2.1 Mechanical Analysis

Mechanical testing (tensile testing and hardness testing) was used to determine whether the mechanical properties of microwave sintered tin alloys (pewter) falls within the specified range for cast pewter. The most influential parameters would include sintering time, sintering temperature and compaction load for both sintering methods.

Density

Of interest in this work is the relationship between the powder compact pressing force, the resulting green density and subsequent sintered density and their effect on mechanical properties. The green compacts pressed at 96 MPa produced an average green density (relative to theoretical density) of 80.66% to 80.76% while those pressed at 129 MPa produced an average green density of 84.49% to 84.67% for all the three compositions; 97Sn2Cu1Sb, 94Sn4Cu2Sb and 91Sn6Cu3Sb (see Tables A1 –A6 in the appendix).

Conventional Sintering

Figure 4.1 (a) – (d) shows the densification behaviour for all the three compositions for varying sintering times and temperatures by conventional vacuum sintering (see Tables A7-A12 in the appendix). There are significant increases in density for all three compositions when the sintering time and temperature are increased. By increasing the sintering time from 60 to 120 minutes at 160°C, the bulk density for the composition of 97Sn2Cu1Sb had reached 86.64% and 88.10% for the 96 MPa and 129 MPa compaction pressures respectively. While increasing the temperature from 160°C to 220°C for the same composition, the samples compacted at 96 MPa produced bulk density of 94.65% while those compacted at 129 MPa produced samples with 98.28% bulk density.

The composition of 94Sn4Cu2Sb showed a more significant increase in the density values upon sintering. At 160°C, doubling the sintering time from 60 to 120 minutes has produced samples with bulk densities of 90.38% and 91.17% for the lower and the higher compaction loads respectively. Meanwhile, the bulk densities have increased to 95.05% and 98.46% when the sintering temperature was increased from 160°C to 220°C for both compaction loads.

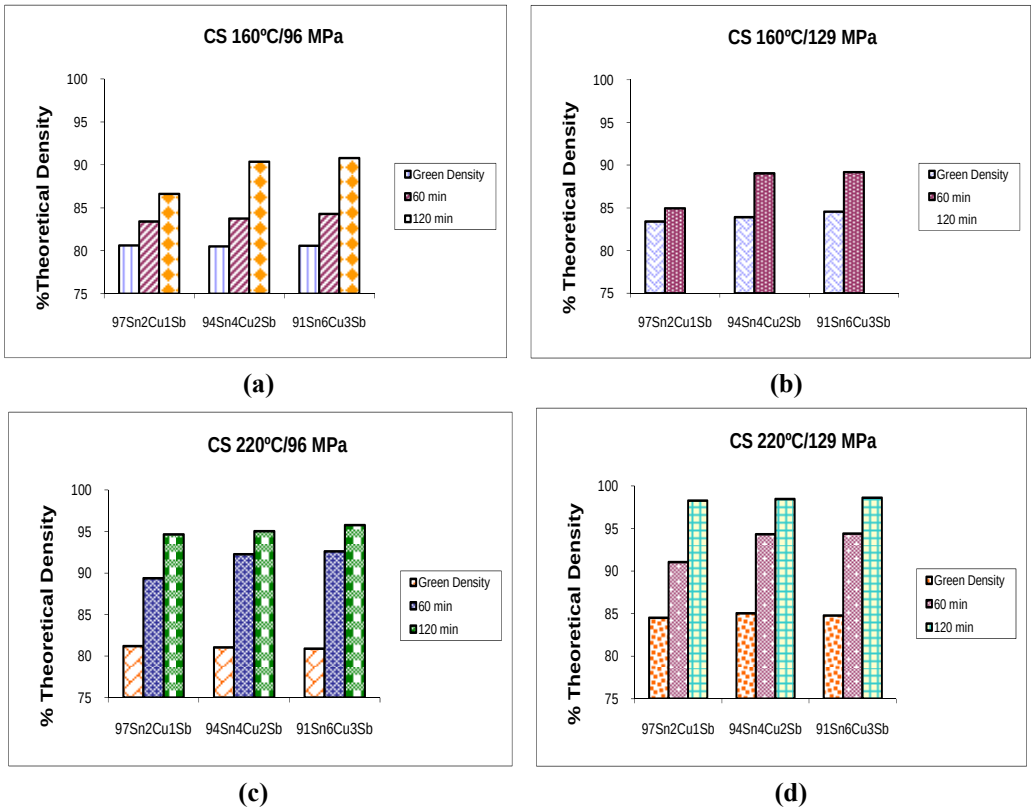

Figure 4.1: Bar charts of density measurements for the conventionally sintered samples for 97Sn2Cu1Sb, 94Sn4Cu2Sb and 91Sn6Cu3Sb compositions

Similarly, the 91Sn6Cu3Sb composition has also shown comparable results with respect to change in bulk density. The samples compacted at 96 MPa and 129 MPa achieved densities with 90.8% and 91.27% of theoretical density respectively when sintered at 160°C for 120 minutes. By increasing the sintering temperature to 220°C, higher densities were reached using both compaction loads after sintering for 120 minutes. The former (96 MPa) increased by 15.4% and the latter (129 MPa) by 13.7%.

Microwave Sintering

Figure 4.2 (a) – (d) shows the densification behaviour for all the three compositions produced by microwave sintering. The sample for the 97Sn2Cu1Sb composition showed a large increase in bulk density, reaching 92.98% and 95.95% of theoretical density for the 96 MPa and 129 MPa compaction pressures respectively when sintered at 160°C. This is higher than the conventionally sintered powder. Doubling the sintering time from 15 minutes to 30 minutes

increased the density by only a small percentage. The lower compaction load increased by 1% and the higher compaction load increased by 2%. Microwave sintering may have showed a low percentage increase but it produced a much higher density at 15 minutes compared with conventional sintering at 60 minutes.

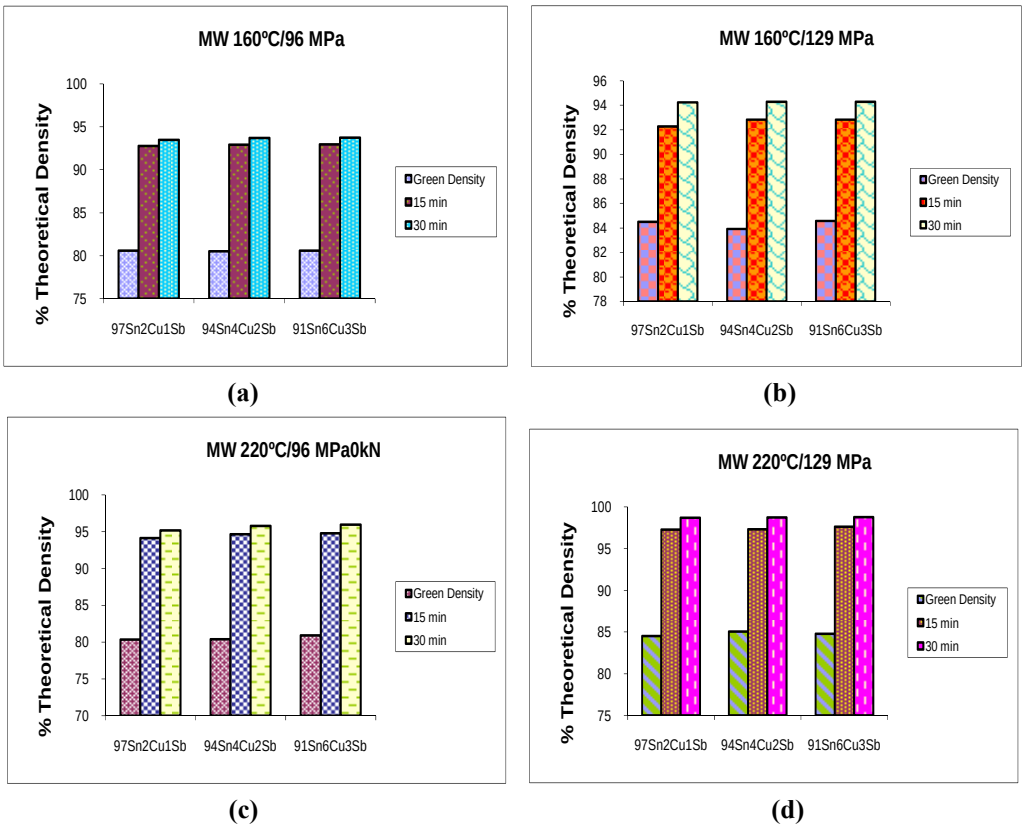

Figure 4.2: Bar charts for the microwave sintered samples for 97Sn2Cu1Sb, 94Sn4Cu2Sb and 91Sn6Cu3Sb compositions

Meanwhile, 94Sn4Cu2Sb and 91Sn6Cu3Sb compositions have produced slightly higher density values after sintering under the same conditions. The former reached sintered densities of 95.78% and 98.75% for the 96 MPa and 129 MPa compaction pressures respectively when sintered for only 30 minutes at 220°C. Similarly, the latter reached 95.95% and 98.79% under the same sintering conditions. Furthermore, Tables A7 – A12, from the appendix, show positive densification values for the sintered compacts which are a clear indication that there was no compact swelling occurring for both the conventional vacuum sintering and the microwave sintering method.

Conventional vs. Microwave Sintering

Both microwave sintering and conventional sintering produced significantly higher density samples by increasing the sintering temperature from 160ºC to 220ºC and also by doubling the sintering time. For conventional sintering, the densification occurs gradually with time. However, for microwave sintering, the densification is quite rapid and sudden. Figure 4.3 shows the densification of microwave sintered and conventionally vacuum sintered powder for the three different compositions. It can be seen that the density values for the microwave sintering have increased marginally by increasing the copper and antimony content since no statistical difference in density was noticed. Meanwhile, the densities for the conventionally sintered samples have increased slightly more than the microwave sintered samples which is evident from the slope of the graph itself.

Microwave sintering produced samples with higher densities (98.7%TD) than conventionally sintered samples (98.28%TD) and traditionally cast pewter from Royal Selangor (98.4%TD) after shorter times (30 minutes). Tables A13-A15 (refer to appendix) also indicate that the percentage of porosity existing in the samples decreases with increasing sintering time and temperature. Moreover, the degree of porosity has decreased significantly with increased Cu and Sb content and this has further enhanced densification.

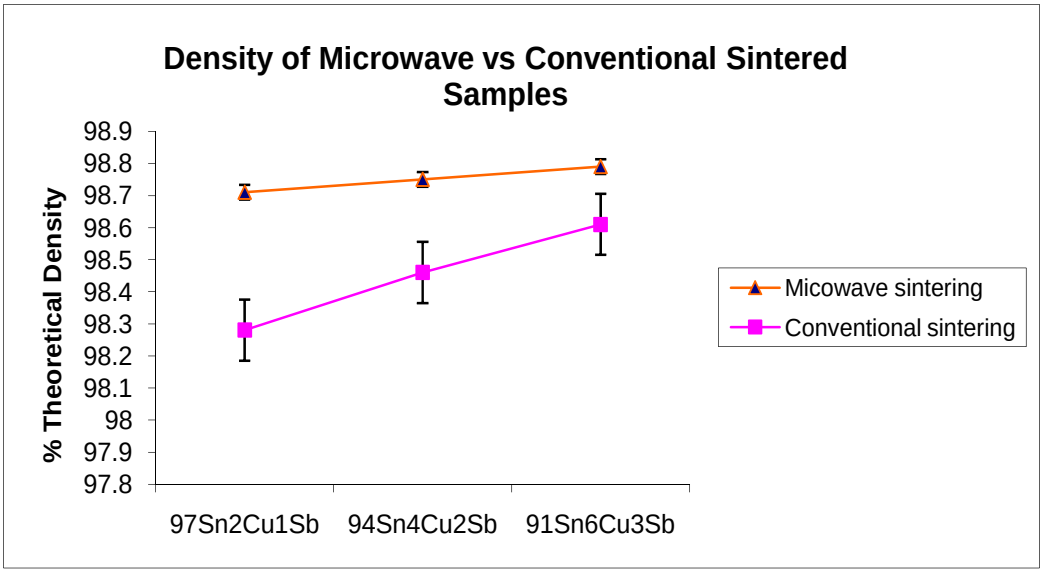

Figure 4.3: Graph of density measurements for microwave (30 min) and conventional (120 min) sintering for 97Sn2Cu1Sb, 94Sn4Cu2Sb and 91Sn6Cu3Sb compositions pressed at 129 MPa and sintered at 220°C

Microhardness

Microhardness testing is useful for measuring the surface hardness of the tin alloy samples or for measuring the hardness of different microstructures by making a series of indentations to describe a profile of the change in hardness. It is another method of characterizing mechanical properties within the sintered pewter alloys.

Conventional Sintering

Figure 4.4 (a) – (d) displays the microhardness values for all three compositions which have been conventionally sintered. Hardness values in the material increase with an increase in sintering time, sintering temperature and compaction load. Higher compaction loads generally result in higher hardness values and higher densities. The conventionally sintered powder increased by about 48% in hardness, from 12.9 HV to 19.1 HV under varying conditions of cold compaction load, sintering temperature and composition. The 94Sn4Cu2Sb and 91Sn6Cu3Sb compositions showed an increase in hardness of 45% from 13.8 HV to 20 HV and 44% from 16.8 HV to 24.2 HV respectively. In general, increasing the Cu and Sb content of the alloy increases the hardness of the material as expected.

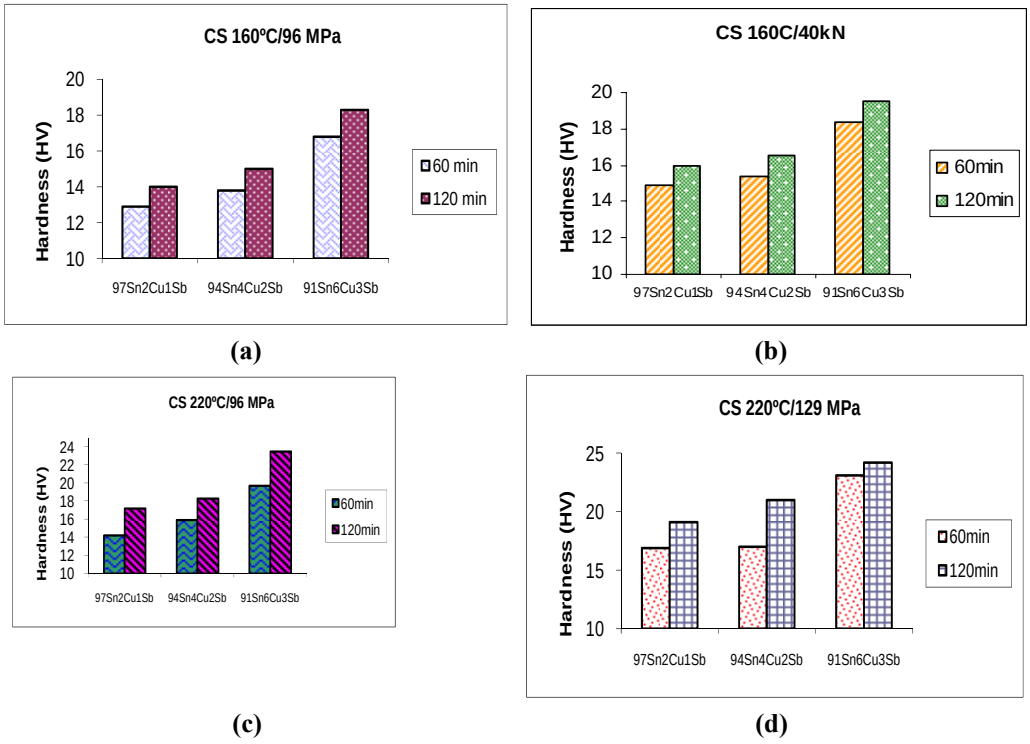

Figure 4.4: Bar charts of microhardness for the conventionally sintered samples for 97Sn2Cu1Sb, 94Sn4Cu2Sb and 91Sn6Cu3Sb compositions

Microwave Sintering

Figure 4.5 (a) – (d) shows the microhardness values of microwave sintered samples for all three compositions. Microwave sintering gave an increase in hardness of 38%, 42% and 46% for the compositions of 97Sn2Cu1Sb, 94Sn4Cu2Sb and 91Sn6Cu3Sb respectively under varying conditions of cold compaction load, sintering temperature and composition. Hardness values have increased with increasing sintering time, temperature and compaction load. A higher percentage increase in hardness is found with the increasing Cu and Sb content. In comparison to conventional sintering, microwave sintered materials lead to improved hardness in shorter sintering times. The hardness level achieved after conventional sintering for 120 minutes, is slightly improved on by microwave sintering for 30 minutes.

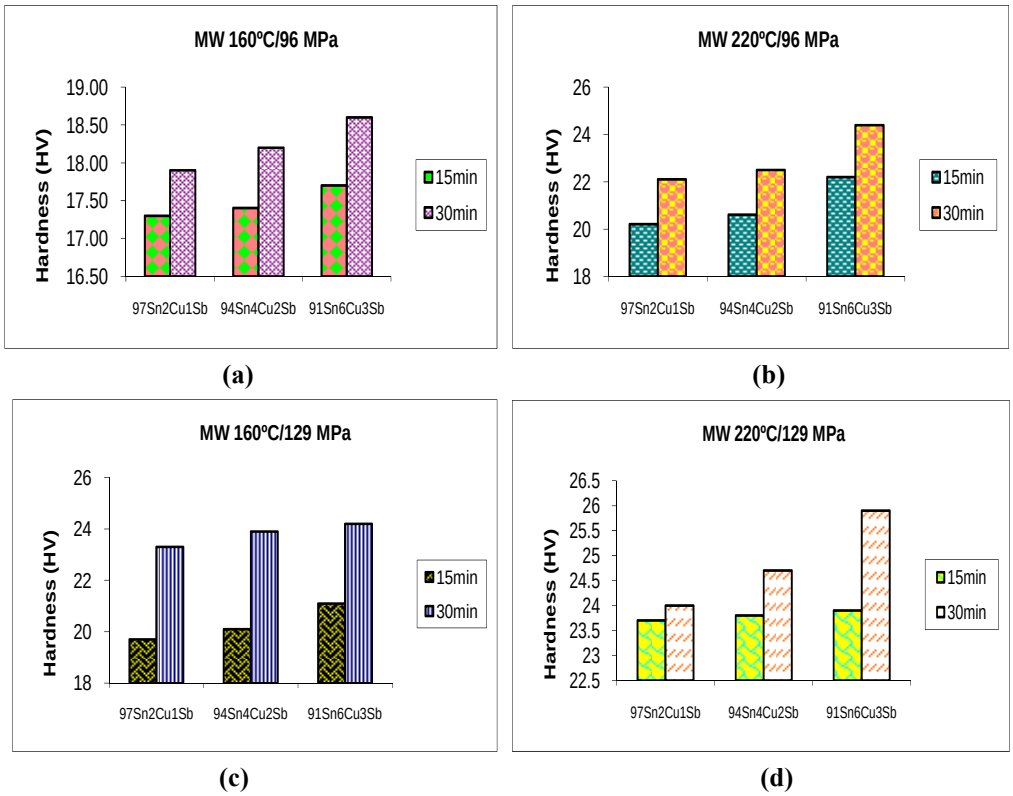

Figure 4.5: Bar charts of microhardness for the microwave sintered samples for 97Sn2Cu1Sb, 94Sn4Cu2Sb and 91Sn6Cu3Sb compositions

Conventional vs. Microwave Sintering

Figure 4.6 clearly shows that microwave sintering produces samples with higher hardness values compared to conventional sintering. Higher green strengths, longer sintering times and higher sintering temperatures result in samples with higher densities and hardness values for both conventional and microwave sintering. The hardness value for microwave sintering was generally about 7 to 25% higher than that for conventional sintering for all three compositions.

By doubling and tripling the amount of Cu and Sb in the alloy, the hardness values increased by 4.7% and 26.7% respectively when conventionally sintered. However when microwave sintered, the hardness of the samples increased by 2.9% and 7.9% respectively. This is attributed to solid solution strengthening from the Cu and Sb additions. The higher the percentage of Cu and Sb added results in higher hardness values. In conclusion, microwave sintering produces pewter samples with higher hardness (24-25.9 HV) compared with the conventionally sintered samples (19.1-24.2 HV) and traditionally cast pewter from Royal Selangor (17-20 HV).

The hardness values obtained can be said to be increasing with increasing density of the pewter alloys (see Figure 4.7). The relationship of hardness with density for the varying sintering conditions for both conventional and microwave sintering gives a clear understanding that the hardness is a function of density. It is interesting to note that the percentage change in hardness after microwave sintering is smaller than that for conventional sintering. Enhanced densification is achieved in microwave sintering as compared to conventional sintering which attributes to the improvement in hardness.

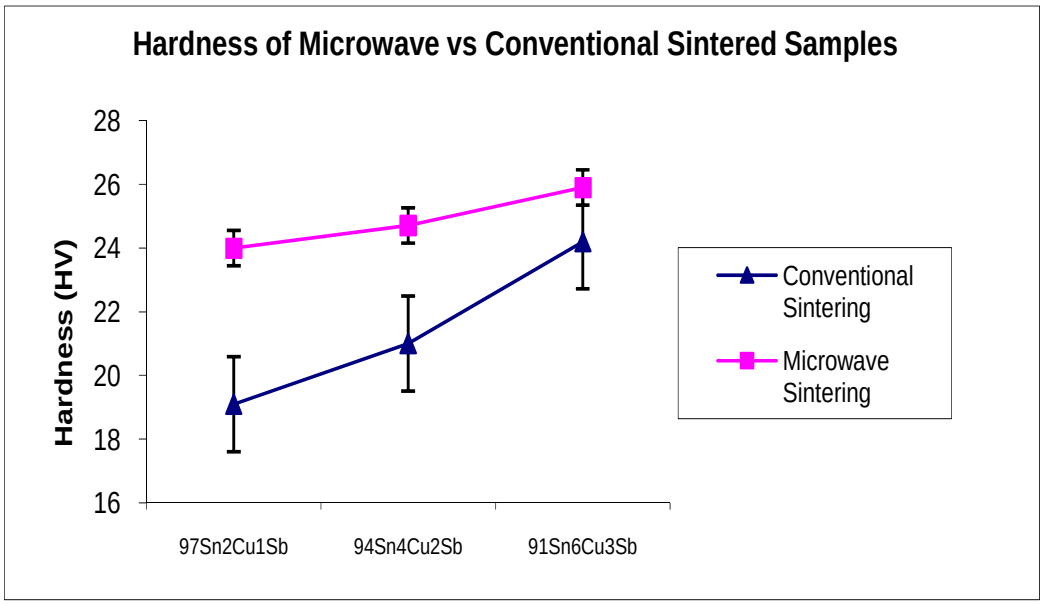

Figure 4.6: Graph of microhardness for microwave (30 min) and conventional (120 min) sintering for 97Sn2Cu1Sb, 94Sn4Cu2Sb and 91Sn6Cu3Sb compositions pressed at 129 MPa and sintered at 220°C

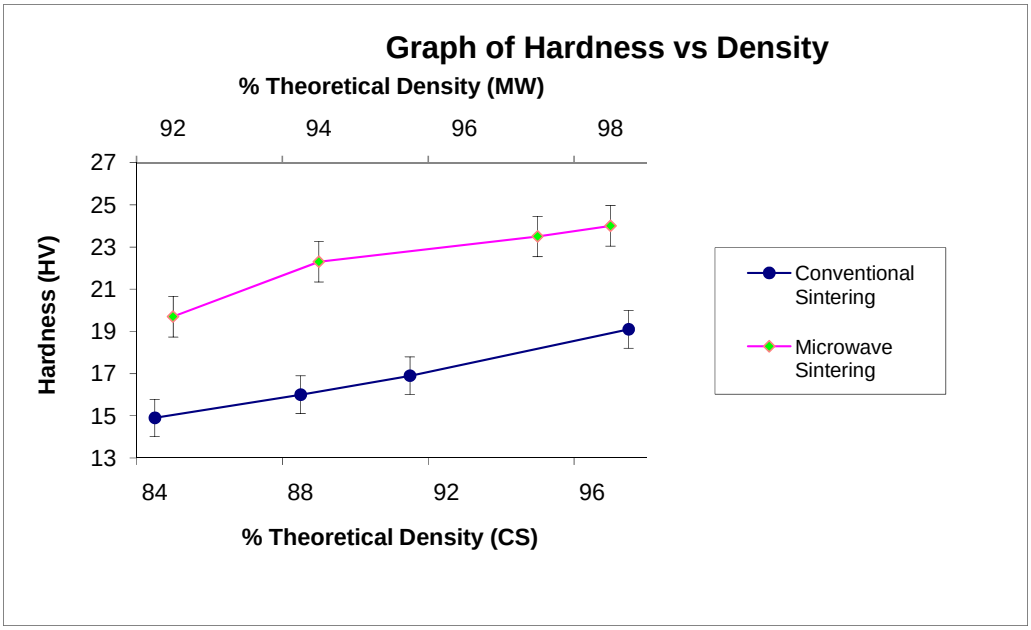

Figure 4.7: Relationship of hardness with density for conventionally sintered (160°C/ 60 min), (160°C/ 120 min), (220°C/ 60 min) and (220°C/ 120 min) and microwave sintered (160°C/ 15 min), (160°C/ 30 min), (220°C/ 15 min) and (220°C/ 30 min) 97Sn2Cu1Sb samples pressed at 129 MPa

Tensile Strength

Tensile strength is an important parameter in engineering materials that are used in structures and mechanical devices. Even though pewter is not used for mechanical devices, tensile strength can still be a good way to characterize the effectiveness of sintering on powder consolidation. In this work longitudinal and transverse strength was determined as a function of the most influential parameters; i.e. sintering time, sintering temperature, sintering method and compaction load.

Conventional Sintering

Tensile properties for samples from both longitudinal and transverse direction indicated that the overall tensile strength for the transverse direction is slightly higher than that for the longitudinal direction. This is found to be true for both sintering methods. This is in accordance with the direction of force applied per unit area across the cross section. Non-uniform pressure is experienced during the compaction. The unidirectional pressure applied on the powder compact from the top of the die is higher across the cross section rather than along the longitudinal direction. By increasing the sintering time and temperature, the tensile strength had increased as well. Nevertheless, the ductility has improved (based on the percentage of strain to fracture) for samples from the transverse direction than from the samples in the longitudinal direction (refer to Tables D1- D6 in the appendix). By increasing the compaction load, an improvement in tensile strength is noticed as well.

For an alloy composition 97Sn2Cu1Sb sintered at 160°C, there was an 18% increase in tensile strength along the transverse direction when the sintering time was increased from 60 minutes to 120 minutes. For samples sintered at 220°C, the increase was 11%. In the longitudinal direction, the samples when sintered at 160°C and 220°C, the tensile strengths were found to be about 2% and 7% lower than in the transverse direction for the same processing conditions. For the other two alloys, a composition of 94Sn4Cu2Sb gave an increase of 11% at 160°C and 15% at 220°C, while a composition of 91Sn6Cu3Sb gave a tensile

strength 20% higher at 160°C and 12% higher at 220°C for the same sintering conditions by doubling the sintering times from 60 minutes to 120 minutes. For the latter two alloys, the longitudinal tensile strengths were 4.6% to 5.6% lower than that for the transverse direction. These can be seen from Figure 4.8 below.

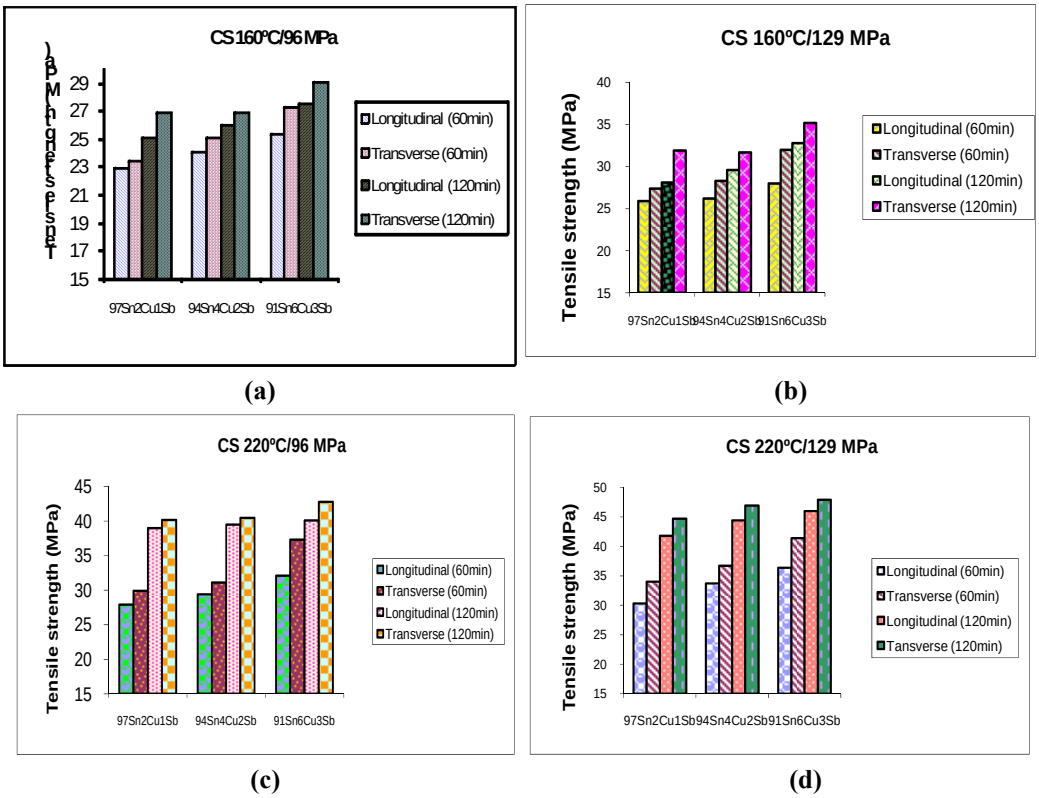

Figure 4.8: Bar charts showing tensile strength properties for the conventional sintered samples for 97Sn2Cu1Sb, 94Sn4Cu2Sb and 91Sn6Cu3Sb compositions

Microwave Sintering

For the 94Sn4Cu2Sb alloy, the tensile strength in the longitudinal direction for the conventionally sintered sample, 94CS8 (220°C/120 min/129 MPa) and the microwave sintered sample, 94MW8 (220°C/30 min/129 MPa) reached values of 44.4 MPa and 43.8 MPa respectively (see Figure 4.9). This was not achievable for the composition of 97Sn2Cu1Sb containing a higher percentage of Sn. However, the tensile strength from the transverse direction was higher with values of 46.9 MPa and 46.0 MPa. These strength values are within the range for cast pewter from Royal Selangor (44 MPa-51 MPa).

The microwave sintered alloy of composition 91Sn6Cu3Sb gave a higher tensile strength than compositions 97Sn2Cu1Sb and 94Sn4Cu2Sb. Tripling the amount of Cu and Sb resulted in higher tensile strength but lower ductility values, with the percentage strain to fracture decreasing by 4-18%.

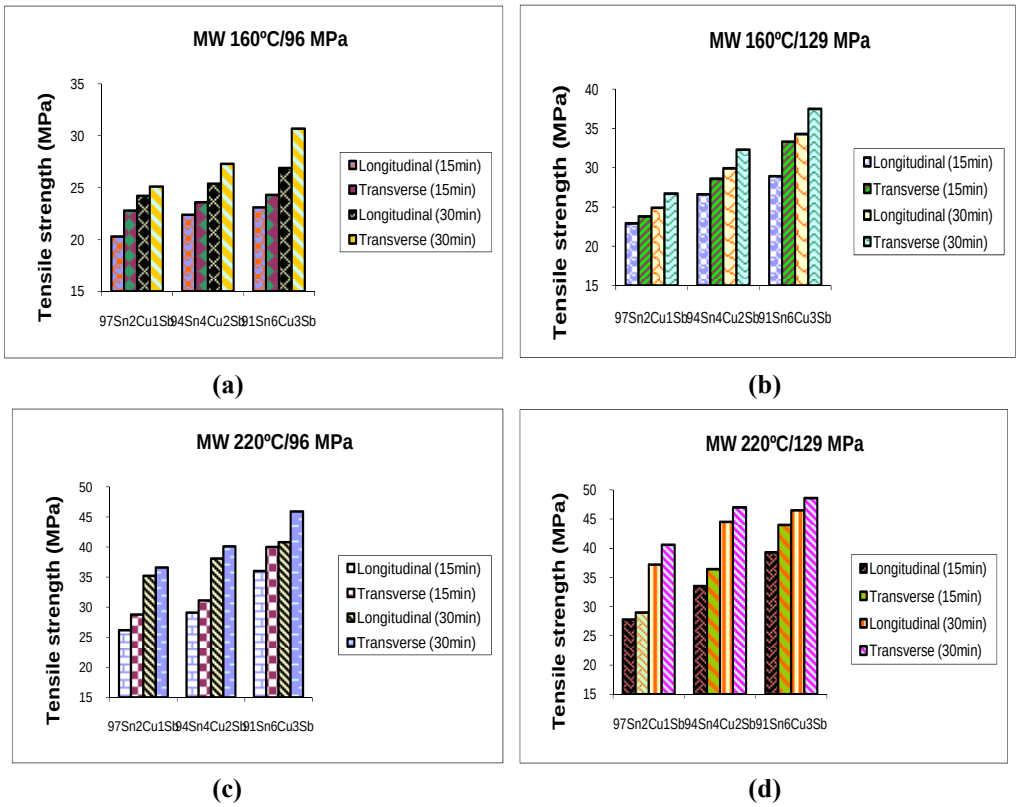

Figure 4.9: Bar charts showing tensile strength properties for the microwave sintered samples for 97Sn2Cu1Sb, 94Sn4Cu2Sb and 91Sn6Cu3Sb compositions

The conventionally sintered sample, 91CS8 (220°C/120 min/129 MPa) and the microwave sintered sample 91MW8 (220°C/30 min/129 MPa), sintered under the same conditions, reached tensile strength values of 46.0 MPa and 46.5 MPa respectively in the longitudinal direction, which is a 4% increase in values obtained for a 94Sn4Cu2Sb alloy composition. However, the same samples in the transverse direction gave tensile strengths of 47.9 MPa and 48.6 MPa respectively.

Conventional vs. Microwave Sintering

The microwave sintered samples in general have produced similar tensile properties to conventionally sintered samples particularly for the compositions 94Sn4Cu2Sb and 91Sn6Cu3Sb as can be seen in Figure 4.10. This may be regarded as an advantage where reasonably similar results can be obtained in a shorter duration of time. The transverse samples sintered at 220°C for both microwave and conventional sintering, produced tensile strengths within the range for cast pewter (44 MPa – 51 MPa).

Figure 4.10 shows the stress-strain curves for microwave and conventionally sintered samples. The tensile data is similar for both conventionally and microwave sintered samples with the same nominal composition. The increase in yield stress with increasing alloying content is apparent. The higher density and hardness in microwave sintered samples are due to the fact that hardness is a function of underlying pores rather than yield point or tensile strength.

From the tensile data given in Tables D1-D6 (refer to appendix), it is clear that the tensile strength for material of composition 91Sn6Cu3Sb, with increased Cu and Sb, is higher than that for the other compositions investigated. Tripling the percentage of Cu and Sb has resulted in a 5-15% increase in tensile strength. However, the ductility, as measured by strain to fracture, has decreased by 3-9% with the addition of Cu and Sb (refer to Tables D1-D6 in the appendix).

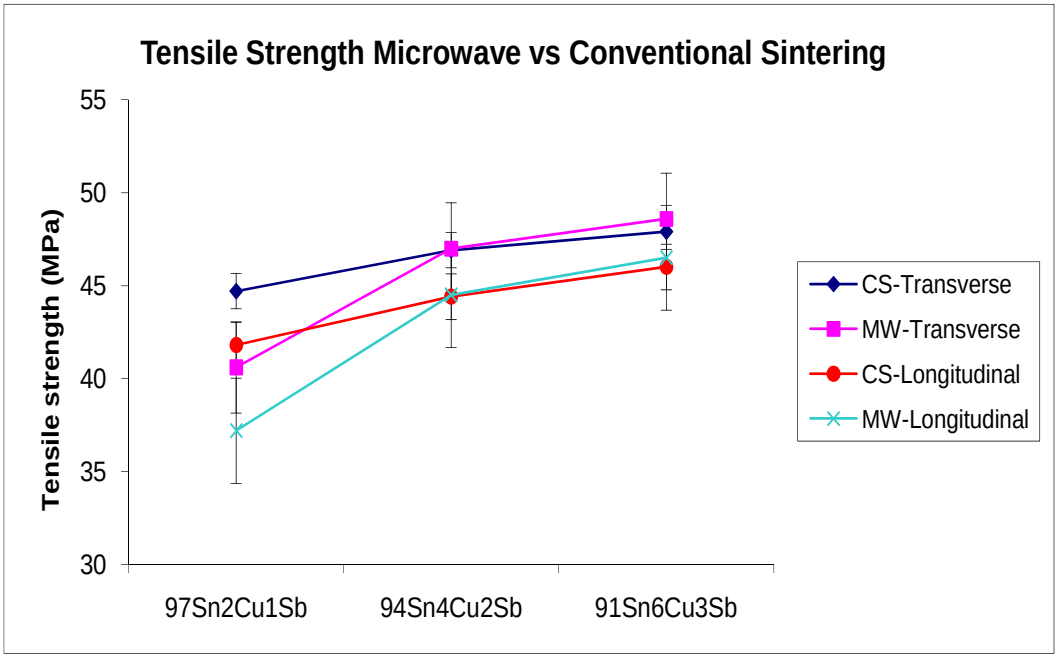

Figure 4.10: Graph showing tensile strength properties for the microwave (30 min) sintered samples and conventionally (120 min) sintered samples for 97Sn2Cu1Sb, 94Sn4Cu2Sb and 91Sn6Cu3Sb compositions pressed at 129 MPa and sintered at 220°C

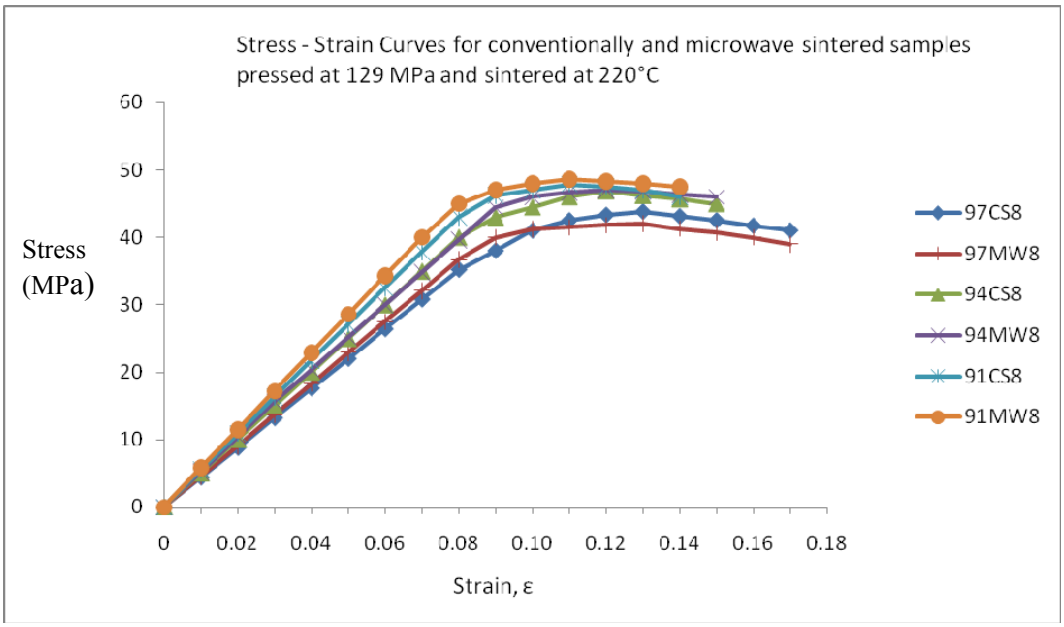

Figure 4.11: Stress – strain curve comparing conventionally sintered (120 min) and microwave sintered (30 min) samples for 91Sn6Cu3Sb, 94Sn4Cu2Sb and 97Sn2Cu1Sb alloys

4.2.2 Structural Analysis

Scanning Electron Microscope (SEM)

This section describes the morphology of samples from SEM images obtained for various sintering conditions for all three compositions; 97Sn2Cu1Sb, 94Sn4Cu2Sb and 91Sn6Cu3Sb. The effects of these sintering conditions and compaction loads on grain growth, pore size and densification are discussed.

Alloy with composition 97Sn2Cu1Sb

Samples from the 97Sn2Cu1Sb alloy that were pressed at 96 MPa (see Figure 4.12 (a)) appeared to have uniformly distributed pores with irregular shape and size when compared with samples that were pressed at 129 MPa (see Figure 4.13 (a)). This is due to the higher compaction load and better densification. The conventionally sintered samples (pressed at 96 MPa) particularly 97CS1 (160°C/ 60 min) and 97CS2 (160°C/ 120 min) had much more porosity and larger sized pores when compared with samples 97CS3 (220°C/60 min) and 97CS4 (220°C/120 min) (see Figure 4.12).

The conventionally sintered samples that were pressed at 129 MPa had less porosity and smaller sized pores as shown in Figure 4.13, particularly for samples 97CS7 (220°C/60min) and 97CS8 (220°C/120min). Table B1 (refer to appendix) gives the estimated percentage of porosity existing in the samples. As the sintering time and temperature increased, the amount of porosity decreased for both compaction loads. When the sintering time was doubled from 60 minutes to 120 minutes, the density increased by 3% when sintered at 160ºC and 8% when sintered at 220ºC.

The microwave sintered samples pressed at 96 MPa produced fewer larger sized pores when sintered at 160ºC (sample 97MW1 (15 min) and 97MW2 (30 min)) compared with conventional sintering. However, when microwave sintered at 220ºC, particularly sample 97MW4 (30 min), the size and quantity of pores had significantly decreased under the same compaction load. For the microwave

sintered samples pressed at 129 MPa (sample 97MW7 (15 min) and sample 97MW8 (30 min)), the size and distribution of porosity was significantly reduced compared with microwave sintered samples pressed at 96 MPa. Even at 160ºC, there were fewer pores and these had a more uniform distribution compared to conventionally sintered material. Moreover, the pores were more regularly shaped. This is due to the fact that the sample is heated from outside to inside using hybrid microwave sintering, unlike conventional sintering that has a reverse heating direction. The uniform distribution of microstructures from the microwave sintered samples is attributed to the uniform volumetric heating. The powder particles which were visible for 97MW3 (220ºC/ 15 min/ 96 MPa) (see Figure 4.14(d)) disappeared as the sintering time was increased to 30 min (97MW4) (see Figure 4.14(e)). As the sintering temperature increased from 160ºC to 220ºC, the sample appeared to have minimal porosity; only 2.8% and 1.31% of porosity was found after 15 and 30 minutes of sintering time respectively. These can be seen clearly in Figures 4.14-4.15.

Microwave sintering in general produced a finer microstructure compared to a conventional sintering process which contributed to the higher density and microhardness. This is attributed to the rapid heating effect of microwave sintering which did not allow sufficient time for grain growth to occur. Sintering temperatures and sintering time had significant effects on the density and porosity of the sintered samples. The pores were generally smaller and were fewer in quantity as the compaction load, sintering time and sintering temperature increased.

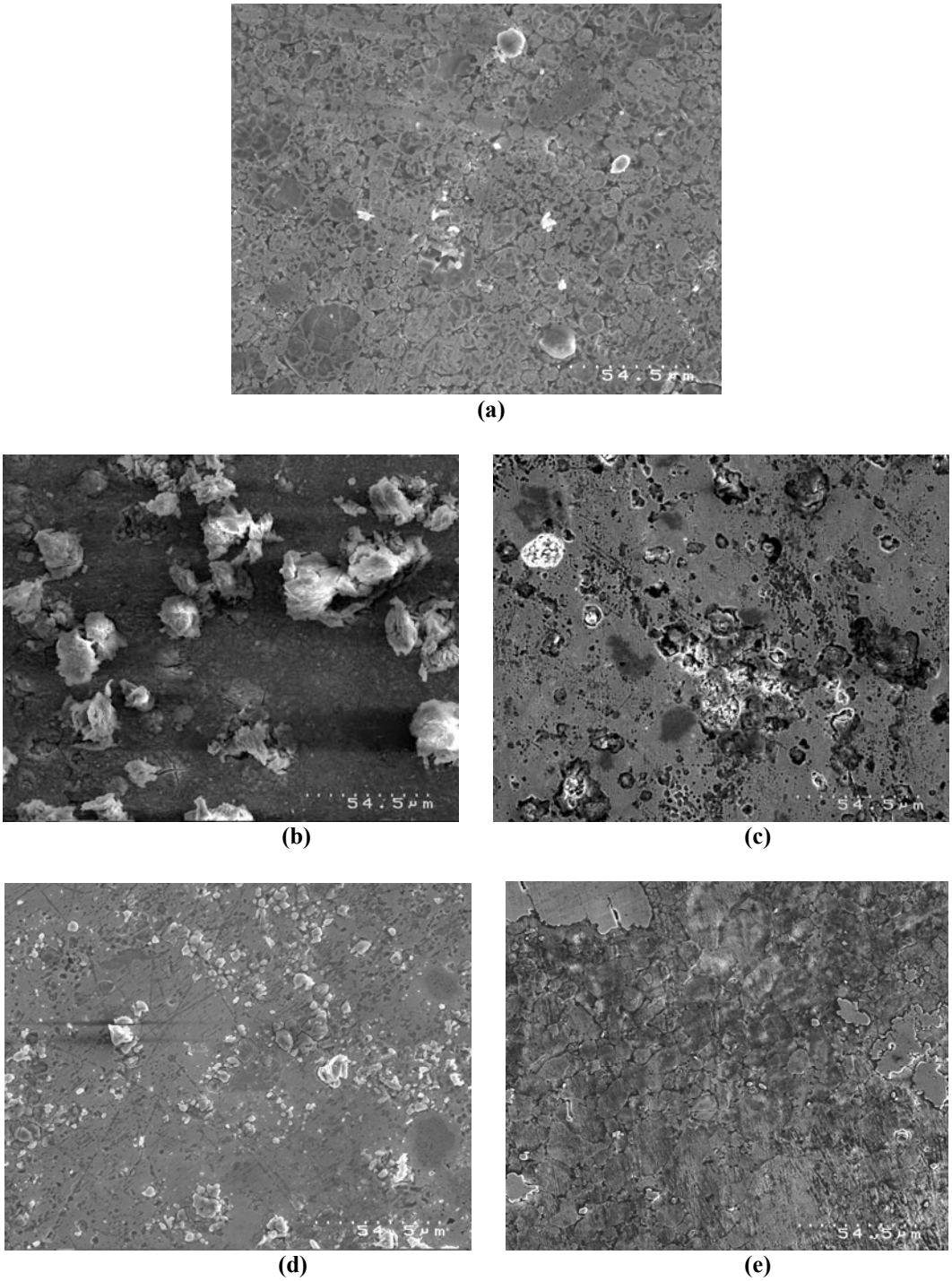

Figure 4.12: Samples of 97Sn2Cu1Sb composition pressed at 96 MPa and conventionally sintered (a) Green compact (b) CS1 (160°C/ 60 min) (c) CS2 (160°C/ 120 min) (d) CS3 (220°C/ 60 min) (e) CS4 (220°C/ 120 min)

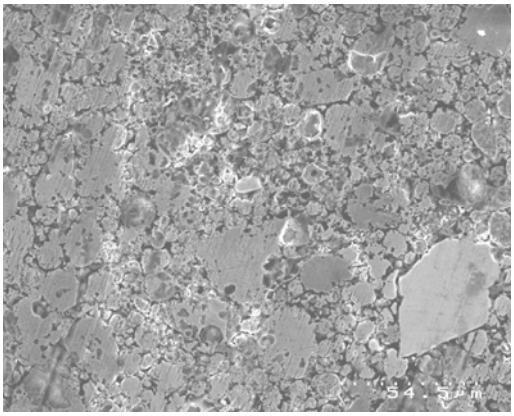

(a)

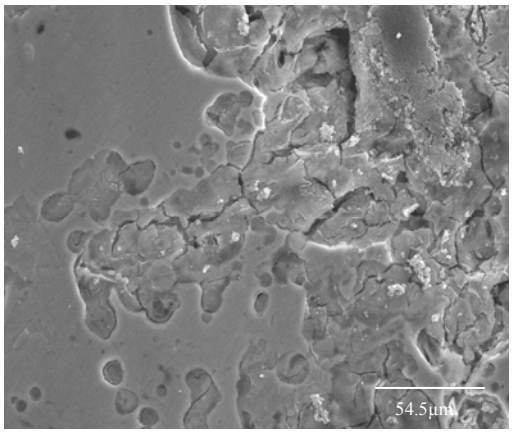

(b)

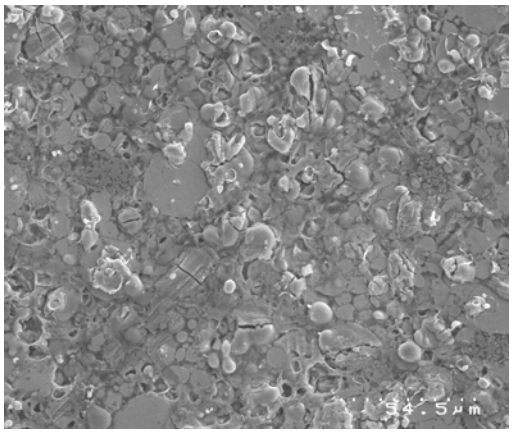

(c)

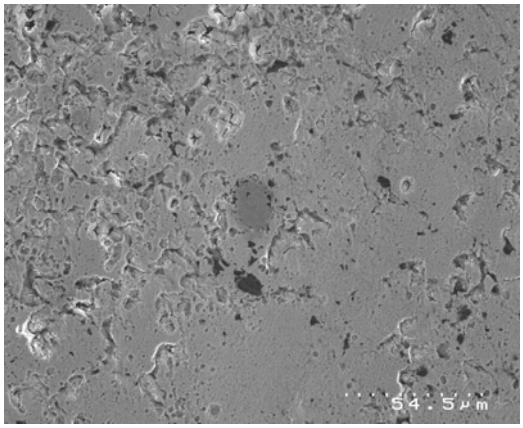

(d)

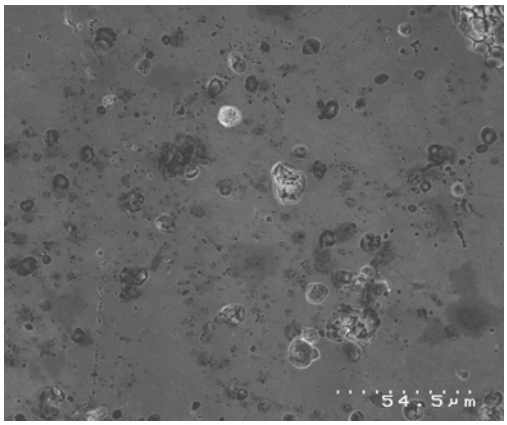

(e)

54.5µm

Figure 4.13: Samples of 97Sn2Cu1Sb composition pressed at 129 MPa and conventionally sintered (a) Green compact (b) CS5 (160°C/ 60 min) (c) CS6 (160°C/ 120 min) (d) CS7 (220°C/ 60 min) (e) CS8 (220°C/ 120 min)

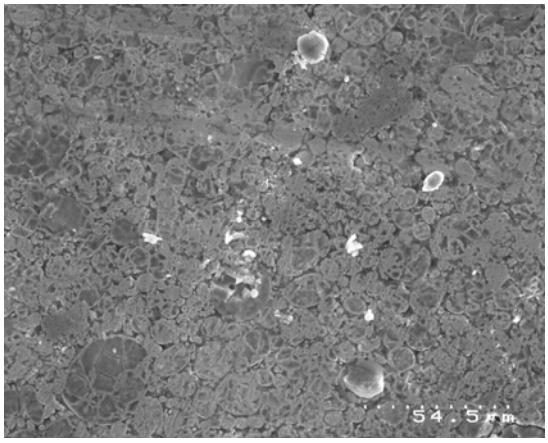

(a)

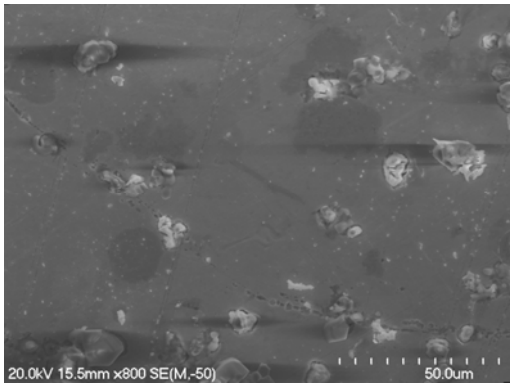

(b)

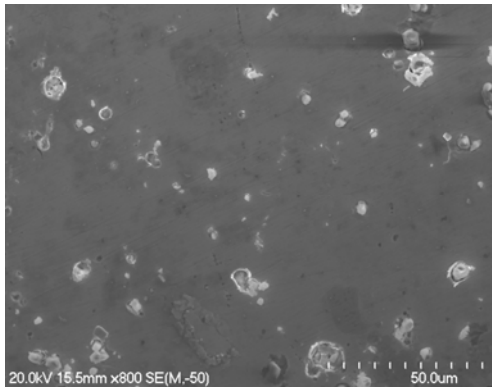

(c)

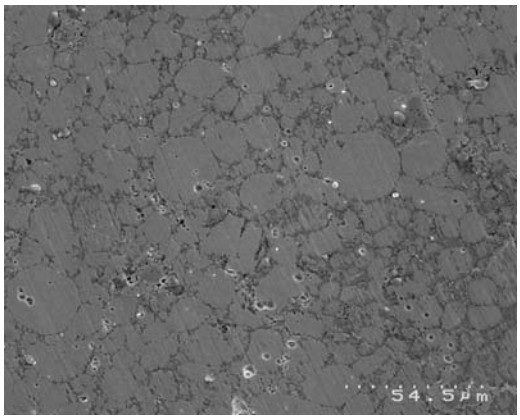

(d)

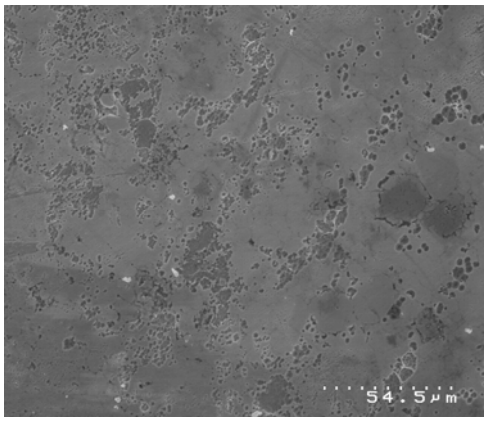

(e)

54.5µm

Figure 4.14: Samples of 97Sn2Cu1Sb composition pressed at 96 MPa and microwave sintered (a) Green compact (b) MW1 (160°C/ 15 min) (c) MW2 (160°C/ 30 min) (d) MW3 (220°C/ 15 min) (e) MW4 (220°C/ 30 min)

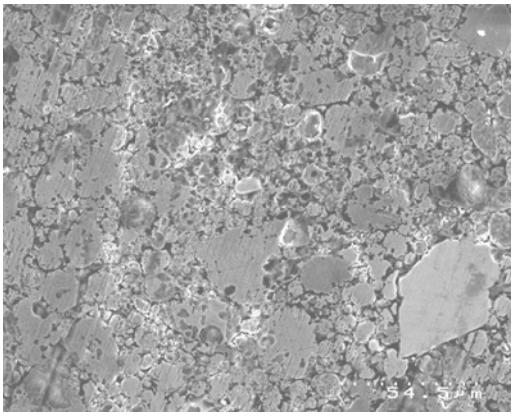

(a)

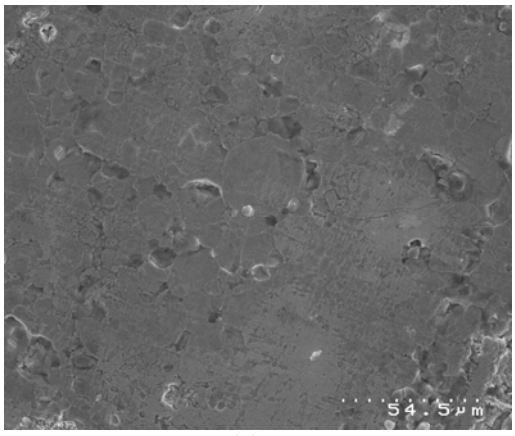

(b)

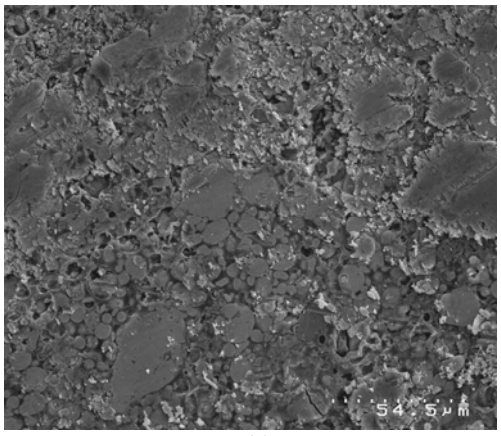

(c)

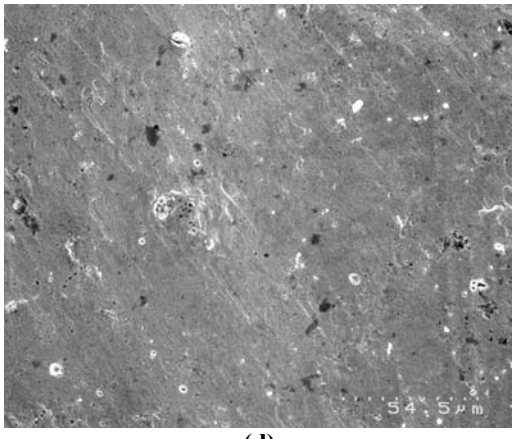

(d)

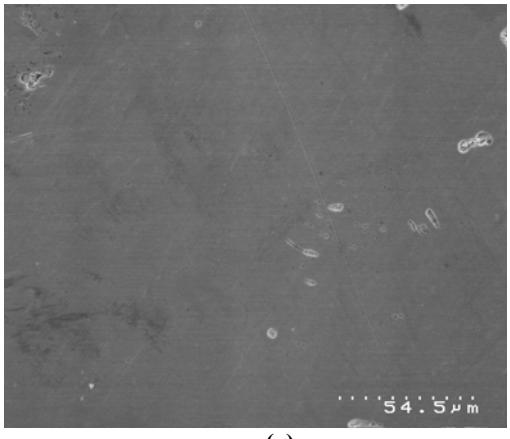

(e)

54.5µm

Figure 4.15: Samples of 97Sn2Cu1Sb composition pressed at 129 MPa and microwave sintered (a) Green compact (b) MW5 (160°C/ 15 min) (c) MW6 (160°C/ 30 min) (d) MW7 (220°C/ 15 min) (e) MW8 (220°C/ 30 min)

Alloy with composition 94Sn4Cu2Sb

Green compacts of 94Sn4Cu2Sb alloy appeared to have uniformly distributed pores with irregular shape. Samples pressed at 96 MPa (see Figure 4.16(a)) have larger pores compared with samples that were pressed at 129 MPa (see Figure 4.17(a)). Figures 4.16-4.19 are the SEM images of samples sintered by both microwave and conventional sintering for the composition 94Sn4Cu2Sb. It can be clearly seen that the conventionally sintered samples, particularly 94CS1 (160°C/60 min) and 94CS2 (160°C/120 min), which had lower green densities, have many large pores (refer to Figure 4.16 (b) and (c)). The size of the pores tends to decrease with increasing sintering time at a higher temperature as shown in Figure 4.16 (d) and (e) for samples 94CS3 (220°C/60 min) and 94CS4 (220°C/120 min) respectively.

Samples with higher green densities naturally had smaller pores due to the higher compaction load which led to better densification. Conventionally sintered samples 94CS5 (160°C/60 min) and 94CS6 (160°C/120 min), as shown in Figure 4.17 (b) and (c), appeared to have fewer larger pores. By increasing the temperature to 220°C, the estimated porosity value from Table B3 (refer to appendix) had decreased from 9.69% (sample 94CS6) to 6.01% for the sample 94CS7 (220°C/60 min). These can be seen in Figure 4.17 (d) and (e). By doubling the sintering time from 60 minutes to 120 minutes, further enhancement in densification was found and the porosity decreased to 1.57% for the sample 94CS8(220°C/120 min).

Microwave sintering on the other hand was more effective in achieving higher densification in a shorter duration of time compared with conventional sintering. From Table B4 (refer to appendix), the porosity for the microwave sintered sample, 94MW1 (160°C/15 min) appeared to have an estimated porosity value of only 7.56%. Meanwhile, the conventionally sintered sample, 94CS1 (160°C/60 min) produced a porosity value of 17.34%. This is a large difference after just 15 minutes.

Microwave sintering produced samples with less porosity and smaller pores than those conventionally sintered. By increasing the sintering time and temperature, microwave sintering led to 1.29% of porosity after 30 minutes for the sample 94MW8 (129 MPa/220°C) while conventional sintering gave 1.57% of porosity after 120 minutes for the sample 94CS8(129 MPa/220°C).

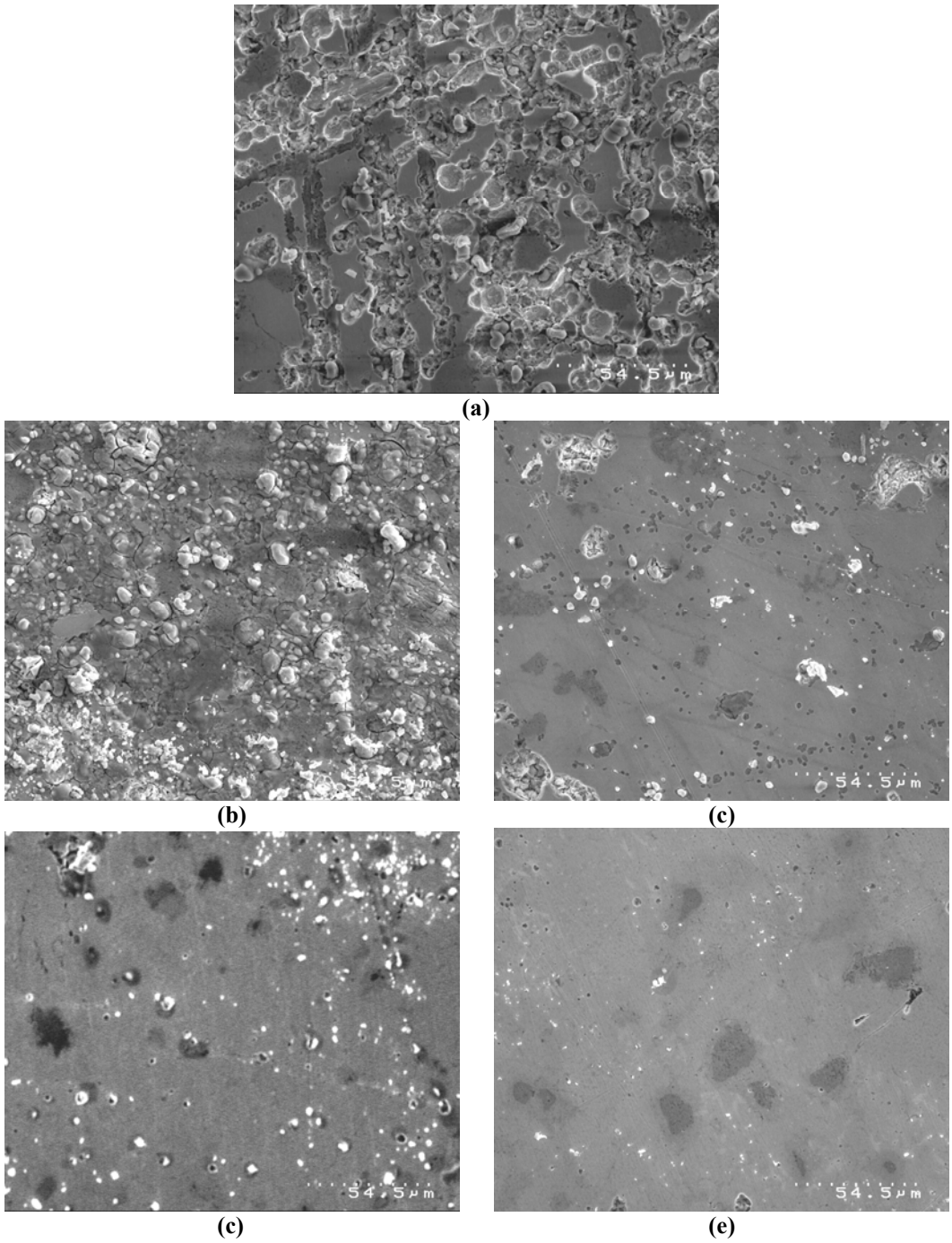

Figure 4.16: Samples of 94Sn4Cu2Sb composition pressed at 96 MPa and conventionally sintered (a) Green compact (b) CS1 (160°C/ 60 min) (c) CS2 (160°C/ 120 min) (d) CS3 (220°C/ 60 min) (e) CS4 (220°C/ 120 min)

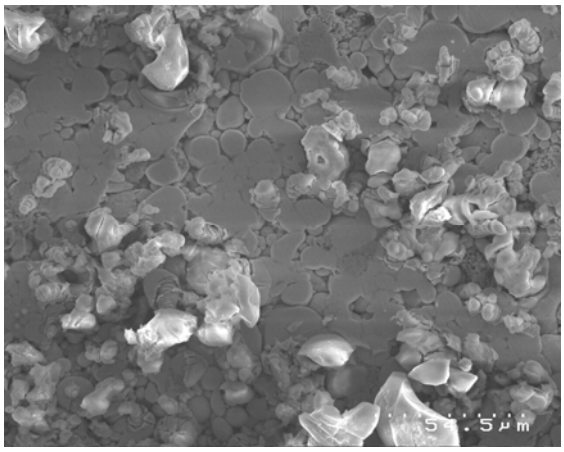

(a)

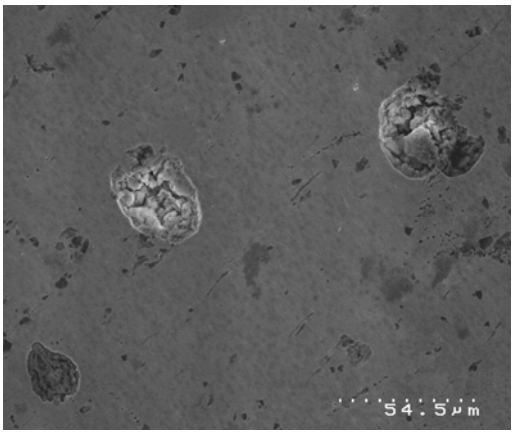

(b)

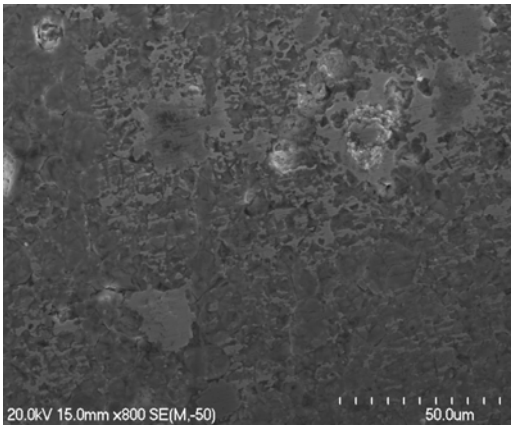

(c)

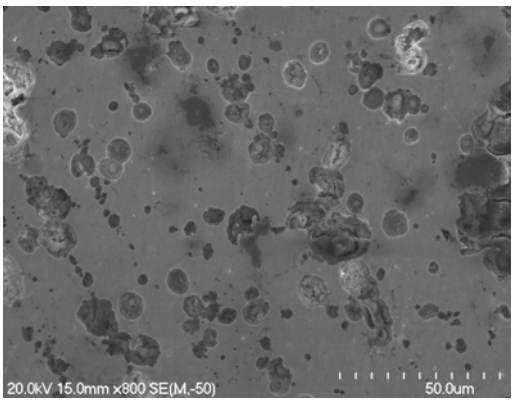

(d)

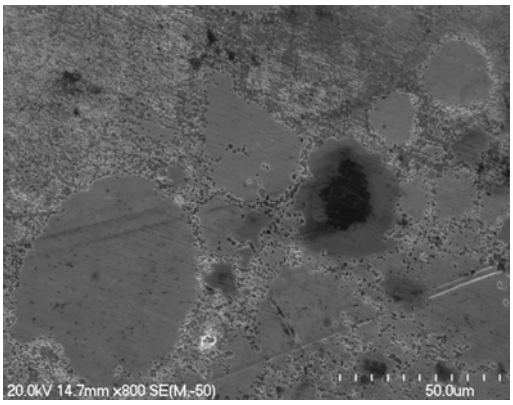

(e)

54.5µm

50.0µm

Figure 4.17: Samples of 94Sn4Cu2Sb composition pressed at 129 MPa and conventionally sintered (a) Green compact (b) CS5 (160°C/ 60 min) (c) CS6 (160°C/ 120 min) (d) CS7 (220°C/ 60 min) (e) CS8 (220°C/ 120 min)

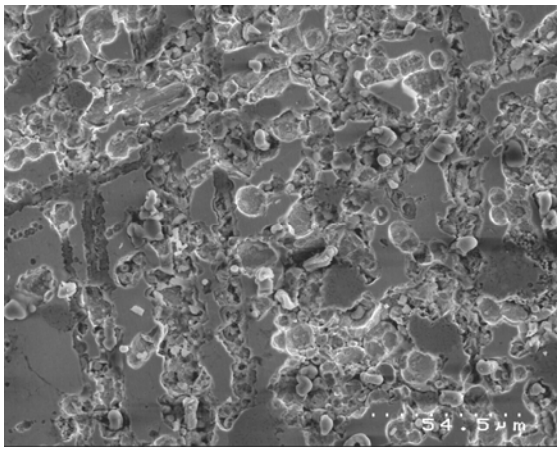

(a)

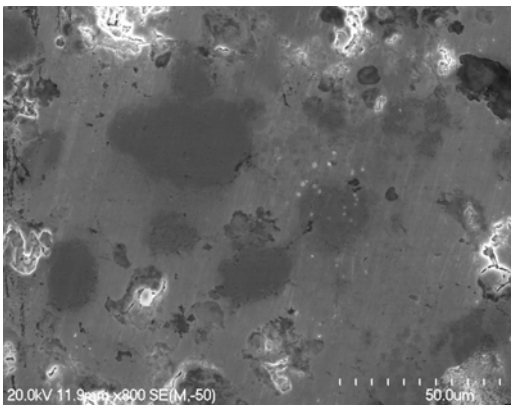

(b)

(c)

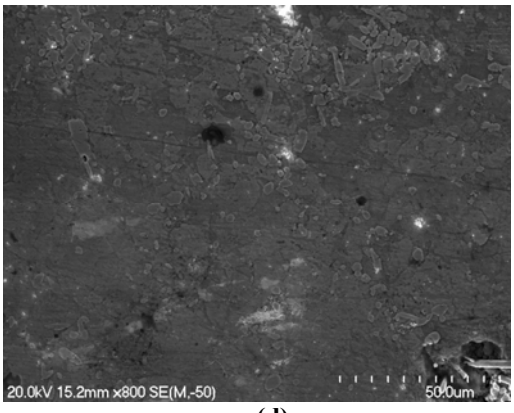

(d)

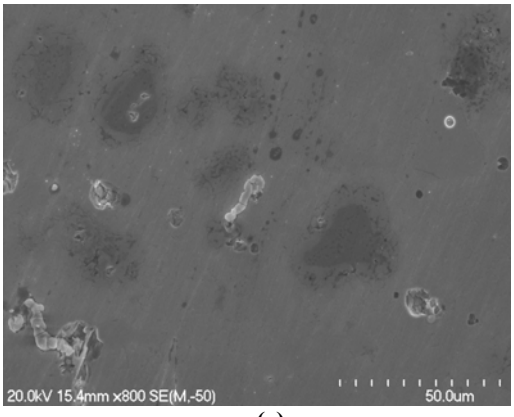

(e)

50.0µm

Figure 4.18: Samples of 94Sn4Cu2Sb pressed at 96 MPa and microwave sintered (a) Green compact (b) MW1 (160°C/ 15 min) (c) MW2 (160°C/ 30 min) (d) MW3 (220°C/ 15 min) (e) MW4 (220°C/ 30 min)

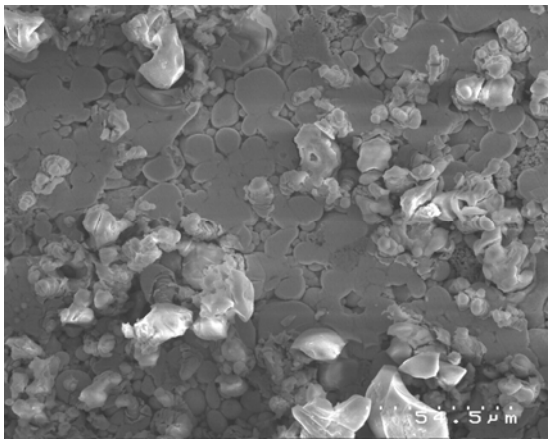

(a)

(b)

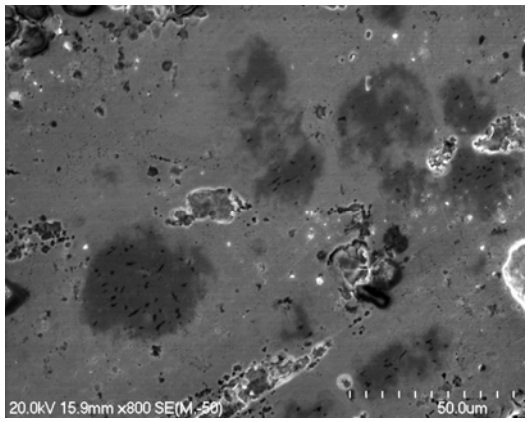

(c)

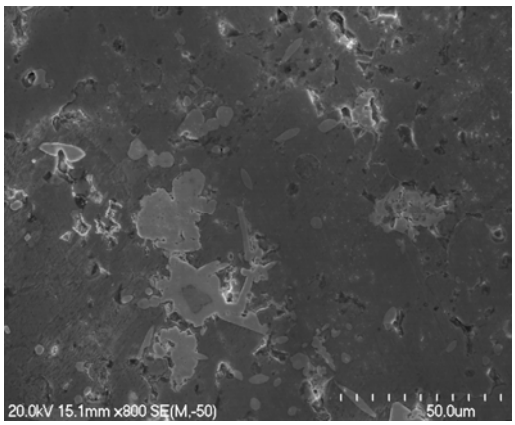

(d)

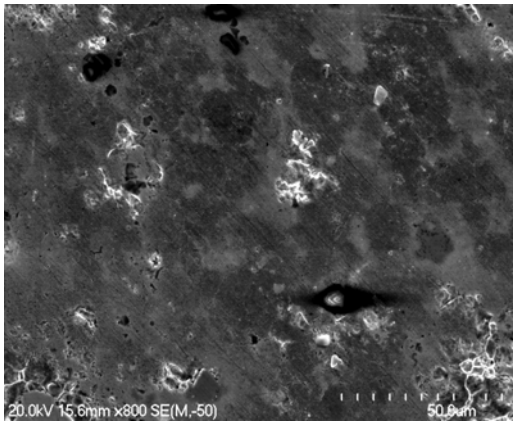

(e)

50.0µm

Figure 4.19: Samples of 94Sn4Cu2Sb composition pressed at 129 MPa and microwave sintered (a) Green compact (b) MW5 (160°C/ 15 min) (c) MW6 (160°C/ 30 min) (d) MW7 (220°C/ 15 min) (e) MW8 (220°C/ 30 min)

Alloy with composition 91Sn6Cu3Sb

Samples of 91Sn6Cu3Sb alloy appear to have irregularly shaped pores which is uniformly distributed. Samples pressed at 96 MPa have larger sized pores (see Figure 4.10 (a)) compared with samples pressed at 129 MPa (see Figure 4.21 (a)). Figures 4.20 to 4.23 are the SEM images of the samples obtained from a 91Sn6Cu3Sb composition. The samples with a lower green density had relatively larger pores than the samples with a higher green density. The percentage of porosity decreases from 16.27% to 4.45% with increasing sintering time and temperature for the samples 91CS1 (160°C/60 min) and 91CS4 (220°C/120 min) respectively. Table B5 (refer to appendix) displays the porosity values for these samples. Meanwhile, samples with a higher green density have decreased porosity from 11.47% to 1.54% with increasing sintering time and temperature for the samples 91CS5 (160°C/60 min) and 91CS8 (220°C/120 min) respectively.

However, after microwave sintering, there are fewer smaller round pores compared with conventional sintering. The microwave sintered samples look more dense and Table B6 (refer to appendix) displays the values of estimated porosity values for the microwave sintered samples. The percentage of porosity for the lower green density samples had decreased from 7.26% to 4.21% with increasing sintering time and temperature. However, for the higher compaction load, the samples show better densification. Porosity for samples 91MW5 (160°C/15 min) and 91MW8 (220°C/30 min) decreased to 7.25% and 1.25% respectively.

Compared with the previous compositions ; 97Sn2Cu1Sb and 94Sn4Cu2Sb, the composition of 91Sn6Cu3Sb with increased content of Cu and Sb, seems to have produced samples with slightly improved microstructural properties i.e.better densification and less porosity.

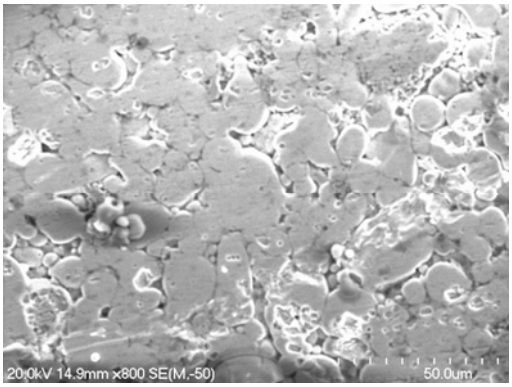

(a)

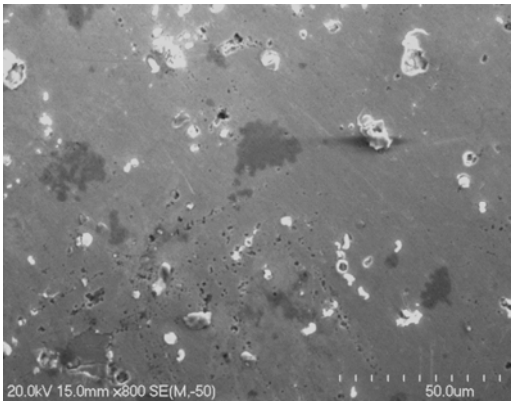

(b)

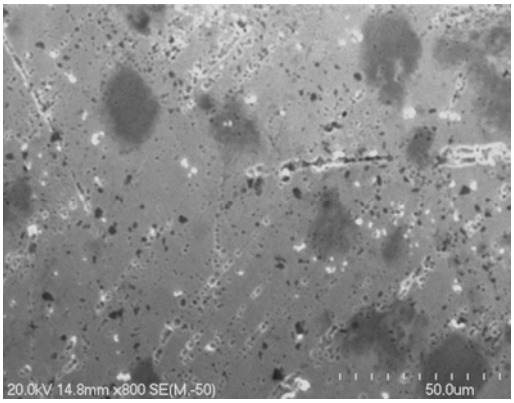

(c)

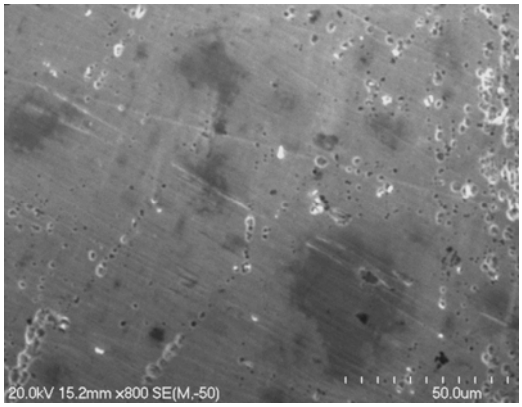

(d)

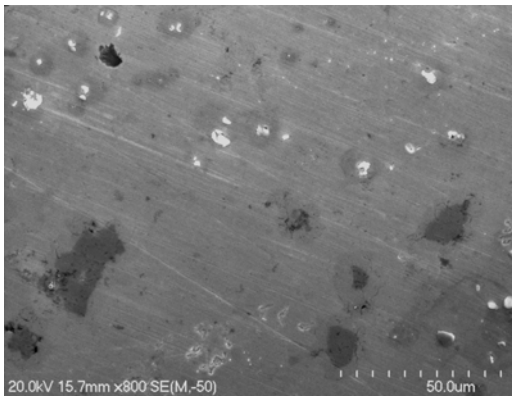

(e)

50.0μm

Figure 4.20: Samples of 91Sn6Cu3Sb composition pressed at 96 MPa and conventionally sintered (a) Green compact (b) CS1 (160°C/ 60 min) (c) CS2 (160°C/ 120 min) (d) CS3 (220°C/ 60 min) (e) CS4 (220°C/ 120 min)

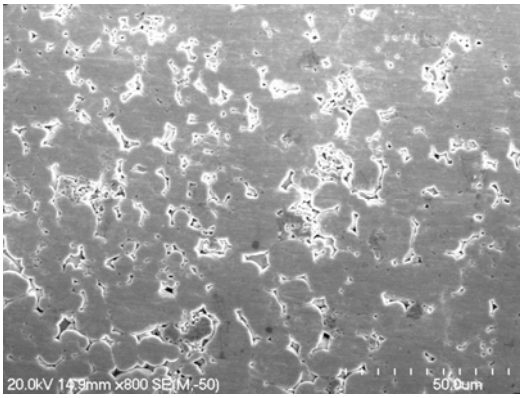

(a)

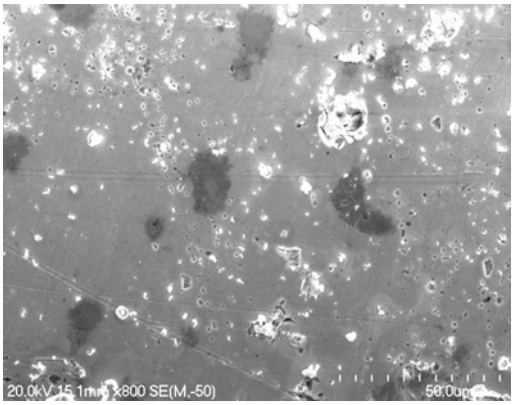

(b)

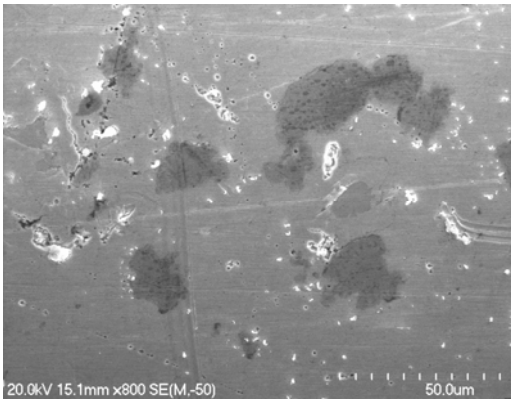

(c)

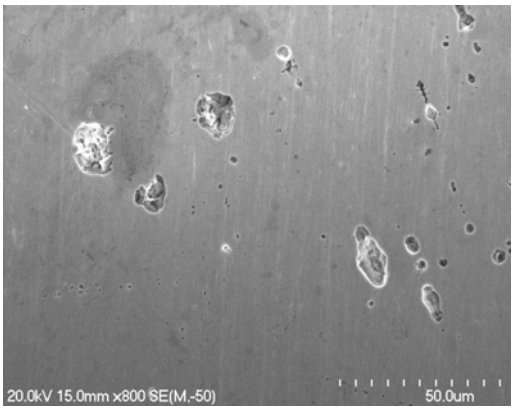

(d)

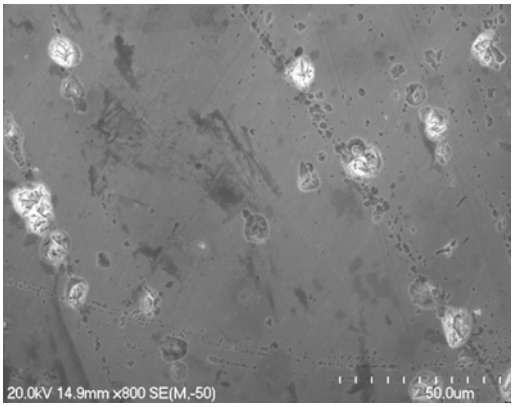

(e)

50.0μm

Figure 4.21: Samples of 91Sn4Cu2Sb composition pressed at 129 MPa and conventionally sintered (a) Green compact (b) CS5 (160°C/ 60 min) (c) CS6 (160°C/ 120 min) (d) CS7 (220°C/ 60 min) (e) CS8 (220°C/ 120 min)

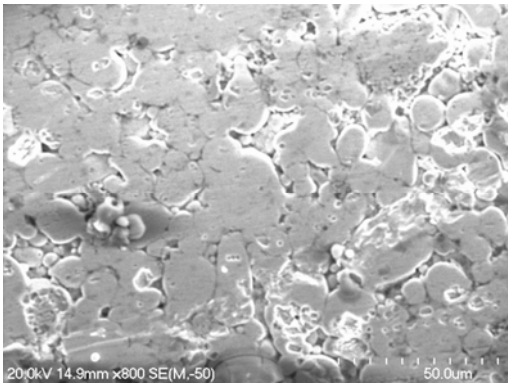

(a)

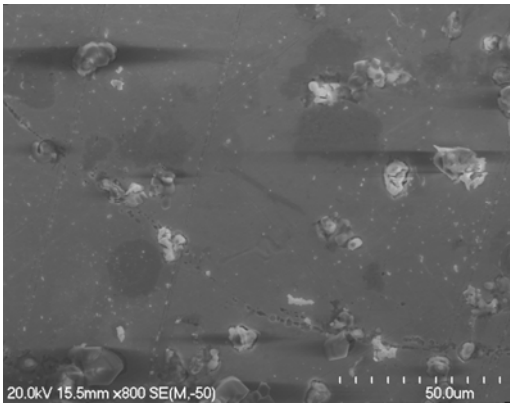

(b)

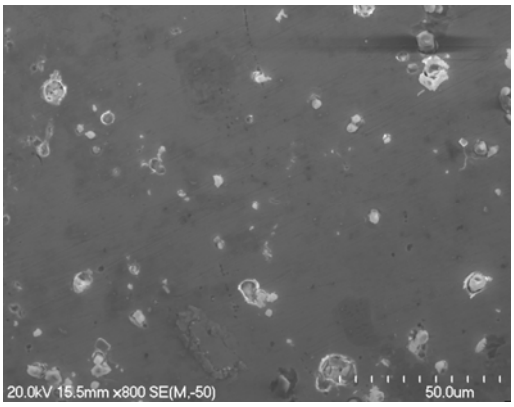

(c)

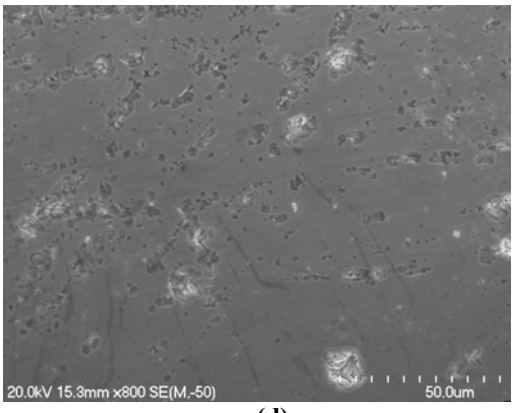

(d)

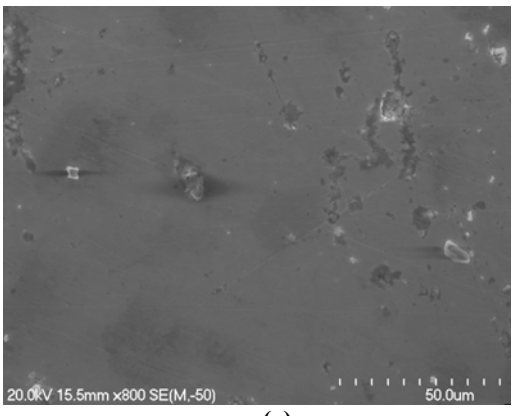

(e)

50.0µm

Figure 4.22: Samples of 91Sn6Cu3Sb composition pressed at 96 MPa and microwave sintered (a) Green compact (b) MW1 (160°C/ 15 min) (c) MW2 (160°C/ 30 min) (d) MW3 (220°C/ 15 min) (e) MW4 (220°C/ 30 min)

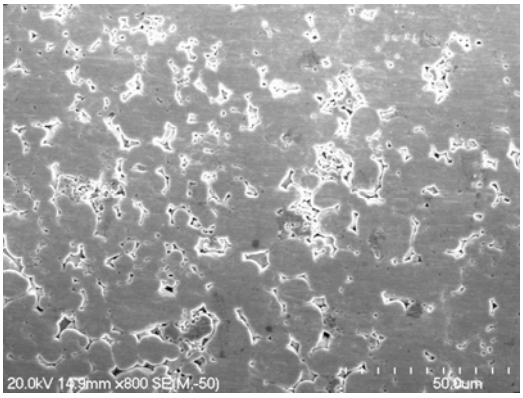

(a)

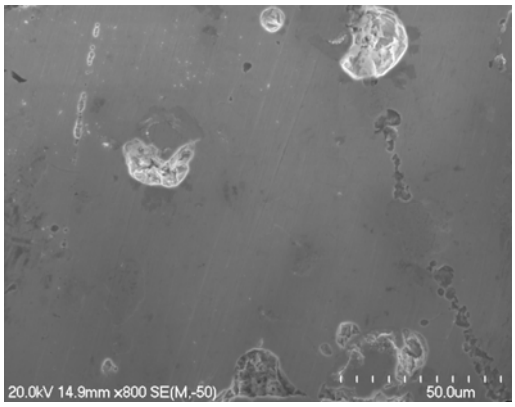

(b)

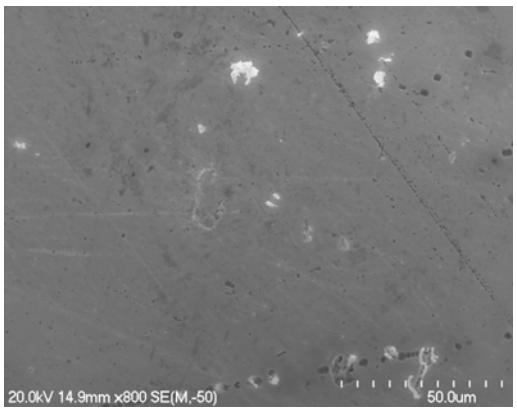

(c)

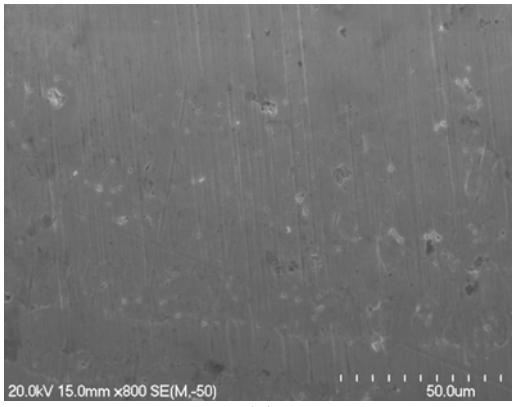

(d)

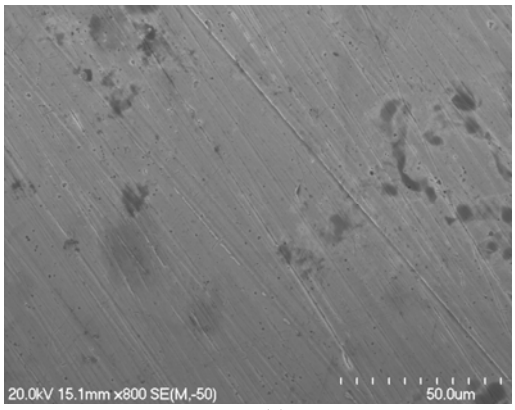

(e)

50.0µm

Figure 4.23: Samples of 91Sn6Cu3Sb composition pressed at 129 MPa and microwave sintered (a) Green compact (b) MW5 (160°C/ 15 min) (c) MW6 (160°C/ 30 min) (d) MW7 (220°C/ 15 min) (e) MW8 (220°C/ 30 min)

Microstructural Evolution and Grain Growth

The effect on grain growth of variations in sintering temperature, sintering time, sintering method, compaction load and different percentages of Cu and Sb in the alloy is analyzed in this section. This analysis helps to characterize microstructural properties of the tin alloys.

Conventional Sintering

In the previous section, the densities of microwave and conventionally sintered samples were compared at various temperatures. However, sintering to full density does not guarantee that the resulting microstructure is desirable. Microstructural features such as the size and shape of the grains and the distribution of pores must all be controlled to achieve the desired properties of the sintered pewter alloy. Grain growth and microstructural evolution of microwave and conventionally sintered samples are compared in this section to determine whether microwave sintering results in any differences in the microstructure and grain size.

Tables A3, A4, A7, A8, A11 and 12 (refer to appendix) show the densification for the conventional and microwave sintered samples for all three compositions. After sintering for 30 minutes at 220ºC, near full density was reached after microwave sintering for all three compositions; 98.71% theoretical density (TD) (97Sn2Cu1Sb), 98.75%TD (94Sn4Cu2Sb) and 98.79% TD (91Sn6Cu3Sb), while it took 120 minutes to reach 98.28% TD(97Sn2Cu1Sb), 98.46%TD (94Sn4Cu2Sb) and 98.51%TD (91Sn6Cu3Sb) with conventional sintering. However, at 160ºC, near full densification was not obtained after conventional sintering. After microwave sintering, near full densification was achieved. For example, densities of 92.26%TD and 94.24%TD were obtained after 15 and 30 minutes respectively in samples cold pressed using the higher compaction load and sintered at 160ºC.

From Tables E1-E3 (refer to appendix), it can be seen that a reasonable amount of grain growth has occurred in the samples with a lower green density when conventionally sintered. This is true for all three compositions of 97Sn2Cu1Sb, 94Sn4Cu2Sb and 91Sn6Cu3Sb. The grain sizes of the green compacts were very similar for all of them; ranging from 15.3 μm to 15.5 μm and 14.1 μm to 14.8 μm for the materials cold pressed at 96 MPa and 129 MPa respectively.

It can be seen from Figure 4.24 (a)-(b), the average grain size for the 97Sn2Cu1Sb alloy increased from 23 μm to 26 μm by doubling the sintering time from 60 minutes to 120 minutes at 160ºC. Using a higher sintering temperature (220ºC), the grain size increased from 27 μm to 29 μm (see Figure 4.24 (c)-(d)). A similar observation was found for samples sintered with higher green densities.

Meanwhile, a 94Sn4Cu2Sb alloy composition had slightly smaller grain growth and smaller average grain size. Samples prepared at a lower compaction load and sintered at 160°C in the conventional furnace resulted in a grain growth from 22 μm to 24 μm when the sintering time was doubled from 60 minutes to 120 minutes. When the sintering temperature was increased to 220°C, the average grain size increased from 26 μm to 28 μm. The higher compaction load samples showed similar results. These can be clearly seen in Figure 4.24 (a)-(d).

The alloy with composition 91Sn6Cu3Sb had smaller grain size and slightly reduced grain growth in general. Conventionally sintering a sample with lower green density at 160°C resulted in a grain growth from 20 μm – 23 μm when the sintering time was doubled to 120 minutes. Meanwhile, sintering at 220°C increased the grain size from 25 μm – 28 μm, which is very similar to those described earlier.

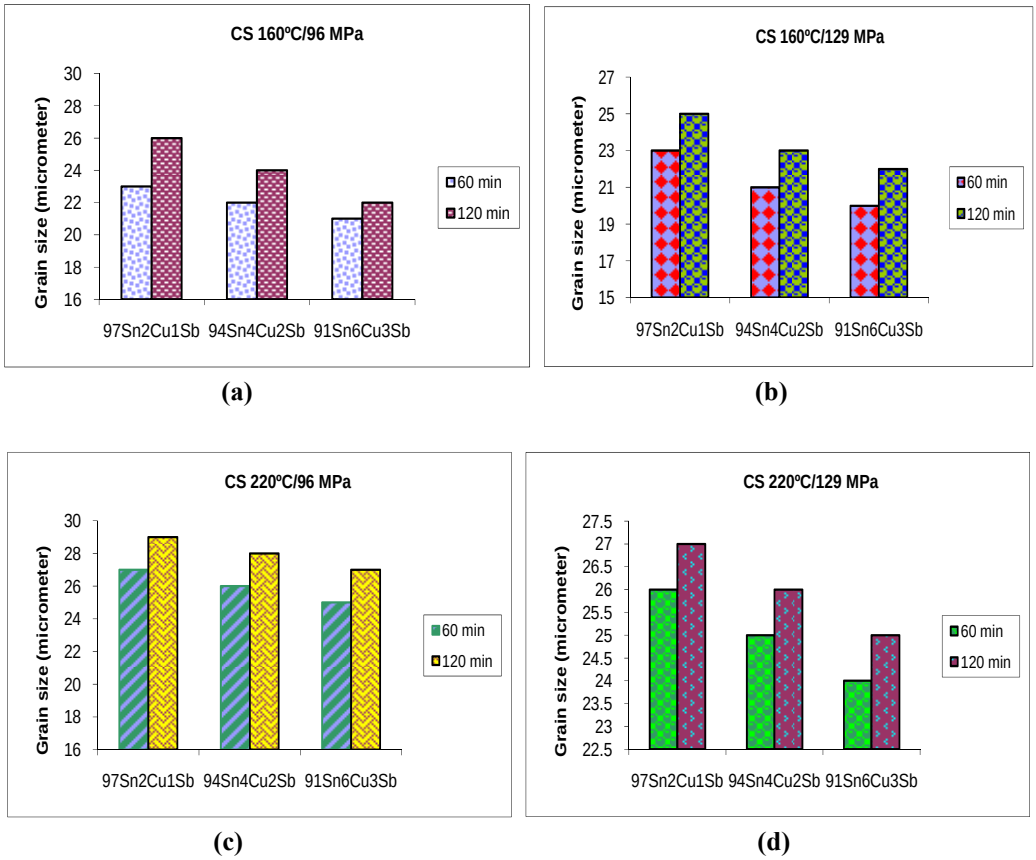

Figure 4.24: Bar charts showing the effect of increasing sintering time and temperature on the grain size for conventional sintered samples for 97Sn2Cu1Sb, 94Sn4Cu2Sb and 91Sn6Cu3Sb compositions

Microwave Sintering

During microwave sintering, the grain growth appeared to be very similar to the grain growth of conventionally sintered samples with increasing sintering time and temperature (see Figure 4.25). An alloy of composition 97Sn2Cu1Sb, cold compacted at 96 MPa, experienced grain growth from an average grain size of 17 µm (sample 97MW1) to 25 µm (sample 97MW4) after microwave sintering with increasing sintering time and temperature. Also, for material cold compacted at 129 MPa, similar observations were noted. Grain growth increased the average grain size from 16 µm (sample 97MW5) to 18 µm (sample 97MW6) after sintering at 160°C and 21 µm (sample 97MW7) to 24 µm (97MW8) after sintering at 220°C.

An alloy of composition 94Sn4Cu2Sb, on the other hand, showed less grain growth compared with alloy composition 97Sn2Cu1Sb. A lower compaction load resulted in slightly more grain growth from an average grain size of 17 µm (sample 94MW1) to 25 µm (sample 94MW4), while the higher compaction load resulted in similar grain growth from 16 µm (sample 94MW5) to 24 µm (sample 94MW8) with increasing sintering time and temperature.

For the alloy composition 91Sn6Cu3Sb, the grain growth during microwave sintering was a little less than that for the alloy with composition 94Sn4Cu2Sb. Material cold compacted at 96 MPa had grain growth from an average grain size of 16µm (sample 91MW1) to 24µm (sample 91MW4) while material cold compacted at 129 MPa had grain growth of 16µm (sample 91MW5) to 23µm (sample 91MW8).

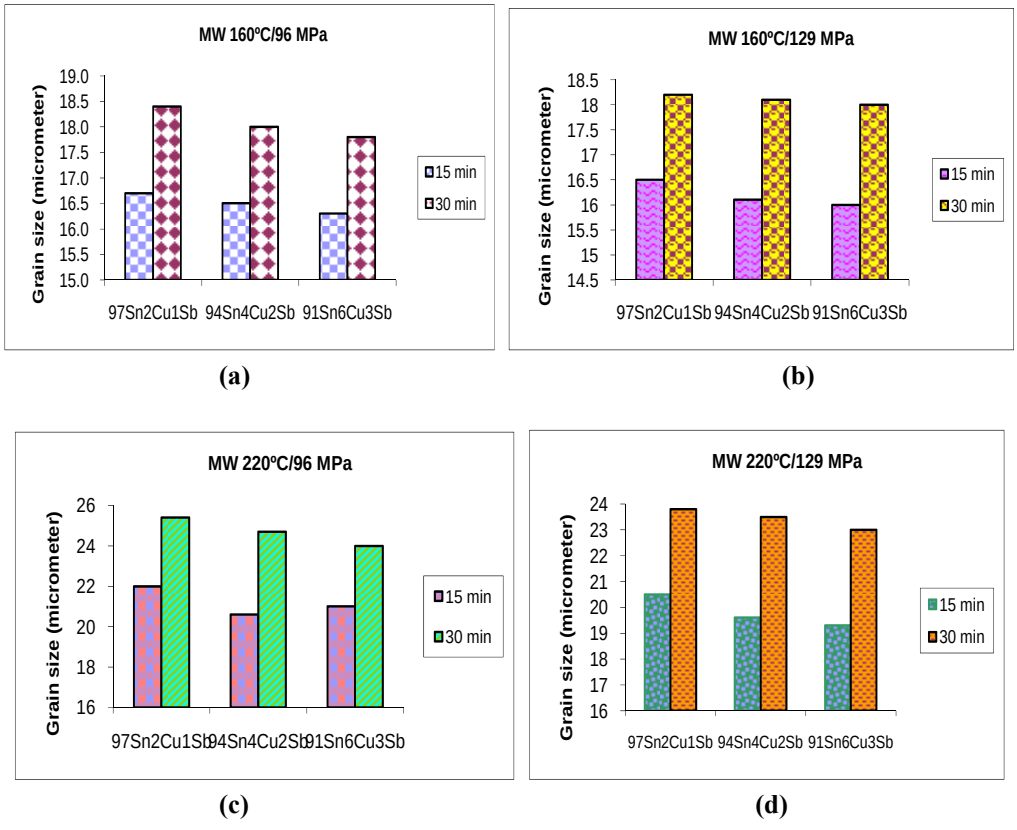

Figure 4.25: Bar charts showing the effect of increasing sintering time and temperature on the grain size for microwave sintered samples for 97Sn2Cu1Sb, 94Sn4Cu2Sb and 91Sn6Cu3Sb compositions

When compared with conventional sintering, microwave sintering resulted in slightly smaller or similar grain growth as can be seen in Figure 4.26. SEM images from Figures 4.12-4.23 revealed that pores are generally smaller in size as the green density, sintering temperature and sintering time increases. This is noticed in all the three compositions; 97Sn2Cu1Sb, 94Sn4Cu2Sb and 91Sn6Cu3Sb. With increasing percentages of Cu and Sb in the tin alloy, the starting grain size is slightly smaller (14.1 μm). This accounts for improved hardness and strength. The grain sizes that appear in conventionally sintered samples are basically very similar (slightly larger) to the grain size obtained in microwave sintered samples (see Figure 4.27).

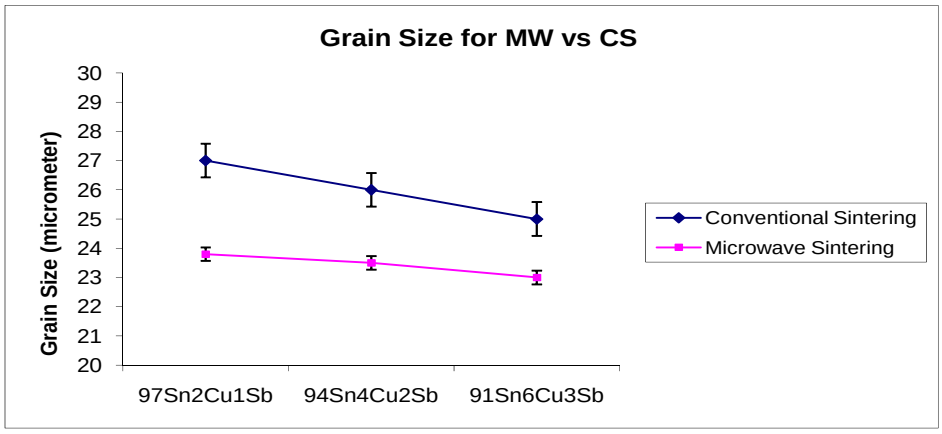

Figure 4.26: Graph of grain size for microwave (30 min) and conventional (120 min) sintered samples for 97Sn2Cu1Sb, 94Sn4Cu2Sb and 91Sn6Cu3Sb compositions pressed at 129 MPa and sintered at 220°C

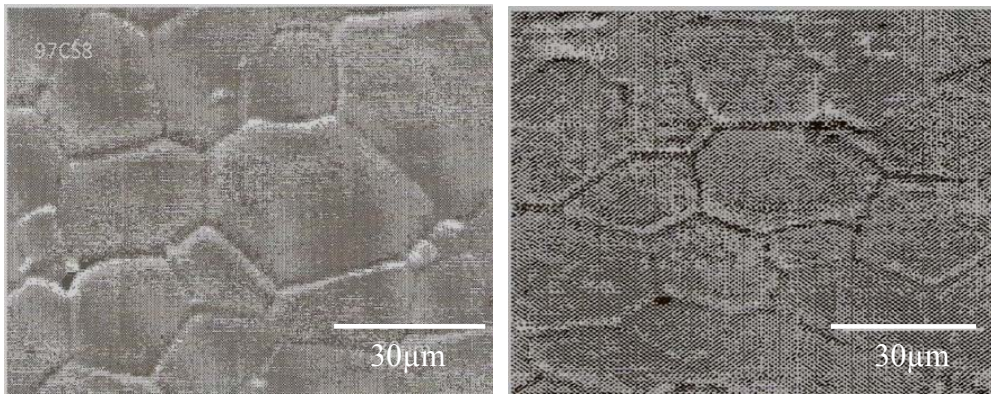

(a) **(b)**

Figure 4.27: Micrographs showing a (a) conventionally sintered sample (120 min) and (b) microwave sintered sample (30 min) for 91Sn6Cu3Sb alloy pressed at 129 MPa and sintered at 220°C

Electron Dispersive X-Ray Spectroscopy (EDS)

EDS was performed on all the tin alloy compositions for each individual sample for the purpose of determining the elemental composition at various selected points. The compositional values obtained are given as percentages and are tabulated accordingly to show the degree to which Cu and Sb have diffused into the base material (Sn). Additionally, the EDS spectrums from an area scan done on the sample have also been included. These EDS spectra reveal the peak of every element detected. This was further verified with the X-Ray maps to clearly see the distribution of Cu and Sb in the alloy. The effects of sintering time, sintering temperature, compaction load and sintering method on the diffusion process were analyzed.

Green Compact

Green compacts pressed at 96 MPa and 129 MPa showed evidence of a homogeneous distribution of Sb which occurred during the mixing process for all three compositions. This can be clearly seen from the X-Ray maps in Figure 4.28. This is further justified by the EDS report from the SEM images (see Figure 4.29) in Tables 4.1-4.3 where the percentages of Sb detected for the three compositions were in the range of 3% or less. This does not indicate any signs of diffusion taking place but indicates a fairly homogeneous distribution of the Sb in the tin alloy. The EDS spectrums (see Figure 4.30) also indicate the presence of tin, copper and antimony in the sample.

The distribution of Cu, on the other hand, did not seem as uniform as the distribution of Sb in all three compositions of 97Sn2Cu1Sb, 94Sn4Cu2Sb and 91Sn6Cu3Sb. The X-Ray maps in Figure 4.28 show some prominent Cu rich areas which have not been uniformly distributed. The EDS report shows evidence of elemental Cu and Sb in green compacts produced at 96 MPa and 129 MPa, which is a clear indication that diffusion has not yet taken place, which is expected since compacts are still in the green and unsintered form.

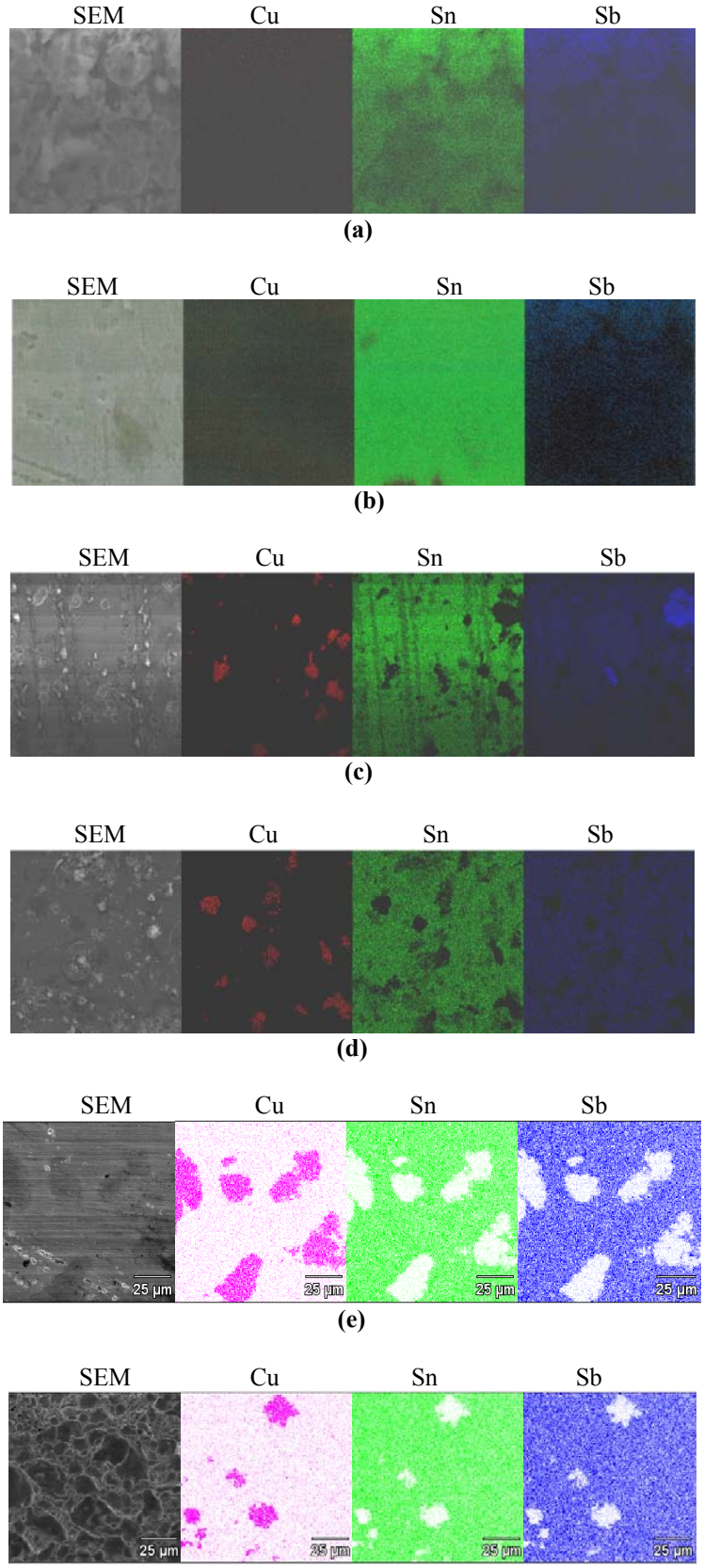

Figure 4.28: X-Ray map of (a) 96 MPa (b) 129 MPa green compact for 97Sn2Cu1Sb composition (c) 96 MPa (d) 129 MPa green compact for 94Sn4Cu2Sb composition (e) 96 MPa (f) 129 MPa for 91Sn6Cu3Sb composition

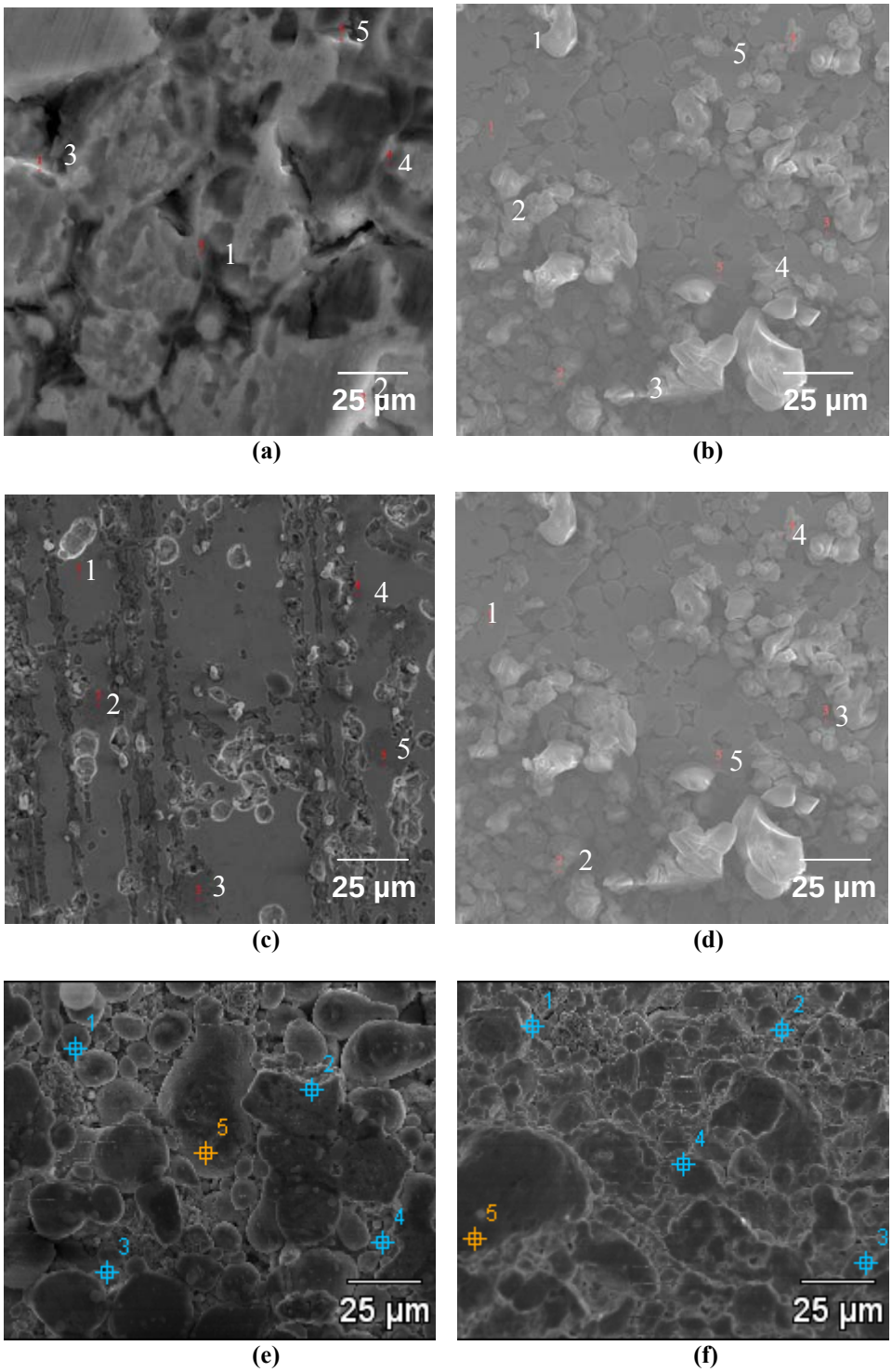

Figure 4.29: SEM image of (a) 96 MPa (b) 129 MPa pressed green compact for 97Sn2Cu1Sb composition (c) 96 MPa (d) 129 MPa pressed green compact for 94Sn4Cu2Sb composition (e) 96 MPa (f) 129 MPa pressed green compact for 91Sn6Cu3Sb composition

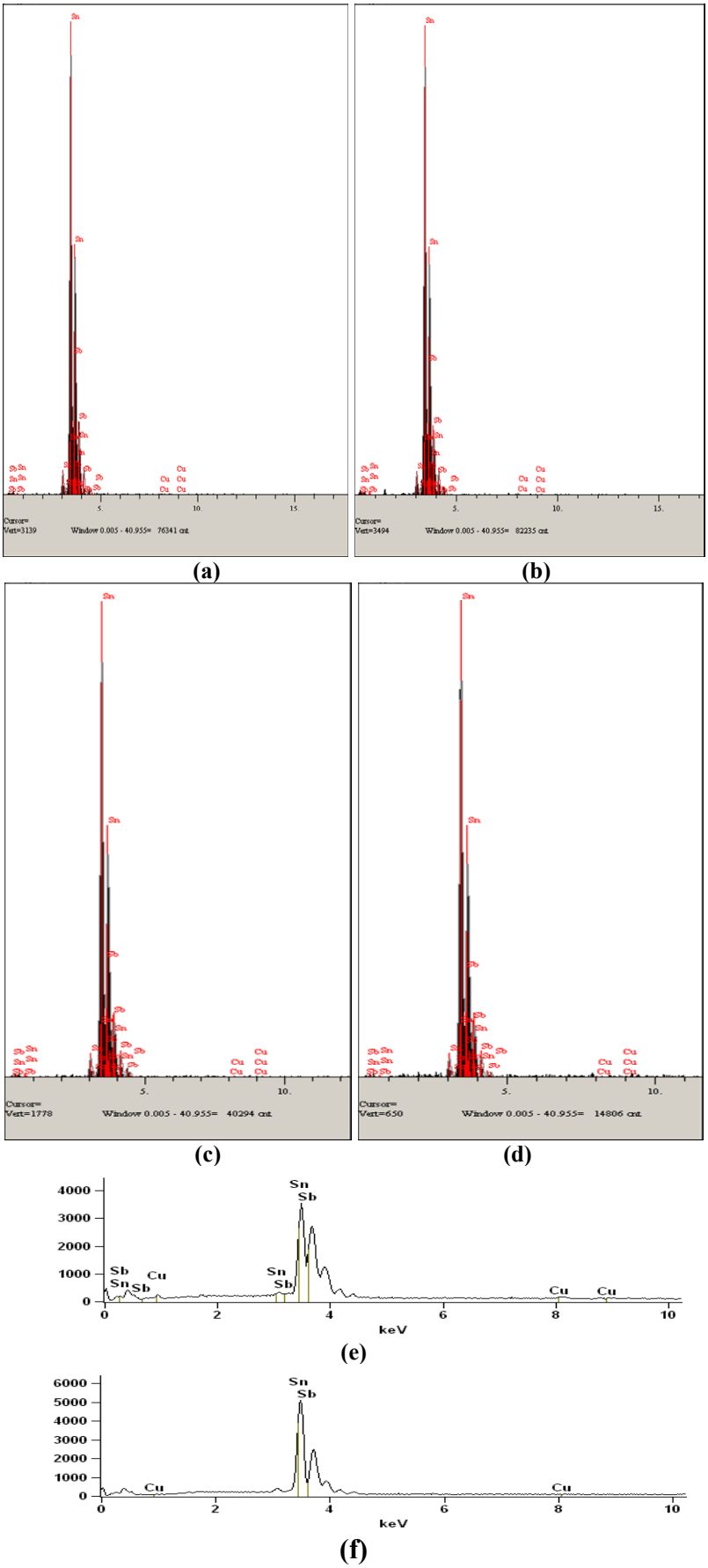

Figure 4.30: EDS Spectrum from an area scan for (a) 96 MPa (b) 129 MPa green compact for 97Sn2Cu1Sb composition (c) 96 MPa (d) 129 MPa green compact for 94Sn4Cu2Sb composition (e) 96 MPa (f) 129 MPa for 91Sn6Cu3Sb composition

Table 4.1: EDS report for green compact of 97Sn2Cu1Sb composition

	weight%		
	Cu-K	Sn-L	Sb-L
97Sn green 96 MPa_pt1	1.79	97.23	0.98
97Sn green 96 MPa_pt2	1.83	97.21	0.96
97Sn green 96 MPa_pt3	1.87	97.18	0.95
97Sn green 96 MPa_pt4	1.93	97.11	0.96
97Sn green 96 MPa_pt5	1.89	97.18	0.93
97Sn green 129 MPa_pt1	1.96	97.06	0.98
97Sn green 129 MPa_pt2	1.95	97.11	0.94
97Sn green 129 MPa_pt3	1.92	97.17	0.91
97Sn green 129 Mpa_pt4	1.90	97.19	0.91
97Sn green 129 MPa_pt5	1.95	97.06	0.99

Table 4.2: EDS report for green compact of 94Sn4Cu2Sb composition

	weight%		
	Cu-K	Sn-L	Sb-L
94Sn green 96 MPa_pt1	3.87	94.23	1.90
94Sn green 96 MPa_pt2	3.96	94.24	1.80
94Sn green 96 MPa_pt3	3.65	94.46	1.89
94Sn green 96 MPa_pt4	3.94	94.21	1.85
94Sn green 96 MPa_pt5	3.82	94.21	1.97
94Sn green 129 MPa_pt1	3.81	94.24	1.95
94Sn green 129 MPa_pt2	3.79	94.32	1.89
94Sn green 129 MPa_pt3	3.89	94.22	1.89
94Sn green 129 Mpa_pt4	3.76	94.28	1.96
94Sn green 129 MPa_pt5	3.94	94.26	1.80

Table 4.3: EDS report for green compact of 91Sn6Cu3Sb composition

	weight%		
	Cu-K	Sn-L	Sb-L
91Sn green 96 MPa_pt1	5.88	91.27	2.85
91Sn green 96 MPa_pt2	5.83	91.22	2.95
91Sn green 96 MPa_pt3	5.72	91.29	2.99
91Sn green 96 MPa_pt4	5.76	91.39	2.85
91Sn green 96 MPa_pt5	5.84	91.27	2.89
91Sn green 129 MPa_pt1	5.89	91.49	2.62
91Sn green 129 MPa_pt2	5.73	91.29	2.98
91Sn green 129 MPa_pt3	5.95	91.31	2.74
91Sn green 129 Mpa_pt4	5.87	91.32	2.81
91Sn green 129 MPa_pt5	5.87	91.27	2.86

Conventional vs. microwave sintering

The X-Ray maps in Figure 4.31 and Figure 4.32 were obtained for conventionally sintered materials (for all three compositions) pressed at 96MPa and sintered at 160ºC and 220ºC respectively. Meanwhile, the X-Ray maps for samples pressed at 129 MPa are shown in Figure 4.33 (160ºC) and Figure 4.34 (220ºC). Both compaction loads reveal similar distributions from the elemental maps, particularly Sn and Sb which appeared to be homogeneously distributed throughout the sample. Cu on the other hand, is reasonably well distributed although there are small clusters of Cu visible in certain parts of the sample particularly for 97Sn2Cu1Sb and 94Sn4Cu2Sb alloys. However, a more homogeneous Cu distribution has been observed in 91Sn6Cu3Sb composition when compared with 97Sn2Cu1Sb and 94Sn4Cu2Sb compositions. This may be due to the fact that a larger amount of Cu (6%) was used and this resulted in a better distribution during mixing.

Similar observations were noticed in microwave sintered samples (see Figures 4.35 - 4.38) when compared with conventionally sintered samples under the same sintering conditions. However, a lesser degree of homogenization of Cu is noticed for the microwave sintered samples when compared with the conventional sintered samples. By increasing the sintering time and temperature, a more homogeneous distribution of Cu is found. The EDS report (refer to Tables F1- F24 in the appendix) obtained from elemental spot analysis performed on these samples (refer to Figures F1- F16 in the appendix) further justifies the distribution of each element.

These X-Ray maps are not evidence to justify diffusion of Cu and Sb into Sn since the green compact had also revealed similar observations and EDS readings. Thus, at this stage, EDS was used as a tool to verify the distribution of each element in the alloy. Diffusion of Cu and Sb into Sn are verified through X-Ray Diffraction (refer to XRD section, page 101).

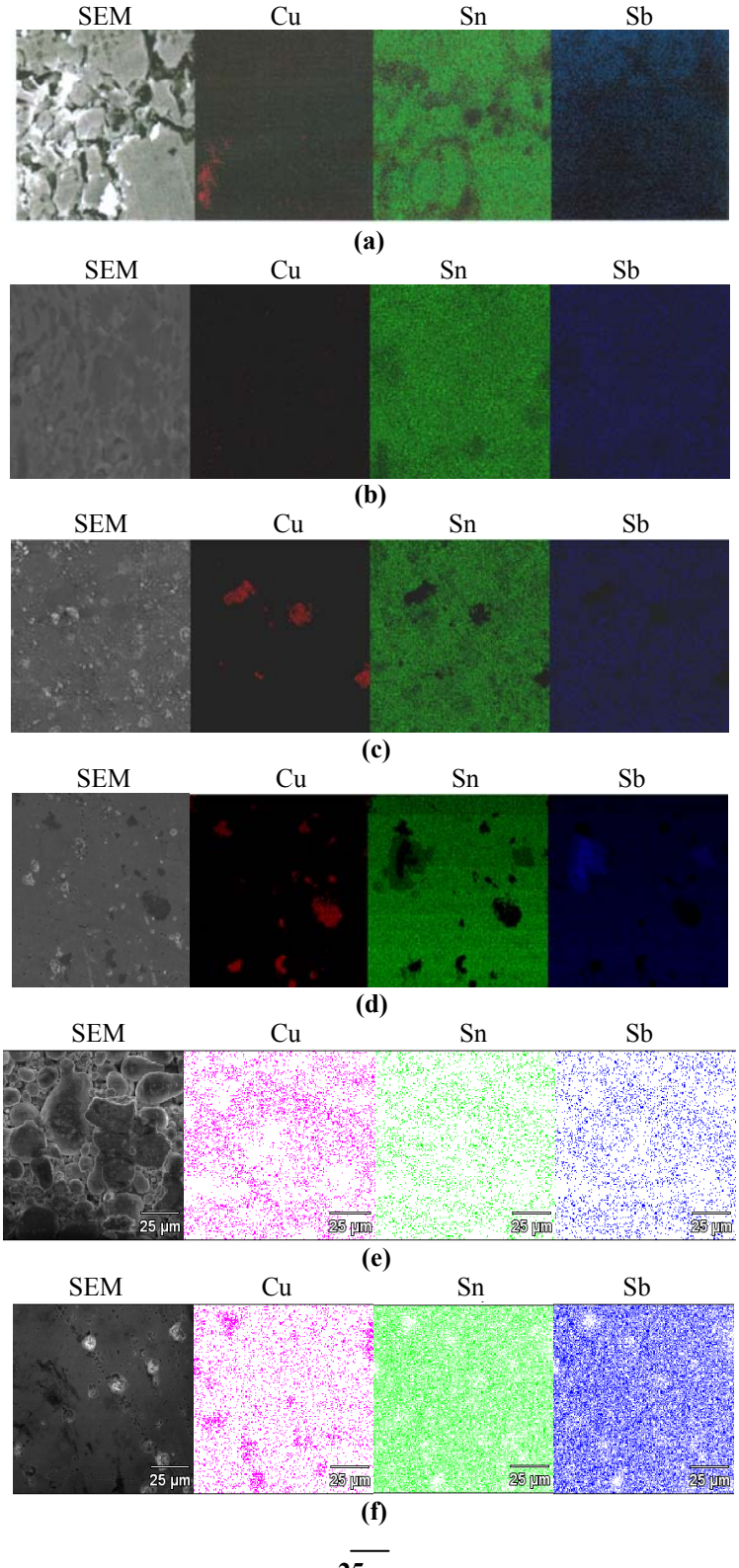

Figure 4.31: X-Ray map for CS samples 96 MPa/160°C (a) 60 min (b) 120 min for 97Sn2Cu1Sb composition (c) 60 min (d) 120 min for 94Sn4Cu2Sb composition (e) 60 min (f) 120 min for 91Sn6Cu3Sb composition

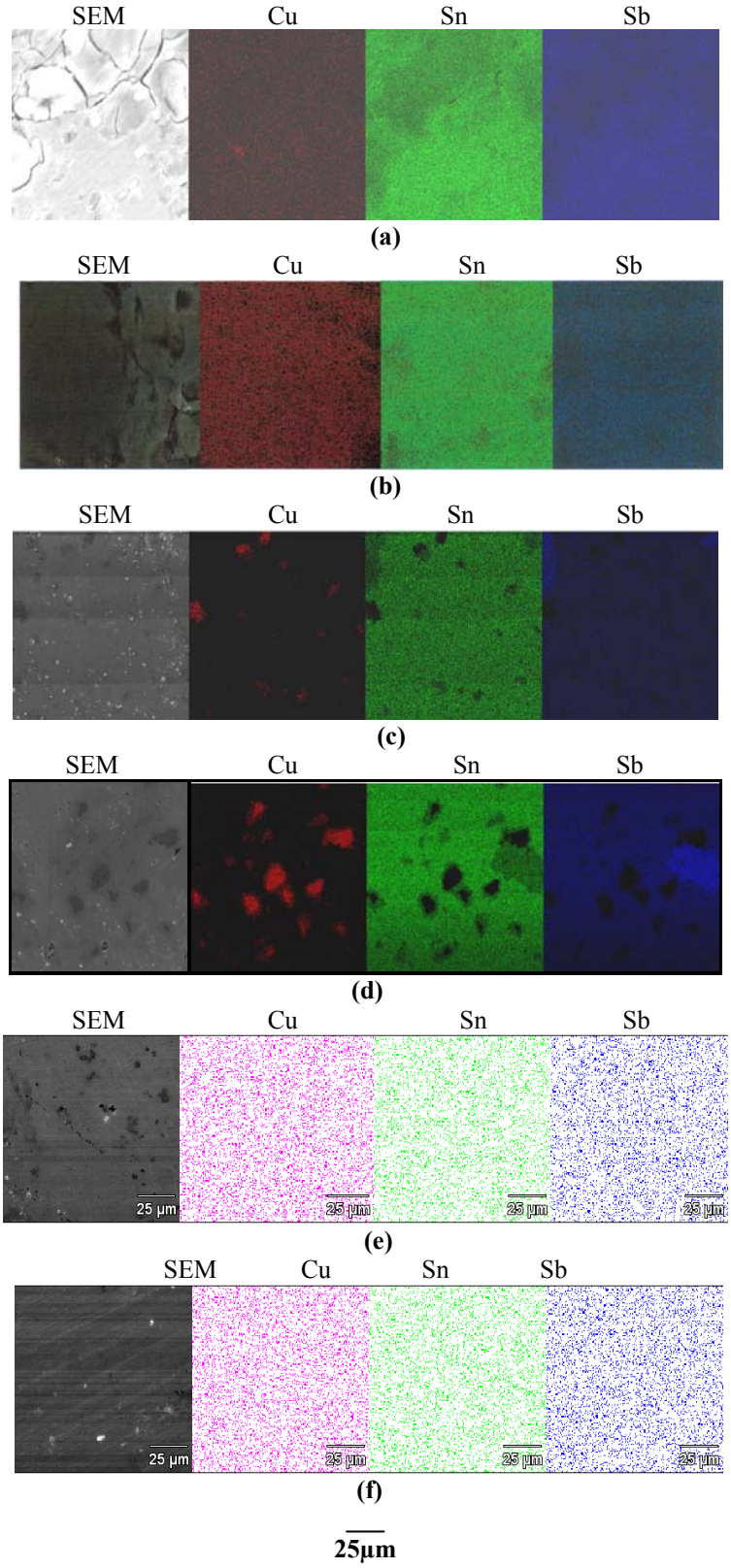

Figure 4.32: X-Ray map for CS samples 96 MPa/220°C (a) 60 min (b) 120 min for 97Sn2Cu1Sb composition (c) 60 min (d) 120 min for 94Sn4Cu2Sb composition (e) 60 min (f) 120 min for 91Sn6Cu3Sb composition

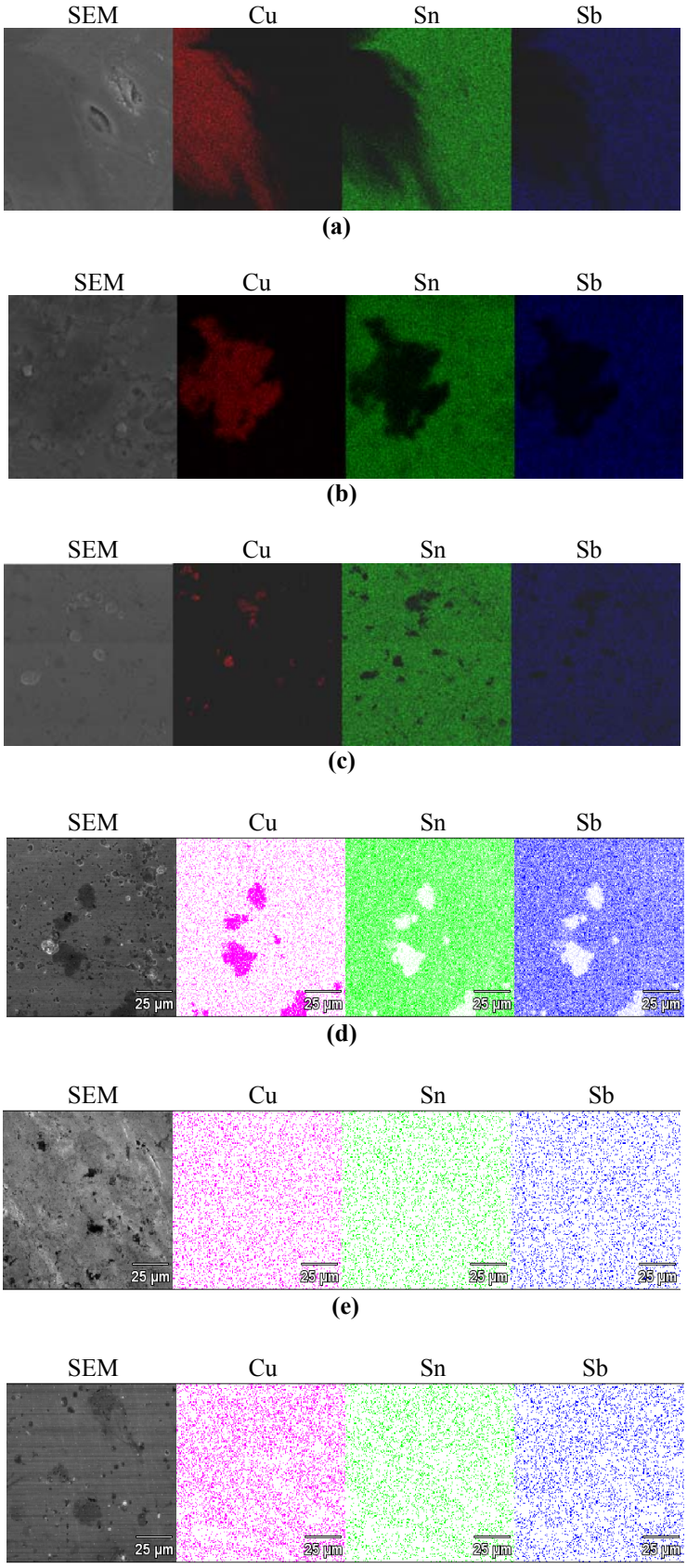

Figure 4.33: X-Ray map for CS samples 129 MPa/160°C (a) 60min (b) 120min for 97Sn2Cu1Sb composition (c) 60min (d) 120min for 94Sn4Cu2Sb composition (e) 60min (f) 120 min for 91Sn6Cu3Sb composition

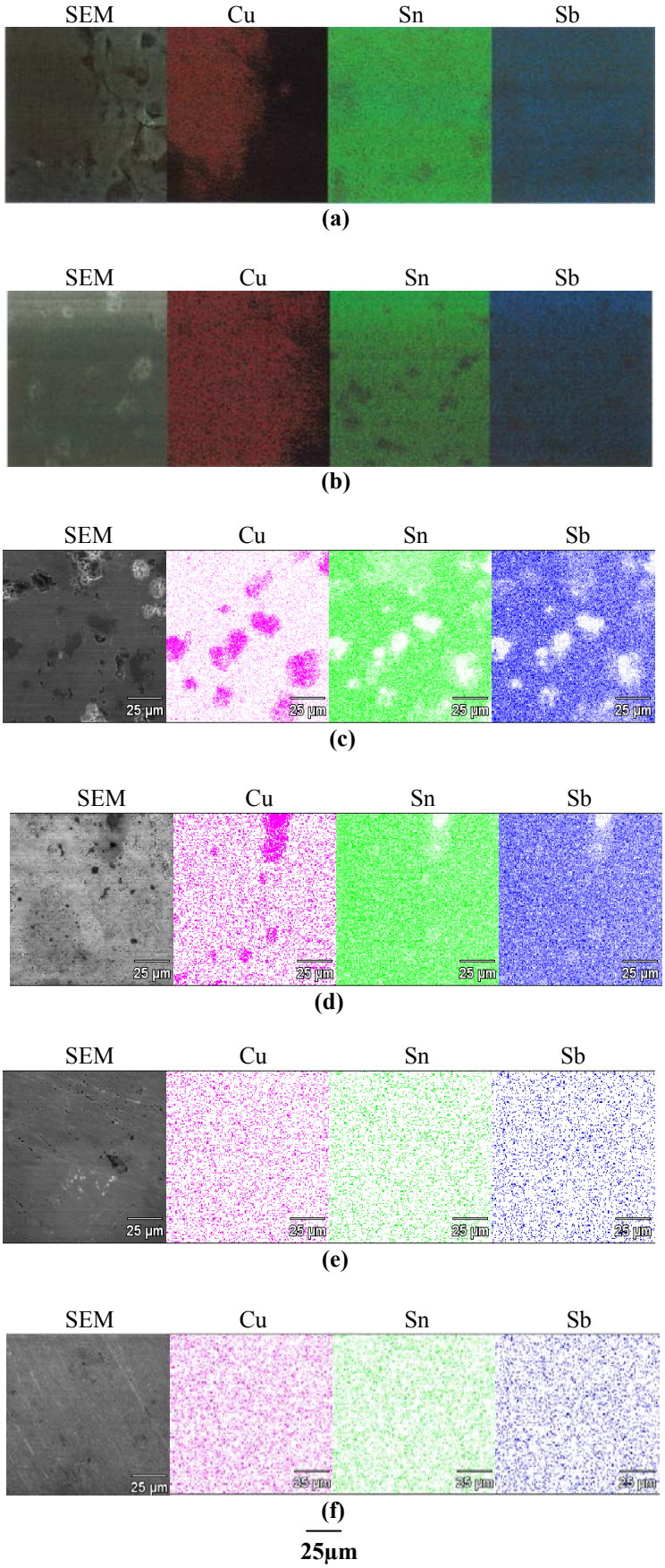

Figure 4.34: X-Ray map for CS samples 129 MPa/220°C (a) 60min (b) 120min for 97Sn2Cu1Sb composition (c) 60min (d) 120min for 94Sn4Cu2Sb composition (e) 60min (f) 120 min for 91Sn6Cu3Sb composition

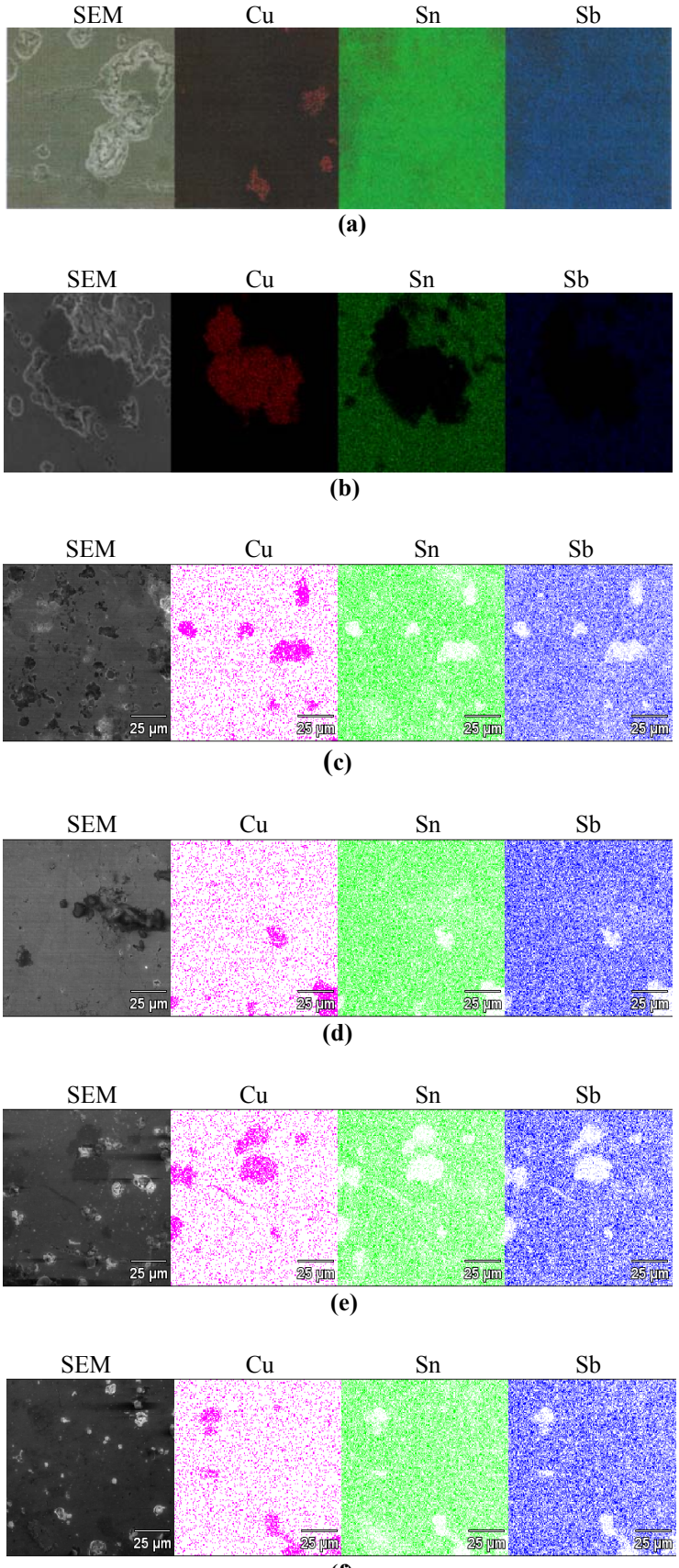

Figure 4.35: X-Ray map for MW samples 96 MPa/160°C (a) 15min (b) 30min for 97Sn2Cu1Sb composition (c) 15min (d) 30min for 94Sn4Cu2Sb composition (e) 15min (f) 30 min for 91Sn6Cu3Sb composition

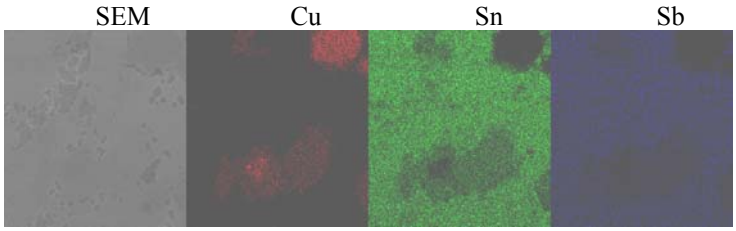

(a)

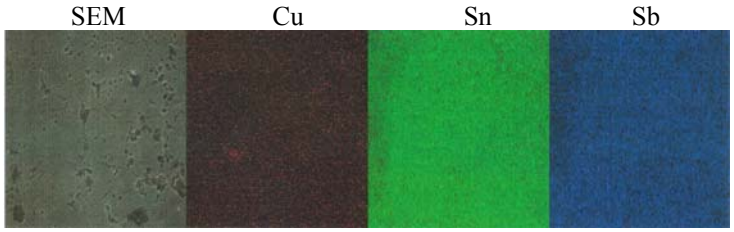

(b)

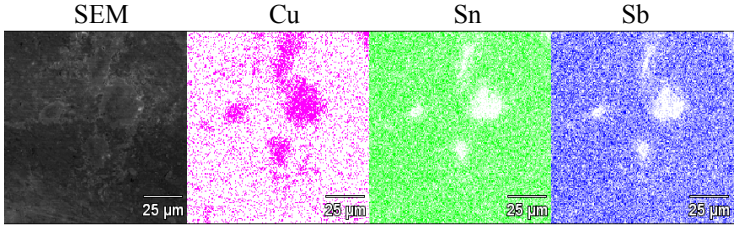

(c)

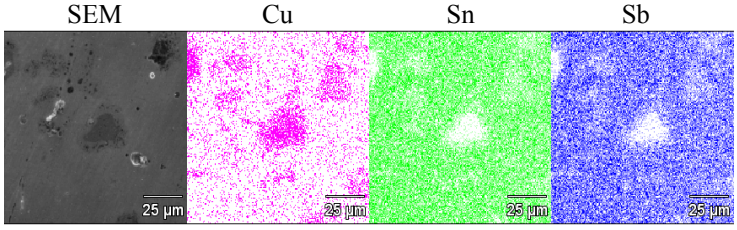

(d)

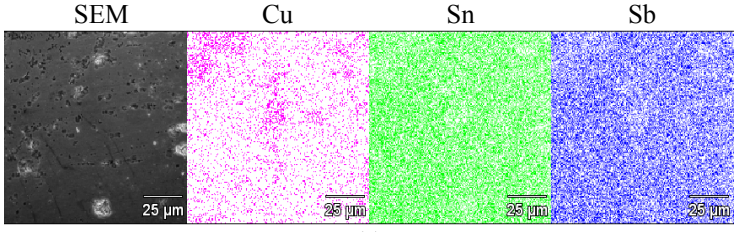

(e)

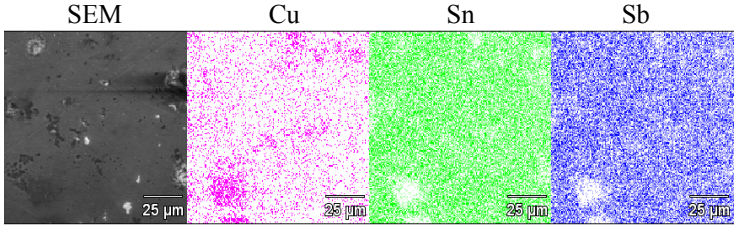

(f)

25µm

Figure 4.36: X-Ray map for MW samples 96 MPa/220°C (a) 15min (b) 30min for 97Sn2Cu1Sb composition (c) 15min (d) 30min for 94Sn4Cu2Sb composition (e) 15min (f) 30 min for 91Sn6Cu3Sb composition

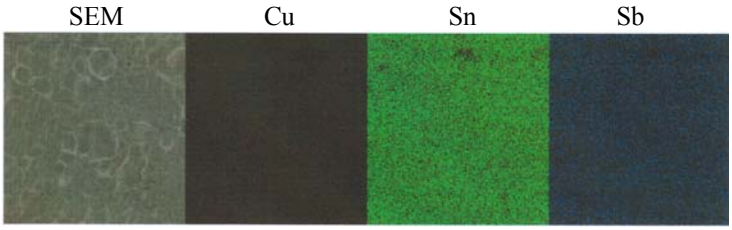

(a)

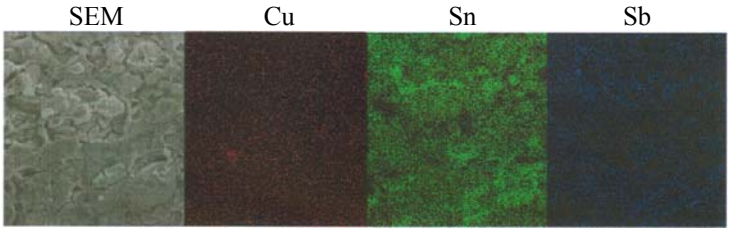

(b)

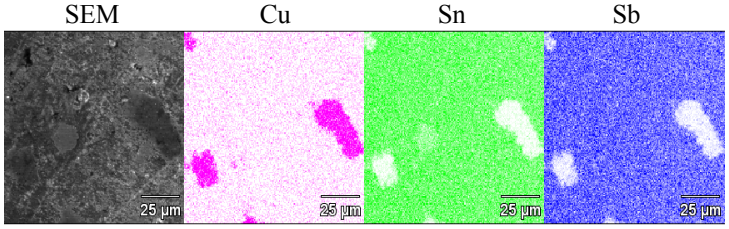

(c)

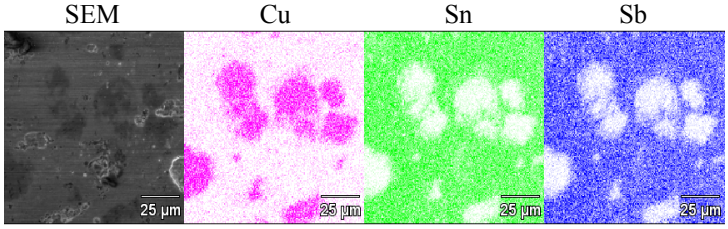

(d)

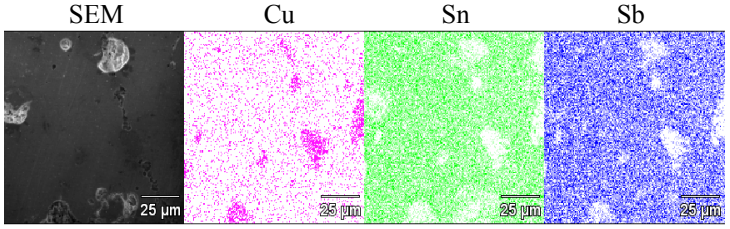

(e)

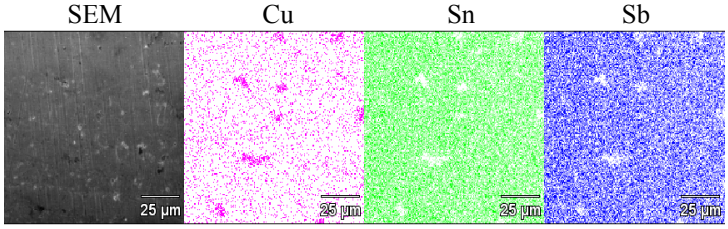

(f)

25µm

Figure 4.37: X-Ray map for MW samples 129 MPa/160°C (a) 15min (b) 30min for 97Sn2Cu1Sb composition (c) 15min (d) 30min for 94Sn4Cu2Sb composition (e) 15min (f) 30 min for 91Sn6Cu3Sb composition

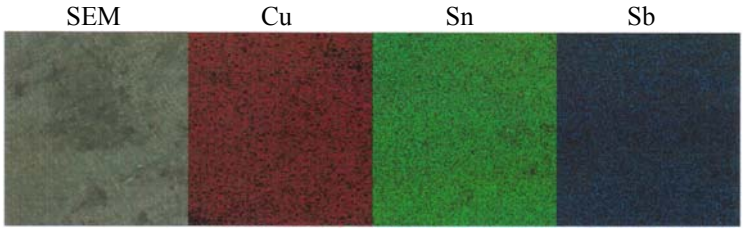

(a)

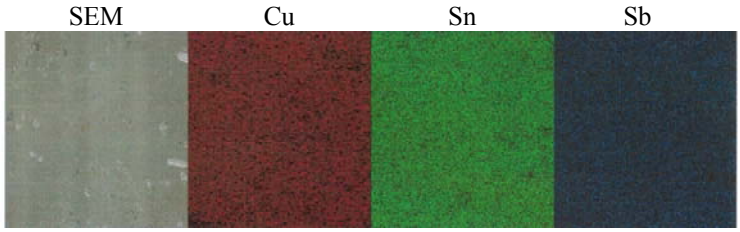

(b)

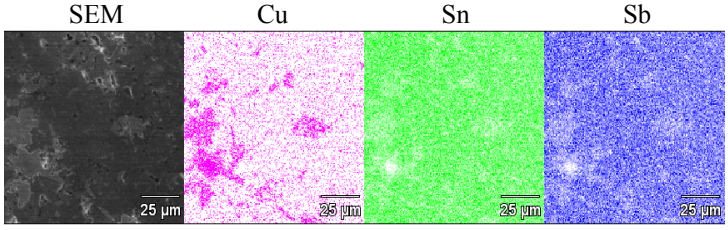

(c)

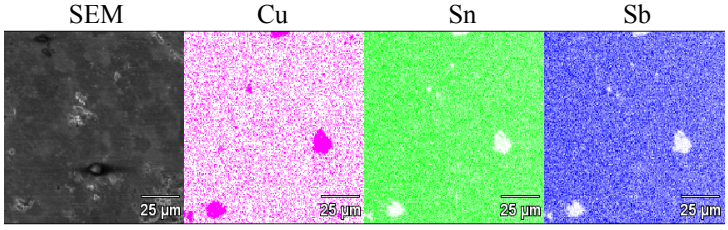

(d)

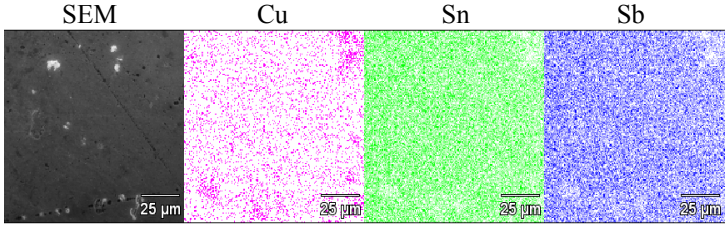

(e)

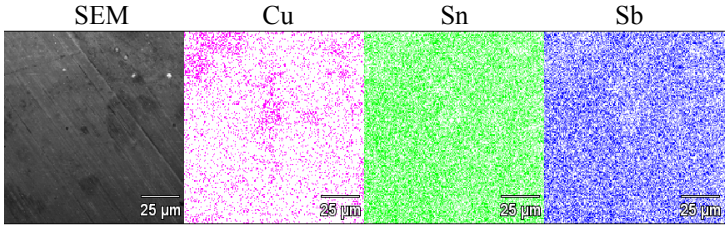

(f)

25µm

Figure 4.38: X-Ray map for MW samples 129 MPa/220°C (a) 15min (b) 30min for 97Sn2Cu1Sb composition (c) 15min (d) 30min for 94Sn4Cu2Sb composition (e) 15min (f) 30 min for 91Sn6Cu3Sb composition

X-Ray Diffraction (XRD)

This section presents data from XRD analysis which is used for identifying the elements present within the samples and also to determine if any new phases are present in the alloys after the sintering process has been completed.

Green compacts

Figure 4.39 shows the XRD peaks for the mixed tin alloy powder for all three compositions of 97Sn2Cu1Sb, 94Sn4Cu2Sb and 91Sn6Cu3Sb. Sn peaks are the most prominent ones for all the three compositions since it is a Sn-based alloy. Additionally, Sb and Cu peaks appear to be visible in all of the compositions because Cu and Sb still exist in their elemental form at this stage, since the Sb and Cu atoms have not diffused during the compaction process. Similar peak patterns were obtained from the green compacts for both compaction loads (refer to Figures G1 – G3 in the appendix).

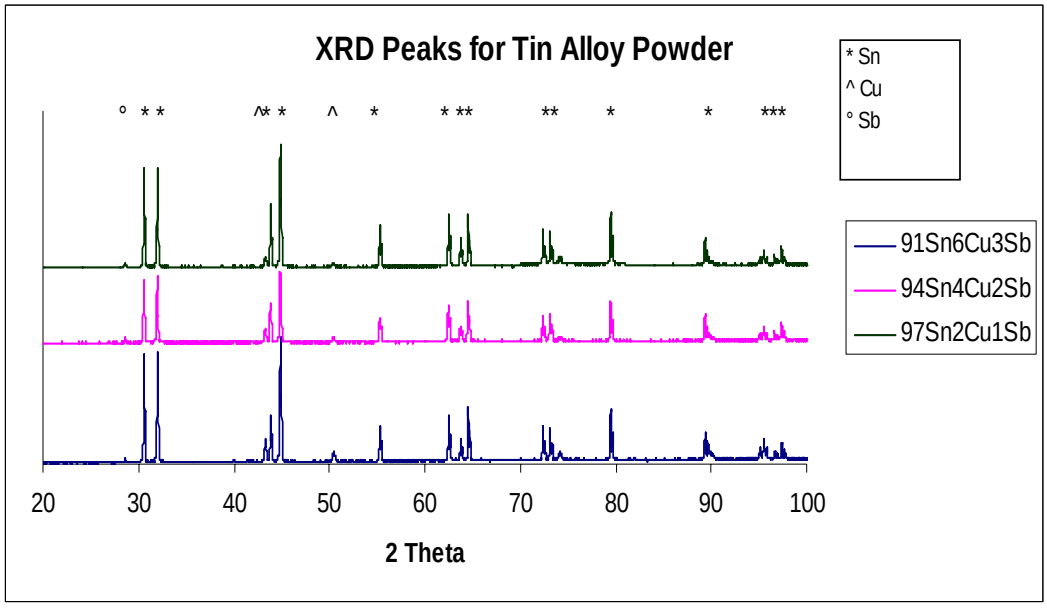

Figure 4.39: XRD peaks for the mixed 91Sn6Cu3Sb, 94Sn4Cu2Sb and 97Sn2Cu1Sb tin alloy powder before compaction

Conventional vs. Microwave Sintering

From Figure 4.40, the XRD peaks for conventional sintering at 160ºC and 220ºC showed similar patterns for all the samples at different sintering times (60 min and 120 min). Since this alloy is a Sn based alloy, only Sn peaks are prominent. Sb atoms completely diffused during the sintering process. This explains why Sb peaks at 2θ value of 28º were not visible at all in the sintered samples. Cu peaks are relatively small, as expected from the small weight percentage in the alloys. The Cu peaks at 2θ values of 43º and 52º were observed to have gradually decreased in its intensity after sintering at 160ºC for 120 minutes.

However, when sintered at 220ºC, the Cu peaks eventually disappeared after sintering for 120 minutes. The higher sintering temperature and longer sintering time results in better diffusion of Cu into the Sn lattice. The XRD results for microwave sintered materials (see Figure 4.41) were similar to those observed in conventionally sintered materials. A reasonably uniform distribution of Sb was found in the tin alloy powder after mixing (from X-Ray maps and EDS reports). However, during cold compaction, there is no evidence of Sb diffusing into Sn. It was evident that the Cu alloying addition formed a solid solution with the Sn. The Sb probably went into solid solution also, but there was no clear XRD evidence to support this.

As for Cu, very small peaks (with decreased intensities) were noticed at 2θ values of 43° and 52°. These Cu peaks were still prominent after microwave sintering at 160ºC as can be seen in Figure 4.41. The peaks did not disappear even after sintering for 30 minutes. However, when microwave sintered at a higher temperature (220ºC), Cu peaks were not visible at all even after sintering for 15 minutes. However, the Cu peaks eventually disappeared with increasing sintering time and temperature. Cu atoms had gradually diffused into Sn lattice and formed a Sn based solid solution with a tetragonal structure. A slight shift in the Sn peaks to smaller angles (to the left in the range of 0.2-0.3°) was noticed for the microwave sintering, while for the conventional sintering, the shift was even smaller than that of microwave sintering (see Figure 4.42). The shift in Sn peaks may be due to the fact that the lattice parameter of the Sn has increased as a result

of the diffusion process of Sb and Cu into Sn. The larger angles of shift in Sn peaks for the microwave sintering justifies that solid solution formation is more pronounced after microwave sintering due to more efficient heating.

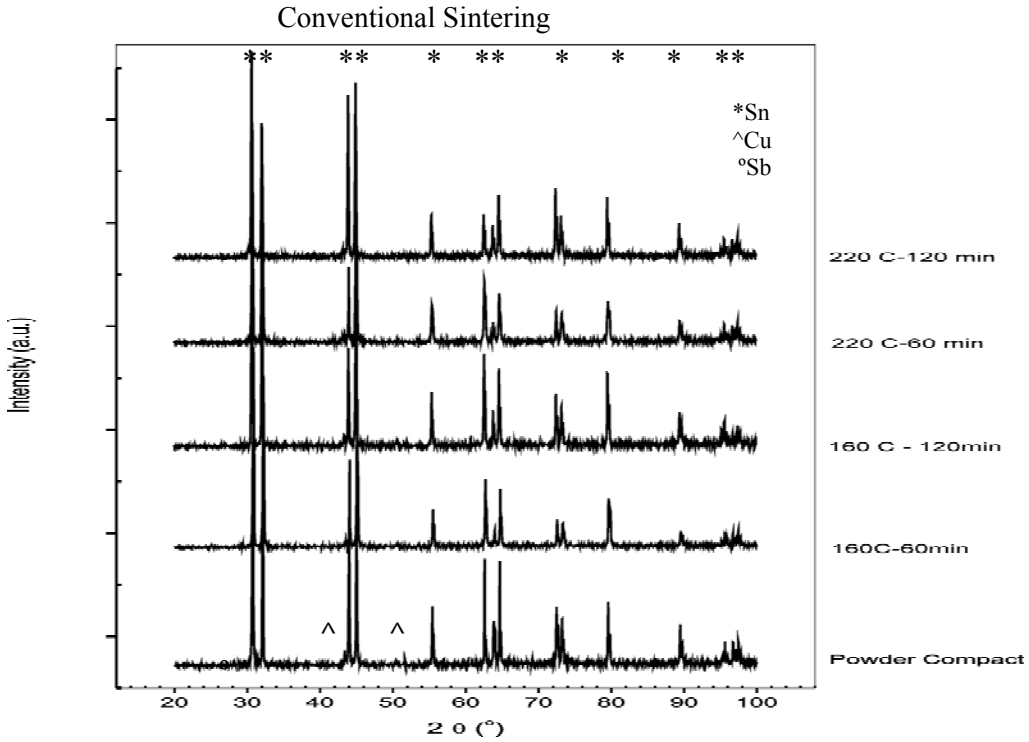

Figure 4.40: XRD peaks comparing different sintering temperatures and sintering times for conventionally sintered 97Sn2Cu1Sb alloy pressed at 129 MPa

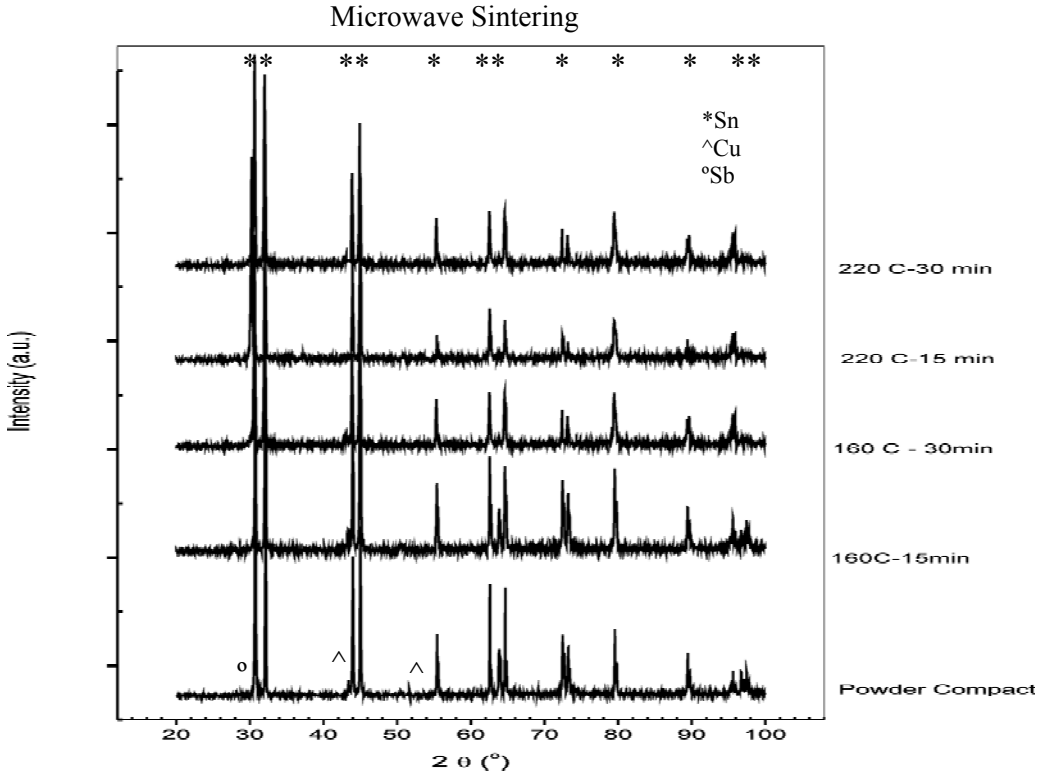

Figure 4.41: XRD peaks comparing different sintering temperatures and sintering times for microwave sintered 97Sn2Cu1Sb alloy pressed at 129 MPa

The XRD peaks for all the other sintered samples for both microwave and conventional sintering have similar peak patterns (refer to Figures G4-G13 at the appendix). However, with different compositions; increasing Cu and Sb content, the shift appeared to be slightly more (~0.5°). From the XRD peaks it was evident that none of the additional phases seen in cast pewter were formed in both microwave and conventionally sintered material. This is further verified by the Sn-Cu-Sb phase diagrams in Figures J1-J3 (refer to appendix) where sintering below the melting point of Sn (232°C) does not form this additional new phase (Cu_6Sn_5). However, for the cast pewter from Royal Selangor, Cu_6Sn_5 (refer to Figure K5 – K6 in the appendix) is formed within the pewter due to higher casting temperature in the range of 275 – 315°C.

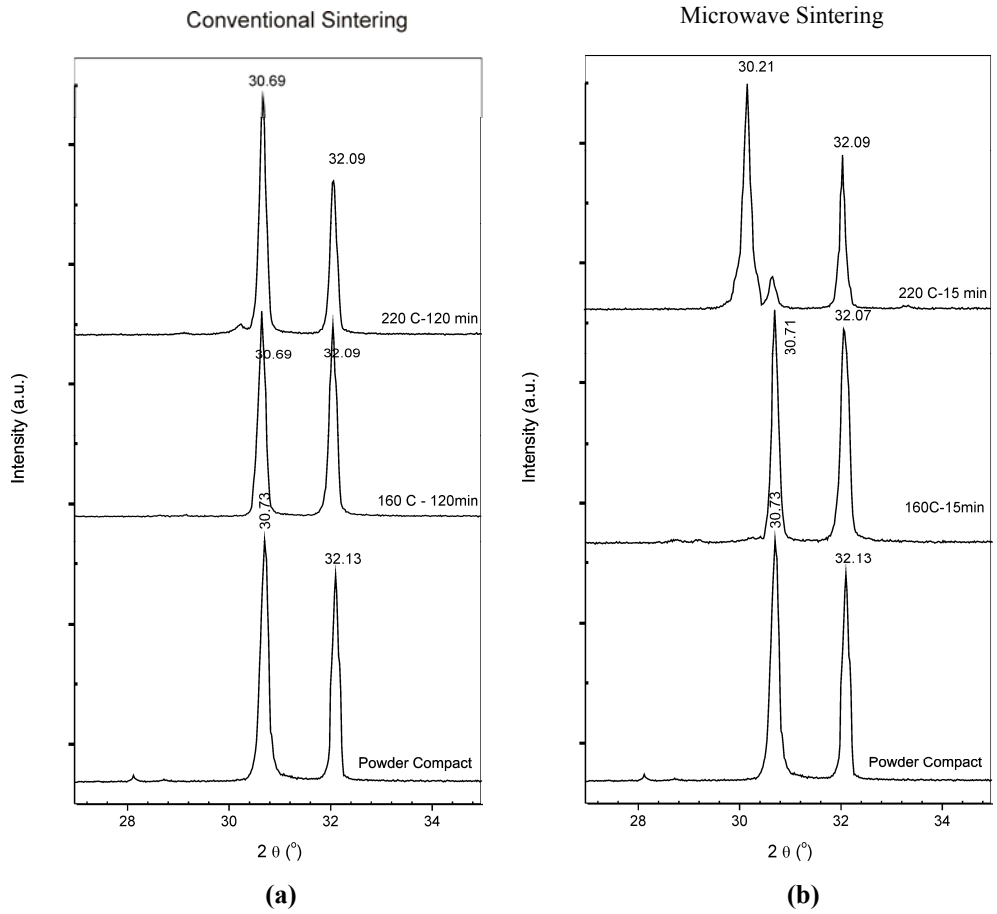

Figure 4.42: Shift in XRD peaks for (a) conventionally sintered and (b) microwave sintered 97Sn2Cu1Sb alloy pressed at 129 MPa at different sintering times

4.2.3 Diffusion Couple Experiments

This section aims to discuss the efficacy of microwave sintering in promoting diffusion, based on separate experiments with Cu-Sn couples and Sb-Sn couples, in order to study the diffusion process at the interface of Cu into Sn and Sb into Sn under various sintering conditions. The most influential parameters to take into account for this part of the study are the sintering time and sintering method i.e. conventional or microwave sintering.

Theory

1. It is well known that for diffusion of a couple in this case Cu-Sn and Sb-Sn, the concentration gradient at a specific point along the diffusion path and the diffusion flux changes with time, t. This is a non-steady state condition because the diffusion profile is time dependent. In this experiment, assuming diffusion into a body from a constant surface source along one dimension, after diffusion for time t, the concentration at a distance x from the surface is [119];

$$\frac{C_x - C_o}{C_s - C_o} = 1 - erf\left(\frac{x}{2\sqrt{Dt}}\right) \quad \textbf{(4.1)}$$

where C_o= initial bulk concentration of the diffusing species ,
C_s = constant surface concentration of the diffusing species and
C_x = concentration at distance x from the interface.
Then modifying it by taking $C_0 = 0$ and C/Cs = concentration of solute atoms' in this case Cu or Sb respectively would give;

$$erf\left(\frac{x}{2\sqrt{Dt}}\right) = 1 - \frac{C}{C_s} \quad \textbf{(4.2)}$$

2. The error function is given by [119];

$$erf(z) = \frac{2}{\sqrt{\pi}} \int_{o}^{z} e^{-(x^2)} \quad \textbf{(4.3)}$$

By taking;

$$z = \frac{x}{2\sqrt{Dt}} \quad \textbf{(4.4)}$$

and plotting the data obtained into a graph of z against x, the diffusion coefficient, *D* can be determined graphically from the slope;

$$slope = \frac{1}{2\sqrt{Dt}} \quad \textbf{(4.5)}$$

3. The coefficient of diffusion, *D* is assumed to be constant at a fixed temperature and can be calculated for comparison purpose using the Arrhenius equation [119];

$$D = A \exp(-Q/RT) \quad \textbf{(4.6)}$$

where A = pre-exponential constant;
(A_{Cu} = 2.4 x 10^{-3} cm^2/s and A_{Sb}= 73 cm^2/s)
Q = energy required to create a point defect and for the point defect to move;
(Q_{Cu}= 33.1kJ/mol and Q_{Sb}=123.1kJ/mol)
R = Gas constant = 8.314472 J/K.mol
T = temperature in Kelvin (493K)

Diffusion Analysis

Figure 4.43 shows the Cu-Sn and Sb-Sn couples in the interface region from which EDS was used to study the concentration of the atoms diffused into Sn across the interface. The values of the elemental concentrations for the Cu and Sb at these points are plotted into Figures 4.44 and 4.45 respectively. An experimental value for the coefficient of diffusion for Cu and Sb has been determined graphically from the slope of the graphs in Figures 4.46 and 4.47 and by using Equation 4.5 for both conventional and microwave sintering for 15 minutes and 30 minutes respectively. These values are tabulated in Table 4.4. The results of this experimental work shown in Figures 4.44 and 4.45 give similar profiles for both Cu and Sb diffusion in Sn after microwave and conventional sintering for both time periods investigated. This indicates that microwave sintering is capable of achieving the same degree of diffusion after the same time as conventional sintering.

The activation energy for Cu and Sb were assumed to be constant in this case since the temperature was fixed at 220°C. It was observed that the diffusion rate of Cu and Sb in Sn from microwave heating was very similar to that obtained from conventional heating. From Table 4.4, it can be summarized that the average value for the coefficient of diffusion for Cu and Sb are 2.15 x 10^{-12} m^2/s and 9.43x10^{-15} m^2/s respectively. These values are of one order of magnitude different from the calculated values under steady state condition (D_{cu} = 7.46x10^{-11} m^2/s and D_{sb} = 6.61x10^{-16} m^2/s).

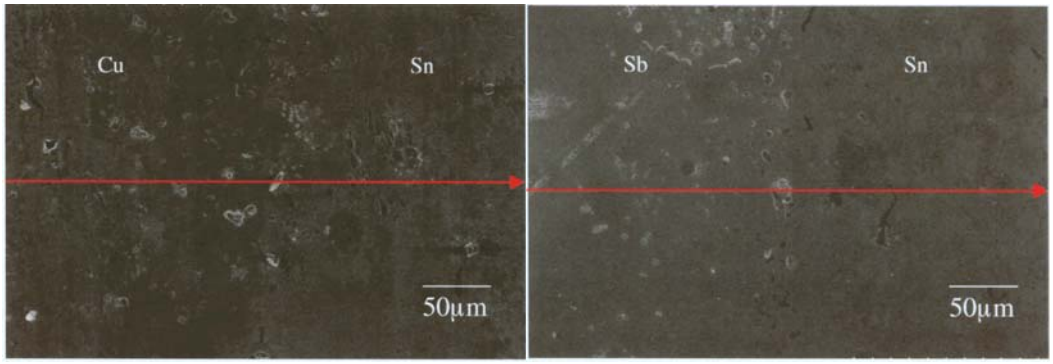

(a) (b)

Figure 4.43: SEM image showing the line scan selected for EDS analysis along the interface of (a) Cu-Sn (b) Sb-Sn

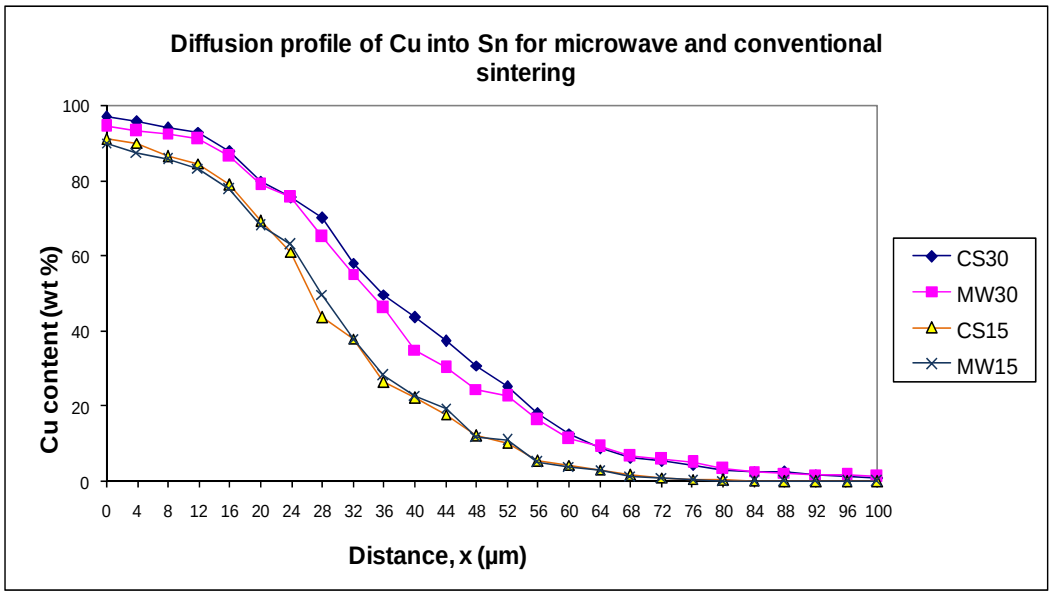

Figure 4.44: Diffusion profile of Cu into Sn for microwave and conventional sintering

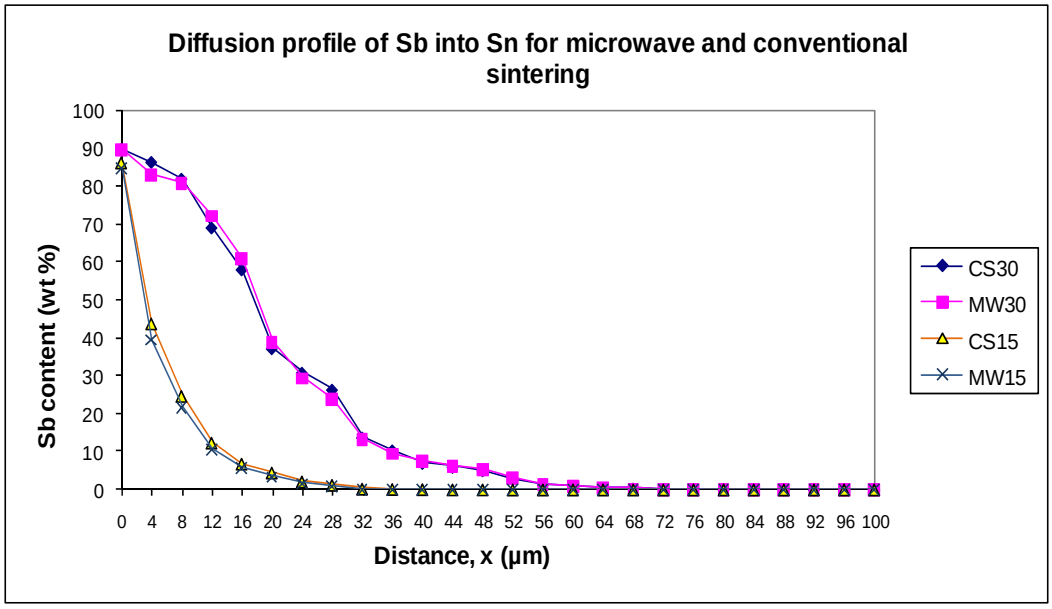

Figure 4.45: Diffusion profile of Sb into Sn for microwave and conventional sintering

Microwaves cause heating within the material through absorption of energy in the atoms. This absorbed energy is transformed into heat. This heat aids in the diffusion process with the coupling effect of the microwaves with the powder particles. Hence, microwave sintering promotes the diffusion of Cu and Sb, but a faster heating rate shortens the processing time. Studies have reported that the diffusivity of Sn into Cu is faster than that of Cu into Sn [30]. However, this is true for sintering bronze (a Cu based alloy) at high temperatures. In this

study, low sintering temperature (below melting point of Sn) was used and diffusion of Sn into Cu or Sn into Sb was not included. Furthermore, pewter alloy is a tin-based alloy and only small proportions of Cu and Sb were added into it.

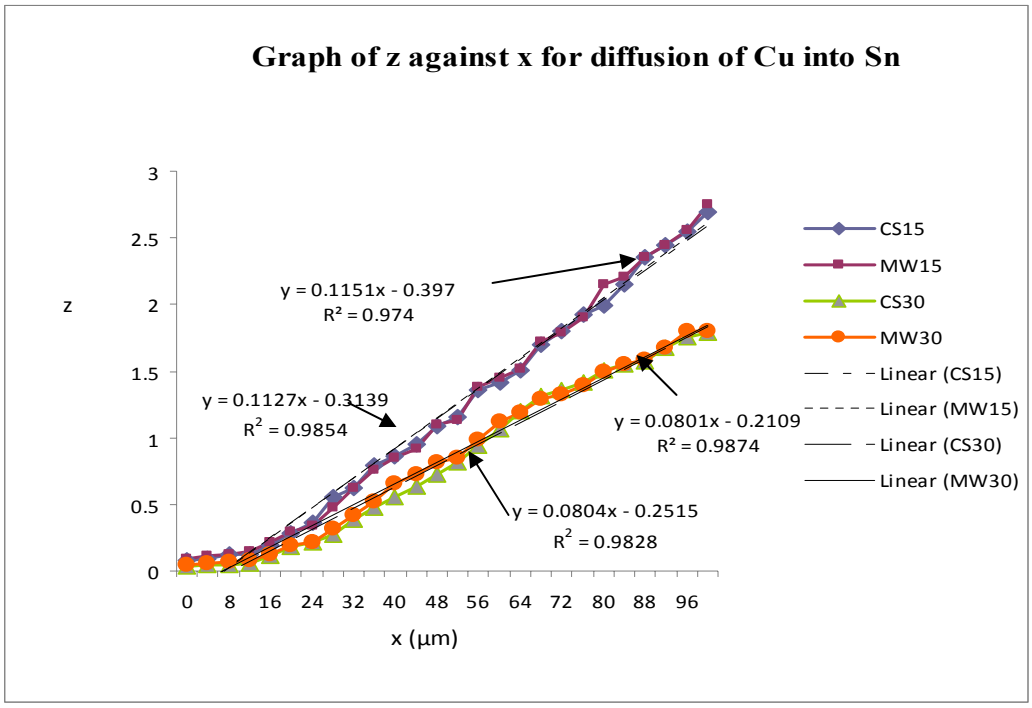

Figure 4.46: Graph of z against x showing the diffusion profile of Cu into Sn for microwave and conventional sintering at different sintering times
MW: Microwave sintering CS: Conventional Sintering

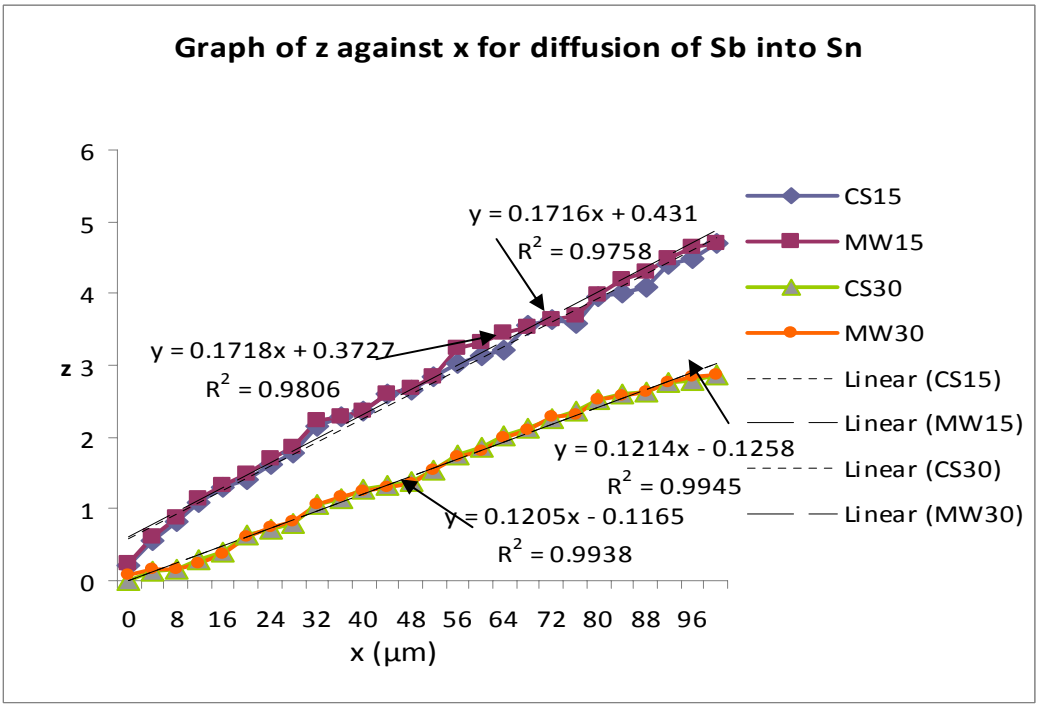

Figure 4.47: Graph of z against x showing the diffusion profile of Sb into Sn for microwave and conventional sintering at different sintering times
MW: Microwave sintering CS: Conventional Sintering

	CS 15	MW15	CS30	MW30
Slope (Sb-Sn)	0.1718	0.1716	0.1214	0.1212
Diffusivity Sb (m^2/s)	9.41E-15	9.43E-15	9.42E-15	9.46E-15
Slope (Cu-Sn)	0.1151	0.1127	0.0804	0.0801
Diffusivity Cu (m^2/s)	2.10E-14	2.19E-14	2.15E-14	2.16E-14

Table 4.4: Diffusivity values for Cu and Sb into Sn via graphical method

However, Acharya and Mukunda [120] have reported that holding the compacts at 200°C for longer times resulted in significant diffusion of Cu into Sn well below 232°C (melting point of Sn). Cu was found to have diffused into the Sn even before the Sn melted, to form η and subsequently ε when heating is prolonged. Nevertheless, as the temperature rises to 700°C the diffusion of Sn into Cu increases, while diffusion of Cu into Sn still continues [120]. Experiments carried out in this work for Sn-Cu couples, revealed that at all temperatures, it is predominantly Cu that diffuses into the Sn, though at 700°C and above, very slow diffusion of Sn into Cu can be detected due to the fact that at high temperatures, the Sn rich phases are capable of dissolving Cu [120], and in comparison the diffusion of Sn into solid Cu is too small to be detected.

Meanwhile, diffusion of Cu and Sb into Sn results in improved densification. The low temperature regions are bypassed by the microwaves where surface–transport-controlled sintering is dominant and preserves the powder surface area to a temperature where bulk transport is significant resulting in volumetric heating [121]. Nevertheless, diffusion of Sb into Sn is seen to be very homogeneous for both sintering methods at various sintering times.

It has been reported by Asante, Terblans and Roos [122] that the diffusion rate of Sn is higher than that of Sb due to activation energy of the atoms, but the segregation energy of Sb is higher than Sn resulting in a repulsive interaction with Sn atoms. This eventually leads to interstitial diffusion of Sb into Sn with the displacement of the Sn atoms. This diffusion process is clearly seen from the X-Ray maps in Figures 4.48 and 4.49 which show the diffusion of Cu and Sb respectively. The diffusion of Sb into Sn is much less than the diffusion of Cu into Sn because the Sb has a lower coefficient of diffusion compared with Cu into Sn.

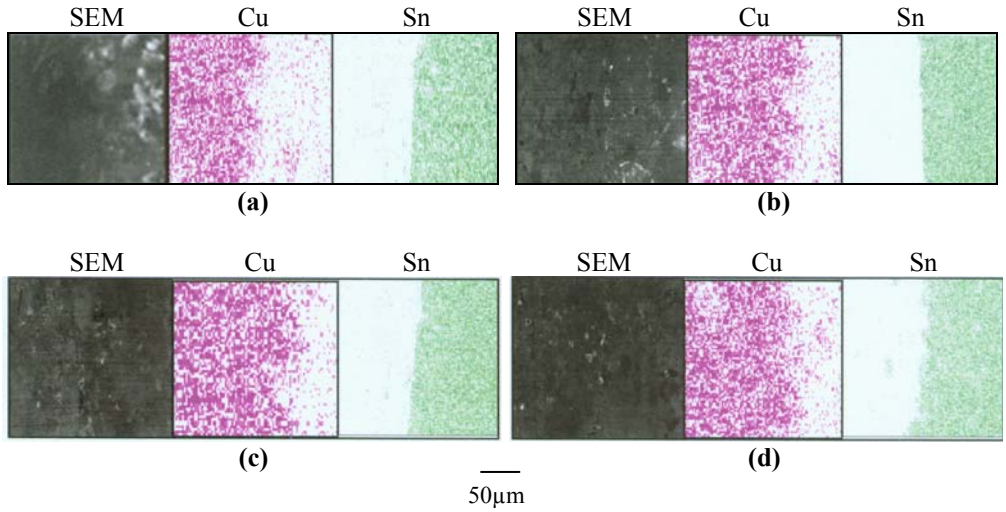

Figure 4.48: X-Ray maps of the Cu-Sn interface couple (a)CS/15min (b)CS/30min (c)MW/15min (d)MW/30min

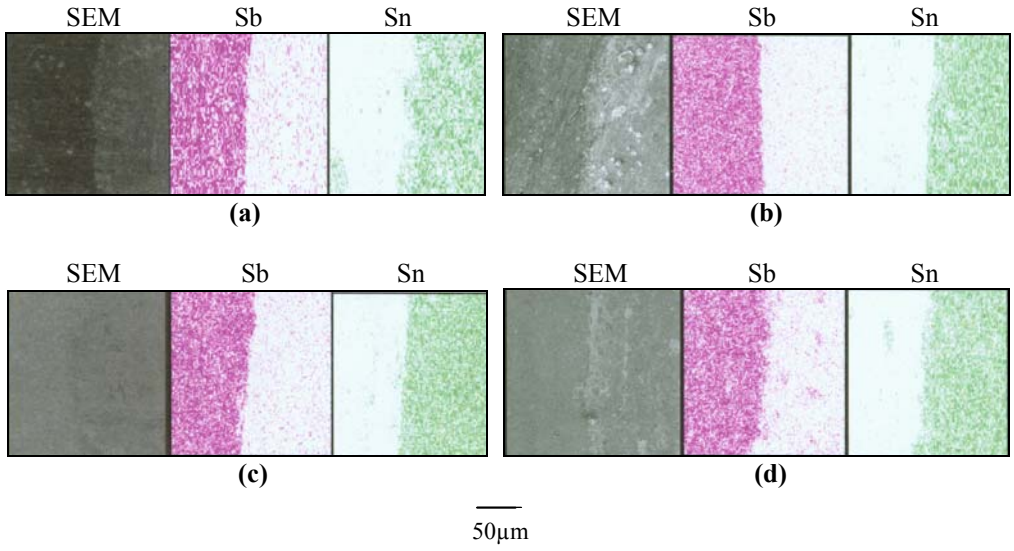

Figure 4.49: X-Ray maps of the Sn-Sb interface couple (a)CS/15 min (b)CS/30 min (c)MW/15 min (d)MW/30 min

4.2.4 Application of Mathematical Modelling to Microwave Sintering

This section aims to discuss the microwave interaction with the tin alloy sample by analysing the effect of microwaves on the skin depth, the electric field distribution, the electromagnetic power density and the absorbed power within the material in order to give a clearer understanding of the process to justify the uniform sintering that takes place within the sample.

Theory

1. The penetration depth of the microwaves at a given frequency "*f*" depends on the electrical and magnetic properties of the material and it is a very important parameter, because it constitutes an upper limit to the thickness of the material which can be heated directly by microwaves.

2. Microwave interaction with metals is restricted to their surface only. This depth of penetration in metals, also known as skin depth (δ), is defined as the distance into the material at which the incident power drops to 1/e (36.8%) of the surface value [123]. The skin depth is mathematically expressed as follows [124]:

$$\delta = \frac{1}{\sqrt{\pi f \mu \sigma}} = 0.029\sqrt{\rho \lambda_0} \qquad \textbf{(4.8)}$$

where: f is the frequency (2.45GHz)
μ is the magnetic permeability
σ_e is the electrical conductivity
ρ is the electrical resistivity
λ_0 is the incident wavelength (12.24cm for 2.45GHz waves)

3. At the beginning of the microwave assisted sintering, the green part can behave like a dielectric material. In this case, the power penetration depth "D_p" is defined as the depth into the material at

which the power flux has fallen to 1/e of its surface value, given by the simplified equation [124]:

$$D = \frac{\lambda_0}{2\pi\varepsilon''}\sqrt{\varepsilon'} \quad \textbf{(4.9)}$$

where ε_0 = permittivity of free space = 8.85×10^{-12} F/m

ε'' = dielectric loss factor

λ_0 = wavelength, measured in, $\lambda 0 = c / f$

f = frequency, measured in Hz

c = 3×10^{10}cm/s speed of light

4. The skin depth of the metal plays an important role in monitoring the power loss during the microwave –metal interaction, which leads to its heating [125]. The tangential component of the magnetic field, Ht, of microwaves induces an electric field, E, at the metal powder surface.

5. The electric field is assumed to decay (at a position x) within the sample according to [126]:

$$E = E_0 \exp\left(\frac{-x}{d}\right) \quad \textbf{(4.10)}$$

where d is the skin depth and E_0 is the electric field in the unloaded cavity (143 V/m). For a multimode microwave source, the magnetic field properties can be considered as equivalent to the electric field [127].

6. The power lost during the interaction of microwave with metal can be related to its surface impedance. The power absorbed per unit area of the conductive surface, P, is expressed as [125]:

$$P = \frac{1}{2}\int_S E.J_S.dV = \frac{1}{2}\sigma\int_V |J_S|^2.dV \quad \textbf{(4.11)}$$

7. From the surface current , J_s, which is expressed as [123]:

$$J_S = \tilde{n}\, X\, H_t \quad \textbf{(4.12)}$$

The power can be further derived as [123]:

$$P = \frac{R_S}{2}\int_S |J_S|^2 dV = \frac{R_S}{2}\int_S |H_t|^2 dV = \frac{2R_S|E_0|^2}{\eta_0^2} \quad \textbf{(4.13)}$$

where R_s is the surface resistivity ($R_s = 1/\sigma\delta$)

σ_e is the electrical conductivity

δ is the skin depth

E_0 is the electrical field amplitude at the surface

η_0 is the impedance of free space (377Ω)

H is the magnetic field

Assuming spherical metal powder of radius, r_p , the electromagnetic power density (P_{EM}) can be expressed as [123]:

$$P_{EM} = \frac{3P}{r_p} = \frac{6R_S|E_0|^2}{\eta_0^2.r_p} \quad \textbf{(4.14)}$$

8. An energy balance, expressed in terms of power transfers is used to determine the temperature rise in the metal powder which is expressed as [123]:

$$\rho C_p\, dT/dt = P_{EM} - P_{conv} - P_{rad} \quad \textbf{(4.15)}$$

where P_{EM} is electromagnetic power density

P_{conv} is power loss per unit volume due to convection

P_{rad} is power loss per unit volume due to radiation

9. Similarly, P_{conv} and P_{rad} are expressed as [123]:

$$P_{conv}\ (n) = hA\ /V\ (T_{n-1}\ -\ T_a\ ) \tag{4.16}$$

$$P_{rad}\ (n) = \sigma\varepsilon A\ /V\ (T_{n-1}^{4}\ -\ T_a^{4}\ ) \tag{4.17}$$

where h is the convective heat-transfer coefficient of incoming gas

A/V is the surface area to volume ratio for compact

σ is the Stefan-Boltzman constant

ε is the effective emissivity of metal powder

T_a is the surrounding temperature

n is the interval

10. The heat transfer coefficient for the argon gas used can be found using the following equation after simplification [128]:

$$h = 0.882\ Pr^{0.33} \tag{4.18}$$

11. The Prandtl Number for this application can be found using [128]:

$$Pr = C_p\mu/k \tag{4.19}$$

where Cp=specific heat

μ=viscosity and

k=thermal conductivity

12. Temperature rise as a function of incremental time domain (Δt) can be written as [123]:

$$T_{rise}\ =\ \Delta t\ /\ \rho C_p\ (\ P_{EM}\ -\ P_{conv}\ -\ P_{rad}\ ) \tag{4.20}$$

Skin Depth

It is well known that the microwave heating of metals is different from that of dielectric materials. An electric field is not induced in metals since metals in general are good electrical conductors. Thus, the induced electric charge remains at the surface of the sample [123]. Microwave interaction with metals is restricted to its surface only. Figure 4.50 shows the variations in skin depth with temperature for Sn, Cu and Sb (calculated from Equation 4.8 shown below) upon interaction with 2.45GHz microwaves. The respective electrical resistivity for each element are summarized in Table G1 (refer to appendix).

$$\delta = \frac{1}{\sqrt{\pi f \mu \sigma}} = 0.029\sqrt{\rho \lambda_0}$$

It is evident that metals with higher electrical conductivity have lower skin depths. For metals, skin depths increase with increasing temperature. This correlates with increasing resistivity as temperature increases. Generally, the skin depth is relatively small in metals. However, the portion of the metal powder that couples with microwaves is high enough to contribute to its heating, which results in volumetric heating in some of the metal powders, provided that they are either submicron or nanosized. However, if coarse powders are used (>100μm), then the heating may be conductive from outside to the interior of the sample [123]. Thus, as the particle size decreases, more uniform heating can be achieved compared with conventional heating.

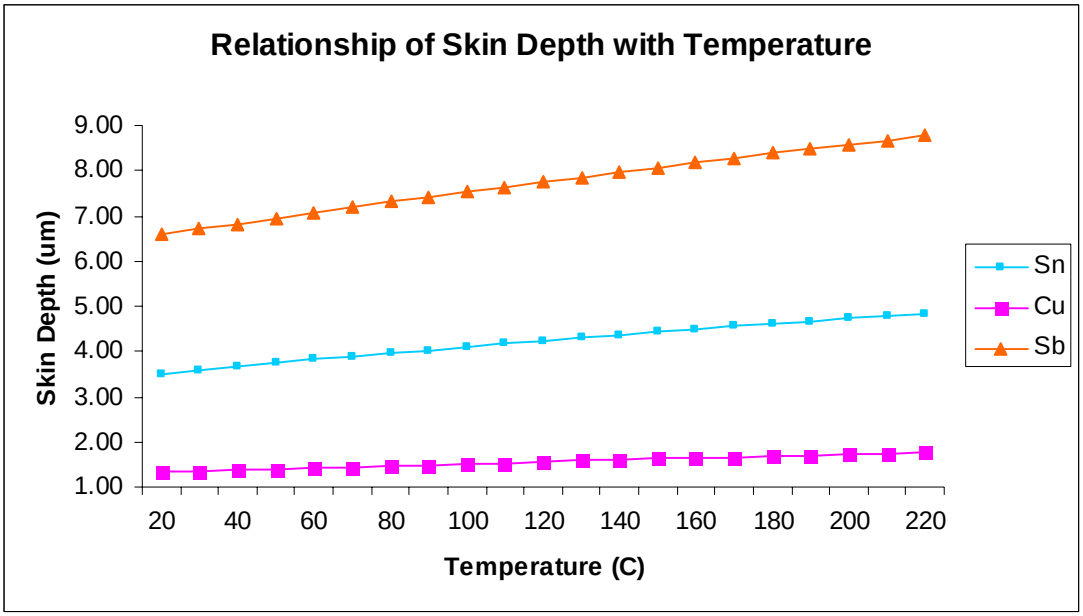

Figure 4.50: Effect of temperature on the calculated skin depth of tin, copper and antimony in 2.45 GHz microwaves

The skin depth of metals plays an important role in determining the power loss during the microwave-metal interaction, which eventually leads to its heating. The tangential component of the magnetic field, H_t, of microwaves induces an electric field, E, at the metal powder surface which then generates surface current. The power lost during the interaction of microwaves with a metal can be related to its surface impedance [125].

Electric Field

The electric field (143V/m) is assumed to decay from the surface of the sample according to Equation 4.10 shown below. The electric field distribution with Sn, Cu and Sb separately at 160°C and 220°C appear to be decaying for these materials as the microwaves penetrate into the sample.

$$E = E_0 \exp\left(\frac{-x}{d}\right)$$

The electric field for Sb decays the least followed by Sn and Cu. Nevertheless, at higher temperature (220°C), the electric field amplitude is slightly higher than at 160°C. The variation of electric field within the sample is very much dependant on the type of material and the sintering temperature used. The higher the conductivity of the material, the faster the decay in the electric field.

Electromagnetic Power Density and Absorbed Power

Figure 4.51 shows the effect of the power absorbed per unit area and electromagnetic power density which were calculated from Equation 4.13 and 4.14 respectively as shown below (refer to Table G2 in the appendix). As the sintering temperature increases, both the absorbed power per unit area and the electromagnetic power density increase as well. This is due to the increasing resistivity with temperature.

$$P = \frac{R_S}{2}\int_S |J_S|^2 dV = \frac{R_S}{2}\int_S |H_t|^2 dV = \frac{2R_S|E_0|^2}{\eta_0^2}$$

$$P_{EM} = \frac{3P}{r_p} = \frac{6R_S|E_0|^2}{\eta_0^2 . r_p}$$

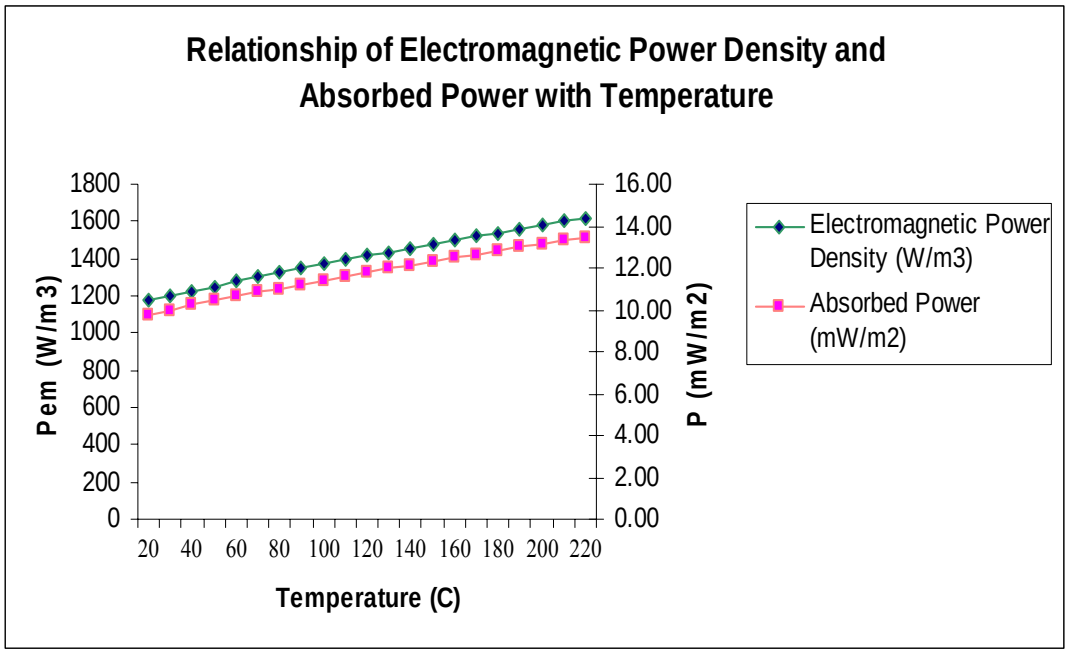

Figure 4.51: The relationship of electromagnetic power density and the absorbed power with temperature in the tin alloy sample

However, the electromagnetic power density for this tin alloy gradually decreases with distance along the furnace. Calculations show that there is very little, or no change in the electromagnetic power density and absorbed power at 160°C and 220°C for the sample region in the furnace. Therefore, there should be no difference in the sintering efficacy in the samples. The calculated electromagnetic power density was 1498.6 Wm^{-3} and the absorbed power was 12.48 mW. The highest values of the power density exist at the surface and eventually decrease further into the tin alloy sample. The decrement in the electromagnetic power density and absorbed power is small. Sintering at higher temperature generates higher values of electromagnetic power density within the sample since it is very much dependent on the surface resistivity. These values were obtained based on the interaction of Sn powder only with microwaves since the pewter alloy is a Sn-based alloy, and consists of more than 90 wt% Sn. Cu and Sb were not included in this calculation.

Heat Losses

In microwave heating, susceptors are used to assist heating in the initial stage. Susceptors are also used to prevent heat loss from the powder compact to the surroundings through radiation. Heat loss through convection also takes place from the sample. Power loss per unit volume due to convection and radiation were calculated using Equation 4.16 and 4.17 respectively as shown below (refer to Tables G3-G4 in the appendix) and the relationship of the power losses with temperature can be seen in Figure 4.52. The power losses seem to increase with increasing temperature. However, the power loss due radiation is far much less than the power loss due to convection.

$$P_{conv}(n) = hA/V(T_{n-1} - T_a)$$

$$P_{rad}(n) = \sigma\varepsilon A/V(T_{n-1}^4 - T_a^4)$$

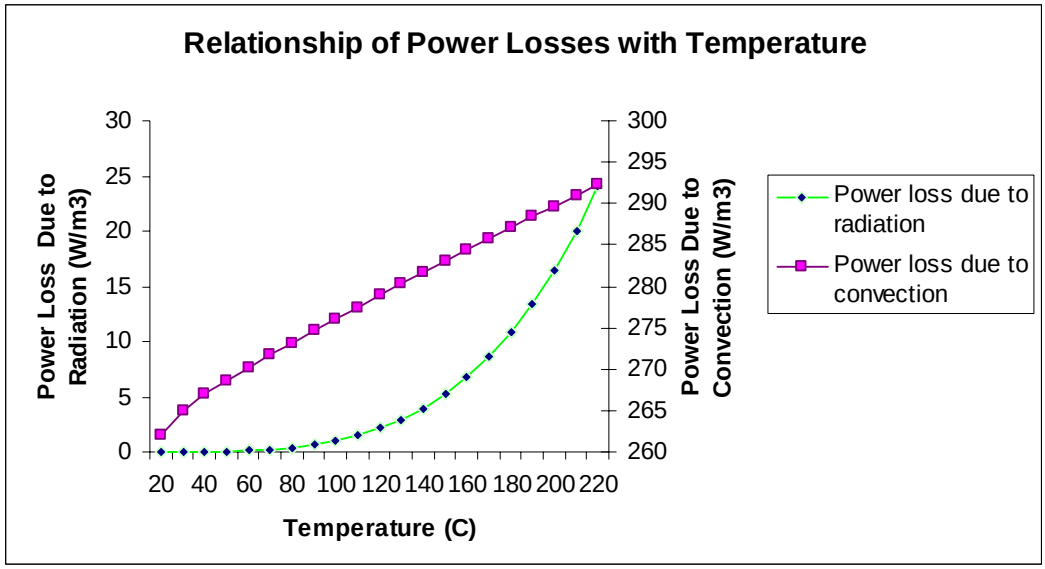

Figure 4.52: The effect of temperature on the power losses due to convection and radiation while sintering the tin alloy using microwave energy

Temperature Rise

The temperature rise is the amount by which the temperature of the sample rises above that of the furnace. Figure 4.53 shows the theoretical temperature rise profile for the microwave sintering of tin alloys used in this experiment. The values were calculated from Equation 4.20 shown below (refer to Table G5 at the appendix). Typically, in the initial stages of heating, the metal powder compacts require susceptor heating [129]. The susceptors aid in a fast temperature rise since they couple with the microwaves. The contribution of the graphite pellets in this case was assumed to be the same as the compacts being heated in the microwave furnace. In other words, the temperature rise of the sample was assumed to be the same as the temperature rise in the pellets because the temperature of the pellets could not be measured with the thermocouple. The thermocouple could only measure the temperature of the sample right in the middle of the microwave furnace. The temperature rise appears to increase exponentially with increasing temperature and remained almost constant after the targeted temperature had been reached.

$$T_{n+1} = T_n + \Delta t / \rho C_p \ (P_{EM} - P_{conv} - P_{rad})$$

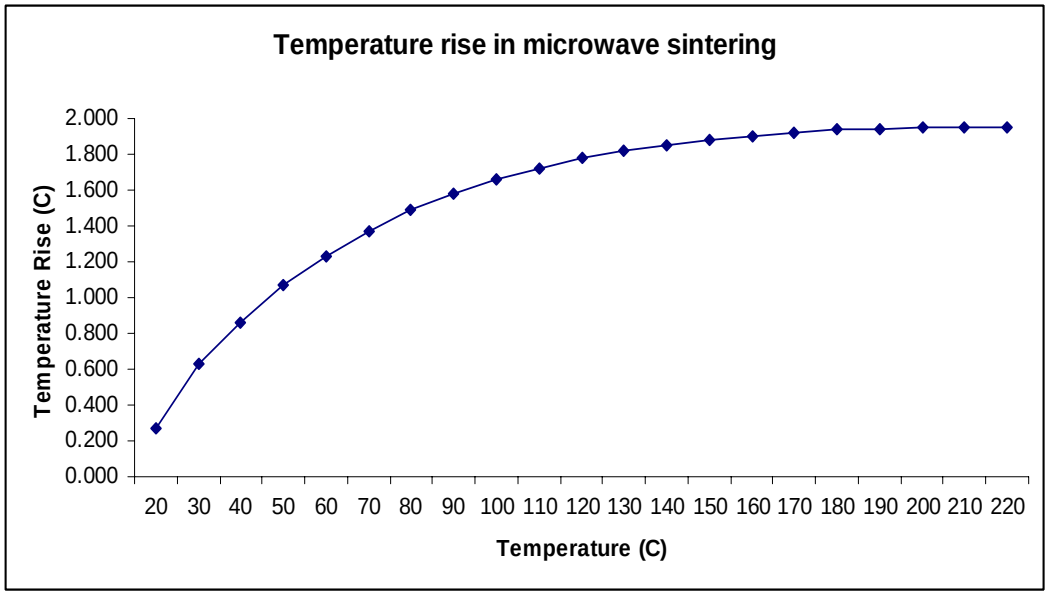

Figure 4.53: The temperature rise for the tin-based alloy sample for microwave sintering at various heating points

4.3 Overall Discussion

The experimental work on the sintering of Sn alloys, presented in this thesis, has shown that cold pressed Sn-alloy compacts can be effectively sintered to almost full density. The rate of heating during microwave sintering is significantly faster than for conventional sintering. There are a few factors that affect the heating behaviour of materials in microwave sintering that require further discussion. Firstly, the size of the powder particles is important. In this research, the Sn alloy powder particle size used had an initial average starting size of 10 μm. The finer the powder size, the higher the heating rate in microwaves since the effective microwave-metal interactive surface is higher [123]. Vaidhyanathan and Rao [130] have also revealed faster heating in finer powder compacts compared with coarser powder compacts. In this experiment, the effect of powder size was not taken into consideration.

Secondly, is the emissivity and conductivity of the metal powder compacts; a maximum attainable temperature increases with decreasing emissivity. Figure 4.50 shows how the skin depth varies with increasing electrical conductivity. Metals with higher electrical conductivity resulted in lower skin depths. However, a more precise experimental determination would be required to predict the heating profiles more accurately. Thirdly, the use of susceptors along with the powder compacts. The rate of heating is increased by using susceptors. Figure 3.8 shows that it takes much longer to reach the targeted temperature without susceptors than with susceptors. In this research, hybrid microwave sintering was applied rather than just direct microwave sintering in order to produce a uniform volumetric two-directional heating.

Finally, the type of susceptors used. The susceptor material also plays an important role. Graphite pellets were selected instead of silicon carbide because silicon carbide was found to absorb too much microwave energy in a short time resulting in a rapid temperature rise. Furthermore, the targeted temperature could not be maintained when sintering at low temperature and an overshoot in temperature occurred when using silicon carbide. The surface area of the

susceptors exposed to microwave energy matters too. The larger the surface area, the more coupling effect takes place between the susceptor material and the microwaves.

Work carried out by Takayama *et al*. [131] has shown that in less dense green parts, microwave heating effects are more volumetric and penetrating. Other authors [132-136] have shown that complex phenomena intervene during microwave assisted sintering of metallic powders, in particular local concentrations of electric field can occur, in excess of the dielectric strength of the medium (air, polymer or glass), leading to arcing, localized melting or very rapid evaporation. Consequently, microwave sintering can proceed at greater speed than conventional heating by virtue of the presence of a more efficient mechanism of mass transport, in the presence of liquid or vapour phases. Moreover, the microwave assisted sintering process can be self-regulating, because the neck formation between powder particles progressively generates longer and longer conductive paths. These lead to a reduction in the electromagnetic field concentration compared with the initial dispersion of particles.

Microwave sintering at 220°C for 30 minutes produced samples with improved densities, hardness values and strengths compared with sintering at 160°C for 30 minutes. Samples sintered at 160°C produced samples with more porosity and less dense parts. Sintering very close to the melting point of the Sn did enhance densification, hardness, strength and resulted in better diffusion of Cu into Sn. This is a known phenomenon whereby, diffusion is very much dependent on the sintering temperature and sintering time. This is verified through the diffusion couple experiments (see Figures 4.44 and 4.45) where longer sintering times have resulted in better diffusion of Cu and Sb into Sn. Conventional sintering on the other hand also produced reasonably good results in terms of density, hardness and tensile strengths. Microwave sintering gave slightly better samples or parity with conventional sintering (in a shorter sintering time), and better than casting. Moreover, more dense green parts did produce slightly better density, hardness and tensile strengths compared with the less dense green parts.

Despite the increase of hardness and tensile strength, with increasing Cu and Sb solute atoms, the samples were found to be brittle as evidenced by negligible plastic deformation at the point of fracture and the low strains to fracture. Sn is probably brittle because it has a tetragonal crystal structure and hence few slip systems for plastic deformation. Increasing the concentration of solute atoms will increase the yield strength of a material. However, there is a limit to how much solute should be added by referring to the phase diagram (refer to Figures J1-J3 in the appendix) in order to avoid forming a second phase. The highest quality pewter contains only a small percentage of Cu and Sb. Nevertheless, in the cast pewter produced by Royal Selangor, a second phase, Cu_6Sn_5, is present because of the higher temperature (275°C – 315°C) of the molten alloy. However, by using powder metallurgy, temperatures are below the melting point of tin and an intermetallic phase does not form under these conditions.

Sintering at 220°C resulted in Sb and Cu diffusing into Sn for microwave sintering which is evident from the XRD peaks (see Figure 4.41). The Sb and Cu peaks have disappeared at higher sintering temperatures and longer sintering times. Additionally, there was a shift in the Sn peaks to lower 2θ angles indicating an increase in the Sn *d* spacing caused by solid solution formation (see Figure 4.42). It is known from Fick's Law that the amount of diffusion depends on sintering time. However, the work carried out on the Sn-Cu and Sn-Sb couples indicated that there is no difference in the diffusivity of Cu and Sb during microwave sintering and conventional sintering.

However, because the heating profile for microwave sintering (see Figure 3.10) allows for faster heating, microwave sintering is a much faster process for achieving the similar end results in terms of grain size and tensile strengths (refer to Tables D1-D6 and Tables E1-E3 in the appendix). The grain size in the microwave sintered material was slightly smaller than that found after conventional sintering. For example 97MW8 (220ºC/30min/129MPa) produced 23.8μm and 97CS8 (220ºC/120min/129MPa) produced 26.9μm. Meanwhile, there was almost no improvement in terms of tensile strength in microwave sintered samples and the conventionally sintered ones. 94MW8 (220ºC/30min/129

MPa) produced a transverse strength of 46.9 MPa and 94CS8 (220ºC/120min/129MPa) produced a transverse strength of 47 MPa.

Microwave sintering has produced slightly improved results in terms of density and hardness when compared with conventional sintering (refer to Tables A1-A12 and C1-C3 in the appendix). 97MW8 (220ºC/30min/129MPa) has produced a theoretical density of 98.28% while 97CS8 (220ºC/120min/129MPa) has produced a theoretical density of 98.71%. Meanwhile, the hardness values for 97MW8 (220ºC/30min/129MPa) and 97CS8 (220ºC/120min/129MPa) are 24.0 HV and 19.1 HV respectively. Grain growth is very much dependent on sintering time and temperature. It is interesting to note that there was little variation in grain size after microwave sintering at 220^{o}C for the three alloy compositions. There was slightly more grain size variation after conventional sintering but this was not significant.

Since the grain sizes obtained from the microwave sintering, after a shorter sintering time, were similar (perhaps marginally smaller) than those obtained after conventional sintering for the same sintering temperatures, improved hardness after microwave sintering is most likely a result of the improved density achievable as a result of volumetric heating. However, the tensile strength of the microwave sintered samples was no better than that found in conventionally sintered samples. This is perhaps not unexpected since hardness measurements are more sensitive to the presence of underlying pores than yield strength.

This investigation has shown that microwave sintering of pewter alloys, prepared using elemental powders, rather than pre-alloyed powders is essentially thermal in nature, rather than the result of an athermal or ‘microwave’ effect. The differences between conventionally sintered samples and microwave sintered samples are largely attributed to the directions of heating i.e. volumetric versus surface heating. This has been partly verified through the diffusion couple experiments whereby microwave and conventionally sintered couples have reached the same levels of diffusion for the same time duration of sintering. However, it is the sintering of the Sn powder, rather than the diffusivities of Cu and Sb, which is important in establishing the final sintered density.

The diffusion of Cu and Sb are important for producing a homogeneous structure and composition. The sintering mechanism involves the replacement of high energy solid-gas interfaces by lower energy solid-solid interfaces, such as grain boundaries. This reduction in interfacial energy is the driving force for sintering, but the mechanism leading to transport of atoms leading to an increase in contact area between powder particles is diffusion, either through the crystal lattice or at the particle surfaces. The contact area between powder particles depends on time and temperature. The rate of sintering decreases with time but increases with increased temperature, since the diffusion coefficient increases with temperature.

Comparing the densities of samples after conventional sintering and microwave sintering at both 160°C and 220°C (refer to Tables A3 and A4 at the appendix), it is clearly evident that there is significantly improved density after shorter sintering time as a result of microwave sintering at 160°C compared with conventional sintering. The differences at 220°C are not quite so marked. This suggests that microwave sintering is more effective in reducing the porosity in the Sn at 160°C and at 220°C achieves a similar density as conventionally sintered material, but after one quarter of the sintering time.

The results from the diffusion couple experiments shown in Figures 4.44 and 4.45 show similar diffusion profiles for the diffusion of copper and antimony after conventional and microwave sintering. The diffusivities of copper and antimony in tin, reported in Table 4.4, give similar values after sintering for 15 minutes and 30 minutes at 220°C. This indicates that there is not a microwave effect that enhances the diffusion process. The achievement of densities after microwave sintering equivalent to those obtained after conventional sintering is almost certain to be a result of the efficient and rapid volumetric heating occurring during microwave sintering.

Microwave sintering of tin alloy samples is effective in producing samples with improved mechanical properties (density, hardness and strength) and structural characteristics (uniform grain size and smaller pores). Through mathematical modelling, it is evident that microwave sintering of tin alloy was

successful because of the sufficient electric field amplitude generated within the sample as a result of the microwave coupling with the material. Moreover, the amount of power losses was quite low. This electric field then generates heat from within the material and promotes volumetric heating and aids the sintering process. The rapid heating in microwave sintered samples and high energy generated inside causes improved densification, and hence, results in higher hardness.

CHAPTER 5
CONCLUSIONS AND RECOMMENDATIONS

5.1 Conclusions

It is expected that in the near future microwave heating could be a promising substitute for conventional processing methods due to its significant advantages, including more rapid heating rate, shortened sintering time, superfine grain size, improved microstructure and much less expensive equipment. In this work a positive outcome has been achieved using both conventional and microwave sintering. This is summarised below:

1. The higher the green density, the higher the sintered bulk density for both sintering methods.

2. Samples conventionally sintered at lower sintering temperature (160ºC), did not achieve any significant improvement when compared with microwave sintered samples in terms of mechanical or structural properties, therefore sintering temperature is an important criteria.

3. Samples conventionally sintered at a higher sintering temperature (220ºC) and for a longer sintering time (120 minutes) resulted in better mechanical and structural properties achieving parity with traditionally cast pewter (from Royal Selangor).

4. Samples microwave sintered at a relatively low sintering temperature (160ºC) achieved similar mechanical properties compared with cast pewter, even at a lower green density.

5. Microwave sintered samples pressed at 129 MPa and sintered for 15 minutes at a higher sintering temperature (220ºC) resulted in improved mechanical and structural properties when compared to both conventional sintering and casting.

6. The diffusion of Cu into Sn is very much influenced by sintering temperature and sintering time. The higher the sintering temperature and the longer the sintering time, the better the diffusion process.

7. Microwave sintering supposedly leads to a finer grain size compared with conventional sintering, but in this research, the difference in grain size between microwave and conventionally sintered samples is marginally small. Grain growth appears to be slightly slower during microwave heating. On the other hand, there is more grain growth during conventional sintering creating a coarser microstructure.

8. Increasing the Cu and Sb content of the pewter alloy simply increases the hardness and strength of the material but at the expense of toughness.

9. A pewter alloy with composition 97%Sn 2%Cu 1%Sb can be consolidated through microwave sintering with a 75% reduction in processing time. Microwave sintering results in higher density and hardness for pewter alloy when compared with conventional sintering,

5.2 Recommendations

Microwave research currently involves a broad range of activity and a wide variety of materials and powders. While there has been much research in microwave processing of metals and alloys, not much has been commercialized mainly due to the limitations and difficulties faced in scaling up operations. The success achieved so far in the laboratory should be exploited for commercialization. Several microwave systems have been developed at the Pennsylvania State University that can circumvent these problems and can be used for commercialization of the technology [137]. Therefore, the future goal will be to convert our laboratory microwave technology successes into commercial successes in specialty material synthesis and sintering.

The following suggestions are recommended for future work:

1. Other material properties such as wear resistance, radial crushing strength and impact testing should be investigated after microwave sintering and find the optimum combination of input parameters.

2. The behaviour of finer powder particle size should be investigated to compare the effect of particle size on microwave sintering efficiency and mechanical properties.

3. Using pre-alloyed pewter powder should also be considered for further work to investigate whether there is any improvement in the diffusion effect.

4. Evacuating the sample in a glass capsule prior to sintering in the microwave should be implemented. However, further study on how to control and monitor the temperature inside the capsule should also be investigated.

5. Attempt to sinter these materials using high heating rate in the conventional furnace as compared to the heating rate used in microwave furnace should be investigated to justify the thermal effects during sintering.

6. A modified design of the microwave should be implemented to the present experimental setup to accommodate larger specimens and to facilitate temperature control.

REFERENCES

1. Schey J.A., "Introduction to manufacturing processes", McGraw Hill, Singapore, 3rd Edition, 2000, pp 441-460

2. Agrawal D.K., "Microwave processing of ceramics ", Current Opinion in Solid State and Materials Science, Volume 3, Issue 5, October 1998, pp 480-485

3. Sorescu M., Diamandescu L., Ramesh P.D., Roy R., Daly A. and Bruno Z., "Evidence for microwave-induced recrystallization in NiZn ferrites", Materials Chemistry and Physics, Volume 101, Issues 2-3, 15 February 2007, pp 410-414

4. Ebadzadeh T. and Valefi M., "Microwave-assisted sintering of zircon", Journal of Alloys and Compounds, In Press, 11 February 2007

5. Agrawal D.K., "Microwave Sintering Of Metals", Materials World, Volume 7, Issue 11, November 1999, pp672-673

6. Agrawal D.K., Microwave Sintering Developments Spur Emergence of New Materials & Technologies ,Materials Research Inst., Penn State University, University Park, Pa. June 7, 2005 (www.industrialheating.com)

7. Roy R, Agrawal D.K, Cheng J.P and Mathis M., Ceramic Trans., 1997, Volume 80, pp3-26

8. Lau Rebecca, "TED Case Studies: Tin Mining In Malaysia-Present and Future", http://www.american.edu/TED/tin.htm, July 1999

9. Carlin J.F., "Mineral Industry Surveys", http://minerals.usgs.gov/minerals

10. Leigh, Barbara, "Batik and pewter: Symbols of Malaysian pianissimo", Journal of Social Issues in Southeast Asia, April 2002

11. http://www.royalselangor.com/rs2/aboutus/php

12. Sutton W.H: American Ceramic Society Bulletin, 1989, 68, (2), 376-386.

13. Sutton W.H: Mater. Res. Soc. Symposium Proceedings, 1992, 269, 3-19.

14. Katz J.D, Annu. Rev. Material Science, 1992, 22, pp153-170

15. Schiffman R.F., Ceramic Trans., 1995, 59, 7-17.

16. Fang Yi., Agrawal D. K, Roy D. M. and Roy R., "Fabrication of transparent hydroxyapatite ceramics by ambient-pressure sintering", Materials Letters, Volume 23, Issues 1-3, April 1995, pp 147-151

17. Brosnan K.H., "Sintering of Alumina Parts with microwave energy", Masters Thesis at the Pennsylvania State University, 2002, pp 2-4.

18. http://www.metal-powder.net

19. Rodiger K., Dreyer K, Gerdes T. and Willert-Porada M., "Microwave sintering of hardmetals ", International Journal of Refractory Metals and Hard Materials, Volume 16, Issues 4-6, 1998, pp 409-416

20. Roy R, Agrawal D.K, Cheng J.P and Gedevanishvili S, *Nature* 399 (1999), p. 668.

21. Sethi G., Upadhyaya A. and Agrawal D.: Science of Sintering, 2003, Volume 35, pp 49-65

22. Willert-Porada, M and Park H.S., in D.E. Clark, J.G.P. Binner and D.A. Lewis, " Microwaves: Theory and Application in Materials Processing V, Am Ceramic Society, Waterville, OH 2001, pp 459-470.

23. Roy R, Agrawal DK, Cheng J. US 6,183,689 B1; 6 February 2001.

24. Takayama S, Saiton Y., Sato M., Nagasaka T., Muroga T. and Ninomiya Y., 9th International Conference on Microwave and High Frequency Heating, Loughborough University, UK, 2003, pp 369-372.

25. Saitou K., "Microwave sintering of iron, cobalt, nickel, copper and stainless steel powders ", Scripta Materialia, Volume 54, Issue 5, March 2006, pp 875-879

26. Panda S.S, Singh V., Upadhyaya A. and Agrawal D., "Sintering response of austenitic (316L) and ferritic (434L) stainless steel consolidated in conventional and microwave furnaces", Scripta Materialia, Volume 54, Issue 12, June 2006, pp 2179-2183

27. Du Y., Courtney T.H. and Lu S.Z., " Gravity-induced sedimentation during melting and liquid phase sintering of Pb-Sn alloys", Acta Materialia 51, 2003, pp 445-456.

28. Upadhyaya D., Ghosh A., Gurumurthy K. R. and Prasad Ram, "Microwave sintering of cubic zirconia ", Ceramics International, Volume 27, Issue 4, 2001, pp 415-418

29. Upadyaya A.and Sethi G., "Effect of heating mode on the densification and microstructural homogenization response of premixed bronze", Scripta Materialia, Volume 56, Issue 6, March 2007, pp 469-472

30. Upadhyaya, A., Tiwari, S.K. and Mishra, P., "Microwave sintering of W–Ni–Fe alloy **",** Scripta Materialia, Volume 56, Issue 1, January 2007, pp 5-8

31. Gupta M and Wong W.L.E. , "Enhancing overall mechanical performance of metallic materials using two-directional microwave assisted rapid sintering", Scripta Materialia, Volume 52, Issue 6, March 2005, pp479-483

32. Wong W.L.E and Gupta M., "Development of Mg/Cu nanocomposites using microwave assisted rapid sintering", Composites Science and Technology, Volume 67, 2007, pp1541-1552

33. Tsay Y., Liu K. S., T. F. Lin and Lin I. N., "Microwave sintering of NiCuZn ferrites and multilayer chip inductors", Journal of Magnetism and Magnetic Materials, Volume 209, Issues 1-3, February 2000,pp 189-192

34. Tsay Chien-Yih, Liu Kuo-Shung and Lin I. -Nan , "Co-firing process using conventional and microwave sintering technologies for MnZn- and NiZn-ferrites", Journal of the European Ceramic Society, Volume 21, Issues 10-11, 2001, pp 1937-1940

35. Peelamedu Ramesh, Grimes Craig, Agrawal Dinesh, and Roy Rustum, " Ultralow dielectric constant nickel-zinc ferrites using microwave sintering", Materials Research Institute, The pensylvania State University, 21 July 2003.

36. Tsay Chien-Yih, Liu Kuo-Shung and Lin I-Nan, "Microwave sintering of $(Bi_{0.75}Ca_{1.2}Y_{1.05})(V_{0.6}Fe_{4.4})O_{12}$ microwave magnetic materials ", Journal of the European Ceramic Society, Volume 24, Issue 6, 2004, pp 1057-1061

37. Yadoji P, Peelamedu R., Agrawal D. and Roy R., **"**Microwave sintering of Ni–Zn ferrites: comparison with conventional sintering", Materials Science and Engineering B, Volume 98, Issue 3, 15 April 2003, pp 269-278

38. Sorescu M., Diamandescu L., Peelamedu R., Roy R. and Yadoji P., "Structural and magnetic properties of NiZn ferrites prepared by microwave sintering ", Journal of Magnetism and Magnetic Materials, Volume 279, Issues 2-3, August 2004, pp 195-201

39. Znamenáčková, M. Lovás, A. Mockovčiaková, Š. Jakabský and Briančin J., "Modification of magnetic properties of siderite ore by microwave energy", Separation and Purification Technology, Volume 43, Issue 2, May 2005, pp 169-174

40. National Research Council Staff, "Microwave Processing of Materials", Washington DC, USA, National Academies Press, 1994, p80.

41. Zhipeng Xie, Jinlong Yang, Yong Huang, "Densification and grain growth of alumina by microwave processing", Materials Letters, Volume 37, Issues 4-5, November 1998, pp 215-220

42. Thostenson E.T. and Chen T.W., "Microwave processing: Fundamentals and Applications", Composites Part A: Applied Science and Manufacturing, Volume 30, Issue 9, September 1999, pp 1055-1071

43. Ananthakumar S., Krishnapriya G., Damodaran A. D. and Warrier K. G. K., "Thermal decomposition characteristics of boehmite gels under microwave heating and associated microstructural features", Materials Letters, Volume 35, Issues 1-2, April 1998, pp 95-99

44. Mathews Tom, Subasri R. and Sreedharan O. M., "A rapid combustion synthesis of MgO stabilized Sr- and Ba-β-alumina and their microwave sintering", Solid State Ionics, Volume 148, Issues 1-2, 1 May 2002, pp135-143

45. Subasri R., Mathews Tom, Sreedharan O. M. and Raghunathan V. S., "Microwave processing of sodium beta alumina", Solid State Ionics, Volume 158, Issues 1-2, February 2003, pp 199-204

46. Subasri R., Mathews Tom and Sreedharan O. M., "Microwave assisted synthesis and sintering of $La_{0.8}Sr_{0.2}Ga_{0.83}Mg_{0.17}O_{2.815}$ ", Materials Letters, Volume 57, Issue 12, March 2003, pp 1792-1797

47. Xu G., Zhuang H., Li W. and Wu F., "Microwave sintering of α/β-Si_3N_4" , Journal of the European Ceramic Society, Volume 17, Issue 8, 1997, pp 977-981

48. Selmi, S. Komarneni, V. K. Varadan and V. V. Varadan, "Microwave sintering of Sb-doped SnO_2 ", Materials Letters, Volume 10, Issue 6, December 1990, pp 235-238

49. Selmi, F. Guerin, X. D. Yu, V. K. Varadan, V. V. Varadan and S. Komarneni, "Microwave calcination and sintering of barium strontium titanate ", Materials Letters, Volume 12, Issue 6, January 1992, pp 424-428

50. Lewis, R. J. Rayne, B. A. Bender, L. K. Kurihara, G-M. Chow, A. Fliflet, A. Kincaid and R. Bruce, "Conventional and high frequency microwave processing of nanophase ceramic materials", Nanostructured Materials, Volume 9, Issues 1-8, 1997, pp 97-100

51. Lin Nan, Lee Wan-Chu, Liu Kuo-Shung, Cheng Hsiu-Fung and Wu Mien-Win, "On the microwave sintering technology for improving the properties of semiconducting electronic ceramics ", Journal of the European Ceramic Society, Volume 21, Issues 10-11, 2001, pp 2085-2088

52. Xie Zhipeng, Yang Jinlong and Huang Yong, "Densification and grain growth of alumina by microwave processing ", Materials Letters, Volume 37, Issues 4-5, November 1998, pp 215-220

53. Xie Zhipeng, Wang Changan, Fan Xudong and Huang Yong , "Microwave processing and properties of Ce–Y–ZrO_2 ceramics with 2.45 GHz irradiation", Materials Letters, Volume 38, Issue 3, January 1999, pp 190-196

54. Thakur O. P., Prakash Chandra and Agrawal D. K., "Dielectric behavior of $Ba_{0.95}Sr_{0.05}TiO_3$ ceramics sintered by microwave", Materials Science and Engineering B, Volume 96, Issue 3, 1 December 2002, pp 221-225

55. Thakur O. P., Prakash Chandra and Agrawal D. K., "Microwave synthesis and sintering of $Ba_{0.95}Sr_{0.05}TiO_3$ ", Materials Letters, Volume 56, Issue 6, November 2002, pp 970-973

56. Chen-Liang Li and Chen-Chia Chou, "Microstructures and electrical properties of lead zinc niobate–lead titanate–lead zirconate ceramics using microwave sintering", Journal of the European Ceramic Society, Volume 26, Issue 7, 2006, pp 1237-1244

57. Sarabjit Singh, O.P. Thakur, D.S. Rawal, Chandra Prakash and K.K. Raina," Improved properties of Sm substituted PCT ceramics using microwave sintering", Materials Letters, Volume 59, Issue 7, March 2005, pp768-772

58. Goldstein, Kaplan W. D. and Singurindi A., "Liquid assisted sintering of SiC powders by MW (2.45 GHz) heating ", Journal of the European Ceramic Society, Volume 22, Issue 11, October 2002, pp 1891-1896

59. Satapathy L.N., Ramesh P.D., Agrawal D. and Roy R., "Microwave synthesis of phase-pure, fine silicon carbide powder", Materials Research Bulletin, Volume 40, Issue 10, 6 October 2005, pp 1871-1882

60. Cheng J.P., Agrawal D.K. and Roy R., " Microwave preparation of transparent alumina ceramics, Am Ceramic Society Bulletin, 1998, 77:211

61. Cheng J.P., Agrawal D.K. and Roy R., "Microwave Processing of transparent ceramics", In Proceedings of the 33rd Microwave Power Symposium, 1998, July 12-15, Chicago, Virginia, USA.

62. Cheng Ji Ping, Agrawal Dinesh, Roy Rustum and Jayan P. S., "Continuous microwave sintering of alumina abrasive grits", Journal of Materials Processing Technology, Volume 108, Issue 1, 1 December 2000, pp 26-29

63. Cheng Ji Ping, Agrawal Dinesh, Zhang Yun Jin and Roy R.," Microwave sintering of transparent alumina", Materials Letters, Volume 56, Issue 4, October 2002, pp 587-592

64. Wang Xinlong, Fan Hongsong, Xiao Yumei and Zhang Xingdong , "Fabrication and characterization of porous hydroxyapatite/β-tricalcium phosphate ceramics by microwave sintering", Materials Letters, Volume 60, Issue 4, February 2006, pp 455-458

65. Ramesh S., Tan C.Y., Bhaduri S.B., Teng W.D. and Sopyan I., "Densification behaviour of nanocrystalline hydroxiapatite bioceramics", Journal of Materials processing Technology, Volume 206, 2008, pp 221-230, doi: 10.1016/j.jmatprotec.2007.12.027

66. Chang H. Y., Liu K. S., Chen H. W., Hu C. T., Lin I. N., Shaw B. J. and Tan J. T., "V-shaped positive temperature coefficient of resistivity (PTCR) characteristics of microwave-sintered $(Sr_{0.4}Pb_{0.6})TiO_3$ ", Materials Chemistry and Physics, Volume 42, Issue 4, December 1995, pp 258-263

67. Chang H.Y., Liu K.S and Lin I.N., "Modification of PTCR behavior of $(Sr_{0\cdot2}Ba_{0\cdot8})TiO_3$ materials by post-heat treatment after microwave sintering ", Journal of the European Ceramic Society, Volume 16, Issue 1, 1996, pp 63-70

68. Piluso P., Gaillard L., Lequeux N. and Boch P., "Mullitization and densification of $(3Al_2O_3 + 2SiO_2)$ powder compacts by microwave sintering", Journal of the European Ceramic Society, Volume 16, Issue 2, 1996, pp 121-125

69. Bykov Y., Gusev S., Eremeev A., Holoptsev V., Malygin N., Pivarunas S., Sorokin A. and Shurov A., "Sintering of nanophase oxide ceramics by using millimeter-wave radiation ", Nanostructured Materials, Volume 6, Issues 5-8, 1995, pp 855-858

70. Bykov Yu., Eremeev A., Egorov S., Ivanov V., Kotov Yu., Khrustov V. and Sorokin A., "Sintering of nanostructural titanium oxide using millimeter-wave radiation", Nanostructured Materials, Volume 12, Issues 1-4, 1999, pp 115-118

71. Chen Ping-Hong, Pan Han-Chang, Chou Chen-Chia and Lin I. -Nan , "Microstructures and properties of semi-conductive $Pb_{0.6}Sr_{0.4}TiO_3$ ceramics using $PbTiO_3$-coated $SrTiO_3$ powders ", Journal of the European Ceramic Society, Volume 21, Issues 10-11, 2001, pp 1905-1908

72. Dervos T., Thirios, Novacovich J., Vassiliou P. and Skafidas P., "Permittivity properties of thermally treated TiO_2 ", Materials Letters, Volume 58, Issue 9, March 2004, pp 1502-1507

73. Hart J. N., Cervini R., Cheng Y.B., Simon G.P. and L. Spiccia Formation of anatase TiO_2 by microwave processing Solar Energy Materials and Solar Cells, Volume 84, Issues 1-4, October 2004, pp 135-143

74. Hart Judy N., Menzies David, Cheng Yi-Bing, Simon George P. and Spiccia Leone, "A comparison of microwave and conventional heat treatments of nanocrystalline TiO_2 ", Solar Energy Materials and Solar Cells, In Press, Corrected Proof, 7 September 2006

75. Marković S., Mitrić M., Cvjetićanin N. and Uskoković D., "Preparation and properties of $BaTi_{1-x}Sn_xO_3$ multilayered ceramics ", Journal of the European Ceramic Society, In Press, Corrected Proof, Available online 23 May 2006.

76. Huang Cheng-Liang, Pan Chung-Long and Hsu Jui-Feng, "Dielectric properties of $(1-x)(Mg_{0.95}Co_{0.05})TiO_3–xCaTiO_3$ ceramic system at microwave frequency ", Materials Research Bulletin, Volume 37, Issue 15, 1 December 2002, pp 2483-2490

77. Hutagalung S.D., Ibrahim M.I. and Ahmad Z.A., "The role of tin oxide addition on the properties of microwave treated $CaCu_3Ti_4O_{12}$", Materials Chemistry and Physics, Volume 112, 2008, pp83-87, doi:10.1016/j.matchemphys.2008.05.020

78. Yu H., Liu H., Luo D. and Cao M., " Microwave synthesis of high dielectric constant $CaCu_3Ti_4O_{12}$", Journal of Materials Processing Technology, Volume 208, 2008, pp 145-148, doi:10.1016/j.matprotec.2007.12.104

79. Mahboob S., Dutta A.B., Prakash C., Swaminathan G., Suryanarayana S.V., Prasad G. Kumar G.S., "Dielectric behaviour of microwave sintered rare earth doped $BaTiO_3$ ceramics", Materials Science and Engineering: B, Volume 134, Issue 1, 25 September 2006, Pages 36-40

80. Ciacchi T., Nightingale S. A. and Badwal S. P. S., "Microwave sintering", Solid State Ionics, Volumes 86-88, Part 2, July 1996, pp 1167-1172

81. Xie Zhipeng, Yang Jinlong and Huang Yong, "Densification and grain growth of alumina by microwave processing ", Materials Letters, Volume 37, Issues 4-5, November 1998, pp 215-220

82. Xie Zhipeng, Wang Changan, Fan Xudong and Huang Yong , "Microwave processing and properties of $Ce–Y–ZrO_2$ ceramics with 2.45 GHz irradiation", Materials Letters, Volume 38, Issue 3, January 1999, pp 190-196

83. Xie Zhipeng, Yang Jinlong, Huang Xiangdong and Huang Yong, "Microwave processing and properties of ceramics with different dielectric loss", Journal of the European Ceramic Society, Volume 19, Issue 3, March 1999, pp 381-387

84. Huang S.G. ,Li L., Van der Biest O. and Vleugels J., "Microwave sintering of CeO_2 and Y_2O_3 co-stabilised ZrO_2 from stabiliser-coated nanopowders", Journal of the European Ceramic Society, In Press, Corrected Proof, Available online 19 May 2006.

85. Goldstein and M. Kravchik, "Sintering of PZT powders in MW furnace at 2.45 GHz ", Journal of the European Ceramic Society, Volume 19, Issues 6-7, June 1999, pp 989-992

86. Goldstein, N. Travitzky, A. Singurindy and M. Kravchik, "Direct microwave sintering of yttria-stabilized zirconia at 2·45 GHz ", Journal of the European Ceramic Society, Volume 19, Issue 12, October 1999, pp 2067-2072

87. Freim J. and McKittrick J. , Katz J. and Sickafus K., "Microwave sintering of nanocrystalline γ-Al_2O_3 ", Nanostructured Materials, Volume 4, Issue 4, July-August 1994, pp 371-385

88. Peelamedu D. Ramesh, Brandon David and Schächter Levi, "Use of partially oxidized SiC particle bed for microwave sintering of low loss ceramics", Materials Science and Engineering A, Volume 266, Issues 1-2, 30 June 1999, pp 211-220

89. Peelamedu Ramesh D., Roy Rustum and Agrawal Dinesh K., "Microwave-induced reaction sintering of $NiAl_2O_4$ ", Materials Letters, Volume 55, Issue 4, 2002, pp 234-240

90. Masatoshi Mizuno, Seizo Obata, Sadatsugu Takayama, Sadataka Ito, Nobuhisa Kato, Toshio Hirai and Motoyasu Sato," Sintering of alumina by 2.45 GHz microwave heating ", Journal of the European Ceramic Society, Volume 24, Issue 2, 2004, pp 387-391 , 8th International Conference on Ceramic Processing

91. Fang Yi, Cheng Jiping and Agrawal Dinesh K., "Effect of powder reactivity on microwave sintering of alumina ", Materials Letters, Volume 58, Issues 3-4, January 2004, pp 498-501

92. Phani A.R. and Santucci S., "Evaluation of structural and mechanical properties of aluminum oxide thin films deposited by a sol–gel process: Comparison of microwave to conventional anneal", Journal of Non-Crystalline Solids, In Press, Corrected Proof, Available online 7 September 2006.

93. Gómez Idalia, Hernández Maryangel, Aguilar Juan and Hinojosa Moisés, "Comparative study of microwave and conventional processing

of MgAl2O4-based materials", Ceramics International, Volume 30, Issue 6, 2004, pp 893-900

94. Subramanian T., Venkatesh P. , Nagarajan K and Vasudeva Rao P. R., "A novel method of sintering UO_2 pellets by microwave heating", Materials Letters, Volume 46, Issues 2-3, November 2000, pp 120-124

95. Yang Jae Ho, Song Kun Woo, Lee Yong Woo, Kim Jong Heon, Kang Ki Won, Kim Keon Sik and Jung Youn Ho ," Microwave process for sintering of uranium dioxide", Journal of Nuclear Materials, Volume 325, Issues 2-3, 15 February 2004, pp 210-216

96. Ravi G. , Praveen V., Panneer Selvam M. and Rao K. J., "Microwave sintering of lead-based relaxor ferroelectric ceramics ", Materials Letters, Volume 36, Issues 1-4, July 1998, pp 191-194

97. Ravi G. , Praveen V., Panneer Selvam M. and Rao K. J., "Microwave-assisted preparation and sintering of mullite and mullite–zirconia composites from metal organics", Materials Research Bulletin, Volume 33, Issue 10, October 1998, pp 1527-1536

98. Travitzky N. A., Goldstein A., Avsian O. and Singurindi A., "Microwave sintering and mechanical properties of Y-TZP/20 wt.% Al_2O_3 composites", Materials Science and Engineering A, Volume 286, Issue 2, 15 July 2000, pp 225-229

99. Vaidhyanathan, Agrawal D. K., Shrout T. R and Fang Yi, "Microwave synthesis and sintering of $Ba(Mg_{1/3}Ta_{2/3})O_3$ ", Materials Letters, Volume 42, Issue 3, January 2000, pp 207-211

100. Völtzke, H. Abicht P., Woltersdorf J. and Pippel E., "Surface modification of pre-sintered $BaTiO_3$ particles ", Materials Chemistry and Physics, Volume 73, Issues 2-3, 15 January 2002, pp 274-280

101. Bhat Mulki H., Miura Anne, Vinatier Phillipe, Levasseur Alain and Rao Kalya J. , "Microwave synthesis of lithium lanthanum titanate", Solid State Communications, Volume 125, Issue 10, March 2003, pp 557-562

102. Panneerselvam M, Agrawal A and Rao K.J.," Microwave sintering of MoSi2–SiC composites", Materials Science and Engineering A, Volume 356, Issues 1-2, 15 September 2003, pp 267-273

103. Panneerselvam M. and Rao K.J.," A microwave method for the preparation and sintering of β′-SiAlON", Materials Research Bulletin, Volume 38, Issue 4, 24 March 2003, pp 663-674

104. Chang Aimin and Jian Jiawen , "The orientational growth of grains in doped $BaTiO_3$ PTCR materials by microwave sintering", Journal of

Materials Processing Technology, Volume 137, Issues 1-3, 30 June 2003, pp 100-101

105. Zhang G., Leparoux S., Liao H. Coddet and C.,"Microwave sintering of poly-ether-ether-ketone (PEEK) based coatings deposited on metallic substrate**",** Scripta Materialia, Volume 55, Issue 7, October 2006, pp 621-624

106. Kaddouri and S. Ifrah, "Microwave-assisted synthesis of $La_{1-x}B_xMnO_{3.15}$ (B = Sr, Ag; x = 0 or 0.2) via manganese oxides susceptors and their activity in methane combustion", Catalysis Communications, Volume 7, Issue 2, February 2006, pp 109-113

107. Cheng-Yu Hsieh, Chun-Nan Lin, Shyan-Lung Chung, Jiping Cheng and Dinesh K. Agrawal, "Microwave sintering of AlN powder synthesized by a SHS method ", Journal of the European Ceramic Society, In Press, Corrected Proof, Available online 3 July 2006.

108. Tun K.S. and Gupta M., " Improving mechanical properties of magnesium using nano-yttria reinforcement and microwave assisted powder metallurgy method", Composites Science and Technology, Volume 67, 2007, pp 2657-2664

109. Tun K.S. and Gupta M.," Effect of heating rate during hybrid microwave sintering on the tensile properties of magnesium and Mg/Y_2O_3 nanocomposite", Journal of Alloys and Compounds, doi:10.1016/j.jallcom.2007.11.047

110. Li Haoxuan, Agrawal Dinesh K., Cheng Jiping and Silsbee Michael R., "Formation and hydration of C_3S prepared by microwave and conventional sintering ",Cement and Concrete Research, Volume 29, Issue 10, October 1999, pp 1611-1617

111. Oh Sung-Tag, Tajima Ken-ichi, Ando Motohide and Ohji Tatsuki, " Fabrication of porous al2O3 by microwave sintering and its properties", Materials Letters, Volume 48, 2001, pp215–218

112. Breval E., Cheng J.P., D.K. Agrawal, P. Gigl, M. Dennis, R. Roy and A.J. Papworth, "Comparison between microwave and conventional sintering of WC/Co composites", Materials Science and Engineering A, volume 391, Issues 1-2, 25 January 2005, pp 285-295

113. VaradaRajan Y.S., Vijayaraghavan L., Krishnamurthy R. and Bhanuprasad V.V., "Performance enhancement through microwave irradiation of K20 carbide tool machining Al/SiC metal matrix composite ", Journal of Materials Processing Technology, Volume 173, Issue 2, 10 April 2006, pp 185-193

114. Kutty M.G., Bhaduri S. and Bhaduri S.B., "Gradient surface porosity in titanium dental implants: relation between processing parameters and microstructure", Journal of Material Science Mater Med., Volume 15, Issue 2, 2004, pp145-150

115. Pan Elizabeth G. and Ravaev Alexander A., "Microwave synthesis of advanced dental ceramic–alloy materials", Materials Letters, Volume 58, Issue 21, August 2004, pp 2679-2683

116. National Research Council Staff, "Microwave Processing of Materials", Washington DC, USA, National Academies Press, 1994, In: http://site.ebrary.com/lib/waikato

117. Fahrenholtz W.G., "Ceramic Engineering 111 Sintering", Ceramic Engineering Department, University of Missouri – Polla, 5 January 2004

118. Mathers, G., "Mechanical Testing – Tensile Testing Part 1", http://www.twi.co.uk/content/jk69.html

119. Brandes E.A. and Brook G.B., "Smithells Metals Reference Book", 7th Edition, The Bath Press, 1992, pp 13-1 – 13-25

120. Acharya, N.N. and Mukunda P.G., "Sintering in the copper-tin system 1: Identification of Phases and Reaction", International Journal of Powder Metallurgy, Volume 31, Issue 1, 1995, pp 63-71

121. German R.M., Sintering Theory and Practice, John Wiley, New York, 1996, In: Upadyaya A.and Sethi G., "Effect of heating mode on the densification and microstructural homogenization response of premixed bronze", Scripta Materialia, Volume 56, Issue 6, March 2007, pp 469-472

122. Asante J.K.O., Terblans J.J. and Roos W.D.," Segregation of Sn and Sb in a ternary Cu(100) SnSb alloy", Applied Surface Science, Volume 252, 2005, pp 1674-1678

123. Mishra P., Sethi G. and Upadhyaya A., " Modeling of Microwave Heating of Particulate Metals", Metallurgical and Materials Transactions B, Volume 37B, October 2006, pp 839-845

124. Meredith, R.J., "Engineers handbook of industrial microwave heating", IEE, 1998, ISBN 0852969163, In: Leonelli C., Veronesi P., Denti L., Gatto A. and Iuliano L., "Microwave assisted sintering of green metal parts", Journal of Materials Processing Technology, 2008, doi:10.1016/j.jmatprotec.2007.11.263

125. Pozar D.M., "Microwave Engineering", 2nd edition, John Wiley & Sons, Toronto, 2001, pp 1-49

126. Darcovich K., Whitfield P.S., Amow G, Shinagawa K and Miyahara R.Y., “A microstructure based numerical simulation of microwave sintering of specialized SOFC materials“, Journal of the European Ceramic Society, Volume 25, Issue 12, 2005, pp 2235-2240

127. Cheng J., Roy R. and Agrawal D., “Experimental Proof of major role of magnetic field losses in microwave heating of metal and metallic composites”, Journal of Material Science Letters, Volume 20, 2001, pp 1561-1563

128. Lin M., “Gas Quenching With Air Products’ Rapid Gas Quenching Gas Mixture”, In: http://www.airproducts.com

129. Gedevanishvilli S., Agrawal D., Roy R. and Vaidyanathan: U.S. Patent 6,512,216, Jan. 2003, pp 1-6, In: Mishra P., Sethi G. and Upadhyaya A., “Modeling of Microwave Heating of Particulate Metals”, Metallurgical and Materials Transactions B, Volume 37B, October 2006, pp 839-845

130. Vaidhyanathan B. and Rao K.J., “High Microwave Susceptibility of $NaH_2PO_4 \cdot 2H_2O$: Rapid Synthesis of Crystalline And Glassy Phosphates with NASICON-Type Chemistry”, Journal of Solid State Chemistry, Volume 132, Issue 2, September 1997, pp 349-354

131. Takayama S., Link G., Miksch S., Sato M., Ichikawa J. and Thumm M., “Behaviour of powder compacts of metals and alloys during millimeter-wave heating, In:Proceedings of the 10^{th} International Conference on Microwave and High Frequency Heating, Modena, Italia, September 12-15

132. Shen L.C. and Kong J.A., Applied Electromagnetism.PWS Publishing Co, pp 552-554, In: Leonelli C., Veronesi P., Denti L., Gatto A. and Iuliano L., “Microwave assisted sintering of green metal parts”, Journal of Materials Processing Technology, 2008, doi:10.1016/j.jmatprotec.2007.11.263

133. Thompson K., Gianchandani Y., Booske J. and Cooper R., J. MEMS, Volume 11, pp 285-292, Minay E.J., In: Leonelli C., Veronesi P., Denti L., Gatto A. and Iuliano L., “Microwave assisted sintering of green metal parts”, Journal of Materials Processing Technology, 2008, doi:10.1016/j.jmatprotec.2007.11.263

134. Veronesi P., Leonelli C., Bassoli E., Gatto A. and Iuliano L., Proceedings of the Microwave Sintering of Green Metal Parts in Sintering 2003 Conference 15-17 September, Penn State University, Pennsylvania, USA, In: Leonelli C., Veronesi P., Denti L., Gatto A. and Iuliano L., “Microwave assisted sintering of green metal parts”, Journal of Materials Processing Technology, 2008, doi:10.1016/j.jmatprotec.2007.11.263

135. Minay E.J., Veronesi P., Cannilo V., Leonelli C., Boccaccini A.R., “Control of pore size by metallic fibres in glass matrix composite foams produced by microwave heating”, Journal of European Ceramics Society, September 2004, Volume 24, Issue 10-11, pp 3203-3208, In: Leonelli C., Veronesi P., Denti L., Gatto A. and Iuliano L., “Microwave assisted sintering of green metal parts”, Journal of Materials Processing Technology, 2008, doi:10.1016/j.jmatprotec.2007.11.263

136. Whittaker A.G., Chemical Materials, Volume 17, page 3428, In: Leonelli C., Veronesi P., Denti L., Gatto A. and Iuliano L., “Microwave assisted sintering of green metal parts”, Journal of Materials Processing Technology, 2008, doi:10.1016/j.jmatprotec.2007.11.263

137. Chan Curtis, “$1Million Grant Establishes Sintering Centre”, Penn State Magazine, 1 March 2000.

APPENDICES

A. Density

A1. 97Sn2Cu1Sb

Table A1: Green density for 30kN press load for 97Sn2Cu1Sb

Sample Name	Sintering Type	Mass (g)	Length (mm)	Width (mm)	Height (mm)	Green density (g/cm3)	% Theoretical Density
97CS1	Conventional Sintering	78.83	30.8	10.1	43.01	5.89	80.34
97CS2		78.79	30.8	10.1	42.98	5.89	80.61
97CS3		78.55	30.8	10.1	42.50	5.94	81.21
97CS4		78.76	30.8	10.1	41.87	6.05	81.73
97MW1	Microwave Sintering	78.81	30.8	10.1	43.25	5.86	80.58
97MW2		78.91	30.8	10.1	42.85	5.92	80.23
97MW3		78.87	30.8	10.1	43.25	5.86	80.34
97MW4		78.89	30.8	10.1	42.79	5.93	80.27

Table A2: Green density for 40kN press load for 97Sn2Cu1Sb

Sample Number	Sample Name	Mass (g)	Length (mm)	Width (mm)	Height (mm)	Green density (g/cm3)	% Theoretical Density
97CS5	Conventional Sintering	78.92	30.8	10.1	41.09	6.17	84.46
97CS6		78.97	30.8	10.1	41.12	6.17	84.45
97CS7		78.75	30.8	10.1	40.98	6.18	84.51
97CS8		78.86	30.8	10.1	41.05	6.18	84.48
97MW5	Microwave Sintering	78.89	30.8	10.1	41.07	6.17	84.47
97MW6		78.73	30.8	10.1	40.95	6.18	84.55
97MW7		78.93	30.8	10.1	41.08	6.18	84.49
97MW8		78.98	30.8	10.1	41.11	6.18	84.49

Table A3: Sintered density at 160°C for 97Sn2Cu1Sb

Sample Name	Sintering Type	Sintering Condition	Mass (g) (air)	Mass (g) (suspended)	Sintered density (g/cm^3)	% Theoretical Density	Densification Parameter
97CS1	Conventional Sintering	30kN/60min	1.89	1.58	6.10	83.40	0.16
97CS2		30kN/120min	1.33	1.12	6.33	86.64	0.31
97CS5		40kN/60min	2.23	1.87	6.19	84.74	0.02
97CS6		40kN/120min	2.05	1.73	6.41	87.64	0.21
97MW1	Microwave Sintering	30kN/15min	2.78	2.37	6.78	92.76	0.63
97MW2		30kN/30min	2.87	2.45	6.83	93.48	0.67
97MW5		40kN/15min	2.9	2.47	6.74	92.26	0.50
97MW6		40kN/30min	3.1	2.65	6.89	94.24	0.63

Table A4: Sintered density at 220°C for 97Sn2Cu1Sb

Sample Name	Sintering Type	Sintering Condition	Mass (g) (air)	Mass (g) (suspended)	Sintered density (g/cm^3)	% Theoretical Density	Densification Parameter
97CS3	Conventional Sintering	30kN/60min	1.96	1.66	6.53	89.38	0.42
97CS4		30kN/120min	2.56	2.19	6.92	94.65	0.72
97CS7		40kN/60min	1.78	1.51	6.59	90.19	0.36
97CS8		40kN/120min	1.64	1.41	7.18	98.28	0.88
97MW3	Microwave Sintering	30kN/15min	2.89	2.47	6.88	94.13	0.70
97MW4		30kN/30min	3.13	2.68	6.96	95.15	0.76
97MW7		40kN/15min	2.94	2.53	7.11	97.28	0.82
97MW8		40kN/30min	3.15	2.71	7.22	98.71	0.92

A2. 94Sn4Cu2Sb

Table A5: Green density for 30kN press load for 94Sn4Cu2Sb

Sample Name	Mass (g)	Length (mm)	Width (mm)	Height (mm)	Green density (g/cm3)	% Theoretical Density
94CS1	78.86	30.8	10.1	42.93	5.91	80.56
94CS2	78.84	30.8	10.1	42.58	5.95	81.20
94CS3	78.82	30.8	10.1	42.65	5.94	81.05
94CS4	78.89	30.8	10.1	42.87	5.92	80.70
94MW1	78.88	30.8	10.1	42.85	5.92	80.73
94MW2	78.93	30.8	10.1	42.98	5.90	80.54
94MW3	78.95	30.8	10.1	43.05	5.90	80.43
94MW4	78.96	30.8	10.1	43.08	5.89	80.38

TableA6: Green density for 40kN press load for 94Sn4Cu2Sb

Sample Name	Mass (g)	Length (mm)	Width (mm)	Height (mm)	Green density (g/cm3)	% Theoretical Density
94CS5	78.96	30.8	10.1	41.27	6.15	83.91
94CS6	78.94	30.8	10.1	41.14	6.17	84.15
94CS7	78.87	30.8	10.1	40.68	6.23	85.03
94CS8	78.89	30.8	10.1	41.05	6.18	84.28
94MW5	78.79	30.8	10.1	40.39	6.27	85.55
94MW6	78.86	30.8	10.1	40.66	6.23	85.06
94MW7	78.87	30.8	10.1	40.74	6.22	84.90
94MW8	78.95	30.8	10.1	41.21	6.16	84.02

Table A7: Sintered density at 160°C for 94Sn4Cu2Sb

Sample Name	Sintering Type	Sintering Conditions	Mass (g) (air)	Mass (g) (suspended)	Sintered density (g/cm3)	% Theoretical Density	Densification parameter
94CS1	Conventional Sintering	30kN/60min	3.5837	3.01	6.14	83.76	0.16
94CS2		30kN/120min	3.4156	2.91	6.63	90.38	0.49
94CS5		40kN/60min	3.7789	3.20	6.53	89.05	0.32
94CS6		40kN/120min	3.5044	2.98	6.68	91.17	0.44
94MW1	Microwave Sintering	30kN/15min	4.0562	3.46	6.80	92.82	0.62
94MW2		30kN/30min	4.0145	3.43	6.87	93.70	0.68
94MW5		40kN/15min	3.7865	3.23	6.80	92.83	0.50
94MW6		40kN/30min	3.6394	3.12	7.01	95.59	0.71

TableA8: Sintered density at 220°C for 94Sn4Cu2Sb

Sample Name	Sintering Type	Sintering Conditions	Mass (g) (air)	Mass (g) (suspended)	Sintered density (g/cm3)	% Theoretical Density	Densification Parameter
94CS3	Conventional Sintering	30kN/60min	3.4140	2.92	6.76	92.26	0.59
94CS4		30kN/120min	3.4102	2.93	6.97	95.05	0.74
94CS7		40kN/60min	3.9281	3.36	6.91	94.33	0.62
94CS8		40kN/120min	3.529	3.04	7.22	98.46	0.90
94MW3	Microwave Sintering	30kN/15min	3.9369	3.37	6.94	94.74	0.73
94MW4		30kN/30min	3.7670	3.23	7.02	95.78	0.78
94MW7		40kN/15min	3.3611	2.89	7.13	97.33	0.82
94MW8		40kN/30min	3.5519	3.06	7.24	98.75	0.92

A3. 91Sn6Cu3Sb

Table A9: Green density for 30kN press load for 91Sn6Cu3Sb

Sample Name	Mass (g)	Length (mm)	Width (mm)	Height (mm)	Green density (g/cm3)	% Theoretical Density
91CS1	78.93	30.8	10.1	42.83	5.92	80.60
91CS2	78.86	30.8	10.1	42.31	5.99	81.52
91CS3	78.82	30.8	10.1	42.62	5.94	80.88
91CS4	78.96	30.8	10.1	42.97	5.91	80.37
91MW1	78.92	30.8	10.1	42.81	5.93	80.63
91MW2	78.96	30.8	10.1	42.99	5.90	80.33
91MW3	78.95	30.8	10.1	42.96	5.91	80.38
91MW4	78.89	30.8	10.1	42.42	5.98	81.34

Table A10: Green density for 40kN press load for 91Sn6Cu3Sb

Sample Name	Mass (g)	Length (mm)	Width (mm)	Height (mm)	Green density (g/cm3)	% Theoretical Density
91CS5	78.98	30.8	10.1	40.85	6.22	84.56
91CS6	78.99	30.8	10.1	40.93	6.20	84.41
91CS7	78.95	30.8	10.1	40.74	6.23	84.76
91CS8	78.92	30.8	10.1	40.71	6.23	84.79
91MW5	78.96	30.8	10.1	40.77	6.23	84.70
91MW6	78.97	30.8	10.1	40.83	6.22	84.59
91MW7	78.96	30.8	10.1	40.75	6.23	84.75
91MW8	78.95	30.8	10.1	40.73	6.23	84.78

TableA11: Sintered density at 160°C for 91Sn6Cu3Sb

Sample Name	Sintering Type	Sintering Conditions	Mass (g) (air)	Mass (g) (suspended)	Sintered density (g/cm3)	% Theoretical Density	Densification parameter
91CS1	Conventional Sintering	30kN/60min	3.9352	3.30	6.20	84.29	0.20
91CS2		30kN/120min	3.9757	3.38	6.67	90.80	0.50
91CS5		40kN/60min	21.1222	17.90	6.56	89.19	0.30
91CS6		40kN/120min	21.1417	17.99	6.71	91.27	0.44
91MW1	Microwave Sintering	30kN/15min	3.8141	3.256	6.83	92.98	0.63
91MW2		30kN/30min	3.8725	3.311	6.89	93.75	0.68
91MW5		40kN/15min	19.6725	16.789	6.82	92.82	0.53
91MW6		40kN/30min	19.5852	16.758	6.93	94.25	0.63

TableA12: Sintered density at 220°C for 91Sn6Cu3Sb

Sample Name	Sintering Type	Sintering Conditions	Mass (g) (air)	Mass (g) (suspended)	Sintered density (g/cm3)	% Theoretical Density	Densification parameter
91CS3	Conventional Sintering	30kN/60min	4.9232	4.20	6.81	92.62	0.62
91CS4		30kN/120min	20.4443	17.54	7.04	95.77	0.78
91CS7		40kN/60min	22.4221	19.19	6.94	94.39	0.63
91CS8		40kN/120min	21.8707	18.85	7.24	98.51	0.90
91MW3	Microwave Sintering	30kN/15min	11.272	9.654	6.97	94.78	0.74
91MW4		30kN/30min	8.244	7.075	7.05	95.95	0.78
91MW7		40kN/15min	19.1004	16.438	7.17	97.61	0.84
91MW8		40kN/30min	22.4998	19.401	7.26	98.79	0.92

B. Porosity

B1. 97Sn2Cu1Sb

Table B1: Porosity for conventional sintered samples for 97Sn2Cu1Sb

Sample Name	Dry weight (g)	Saturated weight (g)	Suspended weight (g)	Volume of open pores Vo (cm^3)	Bulk volume Vb (cm^3)	True volume Vt (cm^3)	Volume of closed pores Vcp (cm^3)	Porosity (%)
97CS1	1.890	1.924	1.58	0.0340	0.34	0.2585	0.0515	19.90
97CS2	1.330	1.456	1.12	0.1260	0.34	0.1819	0.0281	15.42
97CS3	1.960	2.094	1.66	0.1340	0.43	0.2681	0.0319	11.89
97CS4	2.560	2.685	2.19	0.1250	0.50	0.3502	0.0198	5.65
97CS5	2.229	2.368	1.87	0.1390	0.50	0.3049	0.0541	17.73
97CS6	2.048	2.115	1.73	0.0674	0.39	0.2802	0.0378	13.50
97CS7	1.777	1.852	1.51	0.0750	0.34	0.2431	0.0239	9.84
97CS8	1.638	1.741	1.41	0.1030	0.33	0.2241	0.0039	1.75

Table B2: Porosity for microwave sintered samples for 97Sn2Cu1Sb

Sample Name	Dry weight (g)	Saturated weight (g)	Suspended weight (g)	Volume of open pores Vo (cm^3)	Bulk volume Vb (cm^3)	True volume Vt (cm^3)	Volume of closed pores Vcp (cm^3)	Porosity (%)
97MW1	2.780	2.869	2.37	0.0890	0.50	0.3803	0.0297	7.81
97MW2	2.870	2.953	2.45	0.0830	0.50	0.3926	0.0274	6.98
97MW3	2.890	3.011	2.47	0.1210	0.54	0.3953	0.0247	6.24
97MW4	3.130	3.268	2.68	0.1380	0.59	0.4282	0.0218	5.10
97MW5	2.900	3.022	2.47	0.1220	0.55	0.3967	0.0333	8.39
97MW6	3.100	3.246	2.65	0.1460	0.60	0.4241	0.0259	6.11
97MW7	2.944	3.051	2.53	0.1070	0.52	0.4027	0.0113	2.80
97MW8	3.146	3.252	2.71	0.1060	0.54	0.4304	0.0056	1.31

B2. 94Sn4Cu2Sb

Table B3: Porosity for conventional sintered samples for 94Sn4Cu2Sb

Sample Name	Dry weight (g)	Saturated weight (g)	Suspended weight (g)	Volume of open pores Vo (cm^3)	Bulk volume Vb (cm^3)	True volume Vt (cm^3)	Volume of closed pores Vcp (cm^3)	Porosity (%)
94CS1	3.584	3.646	3.01	0.0620	0.64	0.4889	0.0848	17.34
94CS2	3.416	3.522	2.90	0.1061	0.62	0.4660	0.0496	10.65
94CS3	3.414	3.512	2.91	0.0975	0.60	0.4658	0.0382	8.21
94CS4	3.410	3.454	2.92	0.0439	0.53	0.4652	0.0250	5.37
94CS5	3.779	3.858	3.20	0.0795	0.66	0.5155	0.0634	12.29
94CS6	3.504	3.665	2.98	0.1607	0.69	0.4781	0.0463	9.69
94CS7	3.928	4.084	3.36	0.1562	0.72	0.5359	0.0322	6.01
94CS8	3.529	3.640	3.04	0.1108	0.60	0.4814	0.0076	1.57

Table B4: Porosity for microwave sintered samples for 94Sn4Cu2Sb

Sample Name	Dry weight (g)	Saturated weight (g)	Suspended weight (g)	Volume of open pores Vo (cm^3)	Bulk volume Vb (cm^3)	True volume Vt (cm^3)	Volume of closed pores Vcp (cm^3)	Porosity (%)
94MW1	4.056	4.193	3.46	0.1370	0.73	0.5534	0.0418	7.56
94MW2	4.015	4.148	3.43	0.1336	0.72	0.5477	0.0348	6.36
94MW3	3.937	4.064	3.37	0.1266	0.70	0.5371	0.0318	5.92
94MW4	3.767	3.876	3.23	0.1099	0.65	0.5138	0.0227	4.41
94MW5	3.787	3.839	3.23	0.0521	0.61	0.5166	0.0379	7.34
94MW6	3.639	3.762	3.11	0.1230	0.65	0.4965	0.0309	6.22
94MW7	3.361	3.427	2.89	0.0654	0.54	0.4585	0.0126	2.74
94MW8	3.552	3.629	3.06	0.0770	0.57	0.4846	0.0062	1.29

B3. 91Sn6Cu3Sb

Table B5: Porosity for conventional sintered samples for 91Sn6Cu3Sb

Sample Name	Dry weight (g)	Saturated weight (g)	Suspended weight (g)	Volume of open pores Vo (cm^3)	Bulk volume Vb (cm^3)	True volume Vt (cm^3)	Volume of closed pores Vcp (cm^3)	Porosity (%)
91CS1	3.935	4.0263	3.31	0.0911	0.72	0.5369	0.0873	16.27
91CS2	3.976	4.1132	3.38	0.1375	0.74	0.5424	0.0553	10.20
91CS3	4.923	5.2214	4.20	0.2982	1.02	0.6717	0.0545	8.12
91CS4	20.444	20.6487	17.53	0.2044	3.12	2.7891	0.1242	4.45
91CS5	21.122	21.2548	17.91	0.1326	3.34	2.8816	0.3306	11.47
91CS6	21.142	21.2696	17.99	0.1279	3.28	2.8843	0.2674	9.27
91CS7	22.422	22.5982	19.19	0.1761	3.41	3.0589	0.1732	5.66
91CS8	21.871	22.1859	18.84	0.3152	3.34	2.9837	0.0460	1.54

Table B6: Porosity for microwave sintered samples for 91Sn6Cu3Sb

Sample Name	Dry weight (g)	Saturated weight (g)	Suspended weight (g)	Volume of open pores Vo (cm^3)	Bulk volume Vb (cm^3)	True volume Vt (cm^3)	Volume of closed pores Vcp (cm^3)	Porosity (%)
91MW1	3.8141	4.1262	3.26	0.3121	0.87	0.5203	0.0378	7.26
91MW2	3.8725	4.0989	3.31	0.2264	0.79	0.5283	0.0322	6.09
91MW3	11.272	11.4184	9.65	0.1464	1.77	1.5378	0.0842	5.48
91MW4	8.244	8.3985	7.07	0.1545	1.33	1.1247	0.0473	4.21
91MW5	19.6725	19.9625	16.79	0.2900	3.17	2.6838	0.1947	7.25
91MW6	19.5852	19.7586	16.75	0.1734	3.01	2.6719	0.1613	6.04
91MW7	19.1004	19.3687	16.43	0.2683	2.94	2.6058	0.0656	2.52
91MW8	22.4998	22.6314	19.39	0.1316	3.24	3.0695	0.0383	1.25

C. Microhardness

C1. 97Sn2Cu1Sb

Table C1: Microhardness value for both conventional and microwave-sintered samples

Sample name	Sintering Type	Average green (HV)	1st reading (HV)	2nd reading (HV)	3rd reading (HV)	4th reading (HV)	5th reading (HV)	Average (HV)
97CS1	Conventional Sintering	12.4	13.4	13.9	13.1	12.9	12.7	13.2
97CS2			13.8	14.5	14.8	13.7	13.4	14.0
97CS3			14.6	14.9	15.7	14.5	15.5	15.0
97CS4			19.6	14.9	16.1	16.3	19.0	17.2
97CS5		14.5	15.4	14.9	13.8	14.7	15.6	14.9
97CS6			15.9	16.5	15.6	15.7	16.1	16.0
97CS7			17.4	16.9	17.6	15.9	16.8	16.9
97CS8			19.6	18.9	19.1	19.3	18.8	19.1
97MW1	Microwave Sintering	12.4	16.5	17.2	16	19.6	17.3	17.3
97MW2			20.3	19	15.9	16.6	17.5	17.9
97MW3			24.9	23.2	15.7	18.1	18.9	20.2
97MW4			25.9	16.7	28.6	15.8	23.5	22.1
97MW5		14.5	19.9	21.0	18.8	17.0	21.8	19.7
97MW6			28.4	22.5	21.9	20.4	23.3	23.3
97MW7			24.6	22.6	21.0	22.2	28.2	23.7
97MW8			20.5	24.3	29.6	23.9	21.5	24.0

C2. 94Sn4Cu2Sb

Table C2: Microhardness value for both conventional and microwave-sintered samples

Sample name	Sintering Type	Average green (HV)	1st reading (HV)	2nd reading (HV)	3rd reading (HV)	4th reading (HV)	5th reading (HV)	Average (HV)
94CS1	Conventional Sintering	12.1	10.5	11.3	12.6	21.5	13	13.8
94CS2			12.6	16.8	12.9	11.5	21.1	15.0
94CS3			16.9	18.9	18.3	12.1	13.3	15.9
94CS4			18.9	19.6	17.8	20.9	14.3	18.3
94CS5		13.1	15.4	14.9	16.1	14.2	13.9	14.9
94CS6			16.3	14.6	16.8	15.5	16.3	15.9
94CS7			19.7	15.8	19.2	14.8	15.6	17.0
94CS8			20.6	19.8	19.8	21.9	20.5	21.0
94MW1	Microwave Sintering	12.1	18.3	17.8	16.4	18.5	15.9	17.4
94MW2			16.8	18.3	18.6	16.3	19.6	17.9
94MW3			21.8	21.5	19.4	19.6	19.8	20.6
94MW4			23.3	22.8	21.7	21.4	21.8	22.2
94MW5		13.1	19.8	18.9	20.6	19.6	19.7	19.7
94MW6			21.6	22.9	22.6	23.5	21.2	22.4
94MW7			22.8	24.9	23.9	24.6	22.7	23.8
94MW8			26.8	27.9	25.0	24.5	19.3	24.7

C3. 91Sn6Cu3Sb

Table C3: Microhardness value for both conventional and microwave-sintered samples

Sample name	Sintering Type	Average green (HV)	1st reading (HV)	2nd reading (HV)	3rd reading (HV)	4th reading (HV)	5th reading (HV)	Average (HV)
91CS1	Conventional Sintering	14.4	17.4	17.1	17.6	16.8	15.1	16.8
91CS2			17	21.2	17.5	18.9	16.8	18.3
91CS3			21.7	19.3	18.5	18.9	20.3	19.7
91CS4			20.4	25.7	19.6	25.1	26.6	23.5
91CS5		15.3	19.6	16.1	18.9	18.0	19.4	18.4
91CS6			18.2	19.1	18.4	18.9	18.4	18.6
91CS7			26.2	23.3	21.1	23.9	20.8	23.1
91CS8			23.8	25.7	23.8	23.3	24.4	24.2
91MW1	Microwave Sintering	14.4	16.8	16.1	19.7	18.1	17.8	17.7
91MW2			18.8	17.9	18.2	17.8	20.1	18.6
91MW3			18.9	23.9	20.2	28.7	19.4	22.2
91MW4			19.4	20.9	24.1	29.2	28.4	24.4
91MW5		15.3	15.1	22.3	18.3	18.1	19.7	18.7
91MW6			18.8	19.4	18.7	18.5	22.9	19.7
91MW7			23.2	25.3	24.3	22.4	23.7	23.9
91MW8			26.3	26.7	25.7	25.9	24.8	25.9

D. Tensile Strength

D1. 97Sn2Cu1Sb

Table D1: Tensile strength values for longitudinal samples of 97Sn2Cu1Sb

Longitudinal	Maximum Tensile Strength (Mpa)				Strain to fracture
Sample	1st reading	2nd reading	3rd reading	Average	(%)
97CS1	24.351	23.489	20.791	22.9	7.4
97CS2	26.252	23.263	25.702	25.1	8.2
97CS3	26.633	28.750	28.295	27.9	10.1
97CS4	39.536	40.203	37.881	39.2	13.4
97CS5	26.509	25.490	25.652	25.9	7.5
97CS6	27.517	26.664	27.132	27.1	8.4
97CS7	30.066	30.242	30.599	30.3	10.6
97CS8	46.343	39.754	39.173	41.8	16.3
97MW1	21.193	20.046	19.587	20.3	7.1
97MW2	24.450	24.337	23.846	24.2	8.3
97MW3	26.540	27.110	24.887	26.2	9.5
97MW4	32.707	37.627	35.361	35.2	13.3
97MW5	22.442	24.163	22.064	22.9	8.3
97MW6	25.096	25.648	23.934	24.9	9.3
97MW7	28.354	28.430	26.712	27.8	11.0
97MW8	37.488	37.191	36.858	37.2	16.4

Table D2: Tensile strength values for transverse samples of 97Sn2Cu1Sb

Transverse	Maximum Tensile Strength (Mpa)				Strain to fracture
Sample	1st reading	2nd reading	3rd reading	Average	(%)
97CS1	24.717	23.842	21.611	23.4	7.4
97CS2	26.860	27.375	26.442	26.9	8.4
97CS3	30.888	30.915	27.877	29.9	11.0
97CS4	43.369	35.721	41.509	40.2	13.8
97CS5	28.003	26.634	27.549	27.4	7.4
97CS6	31.913	32.481	31.390	31.9	8.2
97CS7	33.234	35.491	33.415	34.0	10.9
97CS8	43.774	47.013	43.219	44.7	16.9
97MW1	23.779	23.034	21.629	22.8	7.1
97MW2	25.073	24.106	26.131	25.1	8.3
97MW3	29.907	28.934	27.624	28.8	9.8
97MW4	36.678	35.842	37.237	36.6	13.5
97MW5	22.781	27.563	21.150	23.8	8.6
97MW6	27.128	25.467	27.549	26.7	9.6
97MW7	29.507	28.079	29.441	29.0	11.5
97MW8	37.945	40.765	43.085	40.6	16.7

D2. 94Sn4Cu2Sb

Table D3: Tensile strength values for longitudinal samples of 94Sn4Cu2Sb

Longitudinal	Maximum Tensile Strength (Mpa)				Strain to fracture
Sample	1st reading	2nd reading	3rd reading	Average	(%)
94CS1	23.082	23.87	24.936	24.0	7.2
94CS2	26.862	25.382	25.387	25.9	7.6
94CS3	28.994	29.859	29.404	29.4	9.4
94CS4	34.706	43.087	37.518	38.4	12.2
94CS5	25.185	26.141	27.385	26.2	7.2
94CS6	28.549	28.845	31.450	29.6	7.9
94CS7	31.963	33.742	35.463	33.7	10.1
94CS8	48.049	41.911	43.283	44.4	15.1
94MW1	22.329	22.143	22.863	22.4	7.1
94MW2	25.083	24.94	26.109	25.4	7.5
94MW3	27.93	30.059	29.407	29.1	9.5
94MW4	38.388	38.549	37.428	38.1	12.1
94MW5	25.247	28.459	26.201	26.6	7.8
94MW6	30.722	27.941	31.054	29.9	8.5
94MW7	34.316	31.996	34.260	33.5	10.3
94MW8	43.693	44.943	44.899	44.5	14.9

Table D4: Tensile strength values for transverse samples of 94Sn4Cu2Sb

Transverse	Maximum Tensile Strength (Mpa)				Strain to fracture
Sample	1st reading	2nd reading	3rd reading	Average	(%)
94CS1	25.425	23.801	26.005	25.1	7.2
94CS2	26.643	26.583	27.155	26.8	7.9
94CS3	31.304	30.907	31.087	31.1	9.8
94CS4	40.325	39.581	40.199	40.0	12.9
94CS5	28.376	30.635	25.871	28.3	7.2
94CS6	30.72	32.176	32.126	31.7	7.8
94CS7	34.386	36.342	39.317	36.7	10.2
94CS8	47.842	43.274	49.499	46.9	15.3
94MW1	23.412	23.798	23.517	23.6	7.1
94MW2	27.974	27.496	26.539	27.3	7.5
94MW3	31.154	30.967	31.078	31.1	9.8
94MW4	41.336	39.66	39.410	40.1	12.9
94MW5	29.866	27.237	28.818	28.6	8.1
94MW6	33.456	32.31	31.083	32.3	9.0
94MW7	33.821	37.839	37.631	36.4	10.5
94MW8	46.591	46.682	47.873	47.0	15.2

D3. 91Sn 6Cu3Sb

Table D5: Tensile strength values for longitudinal samples

Longitudinal	Maximum Tensile Strength (Mpa)				Strain to fracture
Sample	1st reading	2nd reading	3rd reading	Average	(%)
91CS1	25.554	26.213	24.278	25.3	6.9
91CS2	27.233	27.270	27.354	27.3	7.3
91CS3	33.494	32.680	30.238	32.1	9.1
91CS4	37.622	38.375	40.902	39.0	11.5
91CS5	29.319	28.521	26.101	28.0	7.0
91CS6	34.462	29.498	31.859	31.9	7.5
91CS7	33.567	35.136	40.519	36.4	9.7
91CS8	50.231	44.640	43.117	46.0	13.7
91MW1	23.060	22.222	23.969	23.1	6.9
91MW2	25.927	27.010	27.616	26.9	7.2
91MW3	33.071	37.080	37.981	36.0	9.1
91MW4	41.020	45.142	36.281	40.8	11.7
91MW5	29.266	28.457	28.840	28.9	7.4
91MW6	34.541	33.789	34.521	34.3	8.1
91MW7	40.172	38.613	39.230	39.3	9.6
91MW8	46.754	45.398	47.425	46.5	13.6

Table D6: Tensile strength values for transverse samples

Transverse	Maximum Tensile Strength (Mpa)				Strain to fracture
Sample	1st reading	2nd reading	3rd reading	Average	(%)
91CS1	26.236	27.886	27.375	27.2	7.1
91CS2	27.681	30.152	29.427	29.1	7.6
91CS3	39.642	35.357	36.955	37.3	9.4
91CS4	43.503	43.848	41.050	42.8	12.1
91CS5	31.740	32.155	32.250	32.0	7.1
91CS6	35.089	32.756	37.902	35.2	7.6
91CS7	39.916	41.137	43.224	41.4	9.9
91CS8	48.333	47.199	48.032	47.9	13.9
91MW1	24.701	25.416	22.807	24.3	6.9
91MW2	29.024	32.658	30.284	30.7	7.3
91MW3	37.691	40.165	42.161	40.0	9.3
91MW4	42.668	47.555	47.453	45.9	12.0
91MW5	31.222	33.662	34.940	33.3	7.7
91MW6	38.204	36.613	37.717	37.5	8.2
91MW7	45.051	41.676	45.185	44.0	9.8
91MW8	46.092	50.778	48.825	48.6	13.8

E. Grain Size

Table E1: Grain size calculation for 97 Sn2Cu1Sb

	l1	*l2*	*l3*	*l4*	*l5*	*l6*	*lavg*	D (μm)
green30kN	10.71	9.23	10.00	11.54	10.00	10.71	10.37	15.5
green40kN	10.00	11.54	10.00	10.00	7.65	10.00	9.87	14.8
97CS1	15.00	15.71	13.75	20.00	12.50	16.00	15.49	23.2
97CS2	12.73	16.25	20.00	18.33	15.00	22.86	17.53	26.3
97CS3	18.75	20.00	16.67	18.75	20.00	14.44	18.10	27.2
97CS4	23.33	25.00	20.00	17.14	20.00	10.00	19.25	28.9
97CS5	15.71	16.67	15.56	17.50	11.67	14.00	15.19	22.8
97CS6	20.00	23.33	13.33	15.00	8.75	20.00	16.74	25.1
97CS7	16.67	18.75	15.71	17.14	20.00	15.00	17.21	25.8
97CS8	20.00	20.00	15.00	15.00	23.30	14.29	17.93	26.9
97MW1	10.00	10.00	12.50	11.11	11.82	11.54	11.16	16.7
97MW2	11.54	11.54	10.71	10.56	17.78	11.33	12.24	18.4
97MW3	14.29	14.29	14.29	12.50	12.50	20.00	14.65	22.0
97MW4	11.67	20.00	16.67	16.25	18.89	18.00	16.91	25.4
97MW5	8.75	12.73	10.77	11.67	9.33	12.73	11.00	16.5
97MW6	10.77	12.00	10.67	10.91	10.00	14.44	12.14	18.2
97MW7	21.67	11.40	16.25	7.27	14.29	11.00	13.65	20.5
97MW8	15.56	15.00	13.33	12.50	25.00	13.75	15.86	23.8

Table E2: Grain size calculation for 94Sn 4Cu 2Sb

	l1	*l2*	*l3*	*l4*	*l5*	*l6*	*lavg*	D (μm)
green30kN	10.67	10.00	12.50	9.23	10.00	9.38	10.30	15.4
green40kN	10.00	10.00	9.38	8.82	9.38	10.00	9.60	14.4
94CS1	14.00	18.75	15.00	15.00	10.77	15.56	14.85	22.3
94CS2	17.5	14.29	14.29	20.00	14.49	16.67	16.21	24.3
94CS3	20.00	21.43	12.00	10.00	20.00	20.00	17.24	25.9
94CS4	21.43	19.17	21.43	15.00	14.29	21.43	18.79	28.2
94CS5	13.75	9.23	16.67	10.71	15.71	16.00	13.68	20.5
94CS6	15.00	15.00	17.14	15.00	14.00	13.63	14.96	22.4
94CS7	16.67	16.67	16.25	12.50	21.43	17.14	16.78	25.2
94CS8	21.43	20.00	13.64	16.67	18.75	11.54	17.01	25.5
94MW1	11.54	8.33	11.54	15.00	12.50	8.33	11.21	16.8
94MW2	11.67	10.00	11.54	10.00	15.00	13.63	11.97	18.0
94MW3	16.67	12.50	12.22	16.67	14.29	10.00	13.73	20.6
94MW4	18.75	17.50	14.29	18.75	13.00	16.67	16.49	24.7
94MW5	11.54	8.33	10.00	10.77	10.71	13.00	10.73	16.1
94MW6	13.64	14.29	10.00	10.00	12.50	12.00	12.07	18.1
94MW7	11.54	15.00	12.73	10.71	13.00	15.56	13.09	19.6
94MW8	15.00	18.75	16.67	15.00	15.00	13.64	15.68	23.5

Table E3: Grain size calculation for 91Sn 6Cu 3Sb

	l1	*l2*	*l3*	*l4*	*l5*	*l6*	*lavg*	D (μm)
green30kN	8.82	10.71	12.50	10.71	8.33	10.71	10.30	15.4
green40kN	8.82	11.54	8.82	8.33	8.33	10.71	9.43	14.1
91CS1	11.54	12.50	15.00	15.00	16.67	12.50	13.87	20.8
91CS2	16.67	15.00	16.67	15.00	15.00	11.54	14.98	22.5
91CS3	15.00	10.00	21.43	16.67	16.67	18.75	16.42	24.6
91CS4	16.67	21.43	16.67	16.67	21.43	18.75	18.60	27.9
91CS5	13.64	11.54	12.50	15.00	15.00	10.71	13.07	19.6
91CS6	13.64	16.67	12.50	16.67	13.64	15.00	14.69	22.0
91CS7	15	15	16.67	16.67	18.75	15.00	16.18	24.3
91CS8	18.75	16.67	13.64	16.67	18.75	21.43	17.65	26.5
91MW1	10.71	11.54	10.71	10.00	11.33	12.50	10.71	16.1
91MW2	11.54	11.54	12.50	11.54	10.00	12.50	11.60	17.4
91MW3	16.67	16.67	12.50	11.54	12.50	13.64	13.92	20.9
91MW4	16.67	15.00	13.64	18.75	18.75	13.64	16.08	24.1
91MW5	11.54	11.54	8.82	9.43	11.54	11.54	10.74	16.1
91MW6	11.54	13.36	12.50	11.54	12.50	11.54	12.16	18.2
91MW7	13.64	13.64	12.50	13.64	12.50	11.54	12.91	19.4
91MW8	13.64	11.54	16.67	16.67	15.00	18.75	15.38	23.1

F. Electron Dispersive X-Ray Spectroscopy (EDS)

F1. Conventional Sintering at 160ºC for 96 MPa pressed samples

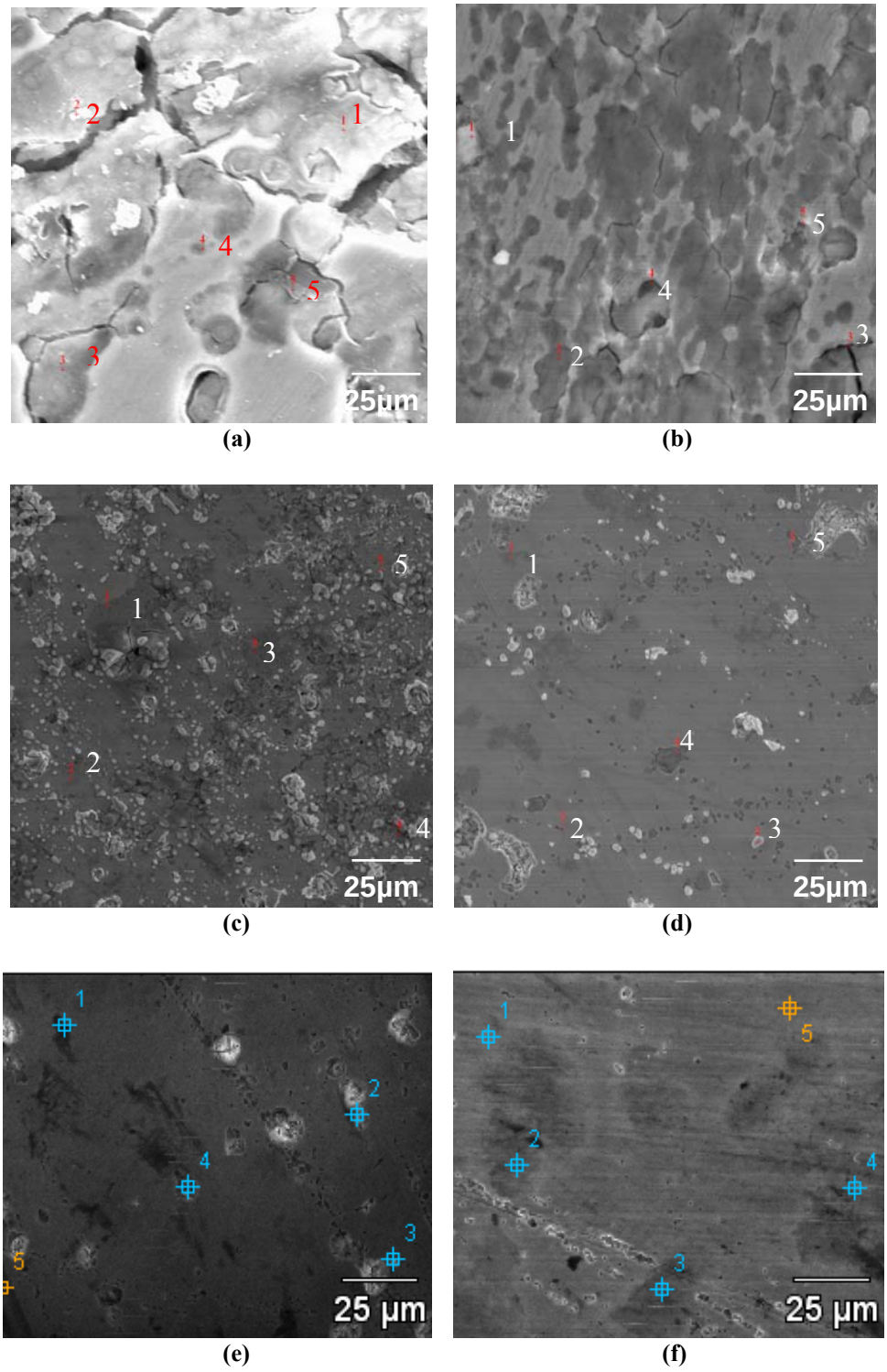

Figure F1: SEM image for conventional sintering at 160°C for the 96 MPa pressed samples (a) 60 min (b) 120 min for 97Sn2Cu1Sb composition (c) 60 min (d) 120 min for 94Sn4Cu2Sb composition (e) 60 min (f) 120 min for 91Sn6Cu3Sb composition

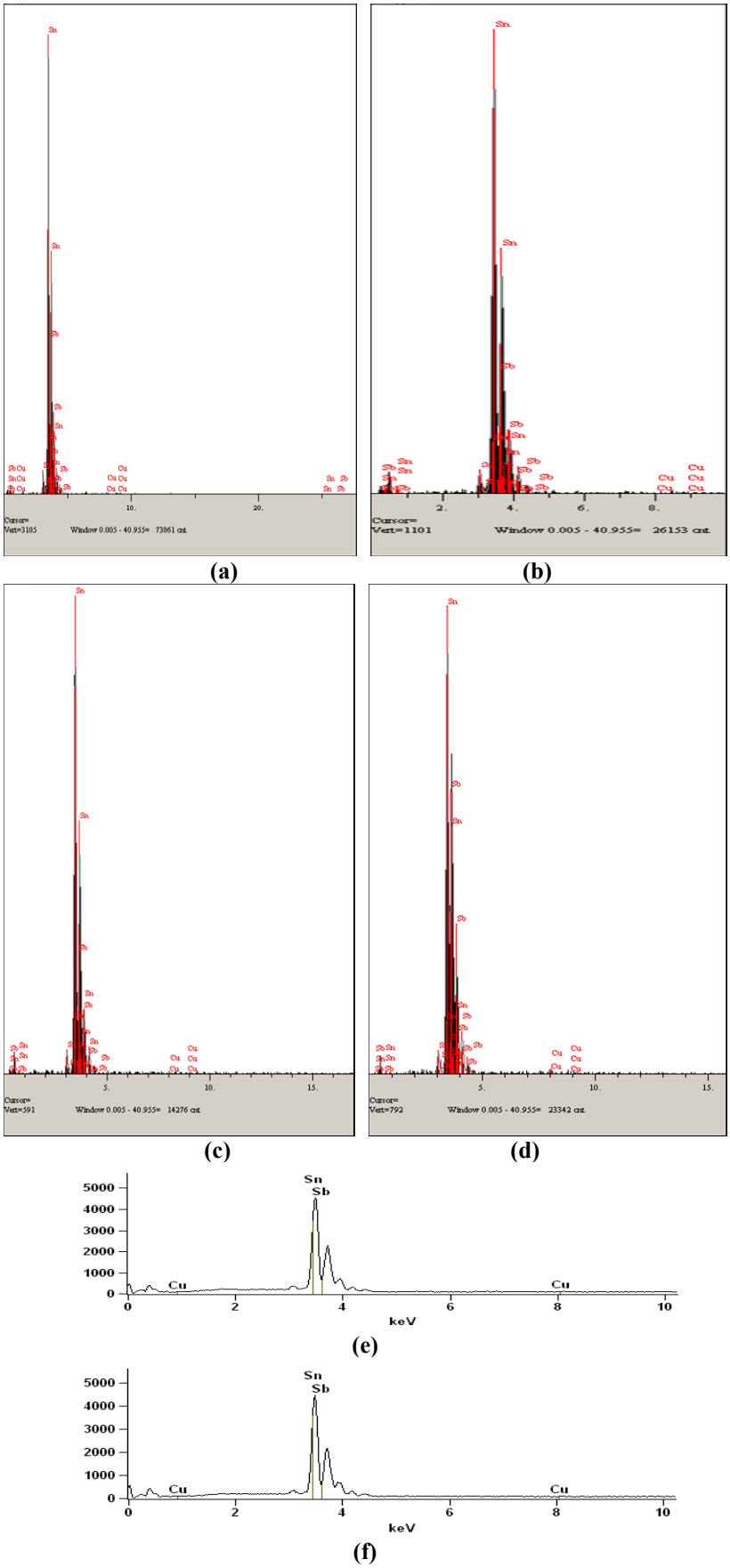

Figure F2: EDS spectrum for samples 96 MPa/160°C (a) 60 min (b) 120 min for 97Sn2Cu1Sb composition (c) 60 min (d) 120 min for 94Sn4Cu2Sb composition (e) 60 min (f) 120 min for 91Sn6Cu3Sb composition

Table F1: EDS report for samples 97CS1 (96 MPa/160°C/60 min) and 97CS2 (96 MPa/160°C/120 min)

	weight%		
	Cu-K	Sn-L	Sb-L
97CS1_pt1	1.54	97.69	0.77
97CS1_pt2	1.64	97.45	0.91
97CS1_pt3	1.42	97.84	0.74
97CS1_pt4	1.76	97.32	0.92
97CS1_pt5	1.46	97.86	0.68
97CS2_pt1	1.52	97.57	0.91
97CS2_pt2	1.46	97.87	0.67
97CS2_pt3	1.87	97.65	0.48
97CS2_pt4	1.36	97.93	0.71
97CS2_pt5	1.77	97.54	0.69

Table F2: EDS report for samples 94CS1 (96 MPa/160°C/60 min) and 94CS2 (96 MPa/160°C/120 min)

	weight%		
	Cu-K	Sn-L	Sb-L
94CS1_pt1	3.67	94.54	1.79
94CS1_pt2	3.34	94.84	1.82
94CS1_pt3	3.78	94.34	1.88
94CS1_pt4	3.94	94.65	1.41
94CS1_pt5	3.53	94.89	1.58
94CS2_pt1	3.63	94.42	1.95
94CS2_pt2	3.67	94.89	1.44
94CS2_pt3	3.35	94.86	1.79
94CS2_pt4	3.27	94.77	1.96
94CS2_pt5	3.83	94.84	1.33

Table F3: EDS report for samples 91CS1 (96 MPa/160°C/60 min) and 91CS2 (96 MPa/160°C/120 min)

	weight%		
	Cu-K	Sn-L	Sb-L
91CS1_pt1	5.33	91.94	2.73
91CS1_pt2	5.28	91.91	2.81
91CS1_pt3	5.43	91.96	2.61
91CS1_pt4	5.25	91.77	2.98
91CS1_pt5	5.21	91.85	2.94
91CS2_pt1	5.26	91.86	2.88
91CS2_pt2	5.32	91.87	2.81
91CS2_pt3	5.41	91.98	2.61
91CS2_pt4	5.29	91.99	2.72
91CS2_pt5	5.32	91.98	2.70

F2. Conventional Sintering at 220°C for 96 MPa pressed samples

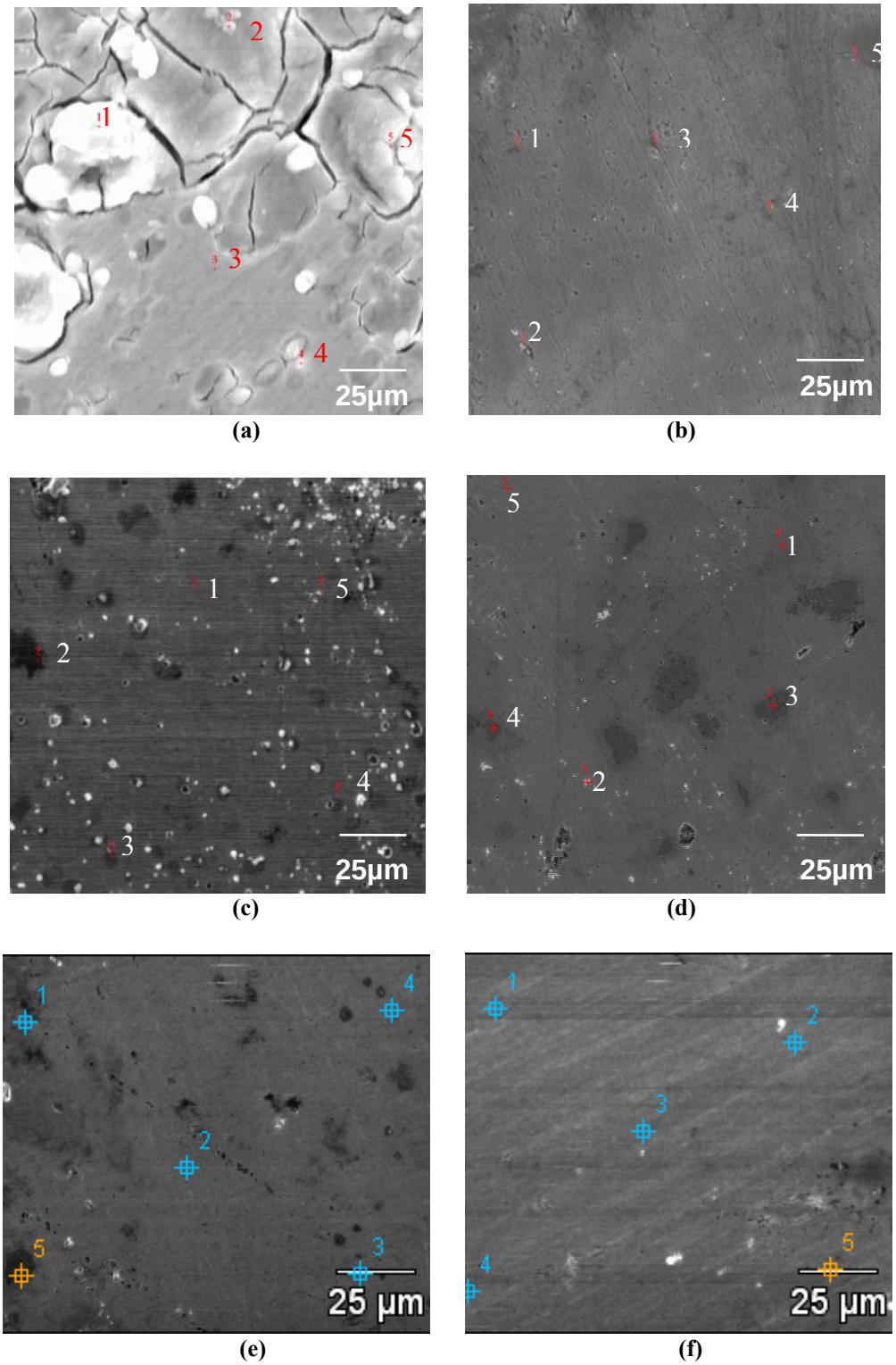

(a) (b) (c) (d) (e) (f)

Figure F3: SEM image of conventional sintering at 220°C for the 96 MPa pressed samples (a) 60 min (b) 120 min for 97Sn2Cu1Sb composition (c) 60 min (d) 120 min for 94Sn4Cu2Sb composition (e) 60 min (f) 120 min for 91Sn6Cu3Sb composition

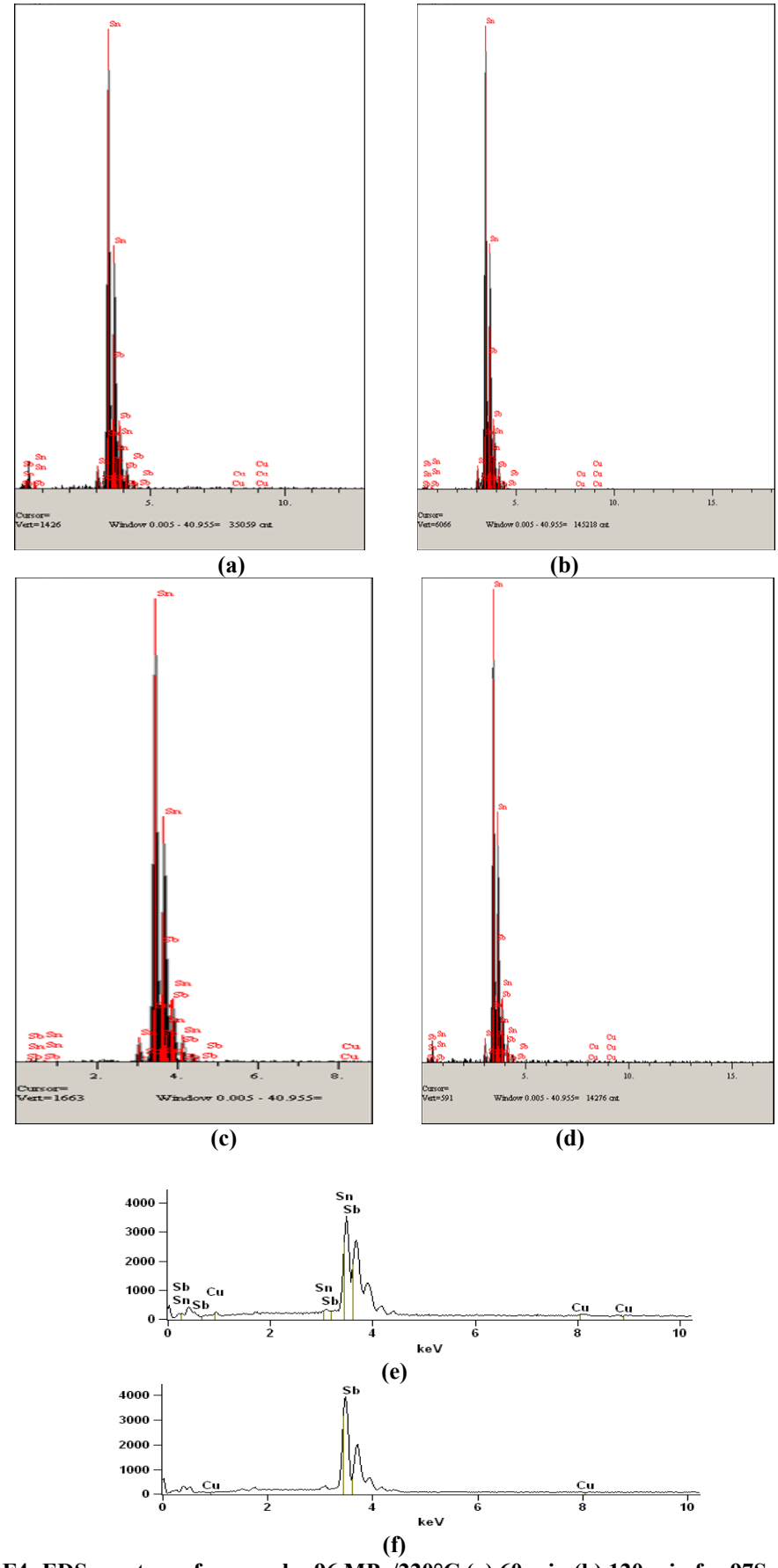

Figure F4: EDS spectrum for samples 96 MPa/220°C (a) 60 min (b) 120 min for 97Sn2Cu1Sb composition (c) 60 min (d) 120 min for 94Sn4Cu2Sb composition (e) 60 min (f) 120 min for 91Sn6Cu3Sb composition

Table F4: EDS report for samples 97CS3 (96 MPa/220°C/60 min) and 97CS4 (96 MPa/220°C/120 min)

	weight%		
	Cu-K	Sn-L	Sb-L
97CS3_pt1	1.21	97.99	0.8
97CS3_pt2	1.39	97.86	0.75
97CS3_pt3	1.32	97.72	0.96
97CS3_pt4	1.11	97.95	0.94
97CS3_pt5	1.29	97.92	0.79
97CS4_pt1	1.35	97.89	0.76
97CS4_pt2	1.67	97.83	0.5
97CS4_pt3	1.45	97.68	0.87
97CS4_pt4	1.47	97.85	0.68
97CS4_pt5	1.66	97.97	0.37

Table F5: EDS report for samples 94CS3 (96 MPa/220°C/60 min) and 94CS4 (96 MPa/220°C/120 min)

	weight%		
	Cu-K	Sn-L	Sb-L
94CS3_pt1	3.21	94.99	1.80
94CS3_pt2	3.69	94.41	1.90
94CS3_pt3	3.42	94.75	1.83
94CS3_pt4	3.71	94.86	1.43
94CS3_pt5	3.64	94.68	1.68
94CS4_pt1	3.55	94.87	1.58
94CS4_pt2	3.42	94.84	1.74
94CS4_pt3	3.47	94.72	1.81
94CS4_pt4	3.51	94.53	1.96
94CS4_pt5	3.48	94.63	1.89

Table F6: EDS report for samples 91CS3 (96 MPa/220°C/60 min) and 91CS4 (96 MPa/220°C/120 min)

	weight%		
	Cu-K	Sn-L	Sb-L
91CS3_pt1	5.31	91.94	2.75
91CS3_pt2	5.22	91.95	2.83
91CS3_pt3	5.37	91.96	2.67
91CS3_pt4	5.29	91.87	2.84
91CS3_pt5	5.17	91.95	2.88
91CS4_pt1	5.36	91.97	2.67
91CS4_pt2	5.26	91.67	3.07
91CS4_pt3	5.41	91.92	2.67
91CS4_pt4	5.19	91.96	2.85
91CS4_pt5	5.36	91.98	2.66

F3. Conventional Sintering at 160ºC for 129 MPa pressed samples

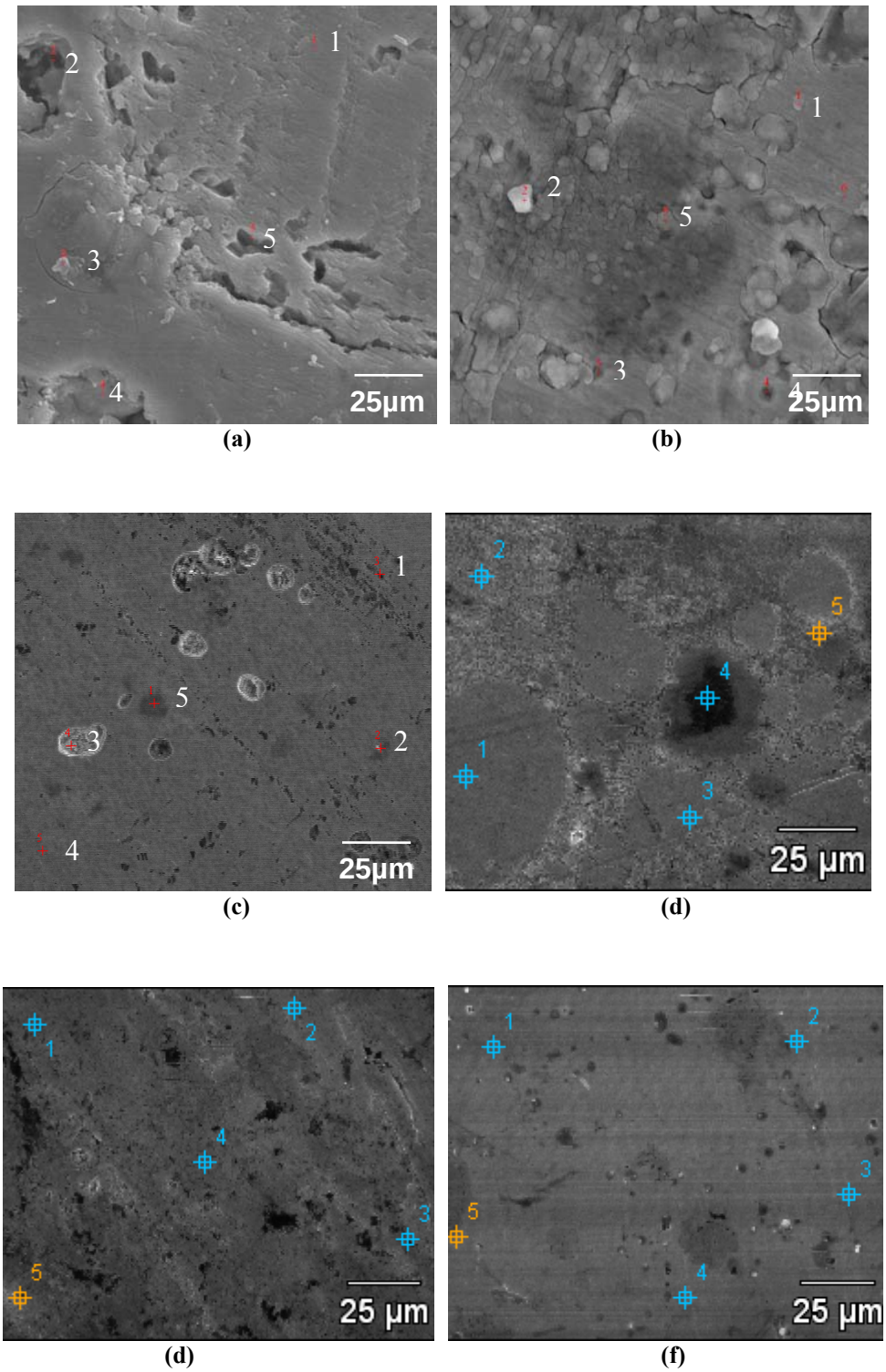

Figure F5: SEM image of conventional sintering at 160°C for the 40kN pressed samples (a) 60min (b) 120min for 97Sn2Cu1Sb composition (c) 60min (d) 120min for 94Sn4Cu2Sb composition (e) 60min (f) 120min for 91Sn6Cu3Sb composition

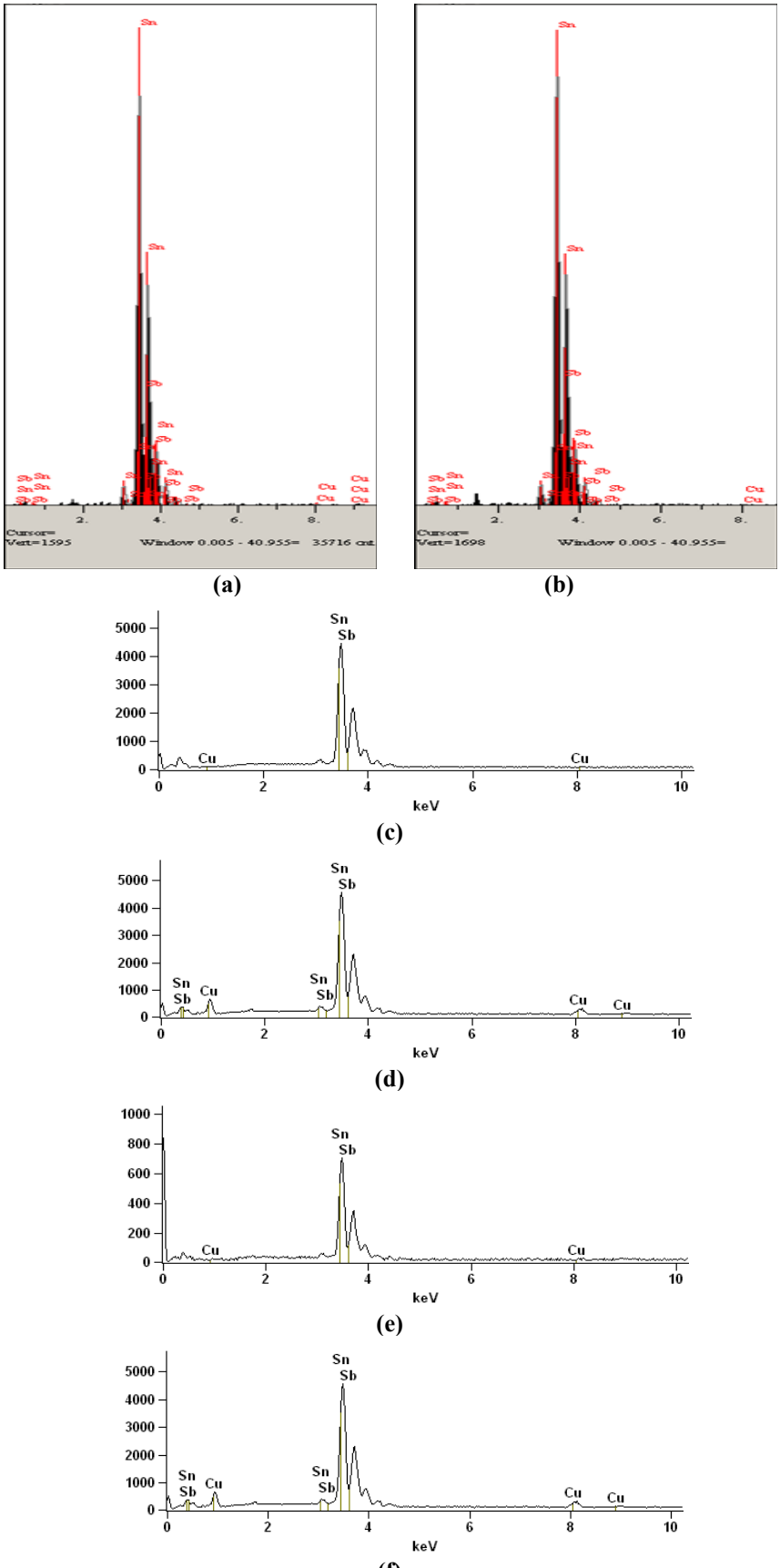

Figure F6: EDS spectrum for samples 40kN/160°C (a) 60min (b) 120min for 97Sn2Cu1Sb composition (c) 60min (d) 120min for 94Sn4Cu2Sb composition (e) 60min (f) 120 min for 91Sn6Cu3Sb composition

Table F7:EDS report for samples 97CS5(129 MPa/160°C/60min) and 97CS6 (129 MPa/160°C/120min)

	weight%		
	Cu-K	Sn-L	Sb-L
97CS5_pt1	1.53	97.55	0.92
97CS5_pt2	1.52	97.59	0.89
97CS5_pt3	1.59	97.54	0.87
97CS5_pt4	1.43	97.59	0.98
97CS5_pt5	1.36	97.75	0.89
97CS6_pt1	1.52	97.53	0.95
97CS6_pt2	1.57	97.55	0.88
97CS6_pt3	1.38	97.67	0.95
97CS6_pt4	1.68	97.58	0.74
97CS6_pt5	1.57	97.53	0.90

Table F8:EDS report for samples 94CS5(129 MPa/160°C/60min) and 94CS6 (129 MPa/160°C/120min)

	weight%		
	Cu-K	Sn-L	Sb-L
94CS5_pt1	3.27	94.87	1.86
94CS5_pt2	3.32	94.99	1.69
94CS5_pt3	3.11	94.96	1.93
94CS5_pt4	3.27	94.83	1.90
94CS5_pt5	3.19	94.86	1.95
94CS6_pt1	3.29	94.84	1.87
94CS6_pt2	3.32	94.88	1.80
94CS6_pt3	3.45	94.69	1.86
94CS6_pt4	3.47	94.58	1.95
94CS6_pt5	3.78	94.67	1.55

Table F9:EDS report for samples 91CS5(129 MPa/160°C/60min) and 91CS6 (129 MPa/160°C/120min)

	weight%		
	Cu-K	Sn-L	Sb-L
91CS5_pt1	5.41	91.97	2.62
91CS5_pt2	5.24	91.85	2.91
91CS5_pt3	5.39	91.97	2.64
91CS5_pt4	5.32	91.89	2.79
91CS5_pt5	5.42	91.93	2.65
91CS6_pt1	5.36	91.87	2.77
91CS6_pt2	5.56	91.97	2.47
91CS6_pt3	5.44	91.95	2.61
91CS6_pt4	5.23	91.91	2.86
91CS6_pt5	5.41	91.94	2.65

F4. Conventional Sintering at 220ºC for 129 MPa pressed samples

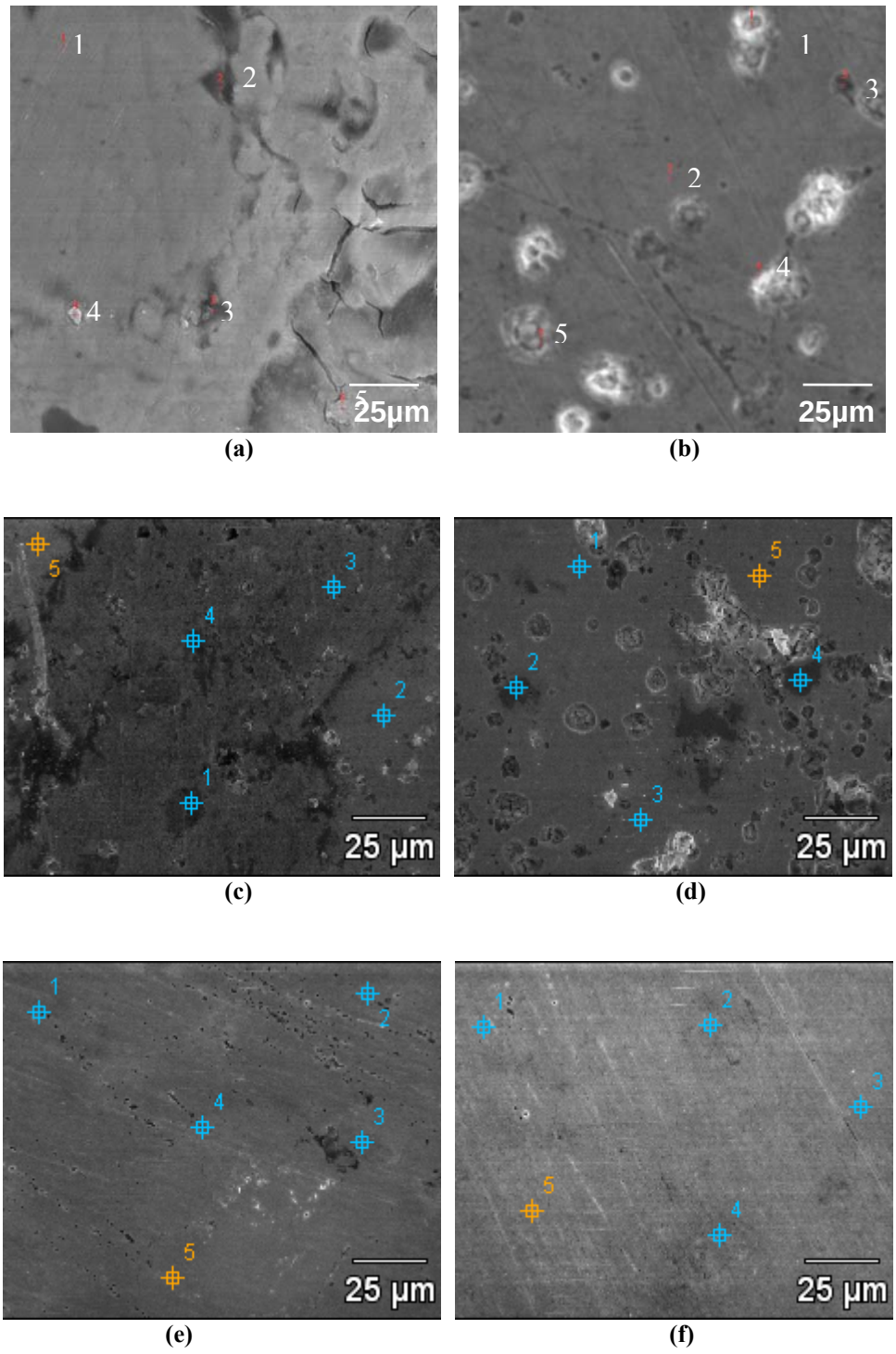

Figure F7: SEM image of conventional sintering at 220°C for the 40kN pressed samples (a) 60min (b) 120min for 97Sn2Cu1Sb composition (c) 60min (d) 120min for 94Sn4Cu2Sb composition (e) 60min (f) 120min for 91Sn6Cu3Sb composition

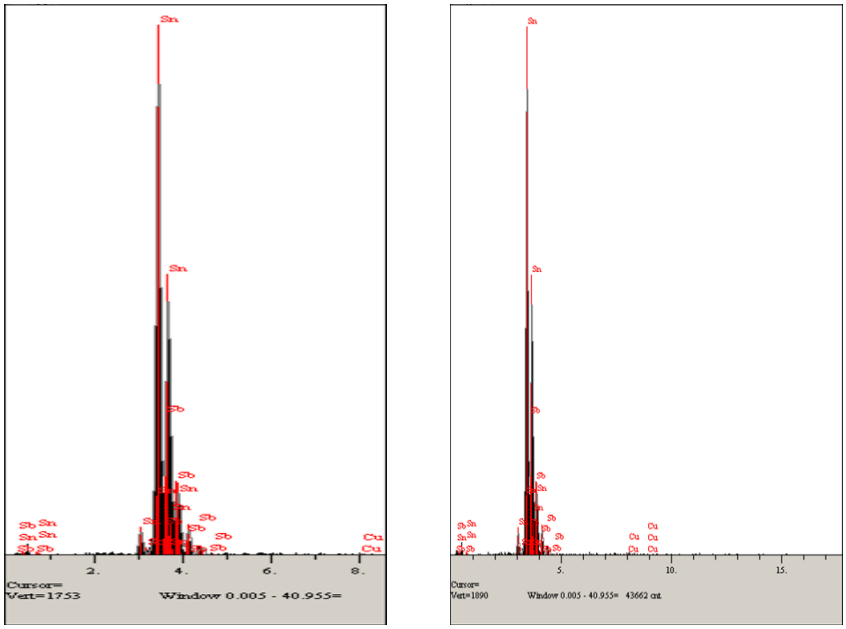

(a) (b)

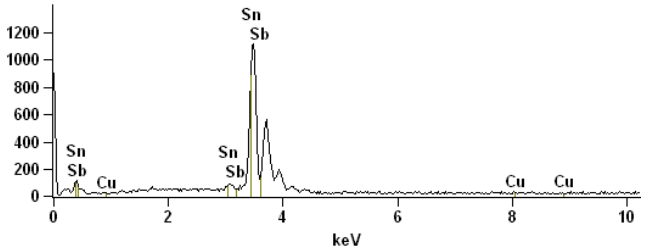

(c)

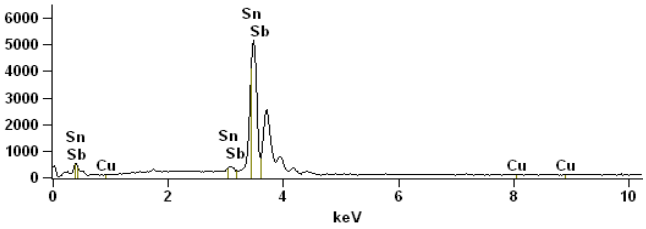

(d)

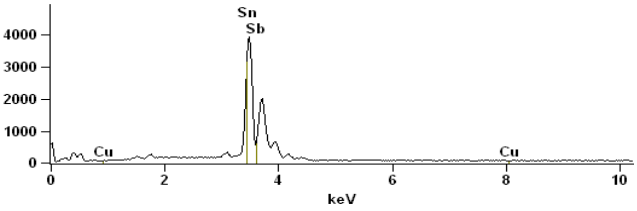

(e)

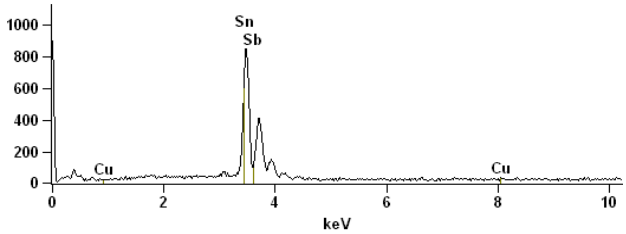

(f)

Figure F8: EDS spectrum for samples 40kN/160°C (a) 60min (b) 120min for 97Sn2Cu1Sb composition (c) 60min (d) 120min for 94Sn4Cu2Sb composition (e) 60min (f) 120 min for 91Sn6Cu3Sb composition

Table F10:EDS report for samples 97CS7(129 MPa/220°C/60min) and 97CS8 (129 MPa/220°C/120min)

	weight%		
	Cu-K	Sn-L	Sb-L
97CS7_pt1	1.56	98.05	0.39
97CS7_pt2	1.45	97.81	0.74
97CS7_pt3	1.29	97.95	0.76
97CS7_pt4	1.32	98.23	0.45
97CS7_pt5	1.86	97.86	0.28
97CS8_pt1	1.22	98.23	0.55
97CS8_pt2	1.23	98.35	0.42
97CS8_pt3	1.42	97.94	0.64
97CS8_pt4	1.14	98.22	0.64
97CS8_pt5	1.05	98.62	0.33

Table F11:EDS report for samples 94CS7(129 MPa/220°C/60min) and 94CS8 (129 MPa/220°C/120min)

	weight%		
	Cu-K	Sn-L	Sb-L
94CS7_pt1	3.33	94.94	1.73
94CS7_pt2	3.27	94.95	1.78
94CS7_pt3	3.46	94.96	1.58
94CS7_pt4	3.27	94.87	1.86
94CS7_pt5	3.19	94.95	1.86
94CS8_pt1	3.26	94.86	1.88
94CS8_pt2	3.32	94.87	1.81
94CS8_pt3	3.41	94.98	1.61
94CS8_pt4	3.29	94.99	1.72
94CS8_pt5	3.32	94.98	1.70

Table F12:EDS report for samples 91CS7(129 MPa/220°C/60min) and 91CS8 (129 MPa/220°C/120min)

	weight%		
	Cu-K	Sn-L	Sb-L
91CS7_pt1	5.39	91.97	2.64
91CS7_pt2	5.34	92.03	2.63
91CS7_pt3	5.36	91.95	2.69
91CS7_pt4	5.27	92.09	2.64
91CS7_pt5	5.42	91.93	2.65
91CS8_pt1	5.36	91.87	2.77
91CS8_pt2	5.57	91.97	2.46
91CS8_pt3	5.48	92.11	2.41
91CS8_pt4	5.28	91.99	2.73
91CS8_pt5	5.45	91.97	2.58

F5. Microwave Sintering at 160ºC for 96 MPa pressed samples

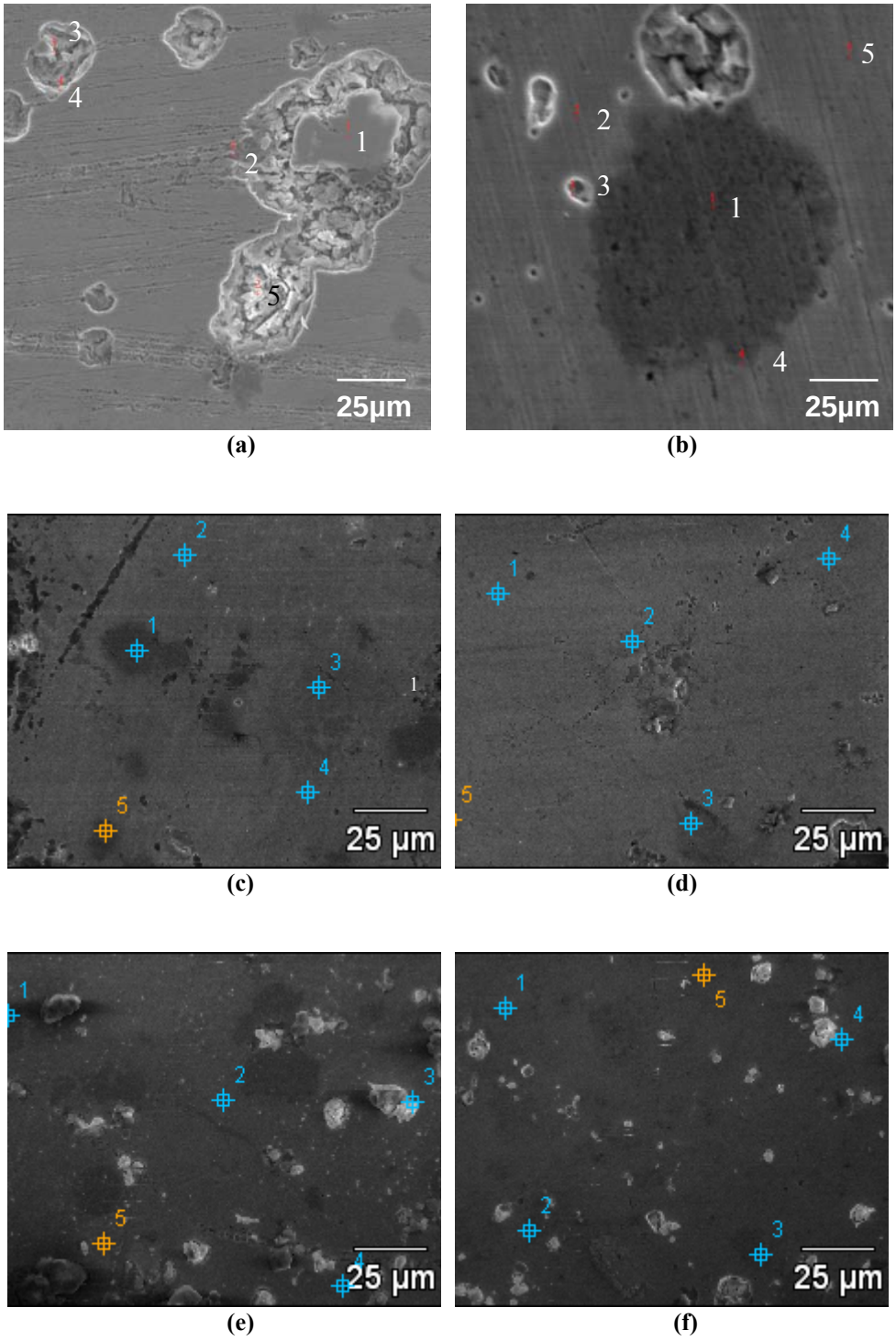

Figure F9: SEM image of microwave sintering at 160°C for the 30kN pressed samples (a) 15min (b) 30min for 97Sn2Cu1Sb composition (c) 15min (d) 30min for 94Sn4Cu2Sb composition (e) 15min (f) 30min for 91Sn6Cu3Sb composition

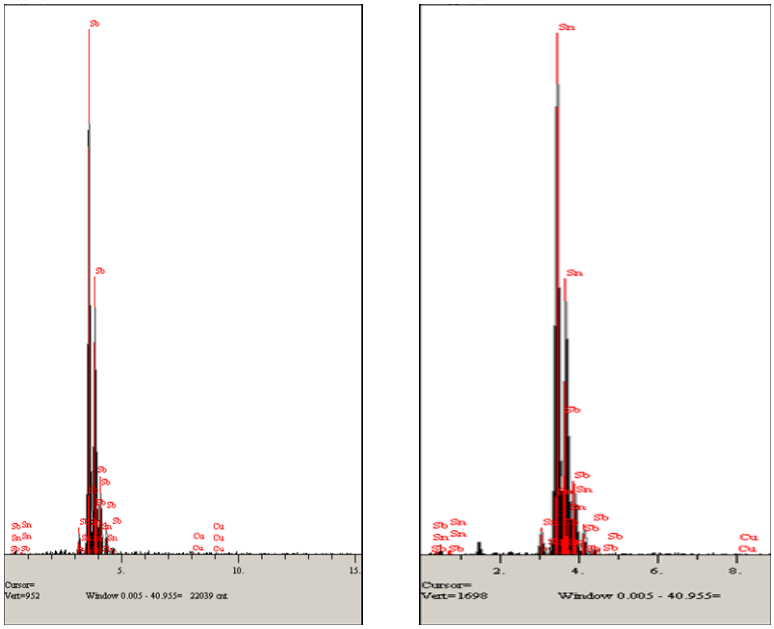

(a) (b)

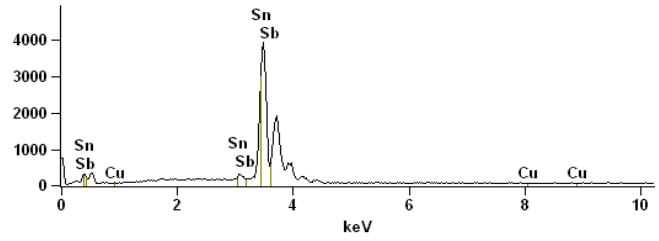

(c)

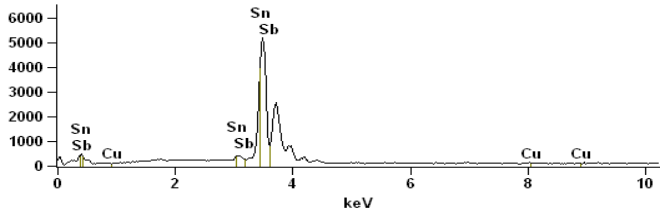

(d)

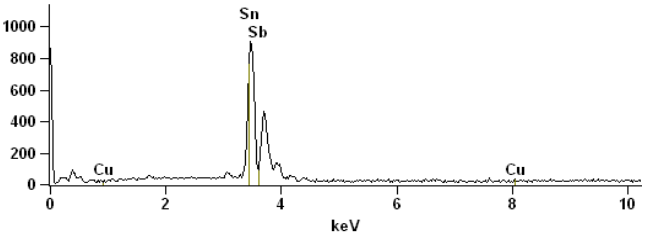

(e)

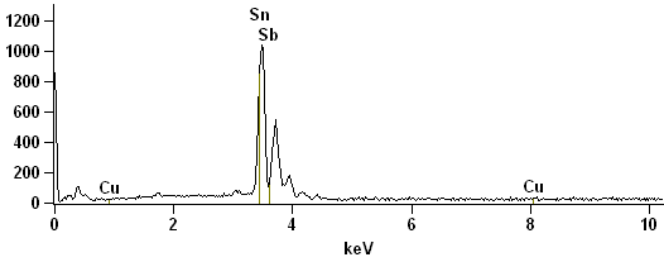

(f)

Figure F10: EDS spectrum for MW samples 30kN/160°C (a) 15min (b) 30min for 97Sn2Cu1Sb composition (c) 15min (d)30min for 94Sn4Cu2Sb composition (e)15min (f) 30 min for 91Sn6Cu3Sb composition

Table F13: EDS report for samples 97MW1 (30kN/160°C/15min) and 97MW2 (30kN/160°C/30min)

	weight%		
	Cu-K	Sn-L	Sb-L
97MW1_pt1	1.52	97.75	0.73
97MW1_pt2	1.49	97.86	0.65
97MW1_pt3	1.39	97.71	0.90
97MW1_pt4	1.35	98.26	0.39
97MW1_pt5	1.87	97.87	0.26
97MW2_pt1	1.29	98.25	0.46
97MW2_pt2	1.33	98.39	0.28
97MW2_pt3	1.48	97.54	0.98
97MW2_pt4	1.24	97.79	0.97
97MW2_pt5	1.47	97.74	0.79

Table F14: EDS report for samples 94MW1 (30kN/160°C/15min) and 94MW2 (30kN/160°C/30min)

	weight%		
	Cu-K	Sn-L	Sb-L
94MW1_pt1	3.31	94.88	1.81
94MW1_pt2	3.29	94.91	1.80
94MW1_pt3	3.48	94.92	1.60
94MW1_pt4	3.27	94.87	1.86
94MW1_pt5	3.22	94.93	1.85
94MW2_pt1	3.28	94.89	1.83
94MW2_pt2	3.35	94.79	1.86
94MW2_pt3	3.41	94.98	1.61
94MW2_pt4	3.31	94.99	1.70
94MW2_pt5	3.38	94.98	1.64

Table F15: EDS report for samples 91MW1 (30kN/160°C/15min) and 91MW2 (30kN/160°C/30min)

	weight%		
	Cu-K	Sn-L	Sb-L
91MW1_pt1	5.29	91.87	2.84
91MW1_pt2	5.49	91.66	2.85
91MW1_pt3	5.39	91.95	2.66
91MW1_pt4	5.38	91.77	2.85
91MW1_pt5	5.46	91.68	2.86
91MW2_pt1	5.36	91.85	2.79
91MW2_pt2	5.67	91.94	2.39
91MW2_pt3	5.81	92.11	2.08
91MW2_pt4	5.38	91.99	2.63
91MW2_pt5	5.47	91.91	2.62

F6. Microwave Sintering at 220ºC for 96MPa pressed samples

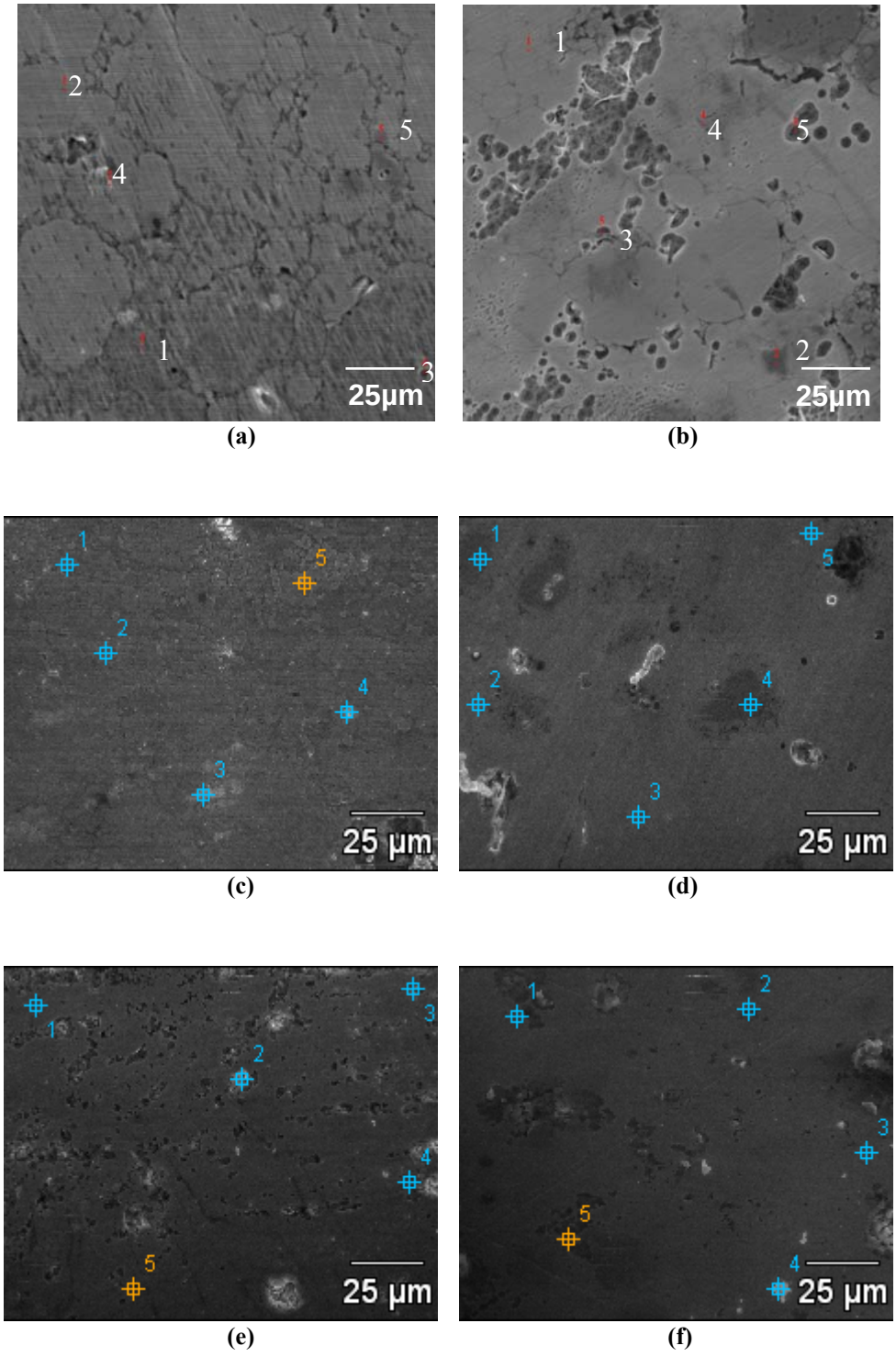

(a) (b)

(c) (d)

(e) (f)

Figure F11: SEM image of microwave sintering at 220°C for the 30kN pressed samples (a) 15min (b) 30min for 97Sn2Cu1Sb composition (c) 15min (d) 30min for 94Sn4Cu2Sb composition (e) 15min (f) 30min for 91Sn6Cu3Sb composition

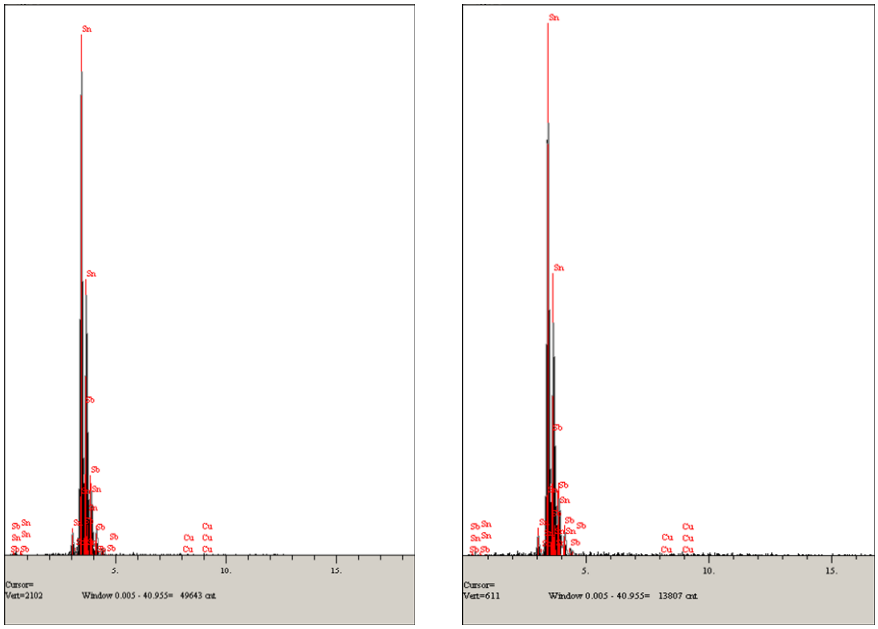

(a) (b)

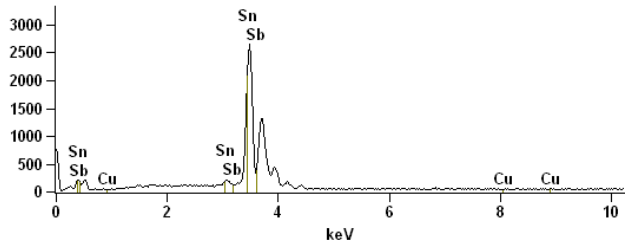

(c)

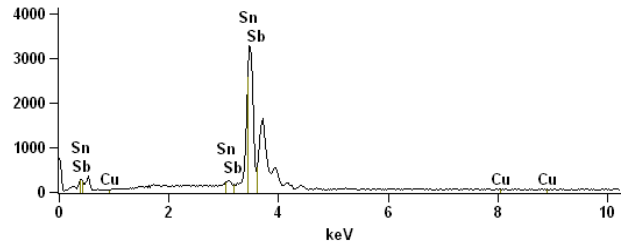

(d)

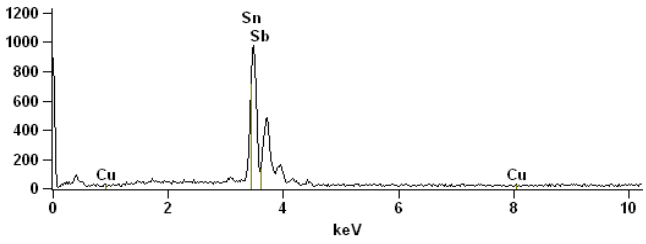

(e)

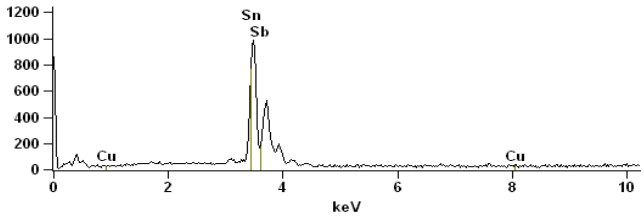

(f)

Figure F12: EDS spectrum for MW samples 30kN/220°C (a) 15min (b) 30min for 97Sn2Cu1Sb composition (c) 15min (d)30min for 94Sn4Cu2Sb composition (e)15min (f) 30 min for 91Sn6Cu3Sb composition

Table F16:EDS report for samples 97MW3 (30kN/220°C/15min) and 97MW4 (30kN/220°C/30min)

	weight%		
	Cu-K	Sn-L	Sb-L
97MW3_pt1	1.66	97.48	0.86
97MW3_pt2	1.55	97.56	0.89
97MW3_pt3	1.29	97.95	0.76
97MW3_pt4	1.62	97.64	0.74
97MW3_pt5	1.83	97.77	0.40
97MW4_pt1	1.62	97.53	0.85
97MW4_pt2	1.63	97.48	0.89
97MW4_pt3	1.42	97.91	0.67
97MW4_pt4	1.14	98.17	0.69
97MW4_pt5	1.35	97.68	0.97

Table F17: EDS report for samples 94MW3 (30kN/220°C/15min) and 94MW4 (30kN/220°C/30min)

	weight%		
	Cu-K	Sn-L	Sb-L
94MW3_pt1	3.38	94.94	1.68
94MW3_pt2	3.37	94.91	1.72
94MW3_pt3	3.56	94.86	1.58
94MW3_pt4	3.39	94.77	1.84
94MW3_pt5	3.29	94.85	1.86
94MW4_pt1	3.29	94.86	1.85
94MW4_pt2	3.42	94.77	1.81
94MW4_pt3	3.49	94.98	1.53
94MW4_pt4	3.36	94.87	1.77
94MW4_pt5	3.56	94.98	1.46

Table F18: EDS report for samples 91MW3 (30kN/220°C/15min) and 97MW4 (30kN/220°C/30min)

	weight%		
	Cu-K	Sn-L	Sb-L
91MW3_pt1	5.39	91.97	2.64
91MW3_pt2	5.39	91.72	2.89
91MW3_pt3	5.36	91.89	2.75
91MW3_pt4	5.29	91.59	3.12
91MW3_pt5	5.53	91.92	2.55
91MW4_pt1	5.36	91.77	2.87
91MW4_pt2	5.59	91.93	2.48
91MW4_pt3	5.52	91.87	2.61
91MW4_pt4	5.68	91.78	2.54
91MW4_pt5	5.49	91.77	2.74

F7. Microwave Sintering at 160ºC for 129 MPa pressed samples

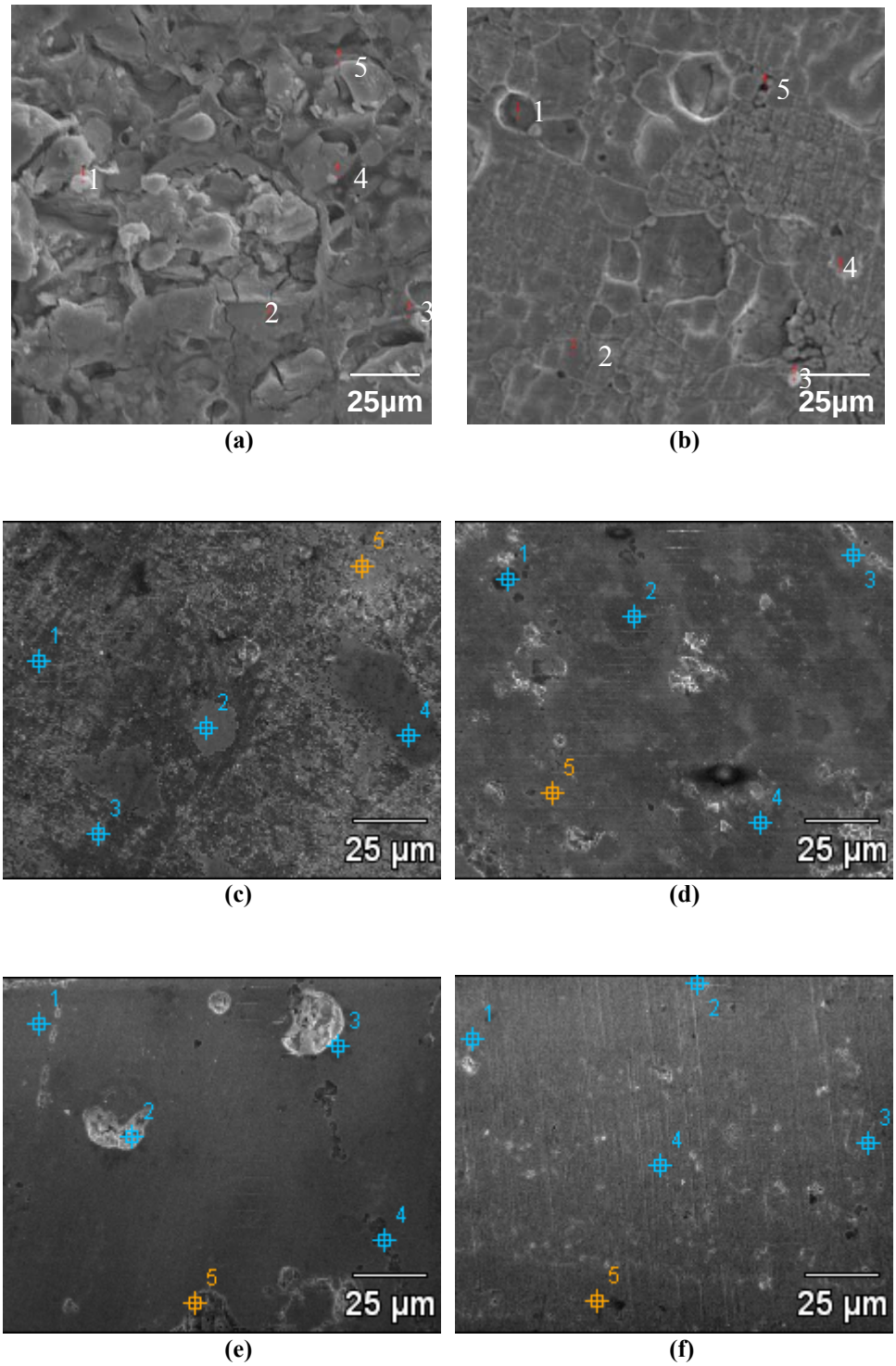

Figure F13: SEM image of microwave sintering at 160°C for the 40kN pressed samples (a) 15min (b) 30min for 97Sn2Cu1Sb composition (c) 15min (d) 30min for 94Sn4Cu2Sb composition (e) 15min (f) 30min for 91Sn6Cu3Sb composition

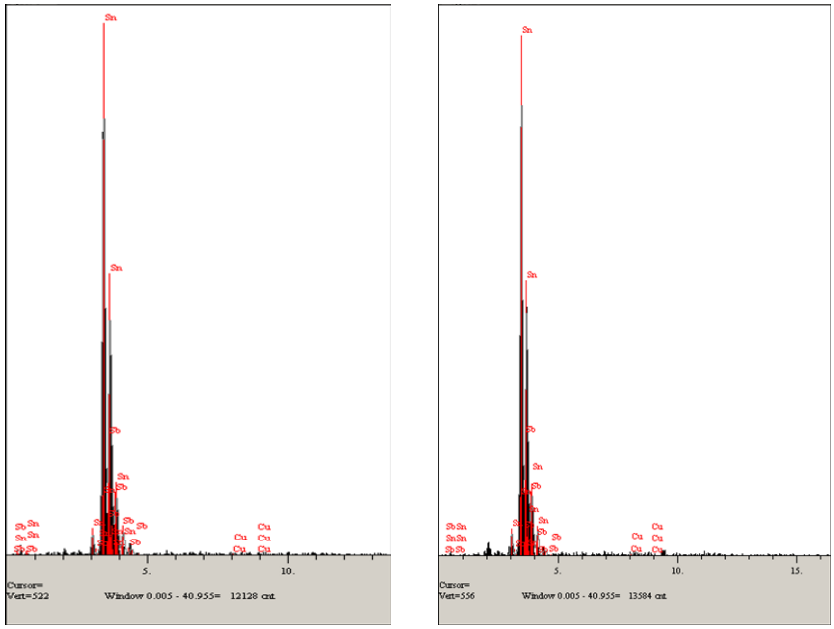

(a) (b)

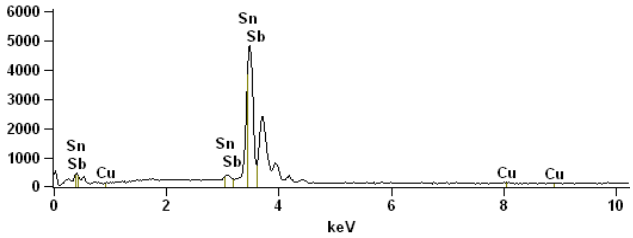

(c)

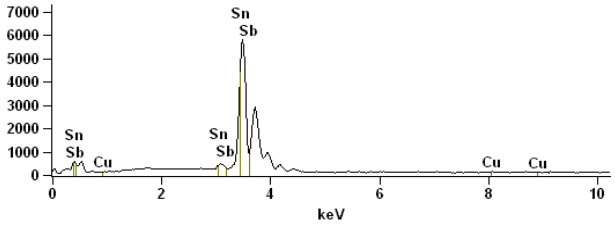

(d)

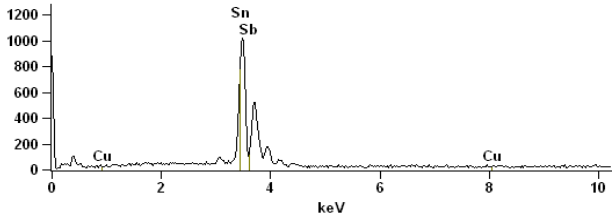

(e)

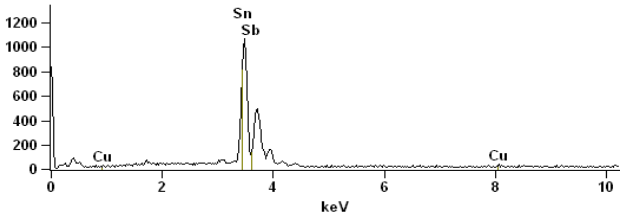

(f)

Figure F14: EDS spectrum for MW samples 40kN/160°C (a) 15min (b) 30min for 97Sn2Cu1Sb composition (c) 15min (d) 30min for 94Sn4Cu2Sb composition (e) 15min (f) 30 min for 91Sn6Cu3Sb composition

Table F19: EDS report for samples 97MW5 (40kN/160°C/15min) and 97MW6 (40kN/160°C/30min)

	weight%		
	Cu-K	Sn-L	Sb-L
97MW5_pt1	1.56	97.95	0.49
97MW5_pt2	1.45	97.81	0.74
97MW5_pt3	1.29	97.95	0.76
97MW5_pt4	1.42	98.03	0.55
97MW5_pt5	1.77	97.86	0.37
97MW6_pt1	1.21	98.23	0.56
97MW6_pt2	1.32	98.35	0.33
97MW6_pt3	1.44	97.94	0.62
97MW6_pt4	1.22	98.02	0.76
97MW6_pt5	1.14	98.22	0.64

Table F20: EDS report for samples 94MW5 (40kN/160°C/15min) and 94MW6 (40kN/160°C/30min)

	weight%		
	Cu-K	Sn-L	Sb-L
94MW5_pt1	3.73	94.74	1.53
94MW5_pt2	3.32	94.85	1.83
94MW5_pt3	3.51	94.76	1.73
94MW5_pt4	3.35	94.81	1.84
94MW5_pt5	3.23	94.95	1.82
94MW6_pt1	3.26	94.86	1.88
94MW6_pt2	3.52	94.77	1.71
94MW6_pt3	3.44	94.98	1.58
94MW6_pt4	3.49	94.79	1.72
94MW6_pt5	3.52	94.68	1.80

Table F21: EDS report for samples 91MW5 (40kN/160°C/15min) and 91MW6 (40kN/160°C/30min)

	weight%		
	Cu-K	Sn-L	Sb-L
91MW5_pt1	5.39	91.86	2.75
91MW5_pt2	5.34	91.73	2.93
91MW5_pt3	5.46	91.85	2.69
91MW5_pt4	5.36	92.09	2.55
91MW5_pt5	5.41	91.91	2.68
91MW6_pt1	5.36	91.82	2.82
91MW6_pt2	5.57	91.87	2.56
91MW6_pt3	5.51	91.61	2.88
91MW6_pt4	5.32	91.94	2.74
91MW6_pt5	5.42	91.92	2.66

F8. Microwave Sintering at 220ºC for 129 MPa pressed samples

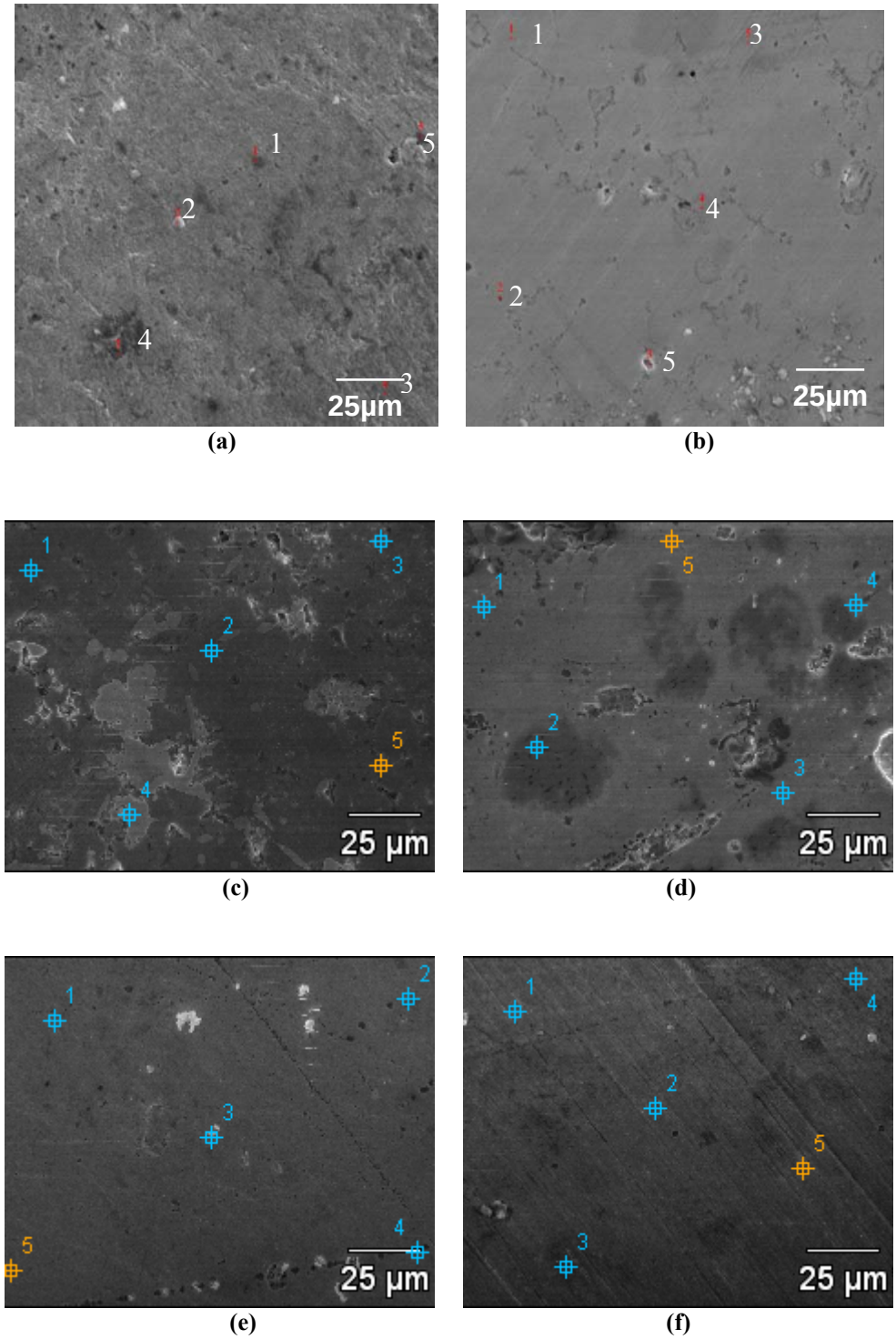

Figure F15: SEM image of microwave sintering at 220°C for the 40kN pressed samples (a) 15min (b) 30min for 97Sn2Cu1Sb composition (c) 15min (d) 30min for 94Sn4Cu2Sb composition (e) 15min (f) 30min for 91Sn6Cu3Sb composition

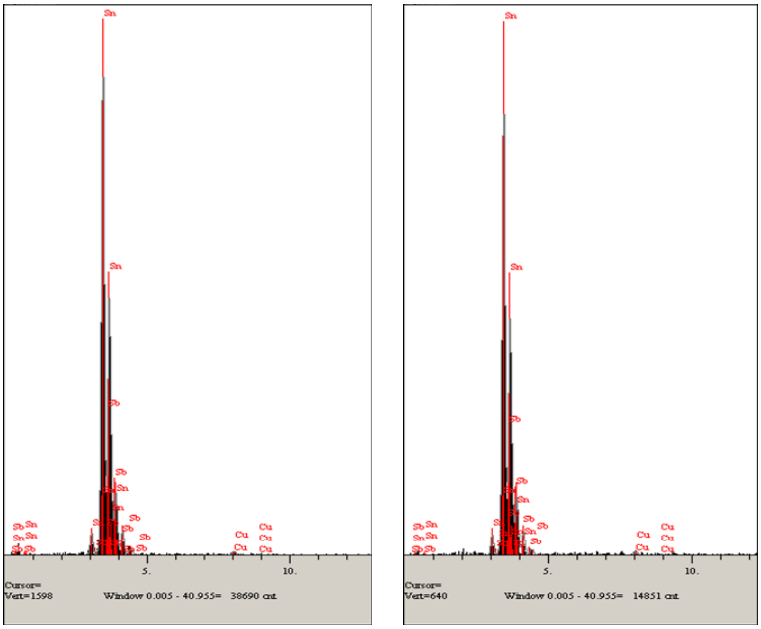

(a) (b)

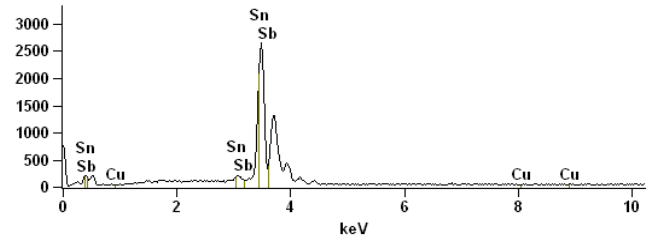

(c)

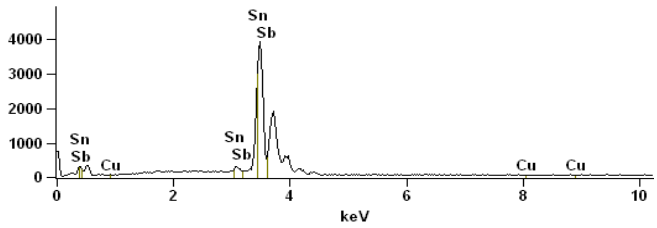

(d)

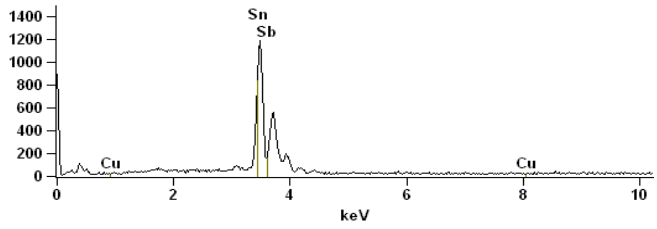

(e)

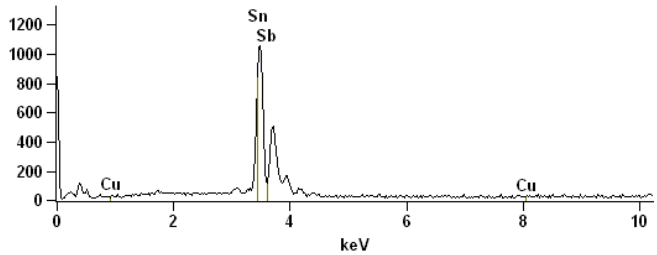

(f)

Figure F16: EDS spectrum for MW samples 40kN/220°C (a) 15min (b) 30min for 97Sn2Cu1Sb composition (c) 15min (d) 30min for 94Sn4Cu2Sb composition (e) 15min (f) 30 min for 91Sn6Cu3Sb composition

Table F22: EDS report for samples 97MW7 (40kN/220°C/15min) and 97MW8 (40kN/220°C/30min)

	weight%		
	Cu-K	Sn-L	Sb-L
97MW7_pt1	1.56	97.87	0.57
97MW7_pt2	1.45	97.76	0.79
97MW7_pt3	1.29	98.05	0.66
97MW7_pt4	1.37	98.10	0.53
97MW7_pt5	1.86	97.86	0.28
97MW8_pt1	1.35	97.83	0.82
97MW8_pt2	1.28	98.05	0.67
97MW8_pt3	1.49	97.94	0.57
97MW8_pt4	1.34	97.72	0.94
97MW8_pt5	1.55	97.51	0.94

Table F23: EDS report for samples 94MW7 (40kN/220°C/15min) and 94MW8 (40kN/220°C/30min)

	weight%		
	Cu-K	Sn-L	Sb-L
94MW7_pt1	3.33	94.79	1.88
94MW7_pt2	3.39	94.87	1.74
94MW7_pt3	3.51	94.91	1.58
94MW7_pt4	3.21	94.79	2.00
94MW7_pt5	3.15	94.95	1.90
94MW8_pt1	3.37	94.86	1.77
94MW8_pt2	3.42	94.87	1.71
94MW8_pt3	3.53	94.98	1.49
94MW8_pt4	3.59	94.99	1.42
94MW8_pt5	3.37	94.98	1.65

Table F24: EDS report for samples 91MW7 (40kN/220°C/15min) and 91MW8 (40kN/220°C/30min)

	weight%		
	Cu-K	Sn-L	Sb-L
91MW7_pt1	5.41	91.92	2.67
91MW7_pt2	5.27	91.77	2.96
91MW7_pt3	5.39	91.95	2.66
91MW7_pt4	5.42	91.89	2.69
91MW7_pt5	5.43	91.93	2.64
91MW8_pt1	5.36	91.87	2.77
91MW8_pt2	5.57	91.97	2.46
91MW8_pt3	5.48	92.11	2.41
91MW8_pt4	5.28	91.99	2.73
91MW8_pt5	5.45	91.97	2.58

G. X-Ray Diffraction (XRD)

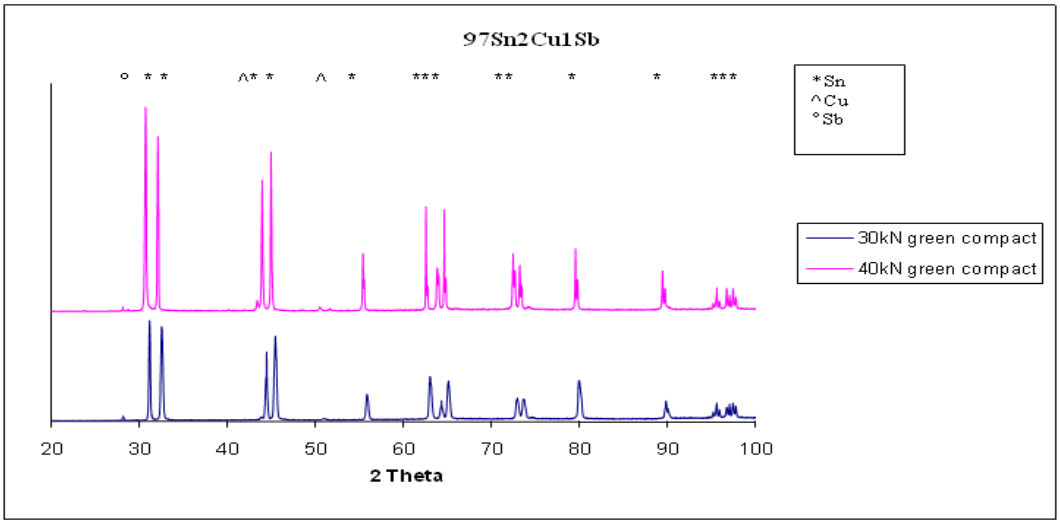

Figure G1: XRD peaks comparing green compacts of 97Sn2Cu1Sb composition at different compaction loads of 96MPa (30kN) and 129MPa (40kN)

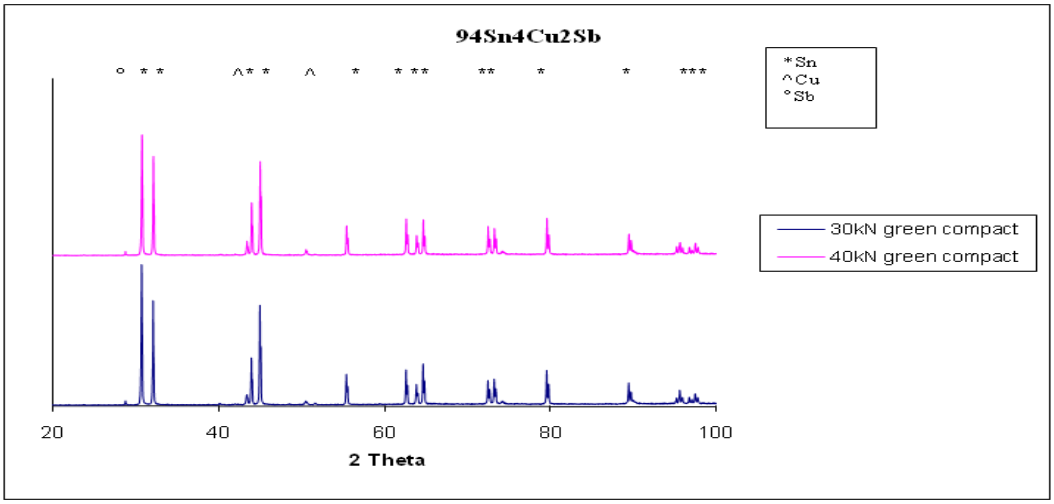

Figure G2: XRD peaks comparing green compacts of 94Sn4Cu2Sb composition at different compaction loads of 96MPa (30kN) and 129MPa (40kN)

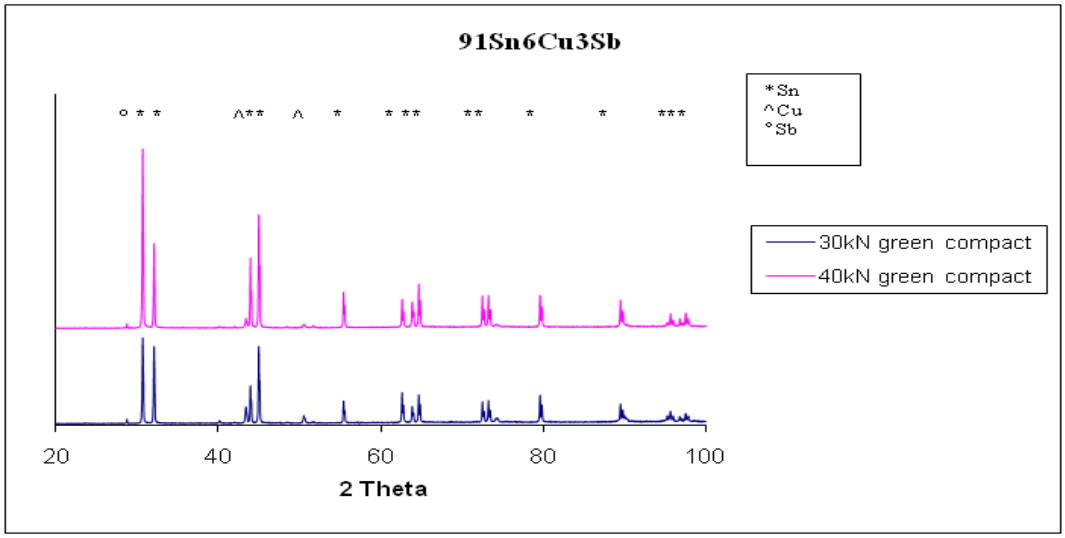

Figure G3: XRD peaks comparing green compacts of 91Sn6Cu3Sb composition at different compaction loads of 96MPa (30kN) and 129MPa (40kN)

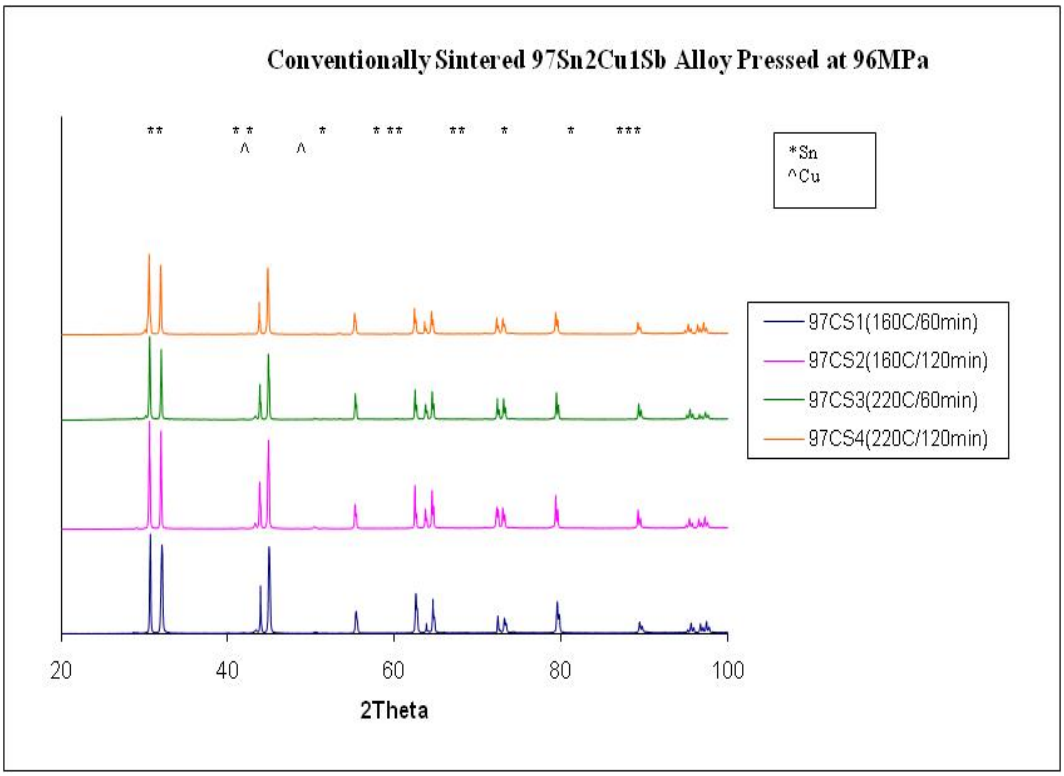

Figure G4: XRD peaks comparing different sintering temperatures and sintering times for conventionally sintered 97Sn2Cu1Sb alloys pressed at 96 MPa

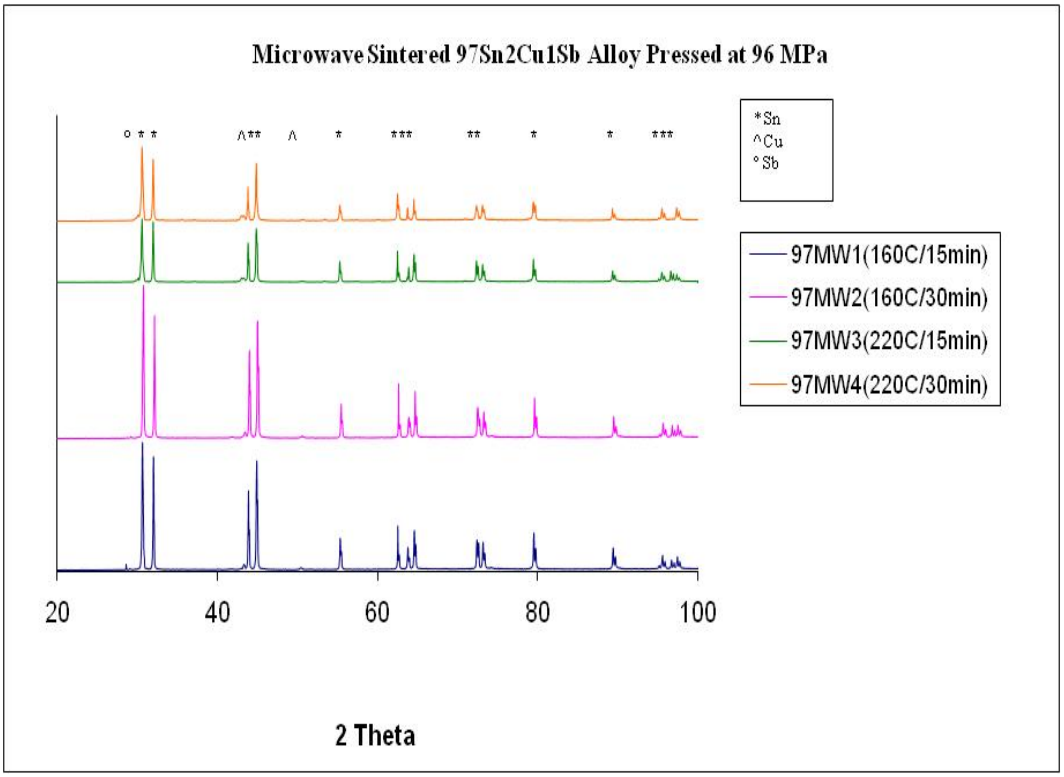

Figure G5: XRD peaks comparing different sintering temperatures and sintering times for microwave sintered 97Sn2Cu1Sb alloys pressed at 96 MPa

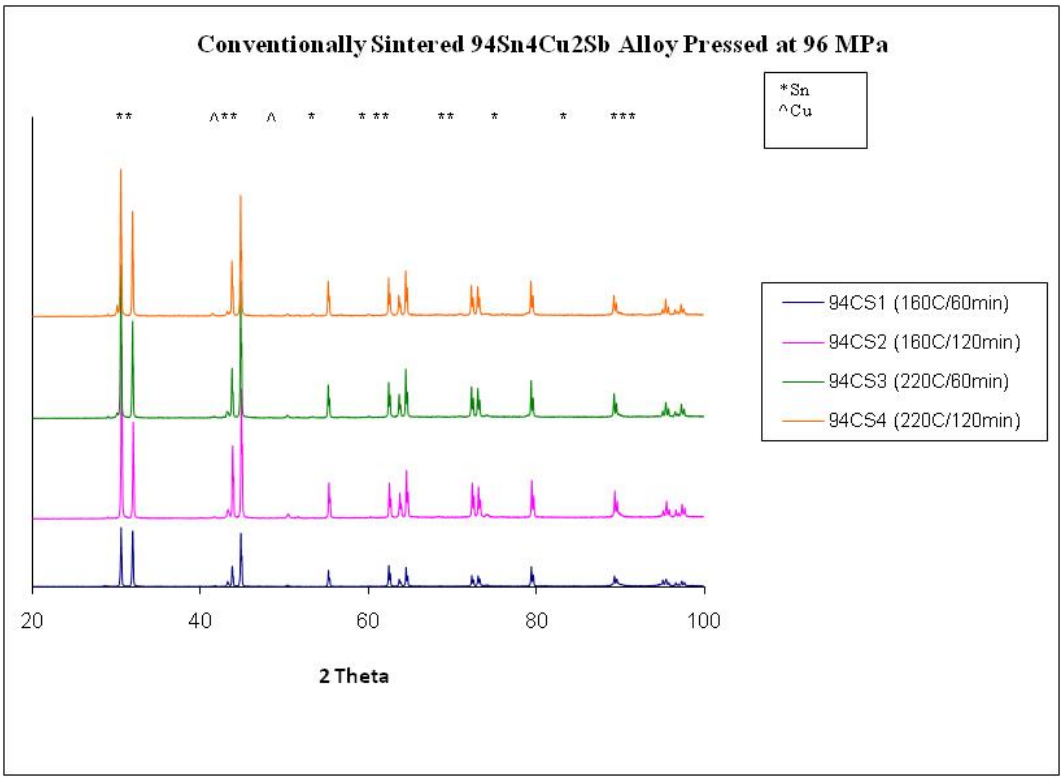

Figure G6: XRD peaks comparing different sintering temperatures and sintering times for conventionally sintered 94Sn4Cu2Sb alloys pressed at 96 MPa

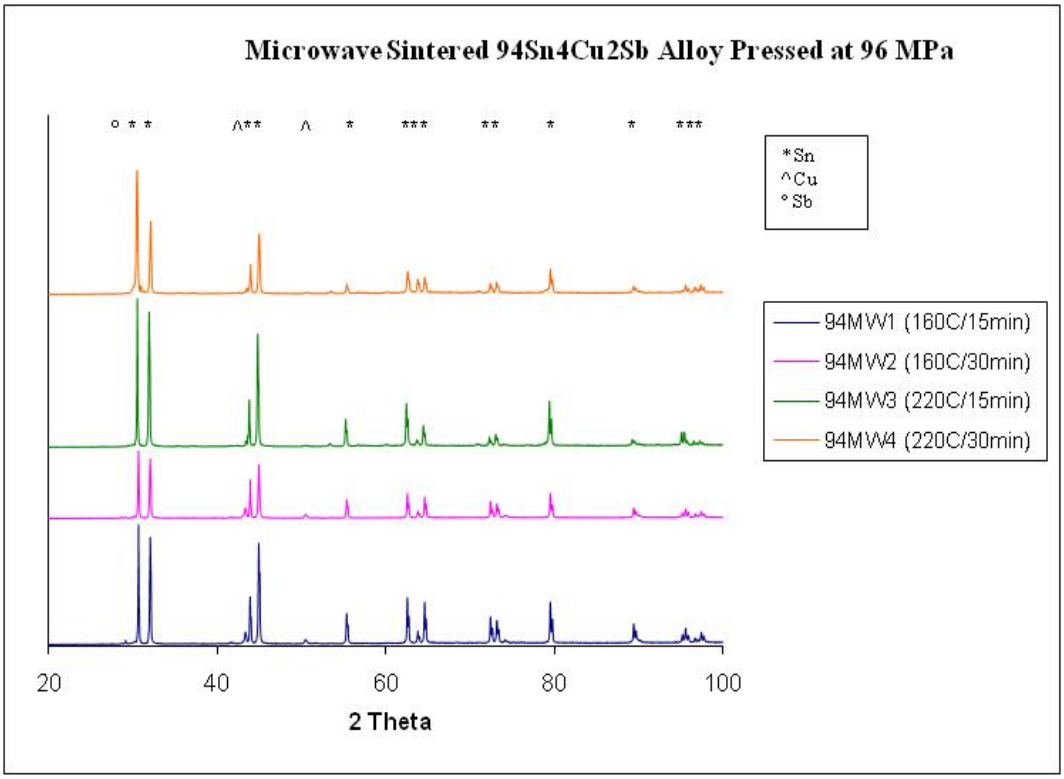

Figure G7: XRD peaks comparing different sintering temperatures and sintering times for microwave sintered 94Sn4Cu2Sb alloys pressed at 96 MPa

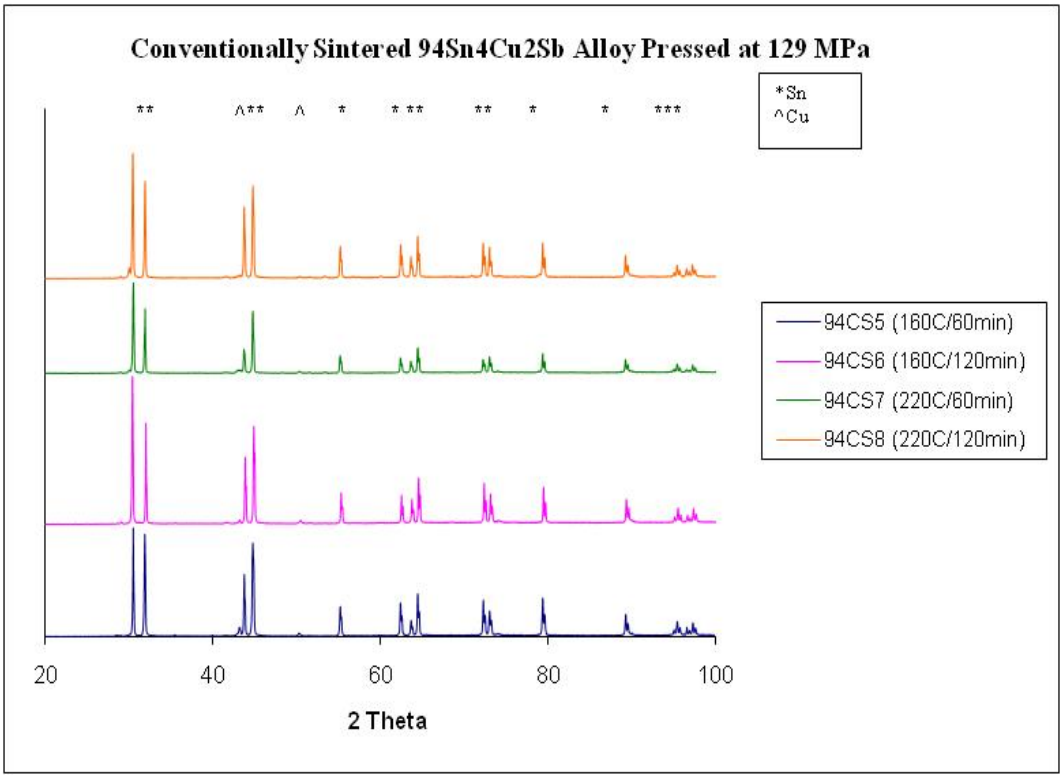

Figure G8: XRD peaks comparing different sintering temperatures and sintering times for conventionally sintered 94Sn4Cu2Sb alloys pressed at 129 MPa

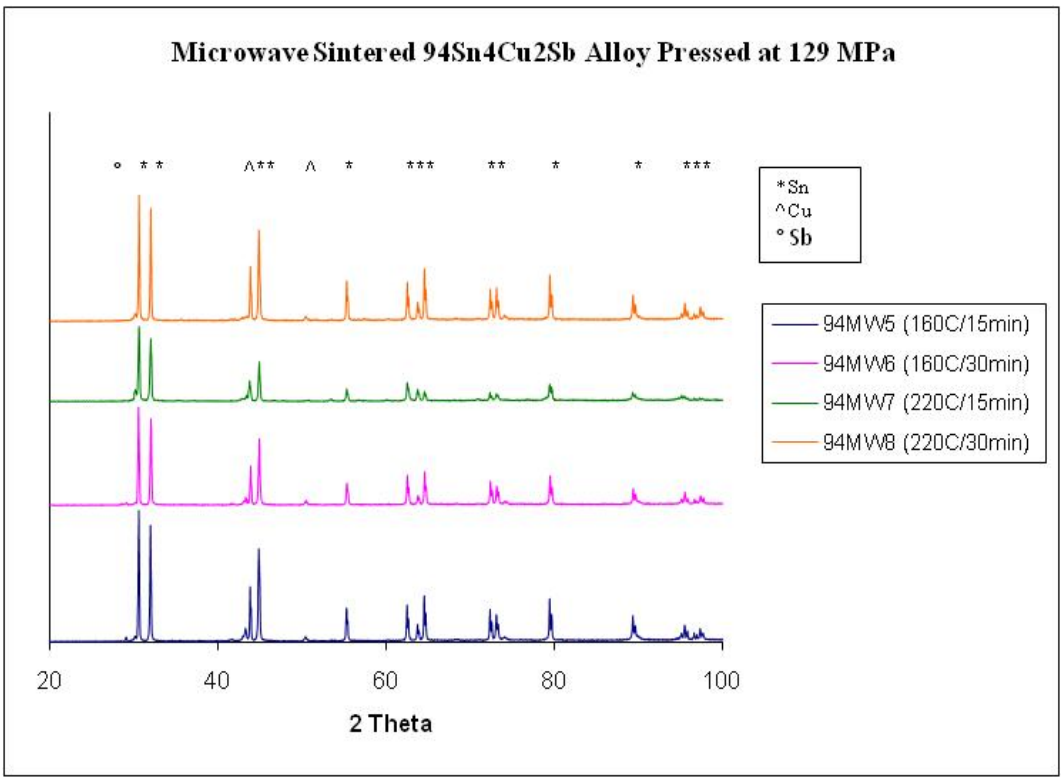

Figure G9: XRD peaks comparing different sintering temperatures and sintering times for microwave sintered 94Sn4Cu2Sb alloys pressed at 129 MPa

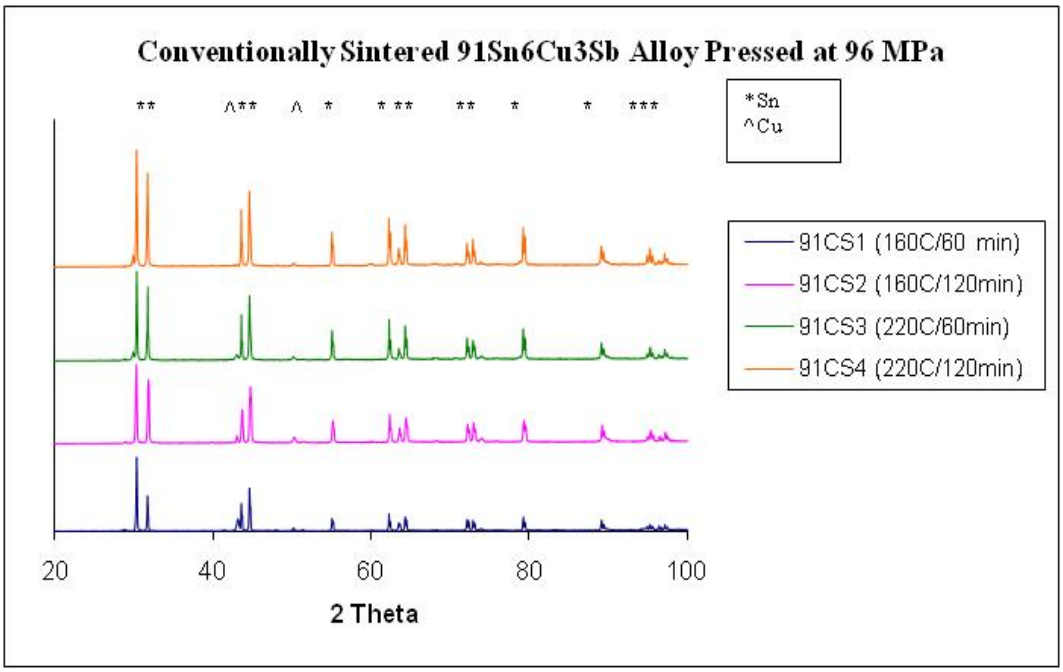

Figure G10: XRD peaks comparing different sintering temperatures and sintering times for conventionally sintered 91Sn6Cu3Sb alloys pressed at 96 MPa

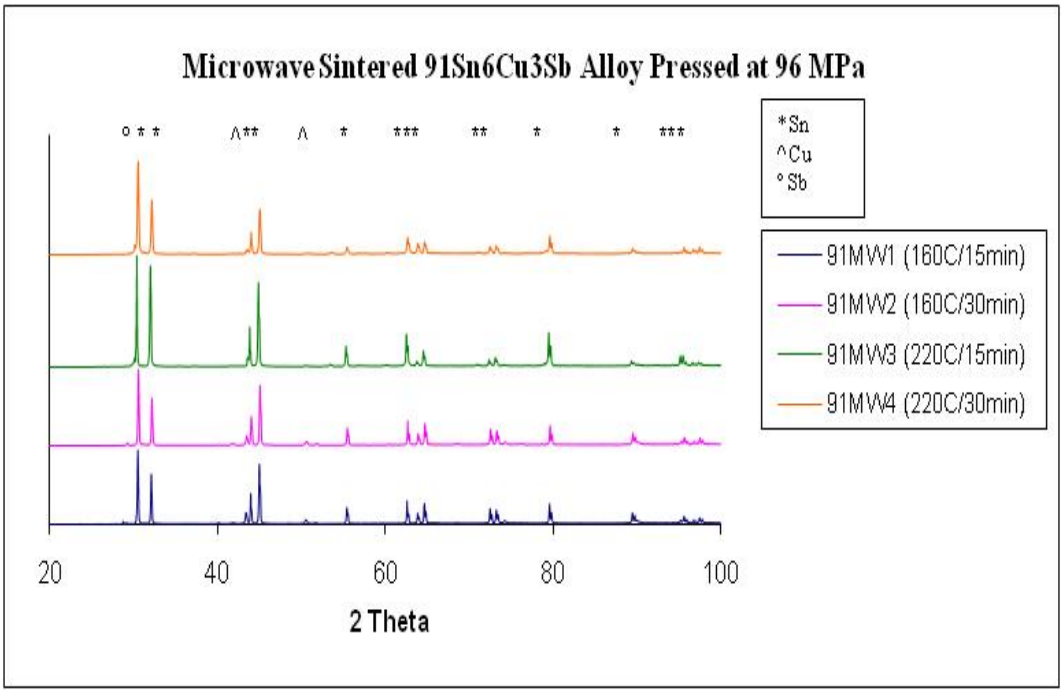

Figure G11: XRD peaks comparing different sintering temperatures and sintering times for microwave sintered 91Sn6Cu3Sb alloys pressed at 96 MPa

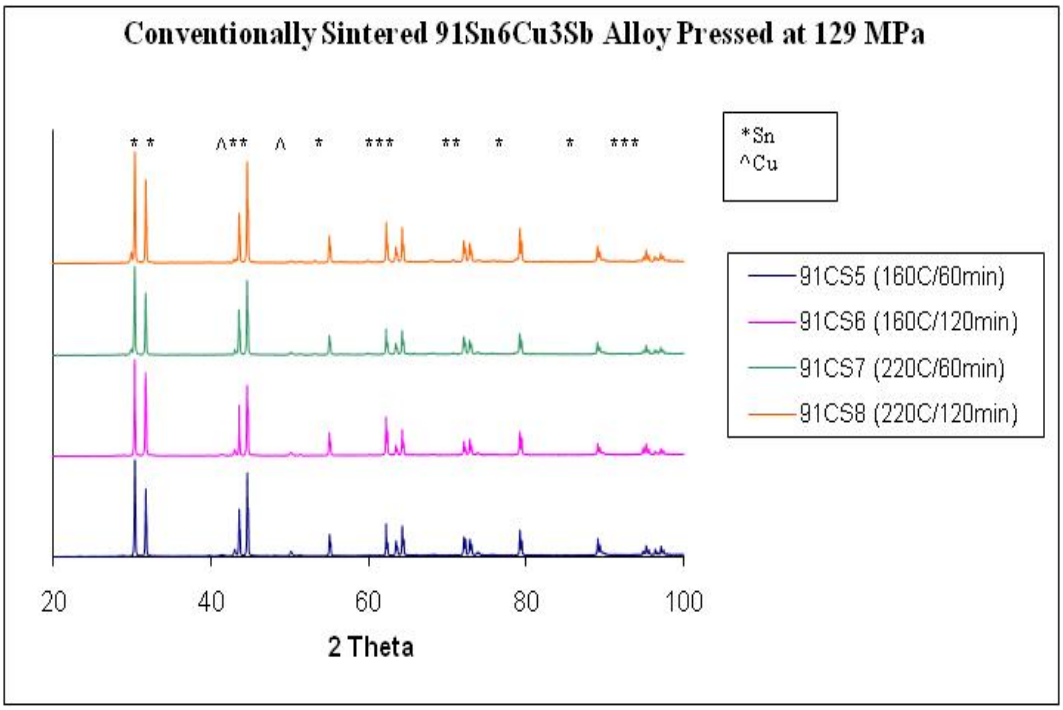

Figure G12: XRD peaks comparing different sintering temperatures and sintering times for conventionally sintered 91Sn6Cu3Sb alloys pressed at 129 MPa

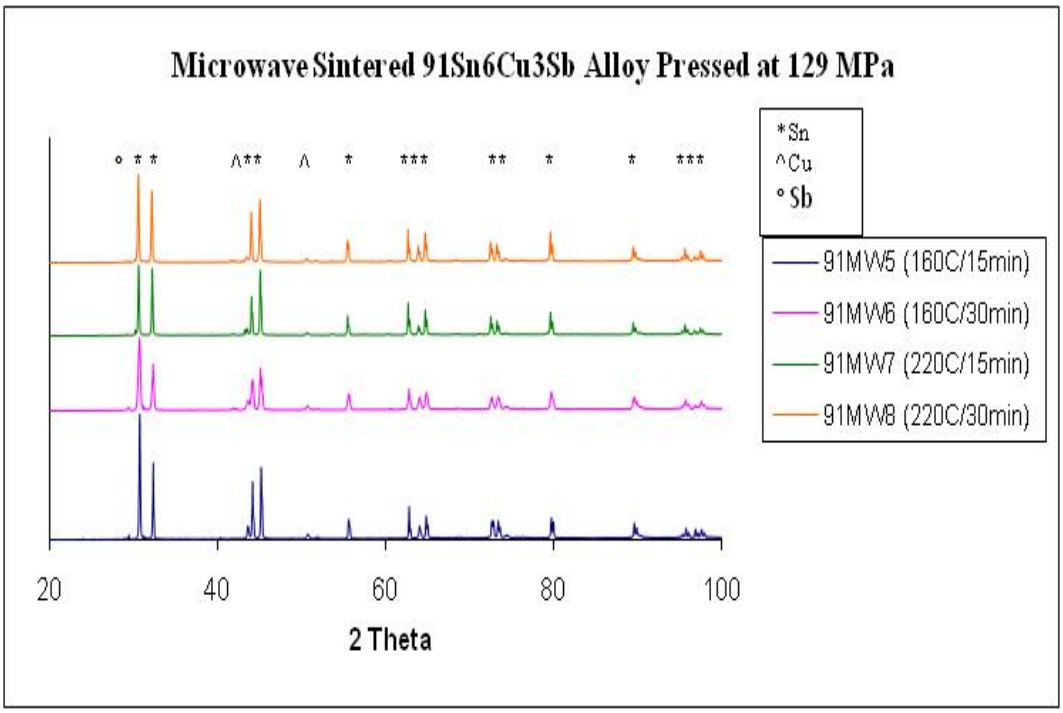

Figure G13: XRD peaks comparing different sintering temperatures and sintering times for microwave sintered 91Sn6Cu3Sb alloys pressed at 129 MPa

H. Diffusion Couple Experiments

Table H1: Values of the concentration for Cu into Sn obtained using EDS at various points from the interface for Conventional and Microwave Sintering at 220°C

x (µm)	Concentration of Cu for CS (15 min)	Concentration of Cu for CS (30min)	Concentration of Cu for MW (15min)	Concentration of Cu for MW (30min)
0	91.22	96.91	90.02	94.36
4	90.10	95.60	87.60	93.30
8	86.58	94.08	85.58	92.58
12	84.54	93.04	83.34	91.04
16	78.82	87.64	77.65	86.54
20	69.21	80.00	68.17	78.82
24	61.07	75.56	63.06	75.57
28	43.67	70.25	49.72	65.09
32	38.06	58.13	38.06	55.25
36	26.39	49.73	28.25	46.21
40	22.39	43.67	22.93	35.06
44	17.91	37.30	19.57	30.19
48	12.32	30.86	11.98	24.62
52	10.39	25.27	11.01	22.77
56	5.45	18.05	5.11	16.55
60	4.46	12.92	4.02	11.42
64	3.28	8.83	3.16	9.33
68	1.62	6.41	1.49	6.91
72	1.09	5.56	1.13	6.06
76	0.66	4.47	0.71	4.97
80	0.48	3.22	0.24	3.41
84	0.23	2.81	0.18	2.77
88	0.11	2.54	0.09	2.41
92	0.05	2.00	0.05	1.98
96	0.04	1.32	0.03	1.82
100	0.02	1.15	0.01	1.21

Table H2: Error function values and the z values obtained for Cu into Sn

x (μm)	erf(z) CS15	erf(z) CS30	erf(z) MW15	erf(z) MW30	z CS15	z CS30	z MW15	z MW30
0	0.0878	0.0309	0.0998	0.0564	0.08	0.03	0.09	0.05
4	0.0990	0.0440	0.1240	0.0670	0.09	0.04	0.11	0.06
8	0.1342	0.0592	0.1442	0.0742	0.12	0.05	0.13	0.07
12	0.1546	0.0696	0.1666	0.0896	0.13	0.06	0.15	0.08
16	0.2118	0.1236	0.2235	0.1346	0.19	0.11	0.21	0.12
20	0.3079	0.2000	0.3183	0.2118	0.28	0.18	0.29	0.19
24	0.3893	0.2444	0.3694	0.2443	0.36	0.22	0.34	0.22
28	0.5633	0.2975	0.5028	0.3491	0.55	0.27	0.48	0.32
32	0.6194	0.4187	0.6194	0.4475	0.62	0.39	0.62	0.42
36	0.7361	0.5027	0.7175	0.5379	0.79	0.48	0.76	0.52
40	0.7761	0.5633	0.7707	0.6494	0.86	0.55	0.85	0.66
44	0.8209	0.6270	0.8043	0.6981	0.95	0.63	0.92	0.73
48	0.8768	0.6914	0.8802	0.7538	1.09	0.72	1.10	0.82
52	0.8961	0.7473	0.8899	0.7723	1.15	0.81	1.13	0.85
56	0.9455	0.8195	0.9489	0.8345	1.36	0.94	1.38	0.98
60	0.9554	0.8708	0.9598	0.8858	1.42	1.06	1.45	1.12
64	0.9672	0.9117	0.9684	0.9067	1.51	1.20	1.52	1.19
68	0.9838	0.9359	0.9851	0.9309	1.70	1.31	1.72	1.29
72	0.9891	0.9444	0.9887	0.9394	1.80	1.36	1.79	1.33
76	0.9934	0.9553	0.9929	0.9503	1.92	1.42	1.90	1.39
80	0.9952	0.9678	0.9976	0.9659	1.99	1.51	2.15	1.50
84	0.9977	0.9719	0.9982	0.9723	2.15	1.55	2.21	1.55
88	0.9989	0.9746	0.9991	0.9759	2.35	1.57	2.35	1.58
92	0.9995	0.9800	0.9995	0.9802	2.45	1.68	2.45	1.67
96	0.9996	0.9868	0.9997	0.9818	2.55	1.75	2.56	1.80
100	0.9998	0.9885	0.9999	0.9879	2.70	1.79	2.75	1.81

H2. Sb-Sn Interface

Table H3: Values of the concentration for Sb into Sn obtained using EDS at various points from the interface for Conventional and Microwave Sintering at 220°C

x (µm)	Concentration of Sb for CS (15 min)	Concentration of Sb for CS (30min)	Concentration of Sb for MW (15min)	Concentration of Sb for MW (30min)
0	86.05	89.90	85.02	89.87
4	43.67	86.52	39.61	83.21
8	24.62	82.10	21.86	81.01
12	12.32	69.21	10.69	72.37
16	6.81	58.13	5.81	61.07
20	4.46	37.30	3.39	38.83
24	2.12	30.86	1.56	29.53
28	1.23	26.39	0.89	24.05
32	0.23	13.76	0.15	13.39
36	0.13	10.39	0.13	9.52
40	0.08	7.03	0.09	7.71
44	0.02	6.00	0.02	6.40
48	0.02	5.10	0.02	5.45
52	0.01	2.84	0.01	3.05
56	0.00	1.34	0.00	1.50
60	0.00	0.89	0.00	1.05
64	0.00	0.43	0.00	0.49
68	0.00	0.27	0.00	0.31
72	0.00	0.14	0.00	0.13
76	0.00	0.09	0.00	0.11
80	0.00	0.04	0.00	0.04
84	0.00	0.03	0.00	0.03
88	0.00	0.02	0.00	0.02
92	0.00	0.01	0.00	0.01
96	0.00	0.01	0.00	0.01
100	0.00	0.01	0.00	0.01

Table H4: Error function values and the z values obtained for Sb into Sn

x (μm)	erf(z) CS15	erf(z) CS30	erf(z) MW15	erf(z) MW30	z CS15	z CS30	z MW15	z MW30
0	0.2227	0.1010	0.2763	0.1013	0.20	0.01	0.25	0.09
4	0.5633	0.1348	0.6039	0.1679	0.55	0.12	0.60	0.15
8	0.7538	0.1790	0.7814	0.1899	0.82	0.16	0.87	0.17
12	0.8768	0.3079	0.8931	0.2763	1.09	0.28	1.14	0.25
16	0.9319	0.4187	0.9419	0.3893	1.29	0.39	1.34	0.36
20	0.9554	0.6270	0.9661	0.6117	1.42	0.63	1.50	0.61
24	0.9788	0.6914	0.9844	0.7047	1.63	0.72	1.71	0.74
28	0.9877	0.7361	0.9911	0.7595	1.77	0.79	1.85	0.83
32	0.9977	0.8624	0.9985	0.8661	2.16	1.05	2.24	1.06
36	0.9987	0.8961	0.9987	0.9048	2.28	1.15	2.27	1.18
40	0.9992	0.9297	0.9991	0.9229	2.36	1.28	2.35	1.25
44	0.9998	0.9400	0.9998	0.9360	2.61	1.33	2.60	1.31
48	0.9998	0.9490	0.9998	0.9455	2.66	1.38	2.68	1.36
52	0.9999	0.9716	0.9999	0.9695	2.83	1.55	2.85	1.53
56	1.0000	0.9866	1.0000	0.9850	3.03	1.75	3.23	1.72
60	1.0000	0.9911	1.0000	0.9895	3.12	1.85	3.32	1.81
64	1.0000	0.9957	1.0000	0.9951	3.22	2.02	3.45	1.99
68	1.0000	0.9973	1.0000	0.9969	3.55	2.12	3.54	2.09
72	1.0000	0.9986	1.0000	0.9987	3.65	2.26	3.64	2.28
76	1.0000	0.9991	1.0000	0.9989	3.59	2.35	3.68	2.31
80	1.0000	0.9996	1.0000	0.9996	3.95	2.51	3.98	2.53
84	1.0000	0.9997	1.0000	0.9997	4.00	2.59	4.20	2.57
88	1.0000	0.9998	1.0000	0.9998	4.10	2.62	4.30	2.63
92	1.0000	0.9999	1.0000	0.9999	4.40	2.75	4.50	2.77
96	1.0000	0.9999	1.0000	0.9999	4.50	2.79	4.65	2.83
100	1.0000	0.9999	1.0000	0.9999	4.69	2.88	4.70	2.86

I. Mathematical Modelling

Table I1: Calculated skin depth values for Sn, Cu and Sb in the microwave

Temperature (°C)	Electrical resistivity (Sn), ρ (μΩm)	Skin depth (Sn), δ (μm)	Electrical resistivity (Cu), ρ (μΩm)	Skin depth (Cu), δ (μm)	Electrical resistivity (Sb), ρ (μΩm)	Skin depth (Sb), δ (μm)
20	0.120	3.51	0.017	1.32	0.420	6.58
30	0.125	3.59	0.018	1.35	0.436	6.70
40	0.131	3.67	0.018	1.37	0.453	6.83
50	0.136	3.74	0.019	1.40	0.469	6.95
60	0.142	3.82	0.020	1.42	0.486	7.07
70	0.147	3.89	0.020	1.45	0.502	7.19
80	0.152	3.96	0.021	1.47	0.518	7.30
90	0.158	4.03	0.022	1.49	0.535	7.42
100	0.163	4.10	0.022	1.52	0.551	7.53
110	0.169	4.17	0.023	1.54	0.567	7.64
120	0.174	4.23	0.024	1.56	0.584	7.75
130	0.179	4.30	0.024	1.58	0.600	7.86
140	0.185	4.36	0.025	1.60	0.617	7.97
150	0.190	4.42	0.026	1.62	0.633	8.07
160	0.196	4.49	0.026	1.64	0.649	8.18
170	0.201	4.55	0.027	1.67	0.666	8.28
180	0.206	4.61	0.028	1.69	0.682	8.38
190	0.212	4.67	0.028	1.71	0.698	8.48
200	0.217	4.73	0.029	1.73	0.715	8.58
210	0.223	4.79	0.030	1.75	0.731	8.68
220	0.228	4.84	0.030	1.76	0.748	8.77

Table I2: Calculated power values at the surface of the sample with respect to temperature

Temp (°C)	**Electrical resistivity ρ (μΩm)**	**Specific Heat Capacity Cp (J/kgK)**	**Skin depth δ (μm)**	**Electrical conductivity σ (Ω-1m-1)**	**Surface Resistivity Rs (Ω-1)**	**Power Absorbed P (mW)**	**Pem (W/m3)**
20	0.120	220.72	3.51	8369808.7	0.0340	9.78	1174
30	0.125	222.94	3.59	8009386.3	0.0348	10.00	1200
40	0.131	225.15	3.67	7678723.6	0.0355	10.21	1226
50	0.136	227.37	3.74	7374280.8	0.0362	10.42	1251
60	0.142	229.59	3.82	7093058.2	0.0369	10.63	1275
70	0.147	231.81	3.89	6832496.9	0.0376	10.83	1299
80	0.152	234.03	3.96	6590400.6	0.0383	11.02	1323
90	0.158	236.25	4.03	6364873.6	0.0390	11.22	1346
100	0.163	238.47	4.10	6154271.1	0.0396	11.41	1369
110	0.169	240.69	4.17	5957159.2	0.0403	11.59	1391
120	0.174	242.91	4.23	5772281.9	0.0409	11.78	1413
130	0.179	245.13	4.30	5598534.3	0.0416	11.96	1435
140	0.185	247.34	4.36	5434940.7	0.0422	12.14	1457
150	0.190	249.56	4.42	5280636.4	0.0428	12.32	1478
160	0.196	251.78	4.49	5134852.0	0.0434	12.49	1499
170	0.201	254.00	4.55	4996900.7	0.0440	12.66	1519
180	0.206	256.22	4.61	4866167.9	0.0446	12.83	1539
190	0.212	258.44	4.67	4742101.3	0.0452	13.00	1559
200	0.217	260.66	4.73	4624203.7	0.0457	13.16	1579
210	0.223	262.88	4.79	4512026.3	0.0463	13.32	1599
220	0.228	265.10	4.84	4405162.5	0.0469	13.48	1618

Table I3: Calculated values for power losses due to convection

Ta (°C)	Cp (J/mol.K)	*Prandtl Number	h (W/m2K)	Area, A (m2)	Volume (m3)	Pconv (W/m3)
20	20.786	0.02666	0.267	0.0012936	1.30654E-05	262
30	21.161	0.02714	0.268	0.0012936	1.30654E-05	265.0
40	21.535	0.02762	0.270	0.0012936	1.30654E-05	267.0
50	21.91	0.02810	0.271	0.0012936	1.30654E-05	268.7
60	22.285	0.02858	0.273	0.0012936	1.30654E-05	270.2
70	22.659	0.02906	0.274	0.0012936	1.30654E-05	271.7
80	23.034	0.02954	0.276	0.0012936	1.30654E-05	273.1
90	23.408	0.03002	0.277	0.0012936	1.30654E-05	274.6
100	23.783	0.03050	0.279	0.0012936	1.30654E-05	276.0
110	24.158	0.03098	0.280	0.0012936	1.30654E-05	277.5
120	24.532	0.03146	0.282	0.0012936	1.30654E-05	278.9
130	24.907	0.03194	0.283	0.0012936	1.30654E-05	280.3
140	25.282	0.03242	0.284	0.0012936	1.30654E-05	281.7
150	25.656	0.03290	0.286	0.0012936	1.30654E-05	283.0
160	26.031	0.03338	0.287	0.0012936	1.30654E-05	284.4
170	26.406	0.03386	0.289	0.0012936	1.30654E-05	285.7
180	26.78	0.03434	0.290	0.0012936	1.30654E-05	287.1
190	27.155	0.03482	0.291	0.0012936	1.30654E-05	288.4
200	27.530	0.03530	0.293	0.0012936	1.30654E-05	289.7
210	27.904	0.03578	0.294	0.0012936	1.30654E-05	291.0
220	28.279	0.03626	0.295	0.0012936	1.30654E-05	292.3

* Prandtl Number, Pr= $C_p\mu/k$ where Cp=specific heat, μ=viscosity and k=thermal conductivity

Table I4: Calculated values for power losses due to radiation

Ta (°C)	σ (W/m2C4)	ε	Prad (W/m3)
20	2.60E-09	0.04	0
30	2.60E-09	0.04	0.01
40	2.60E-09	0.04	0.02
50	2.60E-09	0.04	0.06
60	2.60E-09	0.04	0.13
70	2.60E-09	0.04	0.25
80	2.60E-09	0.04	0.42
90	2.60E-09	0.04	0.67
100	2.60E-09	0.04	1.03
110	2.60E-09	0.04	1.51
120	2.60E-09	0.04	2.13
130	2.60E-09	0.04	2.94
140	2.60E-09	0.04	3.95
150	2.60E-09	0.04	5.21
160	2.60E-09	0.04	6.75
170	2.60E-09	0.04	8.60
180	2.60E-09	0.04	10.81
190	2.60E-09	0.04	13.42
200	2.60E-09	0.04	16.47
210	2.60E-09	0.04	20.02
220	2.60E-09	0.04	24.12

Table I5: Calculated values for temperature rise in the tin alloy in microwaves

Ta (°C)	*Prandtl Number	Pem	ΔP	ρ	T rise (°C)
20	0.02666	1174	1174.000	0.120	0.266
30	0.02714	1200	934.397	0.125	0.631
40	0.02762	1226	958.839	0.131	0.865
50	0.02810	1251	982.275	0.136	1.066
60	0.02858	1275	1004.697	0.142	1.226
70	0.02906	1299	1027.095	0.147	1.368
80	0.02954	1323	1049.445	0.152	1.486
90	0.03002	1346	1070.736	0.158	1.575
100	0.03050	1369	1091.938	0.163	1.658
110	0.03098	1391	1112.031	0.169	1.718
120	0.03146	1413	1131.993	0.174	1.775
130	0.03194	1435	1151.788	0.179	1.822
140	0.03242	1457	1171.388	0.185	1.850
150	0.03290	1478	1189.762	0.190	1.882
160	0.03338	1499	1207.868	0.196	1.898
170	0.03386	1519	1224.671	0.201	1.919
180	0.03434	1539	1241.133	0.206	1.936
190	0.03482	1559	1257.202	0.212	1.939
200	0.03530	1579	1272.838	0.217	1.948
210	0.03578	1599	1287.995	0.223	1.946
220	0.03626	1618	1301.614	0.228	1.951

* Prandtl Number, Pr= $C_p\mu/k$ where Cp=specific heat, μ=viscosity and k=thermal conductivity

J. Phase Diagrams

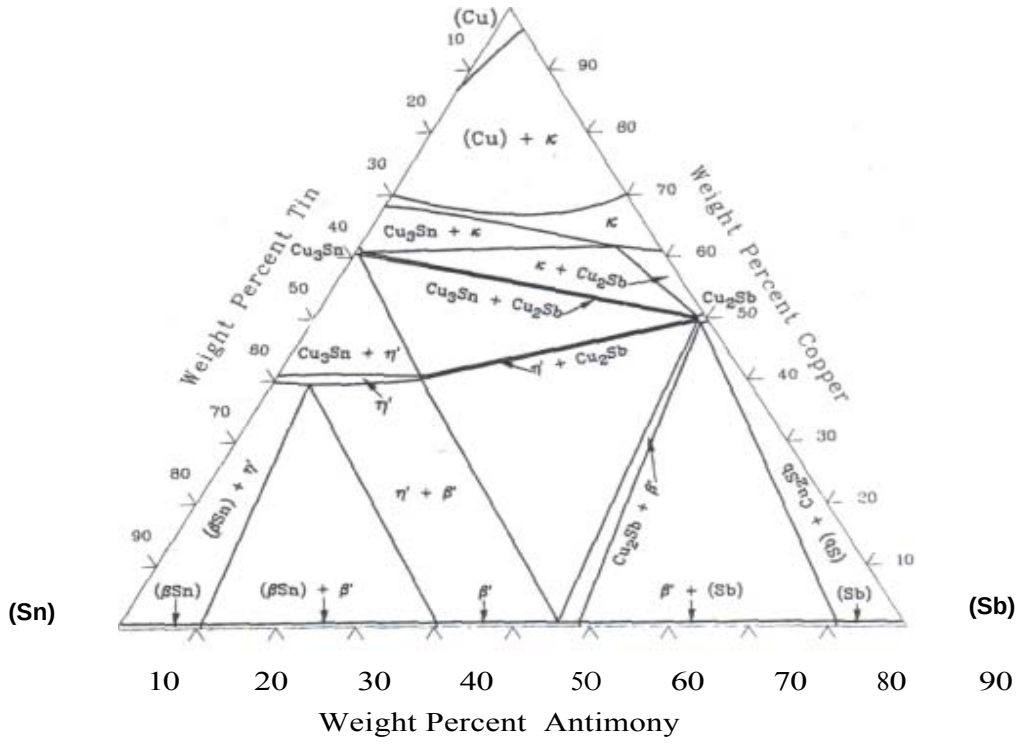

Figure J1: Cu-Sb-Sn phases present at temperatures below the reactions in the solid state [73Bla] (ASME Handbook)

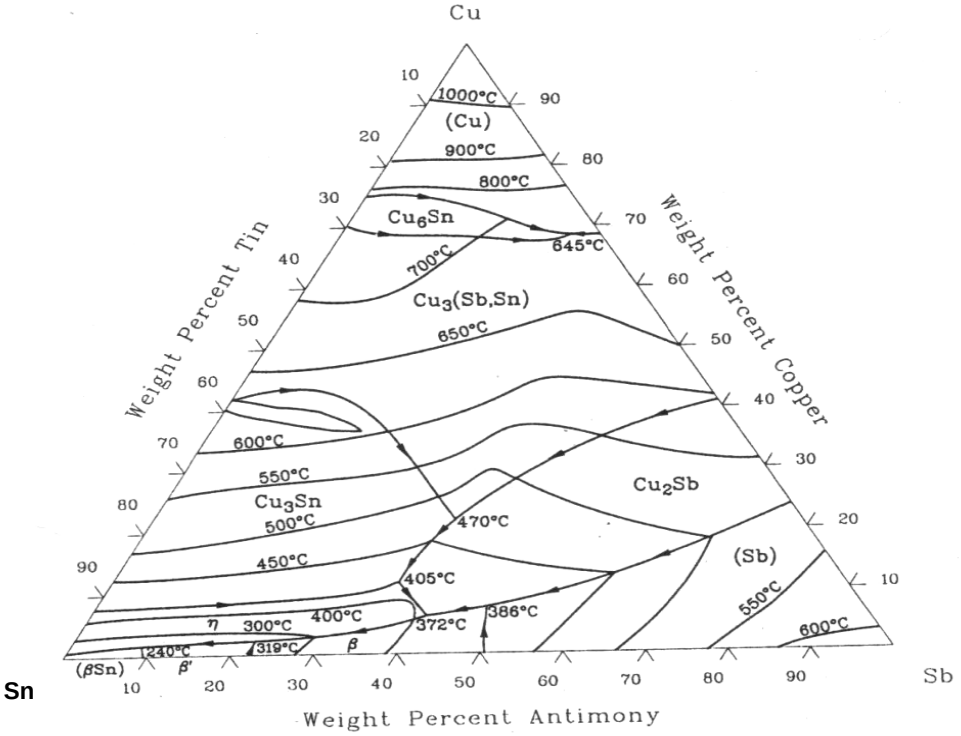

Figure J2: Sn-Cu-Sb liquidus projection [73Bla] (ASME Handbook)

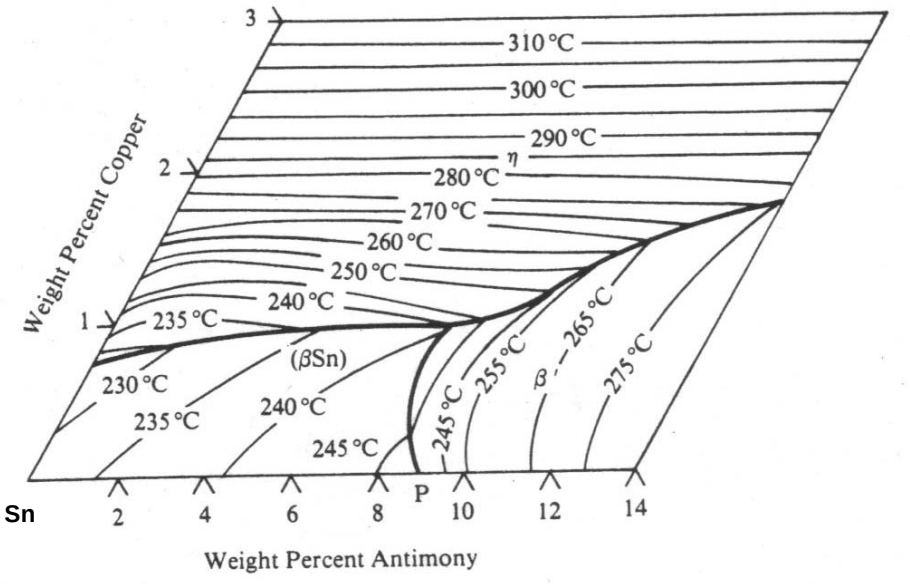

Figure J3: Cu-Sb-Sn (Sn) liquidus projection [73Bla] (ASME Handbook)

K. Micrographs of Cast Pewter

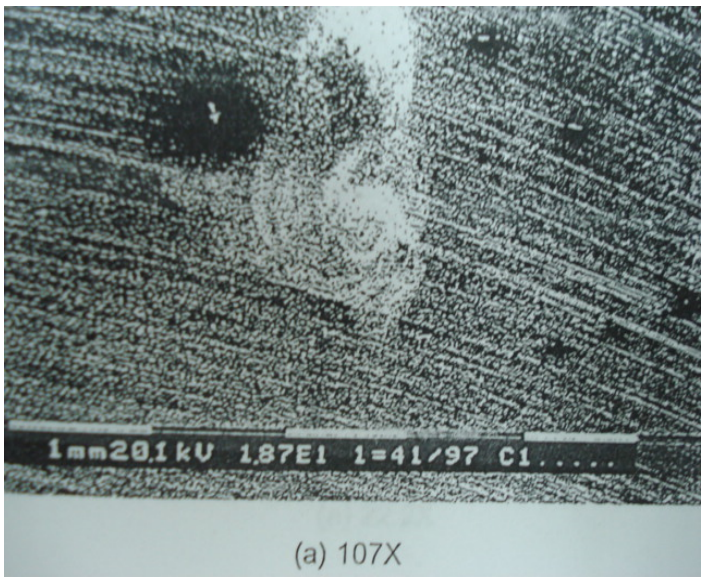

Figure K1: Micrograph of a pewter plate
(The hole is actually porosity in the cast part)
(Courtesy of Royal Selangor, Malaysia)

Figure K2: Close up of the dark pit (from Figure J1) which indicate some metallic crystallites (Courtesy of Royal Selangor, Malaysia)

Figure K3: Optical micrograph showing 200X the microstructure of a pewter piece at the edge (Courtesy of Royal Selangor, Malaysia)

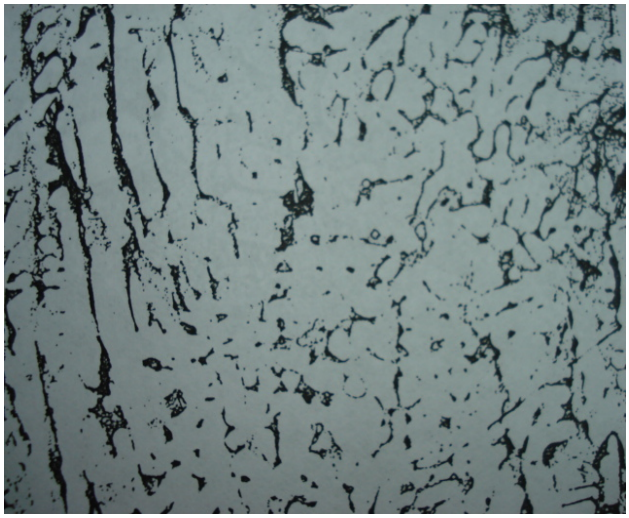

Figure K4: Optical micrograph showing 200X the microstructure of pewter piece at the center (Courtesy of Royal Selangor, Malaysia)

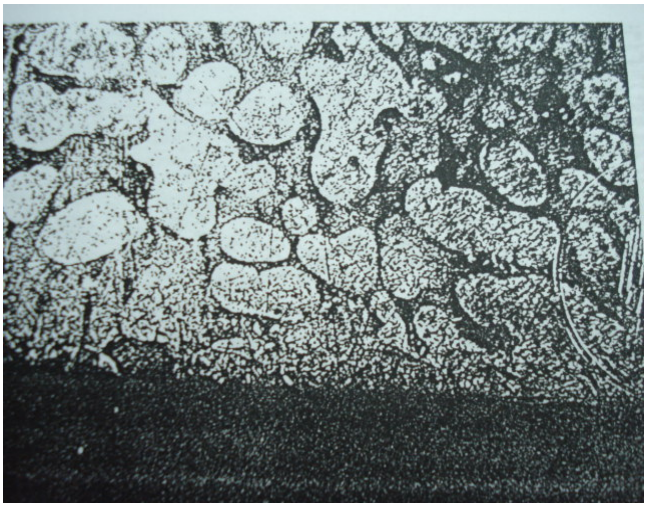

Figure K5: Optical micrograph showing 500X the micro structure of a pewter cast piece with coarse Sn rich dendrites with needles and small particles of Cu6Sn5 (Courtesy of Royal Selangor, Malaysia)

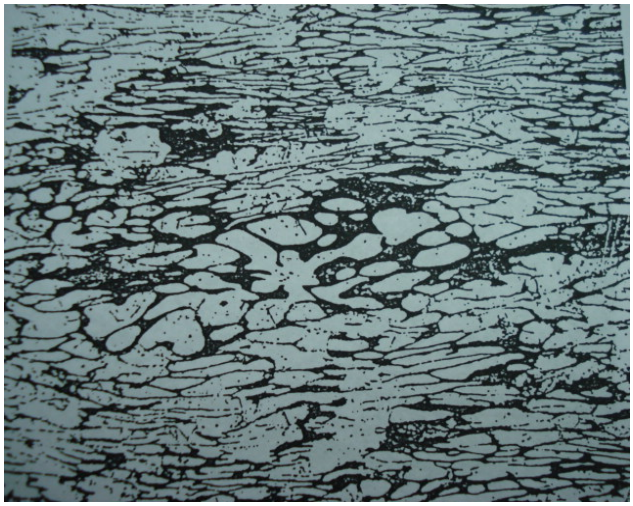

Figure K6: Optical micrograph showing 200X the center of a pewter cast piece- consisting of mainly Sn rich dendrictic grains with fine particles of Cu6Sn5 in tin rich solid solution (Courtesy of Royal Selangor, Malaysia)

Figure K7: Optical micrograph showing 200X the coarse grains of Sn rich dendritic structures in the center of a cast piece (Courtesy of Royal Selangor, Malaysia)

L. The Error Function

The error function, erf is given by:

$$\mathrm{erf}(z) = \frac{2}{\sqrt{\pi}} \int_0^z e^{-(x^2)}\, \mathrm{d}\, x$$

The following table gives values of erf(z) for 0<z<2.8.

Table L1: Values of erf (z)

z	erf(z)	z	erf(z)	z	erf(z)
0	0	**0.55**	0.5633	**1.3**	0.9340
0.025	0.0282	**0.6**	0.6038	**1.4**	0.9523
0.05	0.0564	**0.65**	0.642	**1.5**	0.9661
0.1	0.1125	**0.7**	0.6778	**1.6**	0.9763
0.15	0.168	**0.75**	0.7111	**1.7**	0.9838
0.2	0.2227	**0.8**	0.7421	**1.8**	0.9891
0.25	0.2763	**0.85**	0.7707	**1.9**	0.9928
0.3	0.3286	**0.9**	0.7969	**2**	0.9953
0.35	0.3794	**0.95**	0.8209	**2.2**	0.9981
0.4	0.4284	**1**	0.8427	**2.4**	0.9993
0.45	0.4755	**1.1**	0.8802	**2.6**	0.9998
0.5	0.5205	**1.2**	0.9103	**2.8**	0.9999

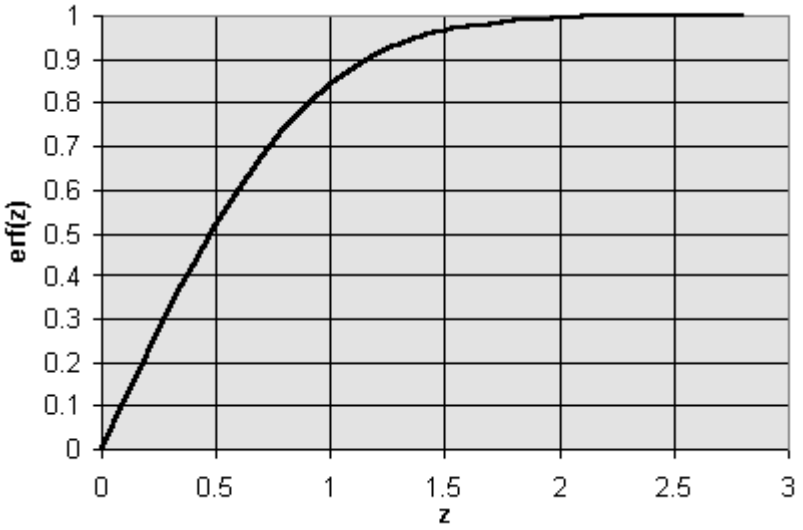

Figure L1: Relationship of erf (z) vs z